Antibacterial nanoparticle - decorated carbon nanotube - reinforced calcium phosphate composites as bone implants

Kiruthika Natesan

Let us know how access to this document benefits you

PHD

Antibacterial nanoparticle - decorated carbon nanotube - reinforced calcium phosphate composites as bone implants

Natesan, Kiruthika

Award date:
2018

Awarding institution:
University of Plymouth

Antibacterial nanoparticle - decorated carbon nanotube - reinforced calcium phosphate composites as bone implants

by

Kiruthika Natesan B.Sc., MRes

A thesis submitted to Plymouth University

in partial fulfilment for the degree of

DOCTOR OF PHILOSOPHY

Plymouth University Peninsula School of Medicine and Dentistry

September 2017

Copyright Statement

This copy of the thesis has been supplied on condition that anyone who consults it is understood to recognise that its copyright rests with its author and that no quotation from the thesis and no information derived from it may be published without the author's prior consent.

To my mum who is a living example of

Courage does not always roar. Sometimes courage is the quiet voice at the end of the day saying,

"I will try again tomorrow"

Acknowledgements

I would like to thank many people for their support and assistance for the past four years without which this work would not be possible. Firstly, a massive thank you to my supervisors Huirong Le, Christopher Tredwin and Richard Handy for believing in me and offering this valuable life changing opportunity to me. A special thanks to Richard Handy for all the effort that he has put in me to shape me as a better researcher especially during the writing of this thesis and to make me realise it is the small things that matter more! I cannot thank Chris enough for always being positive and encouraging, Huirong for showing that engineering is fun, and simple ideas go a long way in engineering. I would also like to thank Alex for being critical about my work and challenging me in every step of my work.

Many thanks must go to the technicians past and present for all the time they have spent training me with all the equipments. A special thanks goes out to Terry and Zoltan for all discussions that we have had and Glen from the microscopy unit for reminding me that life is so much more than just work. A special thanks to Lynn, Andy and Will who went above and beyond to help me throughout the four years. I would also like to acknowledge the administrators from the Engineering, Dental and Biomedical school for their support.

Finally, I would like to thank my family for giving me all the support and encouragement. My deepest gratitude goes to my husband who is my pillar of support, for always giving priority to my needs especially during the writing phase. It is from my husband that I draw my strength and courage to keep going forward. My deep appreciation goes to my friends who never stopped asking me, "When will you finish growing teeth?"

Author's Declaration

At no time during the registration for the degree of Doctor of Philosophy has the author been registered for any other University award without prior agreement of the Graduate Sub-Committee.

Work submitted for this research degree at the Plymouth University has not formed part of any other degree either at Plymouth University or at another establishment. This study was financed with the aid of a studentship from Plymouth University Peninsula School of Medicine and Dentistry.

Relevant scientific seminars and conferences were regularly attended at which work was often presented

Word count of main body of thesis: 51,500

Signed……………………………………………

Date………………………………………………

Antibacterial nanoparticle - decorated carbon nanotube - reinforced calcium phosphate composites as bone implants

Kiruthika Natesan

Abstract

Introduction

Hydroxyapatite (HA) is a biologically active ceramic used in surgery to replace bone. While HA promotes bone growth, it suffers from weak mechanical properties and does not possess any antibacterial property. Multi walled carbon nanotubes (MWCNTs), as one of the strongest and stiffest materials, have the potential to strengthen and toughen HA, thus expanding the range of clinical uses for the material. Furthermore, Silver nanoparticles (Ag NPs) can be decorated to sidewalls of the MWCNTs which could be released over a period of time to prevent infection following surgery. This work sought to develop and characterise Ag NPs- MWCNTs – HA composites in four main areas: 1) production and characterisation of the composite, 2) evaluation of mechanical properties, 3) investigation of antimicrobial property and 4) assessment of biological response to *in vitro* cell culture.

Methods

Pristine (*p*-MWCNTs) and acid treated MWCNTs (*f*-MWCNTs) were decorated with Ag NPs. In the presence of 0.5 wt % Ag NPs-MWCNTs, HA was precipitated by the wet precipitation method in the presence of either poly vinyl alcohol (PVA) or Hexadecyl trimethyl ammonium bromide (HTAB) as the surfactant. Composites were characterised using various techniques and the diameteral tensile strength and compressive strength of the composites were measured. The antibacterial effect of these composites was investigated against clinically relevant microbe, *Staphylococcus aureus.* To determine the

ability of the HOB cells to differentiate and mineralize in the presence of the composite, HOB cells were cultured on the composites for 21 days. Gene expression studies was performed along with the biochemical assays and scanning electron microscopy was used for qualitative analysis. Pure HA was used as control in all the studies.

Results

The study revealed that both the MWCNTs and surfactants play a crucial role in the nucleation and growth of the HA. XRD and FTIR characterisation revealed that HA was the primary phase in all the synthesised powders. Composites made with *f*-MWCNTs were found to have better dispersion and better interaction with the HA compared to composites with *p*-MWCNTs. Although mechanical strength was improved in all the composites, *p*-MWCNTs composites exhibiting maximum strength. Antibacterial studies showed 80% bacterial reduction in the treatment composites compared to pure HA. The biocompatibility study showed reduced activity of the HOB cells, however, no significant difference was observed between the control and the treatments.

Conclusion

This systematic study of the synthesis and properties of the Ag NPs- MWCNTs-HA composites has resulted in improved understanding of the production and processing of these materials and the effect of MWCNTs and silver nanoparticles on primary human osteoblast cells. Additionally, it has yielded interesting biocompatibility result favouring the use of MWCNTs in the development of implants. There is potential to translate Ag NPs-MWCNTs-HA composites into clinically approved product.

Table of Contents

List of Figures

List of Tables

1.Introduction and Literature review

The increasing proportion of older people in the population along with higher expectations of the quality of life has resulted in higher demand for better quality medical implants that are more durable, while remaining biocompatible and safe for the patient. The development of such implants involves a great number of challenges in biomaterials research. For example, in the case of bone implants there are four basic criteria that need to be addressed:

(i)   Superior mechanical strength – bone is one of the strongest organs of the body and the implant material should be capable of functioning efficiently under mechanical stress;

(ii)   Biocompatibility and bioactivity – the implant material should allow and support the proliferation of the osteoblasts (bone cells);

(iii)   Minimal - reactivity – the implant material should not cause any adverse inflammatory response from the body;

(iv)   Regulatory requirements –any implant material intended for human use needs to be approved by the health agencies such as the European Medical Agency (EMA) in the E.U. and the Food and Drug Administration (FDA) in America. The implant material needs to satisfy and pass the safety specifications set out by these agencies for medical devices.

The above mentioned are some of the minimalistic requirements that need to be achieved. With the evolution of antibiotic resistant microbes, meeting basic requirements is not sufficient and the material needs to be patient specific and loaded with antimicrobial agents/ drugs which will combat microbial infection. Several attempts have been made to

solve the current issue by developing composites/nanocomposites which are bioactive and mechanically strong with the ability of delivering antimicrobial agents. However, material synthesis is a highly complicated process. Slight variation in any parameter results either in a new material or in material that is not reproducible. Development of such materials is inefficient, as these materials will not satisfy the legal requirements outlined by the health agencies for the use of an implant material in patients such as:

(i)   Safer than an existing product;

(ii)   Demonstrate the ability to perform better than the existing product in market for the intended used;

(iii)   Limited or no adverse effects on health.

A number of scientific articles are published every year on the various types of materials that could be used as bone implants but they vary significantly based on the type of material, production process and testing standards. The scientific aim of this review is to provide a broad background pertaining to the evolution of implant materials over the years. Emphasis is given to ceramics, nanomaterials and composites while analysing the latest trends, achievements and shortcomings in this area. It is vital to elucidate the purpose for the development of these materials which makes it important to describe the bone structure and complexity involved in it. The contents of the literature then focuses on the different bone replacement options that have been in use and analyses their pros and cons. A detailed yet concise study about nanomaterials and their applications in biomaterials is performed as nanomaterials are widely used in all areas of tissue engineering. Nanomaterials bring their own challenges due to their size and chemistry which still needs better understanding. The

focus then shifts to the use of ceramic composites and their advancement in this field. Finally, the hypothesis and scope of the project is summarised.

1.1   Bone Formation, Structure and Properties

The skeleton is constructed of a hard natural tissue called bone and cartilaginous material. Bone formation, also known as ossification, occurs in two different ways: endochondral ossification and intramembranous ossification. Endochondral ossification is the initial formation stage for most bones in the axial and appendicular skeleton (e.g., femur, tibia, humerus) and starts with a cartilage framework. The cartilage framework is formed from condensed mesenchymal cells which differentiate into chondrocytes and secrete a cartilage extracellular matrix. Once the cartilage framework is completed, it is invaded by a mixture of cells (blood vessels, proliferative, prehypertrophic and hypertrophic chondrocytes and osteoprogenitor cells) first at its centre and then at the ends in a process called primary and secondary ossification, respectively. During primary ossification, which occurs in the middle of the cartilage framework, the osteoprogenitor cells differentiate into osteoblasts which secrete osteoid. The chondrocytes start to secrete enzymes essential for mineral deposition. The hypertrophic chondrocytes secrete growth factors that induce blood vessel sprouting along the length of the cartilage framework (Kini and Nandeesh, 2012). The blood vessels carry the osteoprogenitor, hemopoietic cells and ions deeper into the cartilage framework. The osteoprogenitor cells differentiate into osteoblast cells and use the mineralised framework as a scaffold and begin to secrete osteoid which forms the trabeculae (Felix and Fleisch, 1976, Dereszewski and Howell, 1978, Anderson, 2003, Anderson et al., 2005). The primary ossification occurs during foetal growth and about the time of birth,

secondary ossification happens at both the ends of the long bones. The mesenchymal cells and the blood vessels reach the ends of the bone and the same process is repeated. Postnatal growth continues until the cartilage in the bone is completely replaced reaching maturity. (Mackie et al., 2008). The above mentioned is the process that occurs during fracture healing often treated by cast immobilization.

The other bone formation that occurs in the foetus is the intramembranous ossification where the mesenchymal stem cells differentiate into osteoblast cells without the need for the cartilage framework. Flat bones in the body such as the skull are made by this process. During the intramembranous formation, the ossification centres are formed at certain points. The mesenchymal stem cells proliferate and produce the osteoprogenitor cells which differentiate into osteoblasts. The osteoblasts produce osteoid and the bone matrix which gets surrounded by collagen fibers. The osteoid becomes mineralised and traps osteoblasts which become osteocytes which is then lined with active osteoblasts. The process of mineralisation continues forming the trabeculae leading to the formation of a woven bone which is eventually replaced by lamellar bone. (Kini and Nandeesh, 2012)

The structure of bone can be organised on various levels (i) Macrostructure - cancellous and cortical bone, (ii) Microstructure - Haversian systems, osteons, single trabeculae (iii) Sub - microstructure- lamellae, (iv) Nanostructure - fibrillary collagen and embedded minerals, (v) Sub-nanostructure - molecular structure of constituent elements such as mineral, collagen, and non-collagenous organic proteins. Cortical bones are dense, solid and surrounded by marrow space whereas cancellous bones are composed of

honeycomb-like network of trabecular plates with rods interspaced in the bone marrow compartment (Kini and Nandeesh, 2012). The organic material of bone, namely, collagen forms 30% of the bone providing strength and flexibility. The collagen is stiffened by crystals of inorganic minerals which make up the remaining 70% of the bone. (Seeman and Delmas, 2006). The inorganic minerals are calcium phosphate, calcium carbonate, calcium fluoride, calcium hydroxide and citrate(Murugan and Ramakrishna, 2005). Although, the inorganic component is crystalline, it may also be present in amorphous forms. Details about the composition of bone and the various organic and inorganic phases is provided in Table1.1. These diverse arrangements of material structure work in harmony to perform various mechanical, biological, chemical functions such as structural support, protection, storage of healing cells, and mineral ion homeostasis (Rho et al., 1998).

Table 1.1 Bone composition.

Inorganic phase	Weight %	Organic phase	Weight%
Hydroxyapatite	≈ 60	Collagen	≈ 20
Carbonate	≈ 4	Water	≈ 9
Citrate	≈ 0.9	Non-collagenous proteins	≈ 3
Sodium	≈ 0.7	Primary bone cells: osteoblasts, osteocytes, osteoclasts	
Magnesium	≈0.5		
Other traces: Cl^-, F^-, K^+, Sr^{2+}, Pb^{2+}, Zn^{2+}, Cu^{2+}, Fe^{2+}		Other traces: polysaccharides, lipids, cytokines	

Slightly varied from species to species and from bone to bone (Murugan and Ramakrishna, 2005)

Bone is the framework of the body and plays a vital role in providing the crucial mechanical support required to perform day-to-day activities. The mechanical requirements of bone varies at different parts of the body. Hence, the load bearing ability of the cortical and cancellous bones vary largely (Table 1.2).

Table 1.2 Mechanical properties of bone (Murugan and Ramakrishna, 2005)

Properties	Measurements	
	Cortical bone	Cancellous bone
Young's modulus (GPa)	14-20	0.05-0.5
Tensile Strength (MPa)	50-150	10-20
Compressive strength (MPa)	170-193	7-10
Fracture toughness (MPa m$^{1/2}$)	2-12	0.1
Strain to failure	1-3	5-7
Density (g/cm^3)	18-22	0.1-1.0
Apparent density (g/cm^3)	1.8-2.0	0.1-1.0
Surface/ bone volume (mm^2/mm^3)	2.5	20
Total bone volume (mm^3)	1.4x10^6	0.35x10^6
Total internal surface	3.5x10^6	7.0x10^6

The values mentioned in the table are a rough estimate as the values change depending on various factors such as age, health of the bone, method used to measure the mechanical properties.

In load bearing areas such as the hip and knee, cortical bones must be able to resist deformation but they must also be sufficiently light to allow rapid movement. They must also be able to absorb the energy by deforming, to shorten and widen when compressed and to lengthen and narrow in tension without cracking (Seeman, 2007). If bone is too brittle (unable to deform), the energy imposed during loading will be released by structural failure. Initially this will be in the form of micro cracks, which give way to complete fracture. If bone is too flexible and deforms, it will also crack (Seeman, 2008). Hence, bone is prone to damage and requires suitable replacement/ healing options.

1.2   Bone Replacement Options

Limb transplantation was first described during the 5th century A.D. (Catanzariti and Karlock 1996). The integration of a bone graft is the process by which the donor bone is enveloped and fused with the recipient bone allowing new bone minerals to be deposited in it (Zipfel, Guiot and Fessler 2003). For a long time, autografts were considered as the gold standard as it uses the graft material from the same individual. The main disadvantage of using autografts is the need for surgery to harvest healthy bone from different part of the body. This causes additional discomfort to the patient who are already under chronic pain. Following autografts, allografts were introduced which involves obtaining a tissue or organ from a different member of the same species and grafted to a genetically dissimilar member of the same species. The main issue with allografts is the possibility of transmitting infection and the body may reject the graft and trigger an immune response. To overcome these disadvantages, the xenograft option was developed. The Xenograft approach is similar to

allograft bone replacement method. In this method, the bone graft is obtained from a different species usually from a bovine. The Dutch surgeon Job Van Meekren performed the first registered surgery using a bone xenograft (Hernigou and Homma, 2012). The only advantage is that large quantities of graft can be obtained .The disadvantages are similar to allografts and is not a popular practice as the graft is obtained from an animal usually from a bovine or swine which is unpopular among the patients. For a detailed undertaking of autografts, allografts and xenografts and the complications involved in it, readers are referred to (Arrington et al., 1996, Bauer and Muschler, 2000, Shibuya and Jupiter, 2015). These disadvantages combined with the growing population created the need for the development of better artificial/ synthetic bone grafts.

The key focus for the development of synthetic bone grafts is the ability to blend engineering principles with the body's natural response to tissue damage to attain rapid recovery. This idea coupled with a better understanding of cell signalling and subsequent functionality enables the development multifunctional bioactive scaffolds. A schematic illustration of the criteria for an ideal synthetic bone graft is provided in Figure 1.1. An ideal bone graft should be biochemically stable and promote the growth of native tissues and should not elicit an inflammatory response. It should be capable of providing temporary mechanical support while being able to degrade in a controlled period to enable load transfer. They should not produce any toxic products while degrading and the body should be able to excrete the degrading products safely. The implant should be able to deliver drugs/antimicrobial agents to accelerate the healing process and reduce microbial infection.
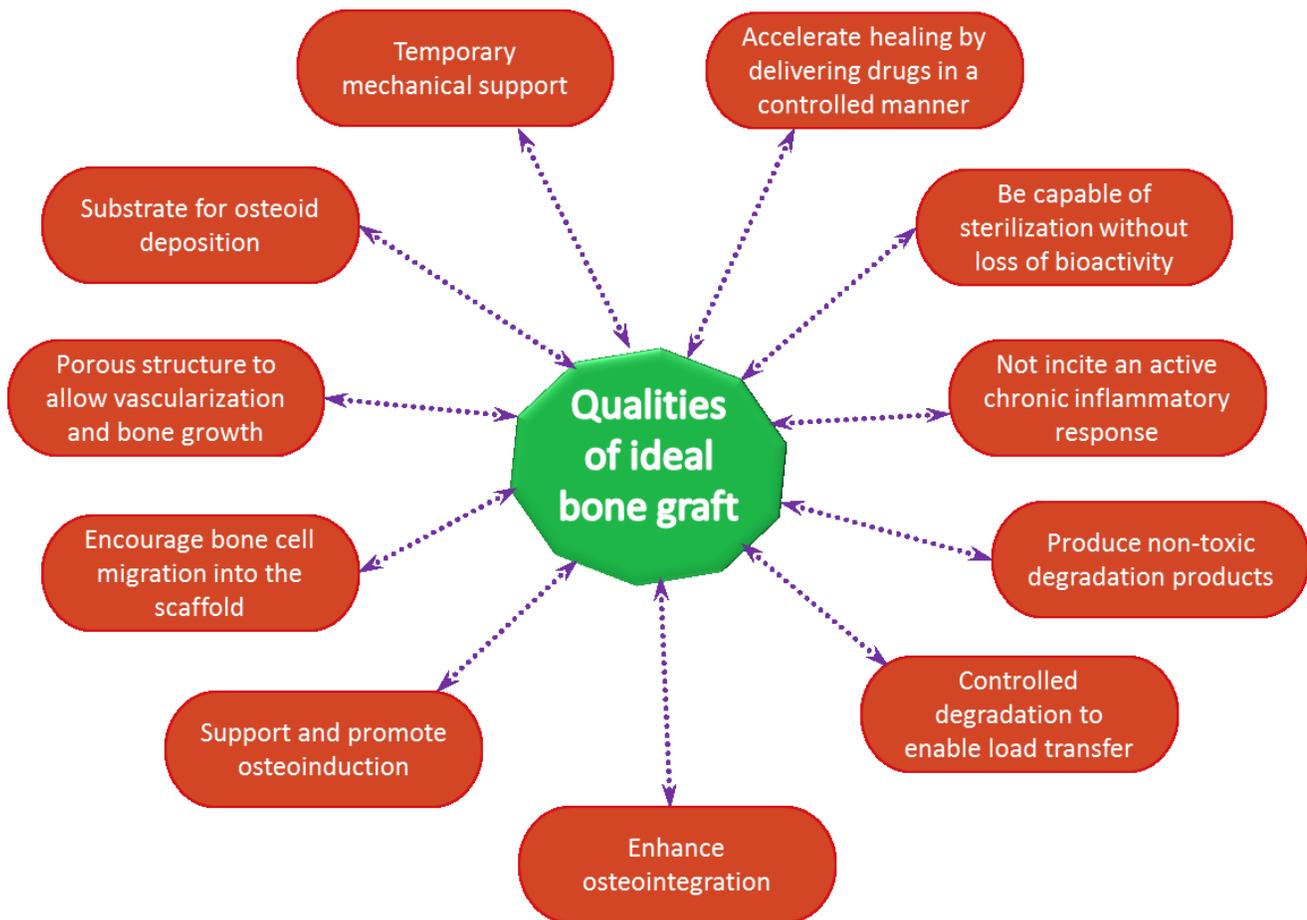
Figure1.1 Illustration of key elements that constitute ideal synthetic bone graft material.

Synthetic bone grafts can be classified into many types based on the nature of the material such as natural, synthetic or composite. Natural materials include biological polymers such as collagen, gelatine, polysaccharides (agarose, alginate, chitosan and hyaluronic acid) and fibrin as well as inorganic minerals such as calcium phosphates (hydroxyapatite and tricalcium phosphate). Synthetic materials are diverse as they can be

engineered from any type of material to exhibit the characteristics of ideal bone graft substitute (Chao Le Meng et al., 2013). However, the main types of synthetic materials currently used for bone implants are metals, ceramics, polymers and composites. Composites can be made by combining natural and synthetic material to produce a hybrid that will exhibit all the qualities of an ideal bone graft substitute.

Naturally derived substitutes have the advantage over synthetic materials in being similar to the chemical composition and crystal structures found in the body. Due to their similarity with bone, naturally derived substitutes are biocompatible and may encourage tissue development by promoting cell adhesion and proliferation without causing adverse inflammatory reaction. When used as *in vivo* implants, the polymers are readily remodelled by natural bone cells to adapt to the internal local environment (Chao Le Meng et al., 2013). For example, one of the commonly used natural polymers is collagen, which is present mainly in the extracellular bone matrix. Owing to the biocompatible properties of collagen, it has been employed in the development of implants. Synthetic HA is usually applied as a reinforcement to overcome the disadvantages of collagen such as such as poor dimensional stability due to *in vivo* swelling, poor mechanical strength and low elasticity (Gorgieva and Kokol, 2011). Ryan et al (2015) produced HA-collagen composites by dispersing HA in the collagen aqueous suspension followed by freeze-drying. They have reported that the dispersion was not uniform and were often aggregated proving that there is no real interaction of HA with collagen fibres. Another method of developing HA-Collagen composites is to nucleate HA on the collagen matrix to improve the interaction. However, as noted by Lin et al (2004) and Yunoki et al (2007) the mechanical property of the composite

was inferior and was not reliable compared to the host bone (Lin et al., 2004, Yunoki et al., 2007). This could partially be due to the difference in the biodegradation of HA and collagen. Another big practical problem with collagen is the cost involved and the poor commercial sources available for this material. For a detailed review of collagen the readers are referred to other reviews in this topic (Bunyaratavej and Wang, 2001, Geiger et al., 2003).

Metals dominate the orthopaedic industry to date. They are non-resorbable and are used in the form of plates, pins, rods and screws which provide rigid internal fixation for damaged bones (Daniels et al., 1990). Currently, titanium and its alloys, cobalt –chromium alloys and stainless steel are widely used as surgical implants. Titanium is chosen over other metals owing to its superior mechanical properties. Moreover, titanium is a reactive metal; it naturally forms an oxide layer on its surface which makes it biocompatible (Kasemo, 1983). In comparison with other alloys, titanium-based materials have low elasticity modulus, varying from 110 to 55 GPa which is approaching the elastic modulus of natural bone (30 GPa) (Vandrovcova and Bacakova, 2011). However, the osseointegrative bioactivity is still not sufficient to attain true adhesion between the implant and the bone, which may ultimately lead to mechanical instability and implant failure. Moreover, since titanium is a reactive metal, it is prone to corrosion (Olmedo et al., 2008). When used in patients as a long-term implant, the metal may induce an inflammatory reaction leading to implant failure. Following titanium alloys, cobalt-chromium alloys are used as bone implants. Unlike titanium implants, cobalt-chromium is corrosion resistant which reduces the likelihood of implant rejection by the body. They are also mechanically strong making them the main choice of metal for hip arthroplasty. However, a study was led by Michel et al., (1991) on the

presence of trace elements in blood serum of patients who had cobalt-chromium implants for 18 years. They showed that compared to the normal levels, the concentration of cobalt and chromium was higher in the patients with the implants and they recorded even higher concentrations in the local area where the implant was placed. The increase in the concentration of these trace metals is due to wear debris which results in loosening the implant which could become toxic, causing adverse local reaction leading to implant failure (Jacobs, 1998, Vandrovcova and Bacakova, 2011). Furthermore, cobalt-chromium alloys have much higher elasticity modulus (240 GPa) which can lead to mechanical failure through loosening or fracture; as the load will not be transferred equally between the natural bone and the implant.

Ceramics such as calcium phosphates, calcium sulphates are another types of materials that are used as bone implants and unlike metals, they are bioresorbable. They degrade over time and are replaced by natural tissue. In particular, synthetic calcium phosphate ceramics holds great promise as a biomaterial for bone implantation compared to the other types of ceramics due to its ability to bond with bone and their similarity to the inorganic phase of natural bone, which is hydroxyapatite (HA), a type of calcium phosphate. One of the first studies reporting the use of calcium phosphate for bone repair was performed by Albee and Morrison in 1920. They reported the use of "triple calcium phosphate" as a stimulus for bone growth. The results indicated that bone fractures, with bone loss, showed rapid bone growth when "triple calcium phosphate" was injected. (Albee, 1920). In the 1970s, calcium phosphate ceramics were synthesized and characterized to be used as bone implants (Monroe et al., 1971, Rejda et al., 1977, Ferraro, 1979). While

bioresorbable material such as tricalcium phosphate (TCP) would seem like an ideal candidate, the degradation process can adversely affect the mechanical integrity of the material and the stability of the material-tissue interface. This compromises the implant-bone system during the resorption and replacement process. It is also difficult to match the resorption rate of the synthetic biomaterial to the repair rate of the bone tissue. Bioactive materials, as intermediate between the two extremes, elicit a biological response at the material interface and bond with the surrounding tissue, yet avoid degradation. This is particularly useful in areas of load bearing as the implant is intended to remain intact for extended periods in the body without causing inflammation or toxic reactions. Hence, this class of synthetic replacement materials should produce promising results. Bioactive ceramics include bioactive glass®, bioactive glass-ceramic and HA, the matrix material of our choice for this study.

Apart from metals and ceramics, polymers are also used in the development of bone implants. The idea behind this accession is their availability in a wide variety of composition, properties and forms that can be fabricated into complex shapes and structures. However, polymers are almost always used in conjunction with ceramics such as HA and TCP as they tend to be too flexible and too weak to meet the mechanical demands of the implants. Synthetic polymers provide certain advantages over natural polymers which makes them an attractive choice for the development of bone implants. For example, synthetic polymers can be manipulated to improve properties such as predictable uniformity, freedom from immunogenicity concern and ability to mass-produce at low cost. Many polymers such as polyetheretherketone (PEEK), polymethylmethacrylate (PMMA) and poly vinyl alcohol (PVA)

have been used in the development of composites (Ramakrishna et al., 2001, Sionkowska, 2011, Baker et al., 2012, Razak et al., 2012).

1.3 Role of Nanotechnology/Nanomaterials in Tissue Engineering

Over the past three decades, a new dimension of synthetic material has evolved by modifying metals, ceramics and polymers at their molecular and nanoscale level rather than manipulating their bulk form. Nanotechnology and nanoscience is the application and study of items smaller than 100nm (at the nanoscale level which is 10^{-9} of a meter) that can be applied in other fields of science such as chemistry, biology, physics, material science and engineering. The European commission states that 'Nanotechnology is the study of phenomena and fine–tuning of materials at atomic, molecular and macromolecular scales, where properties differ significantly from those at a larger scale' (Lioy et al., 2014).

The term 'nanoscale' is defined as size range from approximately 1nm to 100nm (Potocni, 2011). According to the European Commission, a nanomaterial is "A natural, incidental or manufactured material containing particles, in an unbound state or as an aggregate or as an agglomerate and where, for 50% or more of the particles in the number size distribution, one or more external dimension is in the size range of 1-100nm. In specific cases and where warranted by concerns for the environment, health, safety or competitiveness the number size distribution threshold of 50% may be replaced by a threshold between 1 and 50%". However, meeting the length scale criterion of 1-100 nm does not suffice the use of nanomaterials, rather, it is taking advantage of novel properties

such as physical, chemical, mechanical, electrical, optical, magnetic, etc. that results solely because of going to nanoscale from their bulk counterpart (Liu and Webster, 2007, Etheridge et al., 2013). In general, nanoparticles used in the field of biomedical applications range in particle size between 10 and 500 nm. Nanoparticles interact distinctively with bone cells and tissue, depending on their composition, size, and shape Figure 1.2 represents the overview of nanoparticle applications in bone.
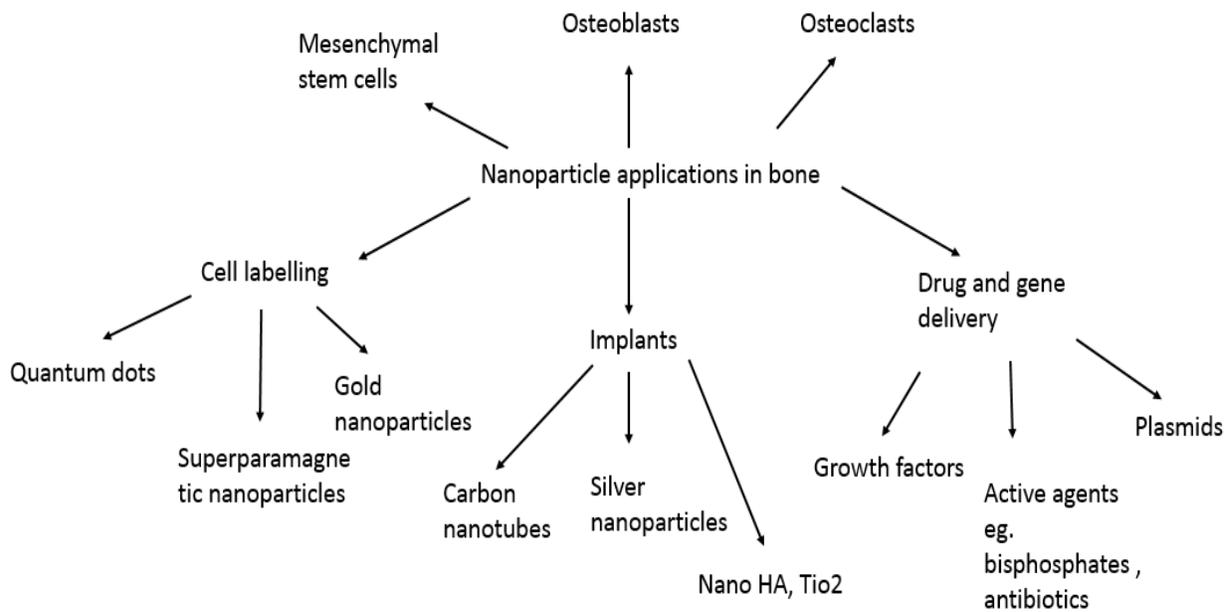
Figure 1.2 schematic representation of the application of nanomaterials related to bone cells.

1.3.1 Carbon Nanotubes

In the last decade the application of carbon based nanomaterials especially carbon nanotubes in tissue engineering has increased. Carbon nanotubes are allotropes of carbon with a cylindrical nanostructure. The walls of CNTs have a hexagonal lattice structure like graphite sheets. Since the start of the 21st century, there has been an increase in the number

of articles related to carbon nanotubes use in biomedical application with 2004 marking the beginning of applying carbon nanotubes in tissue engineering (Correa-Duarte et al., 2004, Harrison and Atala, 2007). Carbon nanotubes are applied in four areas of tissue engineering – cell tracking and labelling, sensing cellular behaviour, augmenting cell behaviour and enhancing tissue matrices which is the area of interest for this study.

There are many different types of CNTs but they are normally categorized as either single walled (SWCNTs) or multi walled (MWCNTs). SWCNTs are made of only one layer of carbon atoms whereas MWCNTs are a collection of nested tubes of continuously increasing diameters. They can range from one outer tube and one inner tube to as many as 100 tubes or more. Each tube is held at a certain distance from either of its neighbouring tubes by interatomic forces.

Important properties of CNTs are high surface area, superior mechanical strength but light weight, abundant electrical properties and excellent chemical and thermal stability (Ajayan, 1999). The tensile strength of MWCNTs has been measured experimentally to be 11-63 GPa with no dependence on the outer wall diameter (Yu et al., 2000). The elastic modulus of CNTs is estimated to be greater than 1 TPa, based on the in-plane elastic modulus of graphite. This value has been confirmed experimentally by Demczyk et al.,(2002). While CNTs have excellent mechanical properties, they can vary widely depending on the production method used to grow the nanotubes, the number of defects in the structure and whether the nanotubes are SWCNTs or MWCNTs. There are three techniques by which CNTs can be synthesized: carbon-arc discharge, laser ablation and chemical vapor deposition (CVD) methods. The first two methods utilize solid-state carbon precursors to provide carbon sources needed for the nanotube growth and involves carbon vaporization at high temperatures (thousands of

degrees Celsius). These methods are well established in producing high-quality and nearly perfect nanotube structures, despite large amounts of by-products associated with them. The CVD method utilizes hydrocarbon gases as sources for carbon atoms and metal catalyst particles as "seeds" for nanotube growth that takes place at relatively lower temperatures (500-1000 °C)(Dai, 2002). CNTs are mostly produced using the CVD method, as it is relatively cheap compared to the other two methods and produces large quantities of CNTs. In the production process, transition-metal catalysts predominantly Fe, Co and Ni, are used. Although they are removed from the raw product, part of the metal is encased in the tubes and cannot be removed completely. When these metal impurities are exposed to the cells they can generate reactive oxygen species (ROS) causing toxicity to the cells (Allegri et al., 2016). The mechanical behaviour of CNTs in composites is complicated as the transfer of strength and stiffness to the matrix depends on the interfacial bonding between the two phases. This is influenced by the wettability of CNTs and interfacial area. Full advantage of the interfacial area cannot be harnessed, as the CNTs tend to agglomerate due to the presence of strong van der waals force which facilitates them to remain twisted and curved in the matrix. Even if the full mechanical property of the CNTs cannot be drawn in due to the limitations, there is a possibility to still enhance the composite.

Medical application of CNTs require knowledge about their bioactivity and toxicity. There are concerns that CNTs may pose a potential health risk due to their similarity to asbestos namely their biopersistance and structure. However, despite their similarities in certain aspects, asbestos and CNTs vary in many physicochemical features such as constituent element, stiffness of the fibres, length and diameter of the tubes and even surface properties. Therefore, the two types of fibres do not necessarily exert similar toxicological

effects. CNTs are durable and does not fragment; hence, their presence in composites could possibly enhance the bioactivity without causing any harmful effect.

In vitro work has shown that several different cell types have been successfully grown on carbon nanotube composites. Zanello et al (2006) studied the osteoblast proliferation and bone formation on pristine and functionalized SWCNTs and MWCNTs. They have found that the cells grew best on pristine SWCNTs and neutrally charged polyethylene glycol-functionalized SWCNTs followed by negatively charged oxidized SWCNTs and zwitterionic poly(aminobenzene sulfonic acid)-functionalized SWCNTs. Recently, Zancanela et al (2016) compared the effect of SWCNTs and MWCNTs on mineralization of osteoblasts. They have shown that osteoblast viability increased in both SWCNTs and MWCNTs at various days and at the end of 21 days, osteoblasts mineralized. They have reported that SWCNTs and MWCNTs are not toxic to osteoblasts at concentrations upto 5×10^{-5} and 1.3×10^{-2} mg/ml respectively. *In vivo* studies have also been performed by Usuai et al (2008) in which they implanted MWCNTs into mouse skull and tibia bones. They have reported that no inflammatory reaction occurred (Abarrategi et al., 2008, Usui et al., 2008).

One of the most important factors governing the biocompatibility of fibrous materials, concerning the removal of foreign particles, is fibre length. Phagocytosis by macrophages is critical in the degradation and clearance of the foreign particles from the body. According to the world health organisation (WHO), asbestos fibres longer than 5μm are considered to be retained in the body and causes fibrosis and fibres shorter than 5μm are not taken into account(Boulanger et al., 2014). If that is the case, then it is suggested that shorter CNTs are biocompatible and nontoxic. There, are still discrepancies in the toxicity report which a

recent review on CNT suggests that the dose, shape, surface chemistry, exposure route and purity all play a vital role in determining the biocompatibility of the CNTs (Zhang et al., 2014). Additionally, several *in vitro* and *in vivo* studies have shown that functionalisation of the CNTs improve their wettability which allows them to disperse even in aqueous solution which in turn improves their biocompatibility (Barrientos-Durán et al., 2014, Paiyz et al., 2014, Tong et al., 2014).

Another concern is the toxicity induced by the presence of catalyst particles as a result of CNT production. One study has shown that ultra-sonicating CNTs for as short as 5 minutes reduces the amount of impurities as the mechanical force promotes the release of impurities form the CNTs into the solution (Toh et al., 2012). Overall, there is a noticeable lack of studies reporting the biological and toxicological properties of CNTs and there is high degree of variation in the methods undertaken to determine the bioactivity /toxicity of CNTs. While reports vary, the majority of research so far suggests that CNTs not only improve the mechanical properties of the composites but also induce bone regeneration and are nontoxic especially when they are functionalized.

Although CNTs have the above mentioned advantages, they do not possess any antimicrobial property which is a key requirement for an implant material. Due to the nature of the CNTs, they can be used in drug delivery. Antimicrobial agents such as silver can be attached to the sidewalls of the CNTs and released in a slow steady manner to curb bacterial infection.

1.3.2 Silver Nanoparticles (Ag NPs)

Bone tissue can become susceptible to infection following injury, during surgical procedures and especially with major invasive surgery such as hip replacement. Two major

types of infection affecting bone are septic arthritis and osteomyelitis, which involves the inflammatory destruction of the joint and bone respectively (Goldenberg, 1998, Lew and Waldvogel, 2004). Staphylococci, in particular *Staphylococcus aureus* are one of the principal causative agents of such infections (Berendt and Byren, 2004). One of the main routes of infection for both osteomyelitis and septic arthritis is often following injury, surgery or implantation of a foreign body, such as joint replacement (Berendt and Byren, 2004). The survival of pathogenic microbes after surgery depends on a number of factors including health of the patient, location of the surgery and infection control in the operating theatre. However, for medical implants there are additional risks with the successful adhesion of microbes to the implant surfaces and their ability to develop into biofilms that can lead to a well-established infection.

The local delivery of antibacterial agents is potentially an advantage over systemic drug administration (standard antibiotics that are supplied orally or intravenously). This is because drugs administered orally have unpredictable absorption due to degradation by stomach acid and enzymes while intravenous drug delivery is distressing to some patients and requires a functioning cannula which is prone to infection and may cause local adverse reaction. Local delivery of antimicrobial agents has the potential to achieve high and sustained local concentrations of the antimicrobial agents without large systemic doses, thus minimizing systemic toxicity, adverse reactions and development of resistant strains of bacteria.

In spite of many advances in biomaterials, a substantial amount of implants become colonized by bacteria and becomes the focus of implant infection. Antibacterial property of silver is related to the quantity of available silver and the rate at which it is released. The

exact mechanism by which silver exhibits its antibacterial action is still not completely understood. Silver is inert in its metallic state but ionizes on contact with an aqueous environment yielding Ag^+ which is believed to be the active antimicrobial agent. The ionized silver is highly reactive as it binds to the tissue proteins causing structural changes in the bacterial cell wall and nuclear membrane leading to cell distortion and death. In spite of its good antibacterial property, it is known that silver may also have adverse effects on human cells depending on many factors such as distance between cells and silver, exposure time and route. The alternate to dissolved silver can be Ag NPs as they have good antibacterial activity and are less toxic to human cells when used in small amounts (Franci et al., 2015).

Ag NPs have a high potential to solve the problem of multidrug –resistant bacteria as bacteria will be less able to develop resistance against silver compared to antibiotics (Rai et al., 2009). Although, the antibacterial effect of Ag NPs has been extensively studied, the mechanism underlying their action has been poorly understood. Many hypotheses has been proposed. One of them suggests that the bacterial cell wall comprises sulfur containing protein with which Ag NPs interact. Once they have entered the bacterial cell, they form a low molecular weight region in the bacteria to which the bacteria conglomerate trying to protect the bacterial DNA. Ag NPs then react with phosphorous containing compounds in DNA (Rai et al., 2009). Further, Ag NPs attacks the respiratory chain, cell division and finally leads to cell death. The antibacterial effect of Ag NPs against gram positive and gram-negative bacteria differ based on their concentration. Kim et al (2007) investigated the antimicrobial activity against *E. coli* and *Staphylococcus aureus*. The results showed that *E. coli* was inhibited at low concentration but it was less effective against *S. aureus.* In addition, Ag NPs have also been proved to breach biofilm formation. Martinez-Gutierrez et al (2013)

studied the antimicrobial activity of Ag NPs against Gram negative (*P. aeruginosa, Acinetobacter baumanni*) and gram positive (*S. aureus and S. mutants*) bacteria. They showed that the Ag NPs killed the bacteria in biofilm however, higher concentrations of Ag NPs was necessary for both the gram types compared to bacteria outside biofilms. They also showed that the anti-biofilm activity of Ag NPs are less profound against the gram-positive bacterial biofilm. They suggest that this could be due to the difference in their cell wall structure (Martinez-Gutierrez et al., 2013). It is clear that Ag NPs have antibacterial activity and this could be exploited in the development of composites for bone implants. Bacterial infection, primarily after surgery could be curbed by the incorporation of Ag NPs as either coatings on metal implants or in composites and could favour the slow release of Ag NPs reducing the need for antibiotics.

Toxicity of Ag NPs to human cells

If Ag NPs are to be incorporated in the development of scaffolds for bone implants, evidence of their bioactivity and toxicity is essential. Depending on the dissolution rate of the Ag NPs from the scaffold, they could pose potential toxic effects to the human cells.

A study led by Pauksch et al (2014) tested the response of primary human mesenchymal stem cells and osteoblasts to Ag NPs. They demonstrated that Ag NPs caused time and dose dependent impairment on both the cell types at concentration of 10μg/g. Ag NPs did not reduce the ability of the cells to differentiate but an increase in cell stress was observed. This suggests that Ag NPs below the concentration of 10μg/g can be used therapeutically but exceeding this limit will be toxic to bone cells. It also means that even if Ag NPs are used at higher concentration the ability of the cells to differentiate is not affected

and in an *in vivo* situation, slow release of moderate concentration will not affect the healing process after surgery and the cells will be replenished over a period of time.

It is unclear whether Ag NPs toxicity is mediated by the particles themselves or by particle dissolution and silver ion release. Albers et al (3013) investigated the cytotoxicity of silver nanoparticles and microparticles on osteoblasts and osteoclasts. They found that Ag NPs exhibited strong cytotoxic effect and microparticles exhibited weak cytotoxic effect. However, they have concluded that the cytotoxic effect of silver nanoparticles is primarily mediated by ionic silver liberation form the nanoparticles (Albers et al., 2013). Only limited number of articles have studied the effect of Ag NPs specifically against bone cells. Overall, in principle, Ag NPs can be used in lower doses for prevention of initial and intermediate stage infection after surgery. Although, they cause some cytotoxicity, it can be reduced by controlling the Ag release rate to accomplish both long-term antibacterial ability and bio integration.

1.4 Composites

Single materials do not always provide all the properties necessary for bone grafting and are very far from the characteristics of a true autogenous bone graft. The ultimate aim is to develop a bone implant which is as close as possible to the mechanical and biological properties of natural bone. The term "composites" can be defined as a heterogeneous combination of two or more materials, differing in morphology or composition on a microscale, in other words microcomposites, which are combined with the aim to improve the mechanical and /or biological properties (Gasser, 2000, Murugan and Ramakrishna,

2005). According to their interaction with the host tissue, composites can be classified as nearly bioinert (Alumina coated biomaterials, carbon-carbon and carbon –PEEK), bioactive (HA-Collagen, HA-PE and HA- Ti-6Al-4V) and bioresorbable (TCP-collagen, TCP-PLA and TCP-PLC). Of particular interest is the development of ceramic composites (HA, TCP) as these mimic the inorganic natural bone component.

1.4.1 Ceramic composites

Ceramics are often preferred over other classes of materials in many applications due to their low density, high rigidity, hardness, and low susceptibility to corrosion. Their main drawback however, is brittleness. Cracks form and quickly propagate through the material in a direction parallel and perpendicular to the applied load, resulting in sudden material failure. In order to prevent the brittle fracture of ceramics and to improve the overall mechanical properties of the ceramics, crack generation and extension of the cracks must be blocked. This can be accomplished by reinforcing the ceramics with high strength and stiff fibrous material. A suitable candidate, CNTs provides both the toughness and tensile strength required by the ceramics to make them less brittle, allowing them to be employed in a wide range of applications including load-bearing areas such as hip and knee joints. The choice of the reinforcing material is crucial in determining the overall success of the ceramic composites. The higher the aspect ratio of the reinforcing material the better the reinforcement. In addition to hindering the development of cracks through the matrix, the reinforcing material should also bear the applied load. The degree of the interfacial bond between the matrix and the fiber determines how well the stress is transmitted from the matrix to the fiber (Wagner et al., 1998). However, the bond between the matrix and reinforcement should not be too strong to hinder the slight flexibility that is required while

load is applied. Other factors to consider are the amount of reinforcement required to support the mechanical properties without eliciting a toxic reaction from the cells and the homogenous dispersion of the reinforcement in the matrix.

In the last twenty years, a large number of publications on calcium phosphate materials, especially on ceramic composites, have appeared in the literature, reflecting a sharp increase in the interest aimed at developing better materials for a broader clinical use (Daculsi, 1998, Vallet-Regí and González-Calbet, 2004, Ambard and Mueninghoff, 2006, Best et al., 2008, Galea et al., 2013). By altering the calcium to phosphate ratio many types of synthetic calcium phosphates can be produced such as monocalcium phosphate (Ca/P - 0.5) , dicalcium phosphate (DCP, Ca/P – 1.0), octa-calcium phosphate (Ca/p – 1.33), triclacium phosphate (TCP, Ca/P – 1.5), hydroxyapatite(HA, Ca/P – 1.67), and tetra-calcium phosphate (Ca/P – 2.0) (Suzuki, 2013, Huang and Cao, 2016). Of the different types of calcium phosphate, HA is greatly studied owing to its resemblance to the inorganic phase of natural bones (elaborated in Chapter 1, section 1.4). Following HA, α and β-tricalcium phosphates are preferred due to their resorbable nature .

Although, a number of studies have been published to illustrate the biocompatibility of the different types of calcium phosphate, they are incomparable due to the difference in the mode of synthesis and characteristics of the material, and *in vitro* experimental design (type of cells, number of days, types of assays and criteria to determine biocompatibility)(Best et al., 2008, Haaparanta et al., 2010), (Xu and Simon, 2005, Zeng et al., 2011). Hence, it is essential to determine the biocompatibility extent of the three main types of calcium phosphates (HA, DCP and TCP) which are much utilized as bone substitutes.

HA is very similar in composition to the mineral phase of bone and is an excellent bone replacement material. Clinically, it has been used in dental and orthopaedic applications for more than 40 years in their bulk form as filler and as coatings. HA is a polycrystalline calcium phosphate ceramic with a hexagonal crystal structure and a stoichiometric Ca/P ratio of 1.67 (Figure 1.3). It is part of the P63/m space group, characterized by a six-fold c-axis perpendicular to three equivalent a-axes at 120° angles to each other. Calcium cations (Ca^{2+}) and phosphate anions (PO_4^{3-}) are arranged around columns of monovalent hydroxyl anions (OH-) (Kay et al., 1964).
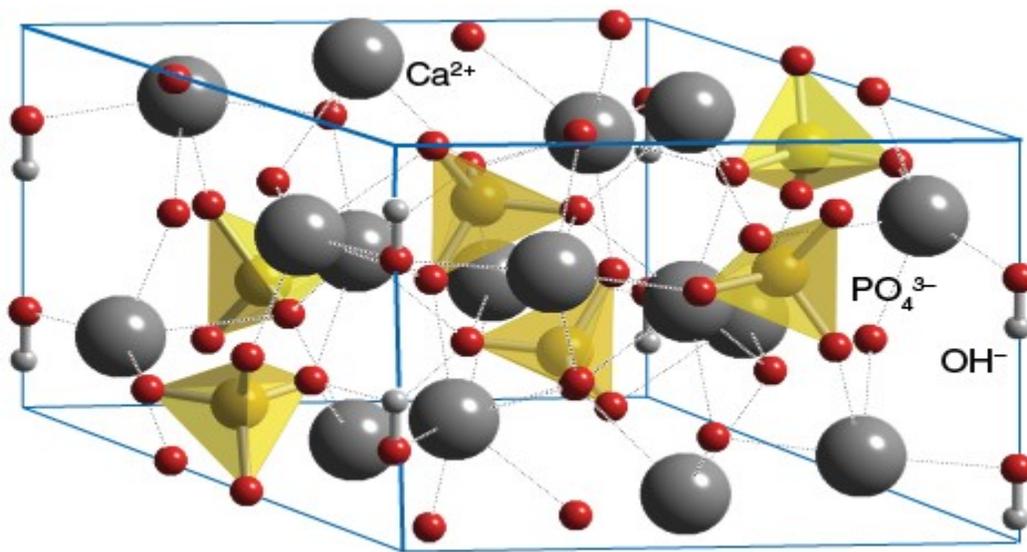
Figure 1.3 Structure of Hydroxyapatite (Greeves, 2017)

The stability of the HA structure is due to the presence of the phosphate group network which provides the skeletal framework. The bioactivity of the ceramic is dependent on the Ca/P ratio as slight alteration produces other types of calcium phosphate such as monocalcium, dicalcium, tricalcium and octacalcium phosphate. Several methods have been

employed for synthesizing HA in the past few decades. Several methods are reported in the literature including solid state reactions, plasma techniques, hydrothermal conditions, and wet chemical methods including aqueous precipitation, hydrolysis and sol-gel processing for HA synthesis. (Koutsopoulos, 2002, Chen et al., 2004, Wang et al., 2006, Nayak, 2010, Sadat-Shojai et al., 2013, Bigi et al., 2004).

By far the most common and simplest method to synthesize large quantities of HA is the aqueous precipitation method. This method involves a wet chemical reaction between a calcium and phosphate precursor under controlled pH and temperature. Typical precursors include calcium hydroxide ($Ca(OH)_2$) with orthophosphoric acid (H_3PO4), calcium nitrate ($Ca(NO_3)_2$) or Calcium acetate ($Ca(CH_3COO)_2$ with diammonium hydrogen phosphate (($NH_4)_2HPO_4$). The last reaction occurs as follows:

$$5Ca\,(CH_3COO)_2.H_2O + 3(NH_4)_2H_2PO_4) \longrightarrow Ca_5\,(PO_4)_3(OH) + 3NH_4\,(CH_3O_2) + 7CH_3CO_2H$$

To successfully synthesize stoichiometric HA, the relative amounts of reactants must be carefully measured to give a Ca/P ratio of 1.67. Synthesis conditions such as starting material, pH, reaction rate, synthesis temperature, aging time and sintering conditions can affect the Ca/P ratio and morphology of the crystals. Once a HA suspension is produced, it is filtered and the resulting slurry is processed. The most common way of approaching this is to dry and crush the powder. This powder is then subject to heat treatment to obtain the final HA powder. It has been shown that the final sintered product is dependent on the initial powder which in turn depends on the synthesis parameters.

Need for Improving HA

Synthetic HA bonds with bone through a complex process of dissolution precipitation and ion exchange. After decades of research on HA, its preparation and properties (including physiochemical, mechanical and biological behavior) are well documented (Suchanek and Yoshimura, 1998, Koutsopoulos, 2002, Janaćkovića et al., 2007, Nayak, 2010, Sadat-Shojai et al., 2013). Although HA is highly bioactive, it does not find application in many areas due to its poor mechanical strength under load conditions. Dense HA has a compressive strength four times that of cortical bone, yet a significantly lower tensile strength and fracture toughness (White et al., 2007).

Over the last thirty years, many materials have been studied as either a possible reinforcement for HA (Particles, fibres and whiskers) or vice versa (polymers such as collagen, gelatine). While mechanical properties of some of these composites increased, there was complication in the matrix – reinforcement reaction or mismatch in the transfer of stress from the reinforcement to the matrix. This section discusses a few HA composite studies in detail.

To enhance the mechanical properties, HA is reinforced with bioinert particulates such as ZrO_2, Al_2O_3, stainless steel, Ti and Mg. Zirconia, as a biologically inert material is expected to improve the mechanical strength of HA without causing any toxic effect. Leong et al., (2013) has shown that HA-ZrO_2 composites exhibit significantly higher mechanical properties compared to pure HA. However, the main issue that has pervaded is the reaction between the two phases. Zirconia affects the decomposition of HA which results in changes in the physical and chemical properties of HA which in turn affects the performance of the implant *in vivo*. Another issue is the formation of secondary phases which reduces the

mechanical properties of the implant. To overcome the problem, Salehi and Fathi, (2010) developed a sol-gel method to produce HA –Zr composite with yttria stabilized Zirconia. They have reported that the decomposition of HA was accelerated at temperatures above 950°C. They have not reported mechanical or biological activity of the composite.

Another area of highly documented HA composites uses Al_2O_3 and Ti as reinforcement to improve the mechanical strength. The use of the two metals limit the performance of the composite due to the interfacial reactions that produces secondary products that deteriorate the property of the composite. These secondary products influence densification, mechanical properties and even degrade the biological properties of the composite. A study led by Yang et al have showed that the interfacial reaction between HA and Ti results in the formation of Ca-P phases like α-TCP and a reaction product $Ca_2Ti_2O_5$ (Yang et al., 2004). Another disadvantage of using Al_2O_3 is the lack of appropriate cellular response from the natural tissue (Ghazanfari and Zamanian, 2013). Finally, other composites have included synthetic polymers such as high-density polyethylene (HDPE), poly ethylene glycol (PEG), PVA and biological glasses. In the case of polyethylene –HA composite, the toughness and elastic modulus is higher than pure HA composites but the tensile strength is far inferior to bone. On the contrary, biological glass can improve the toughness and tensile strength of the composite but large quantities of fillers are required.

In recent years, PVA has gained popularity as a scaffold material as it improves the mechanical stability and flexibility of the scaffolds. PVA is used in the development of scaffolds due to its inherent non-toxicity, non-carcinogenicity, good biocompatilbity and desirable physical properties such as rubbery or elastic in nature and solubility in water at low temperatures (Mollazadeh et al., 2007, Asran et al., 2010). Most of the articles focus on

the use of PVA with collagen or gelatine reinforced nano-HA to improve the mechanical strength of the scaffold. Wang et al (2008) studied the *in vivo* compatibility of HA-PVA-Gelatine composites. They reported that the composite had excellent water swelling behaviour and water absorption in SBF. This allowed the formation of apatite crystals on the composite walls and pores walls while allowing the formation of fibrous tissue around the implant (Wang et al., 2008). In one study led by Zeng et al (2011), HA–PVA composite was developed using solvent casting method. They have demonstrated that the composite was biocompatible with osteogenic cells and the addition of HA in the PVA matrix has reduced the hydrophilicity of PVA. Mechanical results have shown that the interfacial bonding is good between the two materials as there is a reduction in the tensile strength and elongation rate but an increase in the Young's modulus of the composite (Zeng et al., 2011). Since CNTs are known to have high tensile strength, adding CNTs will improve the overall mechanical property of the composite.

1.4.2 HA Composites

The first known publication on HA-CNT composites was in 2004 by Zhao et al. The authors functionalised MWCNTs using nitric acid and sodium dodecyl sulphate (SDS) and the composites were made by nucleating HA in the presence of the CNTs. The authors have reported an increment in the compressive strength of the material from 63MPa to 87MPa for SDS –functionalized MWCNTs and 102 MPa for nitric acid functionalised MWCNTs. (Zhao and Gao, 2004).

There are only a few reports on the development of HA matrix reinforced with MWCNTs. These studies developed HA matrix reinforced with MWCNTs through various process such as sol-gel, spark plasma, ball mill and found that reinforcing HA with CNTs have

improved the mechanical strength of the composite. So far, according to the author's knowledge, Kealley et al. (2006, 2008) is the only author to report a decrease in mechanical properties with the addition of CNTs in the literature. They have prepared composites by adding 2 wt% MWCNTs containing graphite impurities during the precipitation of HA. While the toughness of pure HA and HA-MWCNTs composites remain the same, the hardness of the HA-CNTs decreased compared to pure HA. Kealley et al., (2008) have shown images with clumps of CNTs while in the 2006 paper the author reported homogenous distribution of CNTs. The authors have suggested that the decrease in the mechanical properties could be due to the presence of graphite clumps and removal of the impurities could improve the hardness of the material (Kealley et al., 2006, Kealley et al., 2008). Most studies have functionalised CNTs by oxidation/addition of –OH groups using strong acids (Venkatesan et al., 2011, Maho et al., 2012) or used surfactants that stick to the surface (Hooshmand et al., 2014) to obtain a homogenous dispersion of the CNTs in the matrix but have not reported the effect of this on the growth of the HA crystals.

Most of the HA-CNTs composites are synthesized following the wet precipitation technique as it is the most cost effective and efficient way to introduce CNTs while precipitating HA. A comprehensive literature survey of HA-CNTs bulk composites was undertaken from 2009 to 2017 and is reported in Table 1.3. HA - CNTs used as coatings to improve the performance of metals such as titanium are excluded from the survey.

Table 1.3 HA- CNTs bulk composites for bone implants

Composite characteristics	Aim	Biocompatibility Treatment	Key results		Author
HA-CNTs			Mechanical	Biological	
Sol-gel derived Carboxyl functionalised SWNTs with ε-caprolactam (nylon) and HA composite. Samples with varying quantities of SWNTs were produced.	To enhance mechanical properties of HA.	None reported.	Highest fracture toughness of 3.6 MPa was reported with 1% SWNTs.	Not reported.	(Khanal et al., 2016)
Wet co-precipitation method was used to produce the HA-CNTs composite. Concentration of 5 and 10% CNTs was used for the study.	To determine the effect of CNTs on the structural and biological properties of human G-292 osteoblast cell line.	In vitro cell test was performed for up to 48 hours. MTT, Glutathione, Malondialdehyde and protein assay were performed.	Not reported.	Results show that toxicity occurrence was time and dose dependent. Low dose of CNTs did not reduce cell viability and induce oxidative stress after 2 days.	(Constanda et al., 2016)

Composite characteristics	Aim	Biocompatibility Treatment	Key results		Author
HA-CNTs			**Mechanical**	**Biological**	
Functionalised and raw MWNTs were used to produce the composites. HA powder was ball milled with both types of MWNTs using acetone medium. Composites were made containing 1 and 2 wt.% of MWNTs.	To study the effect of HA-CNT composite on bone regeneration using animal model.	In vivo studies were carried out in adult new Zealand rabbits by creating bony defects at the distal femur. Each treatment type had 4 animals. Observation was carried out for 4 months post operation.	Push out strength test was performed after removing the implants from the animals. After four months, composite with 1wt. % raw MWCNTs showed better strength at 22.45MPa followed by composite with 2 wt. % of functionalised MWNTs which had strength of 24.56 MPa. Pure HA exhibited a strength of 18.48 MPa.	No serious inflammation was observed in any of the implant sites. There was no evidence of adverse local effect like hematoma or edema. All the composites showed considerable *in vivo* new bone formation during the four months. Toxicology studies of the liver and kidneys showed no adverse reaction or accumulation of any implant material. One of the functionalised CNT composite and raw CNT composite proved to be better than the others as well as the control.	(Mukherjee et al., 2016)

Composite characteristics	Aim	Biocompatibility Treatment	Key results		Author
HA-CNTs			**Mechanical**	**Biological**	
HA-CNTs composite was produced through suspension and hot press method with varying quantities of CNTs (0.5, 1, 3 and 5 wt. %).	To determine the mechanical strength of the composite using bending strength as a representative.	Not reported.	Bending strength results showed 70% increase in strength when 3% CNTs are added.	Not reported.	(Salahil, 2016)
3D-printed polycaprolactone, HA and MWNTs composites with varying quantities (1-10%) of MWCNTs was produced. Polymer solution and silicone-doped HA-CNTs suspension was mixed to produce slurry which was used for layer by layer process to build the 3-D structure.	As scaffolds to stimulate bone cell growth.	MG63 osteoblast like cells were seeded on the scaffolds for 6 days.	Compressive yield stress results showed 6 MPa for scaffolds with 0-0.75% CNTs and 1MPa for 10% CNTs.	SEM results showed significant cell adhesion on scaffold with 10% CNTs.	(Gonçalves et al., 2015)

Composite characteristics	Aim	Biocompatibility Treatment	Key results		Author
HA-CNTs			**Mechanical**	**Biological**	
MWCNTs-HA powder was produced by in situ sol-gel process. No description on the quantity of CNTs provided.	To assess the biocompatibility of HA-MWNTs composite with human osteoblast cells.	Human osteoblast sarcoma cell line was used to test the powders. MTT assay was performed to determine cell viability.	Not reported.	The powders were not toxic to the cell line. No detrimental effect on the cell survival or mitochondrial activity was observed.	(Khalid et al., 2015)
Sol-gel production of HA-MWCNTs with varying amounts of MWCNTS (1 and 6%) using SDS and ACUMMER 3100 as dispersant.	Study the biocompatibility of the composites.	*In vitro* studies with human bone marrow stromal cells (hBMSC) for 8 days.	Not reported.	SEM results support biocompatibility of the materials. Cell have adhered and proliferated on the materials with MWCNTs.	(Hooshmand et al., 2014)

Composite characteristics	Aim	Biocompatibility Treatment	Key results		Author
HA-CNTs			**Mechanical**	**Biological**	
HA-CNTs-Ag NPs composite was produced by spark plasma sintering at 950°C with a dwell time of 5 min under uniaxial pressure of 30 MPa in vacuum. Various ratios of HA and Ag ranging between 100 – 86 wt% HA, and 10-1wt% of Ag was used.	To study the antimicrobial, biocompatibility and mechanical properties.	In vitro studies was performed with L292 fibroblast cells for 3 days.	The hardness of the composite with CNTs showed 104% increase compared to pure HA as the hardness value for pure HA was 1.18 GPa and the composites with CNTs was 2.41GPa. The presence of silver had a huge impact on the mechanical properties.	MTT assay results show that the presence of CNTs enhance the adhesion of cells and the presence of silver nanoparticles at low concentrations (1-2 wt%) did not reduce the cell viability.	(Herkendell et al., 2014)
HA-CNTs composite was prepared with varying quantities (0.5%, 1%, 2% and 5%) using ball mill. Pellets were made using uniaxial press following which the samples were sintered at 700°C and 1250°C for 1 h.	Improve the overall properties of synthetic HA.	Hemocompatibility was verified using goat blood. 0.2 ml of goat blood was added to the samples in saline and this was incubated at 37° C for 60 min. The composites were also tested with SBF for a period of 24 weeks.	The composites with 1% CNTs have the highest value of ~ 1.9MPa m$^{1/2}$ for hardness and fracture toughness whereas for flexural strength the composite with 5% CNTS had the highest value of ~35MPa which was 175% increase compared to pure HA.	Hemocompatibility results reveled that hemolysis varied between 0.3 and 5.3 %. Increased apatite formation was reported for samples with 1% CNTs after24 weeks but samples with 2% and 5% CNTs showed increased apatie formation up to 12 weeks after which dissolution occurred.	(Mukherjee et al., 2014)

Composite characteristics	Aim	Biocompatibility Treatment	Key results		Author
HA-CNTs			**Mechanical**	**Biological**	
Polypropylene reinforced with CNF and HA fillers were produced by melt extrusion process. The final composite was injection – molded into rectangular plaques.	To test the mechanical strength and biocompatibility of the composite to be used as bone scaffold.	Human osteoblast sarcoma cells were seeded on the scaffold (n=5) for 10 days. MTT assay was performed to determine cell viability.	Sample with the highest % of CNF showed higher young's modulus and tensile strength which is 2.5 and 33.0 MPa respectively compared to 1.30, 30.0MPa and 2.18 kJm^{-2} for polypropylen.	Compared to Polypropylene (control) there is 78% increase in cell viability in the composite sample.	(Liao et al., 2014)
MWCNTs integrated with HA – polymethyl methacrylate (PMMA) to form composite. 1% functionalised MWCNTs was mixed with homogenous mixture of PMMA and HA prepared by ball milling. This was dried by the freeze –granulation technique to obtain the final composite.	In vivo studies of HA- CNTs composite with varying quantities of MWCNTs.	MG63 cell line was used for in vitro studies which were performed for 14 days. MTT assay and alkaline phosphatase assay was performed to measure cell viability. Adult sheep was used for in vivo implantation.	Hardness and elastic modulus values have been measured. Composites containing functionalised CNTs exhibit high values of 3.5GPa and 69GPa for hardness and elastic modulus respectively.	Cell culture studies showed slower growth rate and lower viable cell density which was decreased by 4% for the treatment composites (n=3) compared to the control (no composites). However, it is reported that the composites are not toxic as high cell viability was achieved for longer periods. No negative reaction was observed after 12 weeks of implantation. No fibrous tissue or inflammation was observed in contact between the cement and bone. In areas of no direct contact, osteoclast like cells were observed.	(Singh et al., 2010)

Composite characteristics	Aim	Biocompatibility Treatment	Key results		Author
HA-CNTs			Mechanical	Biological	
HA-gelatine slurry was prepared in the presence of MWCNTs. Composites with 1-5% MWCNTs were prepared. The slurry was washed and centrifuged to obtain the final product.	To improve the strength of HA – gelatine composite by reinforcing MWCNTs.	*In vivo* biocompatibility was analysed using mice. Different quantities of composites (0, 1,2and 4%) was administered. The experiment was conducted for 30 days.	Flexural strength of the composite increased with the increase in CNTs but no improvement was observed when the concentration went above 4%. With 1% MWCNTs the flexural strength is 9 MPa whereas the elasticity is 2.1 GPa. With 4% MWCNTs the flexural strength is 14MPa but the elastic modulus is approximately 2GPa.	*In vivo* analysis did not show any toxic effect except for the group with 4% MWCNTs after 30 days. The liver and kidneys showed slight alteration.	(Yadav et al., 2010)
HA-Al_2O_3-CNTs composite was prepared by spark plasma sintering technique. Composite composition was (spray dried HA 80 wt. %, Al_2O_3 18.4 wt. % and CNTs 1.6 wt. %) and sintering temperature was 1100°C.	To improve fracture toughness by the addition of Al2O3 and CNTs in HA matrix and to study the cytocompatiblity of the material.	*In vitro* test was performed with Mouse fibroblast (L929) cells. The experiment lasted for 5 days. MTT assay was performed at the end of 3rd and 5th day to analyse the viability of the cells.	Vickers micro indentation showed that there was an increase from 4.0GPa for pure HA to 4.4GPa for the composites. There is a 2.3 times increase in fracture toughness where it is 1.18MPa m$^{1/2}$ for HA and 2.72 MPa m$^{1/2}$ for the composite.	After the 3 and 5 day test there was no significant difference in cell growth between pure HA and the composite. SEM observation has shown attached cells spreading columnar appendages from centre developing filopodia and connecting with neighbouring cells.	(Kalmodia et al., 2010)

Composite characteristics	Aim	Biocompatibility Treatment	Key results		Author
HA-CNTs			**Mechanical**	**Biological**	
HA-MWCNTs composite was prepared by mixing CNTs (2% vol.) with spray dried HA (98% vol.) in ethanol. Spark plasma sintering process was employed to produce the composites.	To study the optimum sintering condition required to employ CNTs in the production of composites and to improve the mechanical strength and assess the biocompatibility of the composite.	An *in vitro* study was carried out with hFOB 1.19 osteoblast like cells for 2 and 4 days. Cells were counted in a haemocytometer.	The authors have reported Youngs modulus value of 131.1GPa and hardness value of 6.86 GPa at a sintering temperature of 1100°C which is a 285% increase compared to the hardness value at sintering temperature at 900°C.	*In vitro* study has shown improved cell adhesion on composites with CNTs than with pure HA. Composites with CNTs have a two fold increase in cells after 4 days compared to pure HA.	(Xu et al., 2009)

Overall, the work on HA-CNT composites has been on fundamental research to develop a safe durable implant and hence different methods are used. Table 1.3 details the different types of HA–CNTs composites that have been synthesised to improve the mechanical and biocompatibility properties. However, the author has not come across a composite that combines the advantages of HA, MWCNTs and PVA to improve the mechanical and biological property of the composites. Moreover, all the studies (Table 1.3) which have performed biochemical assays to confirm the microscopy images have done so only with the cell homogenate and have mostly discarded the conditioned media, which can provide vital clues on the health of the cells while they were still actively proliferating on the composites (Table 1.3).

Similar to the HA- CNTs composites, a number of HA –Ag NPs studies have also been undertaken which are detailed in Table 1.4. Most of the work undertaken is to determine the optimal concentration of Ag NPs required for efficient antibacterial property. However, all the *in vitro* studies have used the standardised disk diffusion susceptibility method which might not be relevant in the clinical setting as the implants will be covered in blood plasma. The presence of aqueous media will change the silver dissolution rate compared to static method used by the studies mentioned in the Table 1.4. In addition, some of the studies have not reported the biocompatibility of the composites with cells. Hence, there is an inconsistency in reporting the biocompatibility of the Ag NPs with the cells.

Table 1.4 HA-AgNPs composites and a review of their role in the development of bone implant composites

HA-AgNPs composites	Aim	Experimental design	Key results		Reference
			Biocompatiblity with cells	Antibacterial activity	
Ag NPs solution was produced from 16 ml of 10^{-2} M AgNO$_3$ and 14ml of 0.5M of glucose monohydroate as reducing agent. The mixture was heated in microwave for 2 min and stirred for 20 min. HA was synthesized using the wet precipitation method and 50 ml of Ag NPs solution was introduced in the HA solution.	Synthesise HA-Ag NPs composites as implant material with antibacterial properties.	Antibacterial activity was tested against *Staphylococcus aureus* using the standardised disk diffusion susceptibility method. Disks containing 0.2gm HA-Ag NPs powder was made and 1x 10^{-6} CFU were used. Pure HA and pure Ag NPs were used as control. Test was performed for 24 h at 37°C.	None reported.	Inhibition of bacterial growth in the Ag NPs was observed whereas the same effect was not observed in the plates containing pure HA and HA-Ag NPs disks due to the low concentration of Ag NPs in the composites. There is no mention of the dissolution of Ag NPs from the composites.	(Charlena et al., 2017)

HA-AgNPs composites	Aim	Experimental design	Key results		Reference
			Biocompatiblity with cells	**Antibacterial activity**	
HA powder was obtained by chemical precipitation and Ag NPs were synthesized in colloidal suspension in the presence of chitosan. The HA powder was immersed in as-prepared Ag NPs colloids to produce HA-Ag NPs with theoretical silver proportion ranging from 0.016 to 0.40 wt%.	To develop a simple adsorption synthesis route for HA-Ag NPs.	Antibacterial activity was tested against *Staphylococcus aureus* and *E.coli* based on the standardised disk diffusion susceptibility method. 1-2 x10^8 CFU was used. Test was performed for 24 h at 37°C.	None reported.	The HA-Ag NPs composites, even with low silver proportions (0.024 wt%) were capable of producing inhibition zones for both *S. aureus* and *E. coli*.	(Andrade et al., 2016)
Ag NPs were formed by the interaction between tannic acid and AgNO$_3$ which was first attached to collagen molecule. The collagen incorporated tAg NPs were made to self-assemble in modified simulated body fluid and HA was allowed to mineralize on the tAg NPs incorporated collagen.	To develop a process to incorporate Ag NPs onto collagen without a crosslinking agent and to mineralize HA.	Antibacterial activity was tested against *Staphylococcus aureus* and *E.coli* based on the standardised disk diffusion susceptibility method and quantitative method. Test was performed for 24 h at 37°C. Biocompatiblity was evaluated with MG63 cells at 1,3 and 7days and was measured using Alamar blue and microscope observation.	Alamar blue assay results showed greater than 80% cell viability for all the composites.	The growth inhibition of up to 31% and 40% were observed against *S. aureus* and *E. coli* respectively.	(Socrates et al., 2015)

HA-AgNPs composites	Aim	Experimental design	Key results		Reference
			Biocompatiblity with cells	**Antibacterial activity**	
HA powder was obtained by wet precipitation method and 1-30 wt% Ag NPs were added to the HA and mixed using mortar and pestle. The resultant powder was calcined at a temperature range of 800-1200 °C	To study the effect of Ag addition on phase stability of HA–Ag composite with respect to calcination temperatures.	Antibacterial activity was tested against *Staphylococcus aureus* based on the standardised disk diffusion susceptibility method. Test was performed for 24 h at 37°C for composites containing 1, 3 and 5 wt% Ag NPs. Biocompatibility was tested with mouse fibroblast cells for composites containing 10 wt% Ag NPs. MTT assay was performed after 48 h.	The MTT assay showed that the composites containing 10 wt % Ag NPs were biocompatible and cell viability was more than 80%.	3wt% concentration of Ag NPs was sufficient to kill the surrounding bacteria.	(Rajendran et al., 2014)

Furthermore, only Herkendell et al (2014) have so far produced HA-CNTs-Ag NPs composite and tested the mechanical, antimicrobial and biocompatible properties. They have not performed in-depth biocompatible analysis as they have tested the composites against L929 fibroblast cells only for 3 days and performed MTT assay (Herkendell et al., 2014). Another study led by Afzal et al (2013) has developed two different types of composites containing HA- 5 wt% Ag NPs and CNTs-5wt% Ag NPs using the spark plasma technique at two temperatures (1700 and 950 °C) under a pressure of 30 MPa with a dwell time of 5 minutes. They have reported that the hardness of the HA- Ag NPs composite has increased compared to pure HA where as in the case of CNTs , pure CNTs showed better hardness. They have reported similar results for the elastic modulus. Their antibacterial results coincide with Herkendell et al's (2014) antibacterial results. Both studies have shown that CNTs promote *E.coli* growth but the presence of Ag NPs reduce the same. They have shown that Ag NPs has a better effect against gram-positive bacteria. However, Afzal et al., (2013) has not tested the biocompatibility of composites and have proclaimed that they can be used for bone substitutes (Afzal et al., 2013).

1.5 Hypothesis and Project design

The main hypothesis being tested in this study is that composite made of HA matrix reinforced with Ag NPs decorated CNTs will serve as bone/ maxillofacial implant, which is biocompatible with antibacterial properties and superior mechanical properties. The HA matrix will be biocompatible with the bone cells and will not elicit any adverse reaction as they will be similar to the inorganic component of natural bone whereas it is expected that the carbon nanotubes will reinforce the composite making it mechanically strong. The carbon nanotubes will form bridges in the cracks and transfer the load

between the tubes and the HA matrix while the silver nanoparticles will provide the antibacterial property to the composites without causing toxicity to the human bone cells. The Ag NPs can achieve the antibacterial property either through the release of consistent small amounts of silver ions or by direct contact with the microbes and inhibit their growth in suspension and prevent the adhesion of bacteria to the surface of the composite. The biocompatibility of the composites was tested with human osteoblast cells and the antibacterial activity was tested against *Staphylococcus aureus* as it plays a crucial role in causing infection following surgery. The mechanical properties of the composite were determined by the testing the tensile and compressive strength of the composites.

The specific objectives were to:

1. Investigate the biocompatibility of HA and compare it with different types calcium phosphate such as dicalcium phosphate and β-tricalcium phosphate;

2. Synthesise Ag NPs-MWCNTs-HA composites (with pristine and functionalised MWCNTs and surfactants) and characterize them using various techniques;

3. Demonstrate the mechanical properties of the composites by performing the diametral tensile strength test and compressive strength test;

4. Determine the biocompatibility of the MWCNTS- HA composites without the presence of Ag NPs *in vitro* by testing the viability and cytotoxic response to the cells to the composites;

5. Demonstrate the antibacterial activity of the Ag NPs- MWCNTs-HA composites against *Streptococcus aureus* and select the composites with good antibacterial property for further study;

6. Investigate the biocompatibility of the Ag NPs- MWCNTs-HA composites with the human osteoblast cells by allowing the cells to differentiate and mineralize in the

presence of the composites and study the viability of the cells by analysing gene expression and cytotoxic response to the composites.

2. Pilot study- Comparison of the biocompatibility of three main types of calcium phosphate used in bone implants

2.1 Introduction

A variety of artificial materials (metals, ceramics, polymers and composites) have been tried over the decades to fill bone defects. Ceramics made from calcium phosphates, calcium sulphates and Bio glass® are of high interest, as they do not tend to induce adverse reaction in patients when used as bone implants. The aim of this study was to compare the biocompatibility of the three phases of calcium phosphate namely hydroxyapatite (HA), dicalcium phosphate (DCP) and β- tricalcium phosphate (β-TCP). The biocompatibility was measured both quantitatively and qualitatively. Based on the results, the most promising composite was chosen to be further enhanced to make it stronger and antibacterial without compromising biocompatibility. All the composites were prepared using the sol-gel technique and characterised to determine the phase purity, shape and size of the crystals. The degree of biocompatibility was measured qualitatively and a simple quantitative method was designed to determine significant biocompatibility differences between the different types of composites.

2.2 Materials and Methods

To compare the biocompatibility of the various phases of calcium phosphate HA, DCP and β-TCP powders were produced in house using the sol-gel technique as explained below. The powders were then mixed with PVA to produce the final composites.

2.2.1 Preparation of the powders

To produce the different mineral powders of calcium phosphate, calcium acetate and ammonium phosphate were mixed in the following molar ratios for:

1. Hydroxyapatite (HA) – 0.1 M calcium acetate and 0.06 M ammonium phosphate

2. Dicalcium phosphate (DCP) - 0.1 calcium acetate and 0.1 M ammonium phosphate

3. β-Tri calcium phosphate (β-TCP) – 0.3 M calcium acetate and 0.2 M ammonium phosphate

These molar concentration were fixed to obtain the appropriate Ca:P ratio which is 1.67 for HA, 1.0 for DCP and 1.50 for β-TCP. Figure 2.1 represents the sol-gel technique used to synthesis the powders for the composites. In a typical experiment, to make 10g of the powders, 200 ml of the appropriate concentration of calcium acetate and 200 ml of ammonium phosphate was added simultaneously into the glass beaker (Figure 2.1). The resulting solutions were stirred at a constant rate of 400 rpm using a magnetic stirrer (dial setting 9, Hotplate/stirrer, RCT basic, IKA Oxford, UK). While stirring, the pH of the solutions was checked periodically and the appropriate pH (HA – 9.5-10, DCP- 7, β-TCP- 9.5-10) was maintained by the addition of 6M sodium hydroxide solution (Figure 2.1). The solution was stirred for 1h at 40 °C and left to mature for 24 h at 40 °C. The resulting dispersions containing the HA, DCP and β-TCP precipitates were then filtered through Whatman® filter paper (WHA1001070, Sigma Aldrich, Irvine, UK) with pore size of 11 μm. The precipitates were washed with ultrapure water and subsequently dried under a vacuum at 60 °C for 24 h respectively (Figure 2.1). The dry precipitate was manually crushed with a glass mortar and pestle to make a fine powder and sintered. Sintering is the process of using high temperature thermal treatment during which phenomena such as consolidation and densification of the dried powders occur leading to the change in the particle shape and size. The dried powders were sintered at various temperatures (HA- 100 °C for 8 h; DCP- 300 °C for 2 h; β-TCP - 1000 °C for 8 h) (Figure2.1)(Wang and Chaki, 1992 , Kivrak and Tas, 1998).
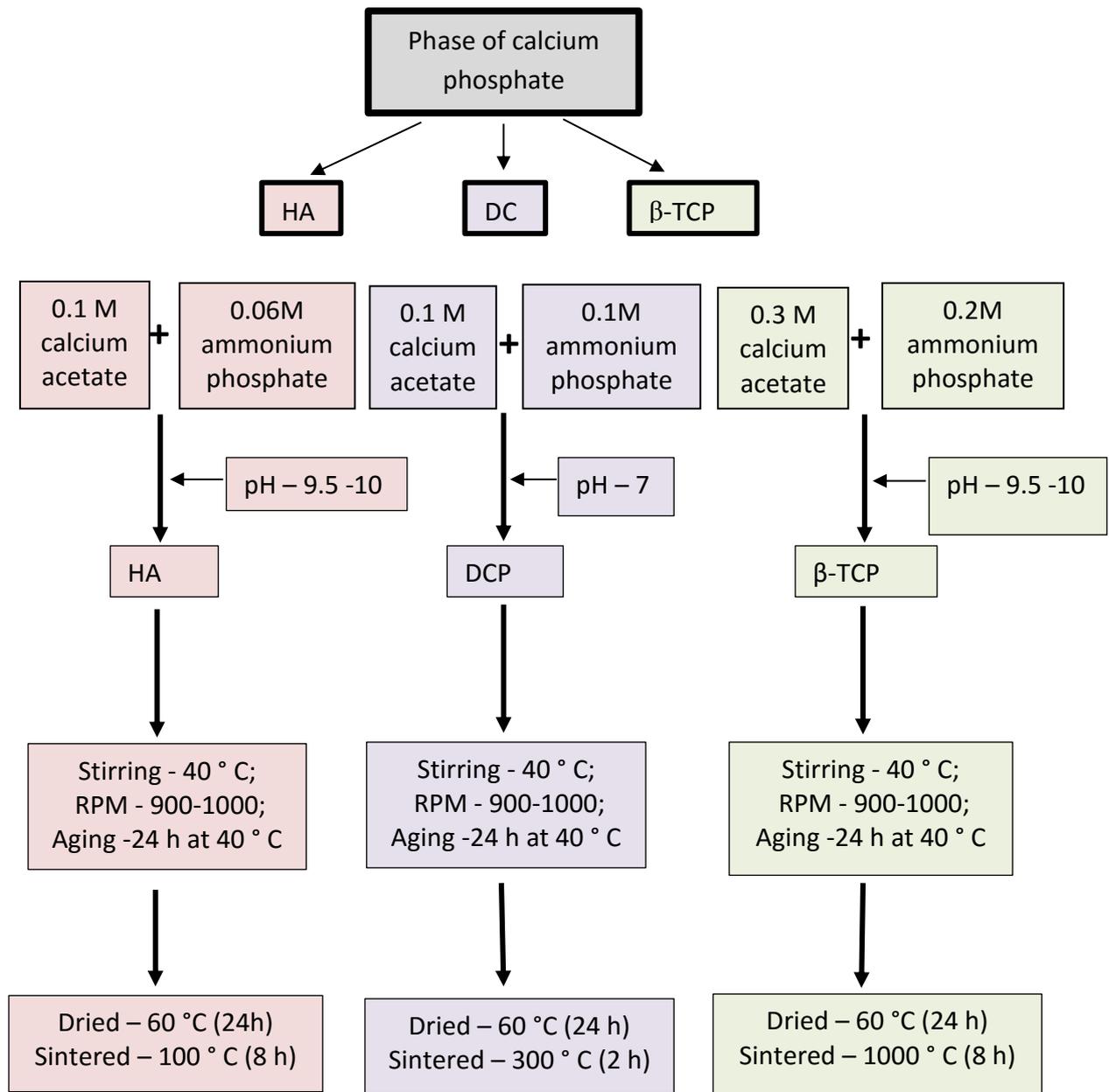
Figure 2.1 Schematic representation of the sol-gel technique used for the synthesis of the different phases of calcium phosphate.

2.2.2 Composite preparation

Before the composite preparation, 20% PVA was prepared and stored at room temperature for later use. Briefly, to make 50 ml of 20 % PVA, 10 g of PVA was added to 50 ml of deionised water which was stirred constantly at 90 ° C until all the PVA was dissolved. To determine the workability of the composite, different ratio combinations

were tried by adding 0.5, 0.8 and 1 mL PVA to 1 g of the powders. The best workable ratio was 1ml and hence 1:1 PVA to calcium phosphate powder ratio was used for all the sample preparation. The composites were hand mixed using a spatula and then inserted and packed into a cylindrical mould with the dimensions of 15x 5 (diameter x height) mm, whose ends were blocked with short cylinders. Pressure was applied on top of the cylinders using a mechanical mini pellet press (Product code: GS03940, Specac, UK) which in turn, compressed the sample inside the mould. The pressure applied on each sample was equivalent to 26 MPa which was held for 1 minute after which, the aluminium cylinders were removed from the moulds. The samples were then placed in an oven at 40 °C for 48 h to dry the composite. Afterwards, the samples were carefully removed from the moulds and stored at room temperature until required for biocompatibility studies.

2.2.3 Composite material characterisation

Physico-chemical characterisation of the produced powders and the final composite was performed to ensure that the intended mineral phases of calcium phosphate were produced. The materials were examined by electron microscopy (Scanning electron microscopy (SEM) and Transmission electron microscopy (TEM)) to study the difference in the morphology of the three phases of calcium phosphate. X-ray diffraction (XRD) is the most common technique to determine crystal structures and atomic spacing and was used to identify the phase purity of the produced powders and Fourier transform infrared spectroscopy (FTIR) analysis was performed to detect the functional groups and characterize covalent bonding information.

2.2.3.1 TEM and SEM analysis of the powders and composites

The powders were examined by TEM and the final composites were analysed by SEM. Briefly, for TEM analysis, approximately 0.05 g of the powders to be analysed (HA,

DCP and β-TCP powders) were dispersed separately in distilled water by sonication for 5 min which was used as the stock solution. All electron microscope observations were made on three sub-samples of each stock. A drop of the relevant dispersion was placed on the copper grid and air dried and subsequently observed at an accelerating voltage of 120 kV using a high resolution TEM (JEOL 1400, JEOL ltd, Japan). The shape of the crystals were observed and the size of the crystals (n=100 crystals) was measured randomly using image J software (Schneider et al., 2012). Care was taken to identify and measure single crystals that were not aggregated. To analyse the final composites by SEM, three separate samples were made from each composite powder and were mounted on conducting carbon stubs and coated with gold in a sputter coater (EMITECH K550, Quorum Technologies, UK). SEM (JEOL JSM -5600LV, JEOL ltd, Japan) images were taken to show the presence of the crystals and PVA in the composites. Images were collected using a 15 kV accelerating voltage.

2.2.3.2 X-Ray Diffraction (XRD) analysis

A crystal consists of a periodic arrangement of the unit cell into a lattice. A unit cell can contain a single atom or atoms in a fixed arrangement. Slight changes in the Ca:P ratio of the reaction mixture and/or sintering temperature during the production of powders can yield other types of calcium phosphates due to the changes in the atomic arrangement of the unit cell. Hence, the phase purity of the sintered powders was determined by XRD. The atomic planes of a crystal causes the reflections of the incident beam of X-rays to interfere with one another as they leave the crystal. This phenomenon is called X-ray diffraction. XRD analysis was performed by colleagues in Nottingham Trent University, UK, using an automated Philips powder diffractometer. Briefly, each specimen was irradiated using copper anode K (alpha) X-ray (CuKα, wavelength 1.5418 Å)

generated by 45 kV and 40mA of current in the cathode-ray source. All data were collected in a 2θ scan mode in the range of 20-40 ° using a step width of 0.03 Å and a 1 sec count time (see (Klug and Alexander, 1954) for discussion of XRD parameters).

2.2.3.3 Fourier transform infrared spectroscopy (FTIR) Analysis

The quality of the materials was also examined by FTIR. Briefly, FTIR involves shining a beam of light that contains many frequencies at the specimen, and then determining which frequencies are absorbed by the specimen. The pattern of the absorbed frequencies is characteristic of the molecular structure of the specimen (review, (Berthomieu and Hienerwadel, 2009). FTIR was used to especially determine the functional groups in the powders and the final composites, which was measured for every new batch that was produced. A Bruker αP FTIR spectrometer (Bruker, UK) was used for the measurements in attenuated total reflection (ATR) mode with an ATR accessory utilizing diamond prism. Spectra were recorded using small amount (approximately 2-5 mg) of each sample (powder and composite), enough to cover the prism. The powders did not require further processing whereas the final composites were ground again in a glass mortar and pestle to obtain a fine powder. Each spectrum was the result of 16 accumulated scans at 4 cm^{-1} resolutions on the same sample.

2.2.3 Experimental design and preparation of the in vitro study

The biocompatibility of the composites was tested with Chinese Hamster ovary (CHO) cells. The cells (supplied by the School of Biomedical Sciences, Plymouth University) were grown in Ham's F-12 medium supplemented with 2mM L-Glutamine (10235122; Thermo Fisher scientific, Loughborough, UK) and 10% foetal bovine serum (11563397; Thermo Fisher scientific, Loughborough, UK), referred to hereafter as "Ham's

F-12". Cells were incubated at 37 °C in a 100% relative humidified atmosphere of air. Stock cultures of CHO cells were grown in 25-cm^2 plastic flasks at 1 - 2 x 10^6 cells/ml of medium with sub culturing carried out every 3 to 4 days until the required amount (3.6x10^3 cells/well) was available.

The experimental design involved exposing the CHO cells to the composites. Before exposing the cells, the composites (d = 15mm x 5mm thickness) were sterilized using 99 % absolute ethanol. The composites were immersed in ethanol for 30 min and placed in sterile petri dishes and dried at 80 °C for 2 h. Using sterile forceps, the composites were carefully placed at the bottom of 24 well plate (flat bottom sterile, tissue culture treated polystyrene microplate; 662160, Greiner bio-one, Stonehouse, UK). The cell culture plate containing all the composites (HA, DCP and β-TCP) was a unit of replication. A total of 6 replicates for two time points (24 h and 7days, n = 3 per time point) were conducted. Each well was seeded with 50 μl of cell culture from the 3rd passage of the stock cell culture and 550 μl of Ham's F-12 was added. The microplates were then incubated for 24 h and 7 days respectively at 37 °C in atmospheric air to allow the cells to grow. For 7-day replicates, the Ham's F-12 media was changed every 48 h to ensure the culture conditions were not limiting. The end points in the experimental design involved measuring the growth of the cells using SEM after 24 h and 7 days and comparing it quantitatively.

2.2.3.1 Cell Morphology

Morphology (shape and appearance) of the cells was regularly observed by light microscope to determine the health of the cells. At the end of the experiment, the presence and health of the cells were determined using SEM. After the media was

removed, the composites with the cells were washed twice with phosphate buffered saline (PBS) and fixed using 2.5% glutaraldehyde in 0.05 M cacodylate buffer at pH 7.4 for 2h. Fixed samples were dehydrated through a graded series of ethanol and then critical point dried. Samples were mounted on conducting carbon stubs and coated with gold in a sputter coater (EMITECH K550, Quorum Technologies, UK). SEM images were collected using a 15 kV accelerating voltage. The observations were conducted systematically, starting at a lower magnification (X30) to examine the distribution of the cells on the composites, and then at a higher magnification (X1000) to observe the morphology of the cell membrane as well as to determine the attachment of cells on the composites.

For the quantitative analysis, four random areas was selected from a grid. Another grid with 100 coordinates was created and 20 coordinates were chosen at random and images taken at the 800x magnification was used to analyse the cell coverage. This was performed on all the four coordinates that were randomly selected previously. The results were then averaged to differentiate the cell growth between the different samples. All the images were process using Image J software (Schneider et al., 2012)

2.2.4 Statistics

All data are presented as mean ± standard error and were analysed using statgraphics software for windows (version XVI.I). After descriptive statistics to determine normality, skewness or kurtosis, parametric data were analysed by one way-ANOVA followed by a post-hoc LSD test and variance check (Levene's test). The non-parametric data were analysed by a Kruskal-Wallis test. All statistical analysis used a 95% confidence limit, so the p values < 0.05 were considered statistically significant.

2.3Results

2.3.1 Characterisation of the composite powders

Figure 2.2 represents the TEM observations of the powders. It is clearly noticed that the crystal structure varied between the three phases of calcium phosphate. HA crystals appear to be short nano-rods (Figure 2.2A) and the average length (n=25) of the crystals was 64.6 ± 26.4 nm. TEM analysis (Figure 2.2B) of DCP shows that they were slightly different to HA crystals; being longer than the HA, average mean length (n=25) of 274.73±75.18nm. They were also wide and flat compared to HA. Figure 2.2C represents β-TCP and the crystals appear to be globular with irregular shape. Their size is in the micrometre scale and the measurements (n=25) were taken between the widest points in the crystal and the average size was 2.5 ± 0.7 μm.

A

200 nm

B

200 nm

C

2 µm
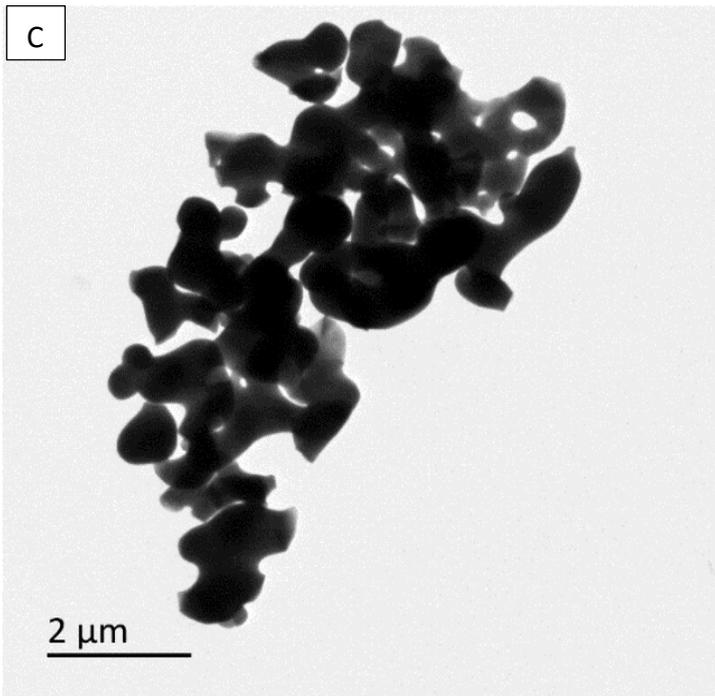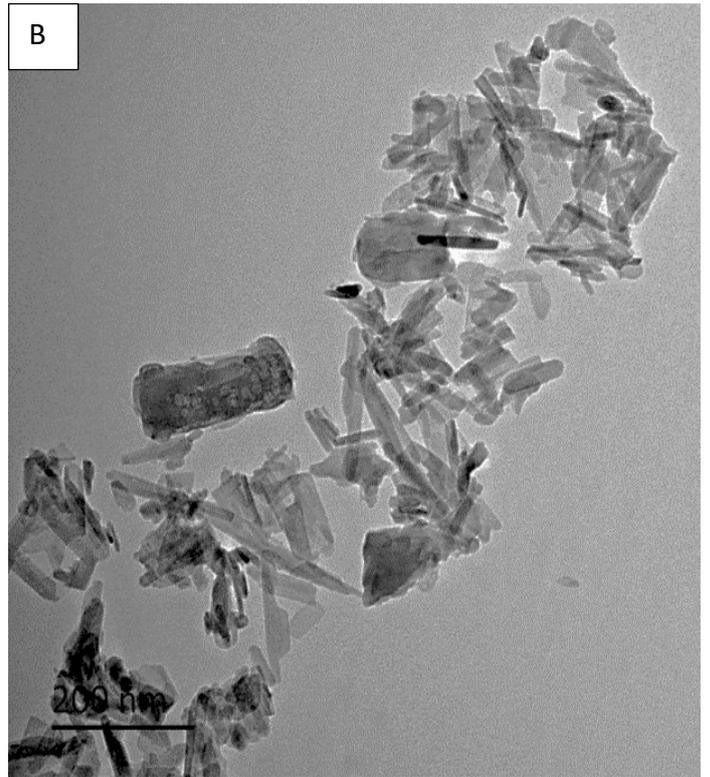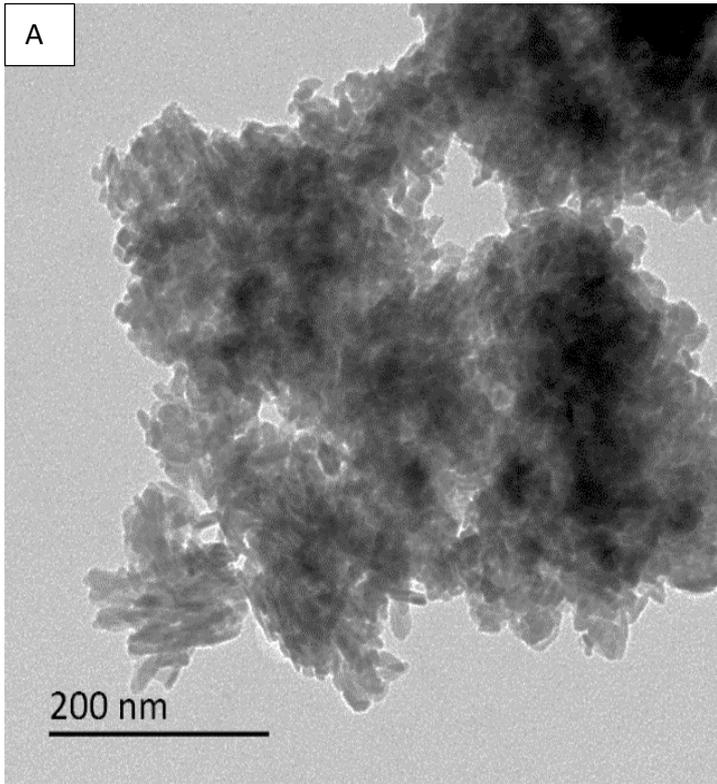
Figure 2.2 TEM images of the three phases of calcium phosphate powders synthesised by the sol-gel technique. (A)HA crystals forming an aggregate (B) DCP crystals are bigger than the HA crystals and did not form aggregates like HA crystals (C) β-TCP crystals are in the µm scale as they are sintered at high temperature.

XRD analysis was performed to determine the crystal structure and phase purity of the HA, DCP and β-TCP powders. XRD patterns of the as synthesized powders are given in Figure 2.3. HA and DCP exhibit broad diffraction peaks whereas in β-TCP powder the peaks are sharp and narrow. The shift in the peaks between the three composites correspond with their respective phases. In HA, a few peaks corresponding to Tricalcium phosphate was observed where as in β-TCP presence of α-TCP was observed.
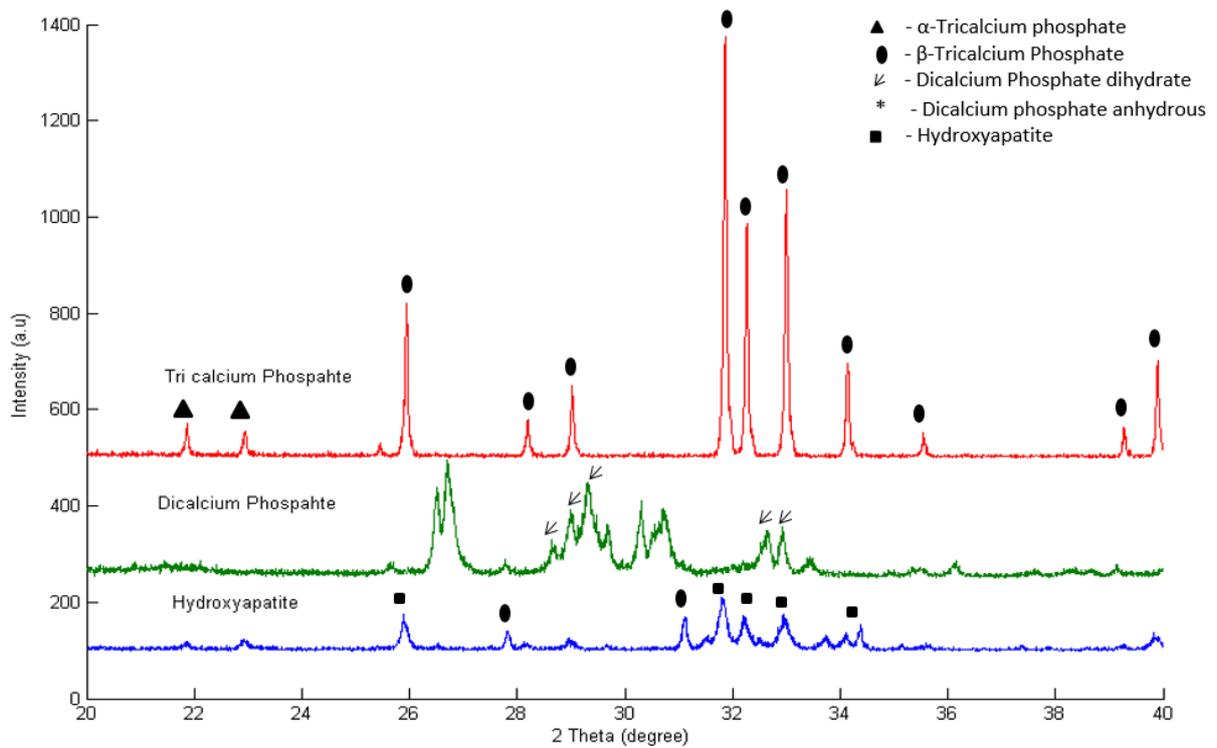
Figure 2.3 XRD analysis of the three phases of calcium phosphate. Different symbols represent the peaks corresponding to the different phases in each spectrum.

FT-IR spectroscopy is an effective tool for structural and functional group investigation at the molecular level. Figure 2.4 (A and B) represents the FTIR absorption peaks of the composite powders. All the major characteristic bands of the respective powders are observed. FTIR spectrum of HA powder shows the presence of most characteristic chemical groups OH- and PO_4^{3-}, CO_3^{2-} as well as HPO_4^{2-} groups that characterize non-stoichiometric HA (Figure 2.4 B). It is of interest to note that the transmittance peak associated with P_2O_7 molecules distinctly appeared at 719 cm^{-1} and 727 cm^{-1} in the spectrum of DCP and β-TCP powders. Presence of DCP is confirmed by the P-O stretching modes between 900- 1200cm^{-1}. PO_4^{3-} groups which are characteristic to β-TCP are observed in β-TCP powders. In HA IR spectrum, OH^- group peaks are observed at 600 and 3361 cm^{-1}, but there are no such peaks in the IR spectrum of β-TCP, which confirms the complete dissolution of HA phase to β-TCP phase in the powder.
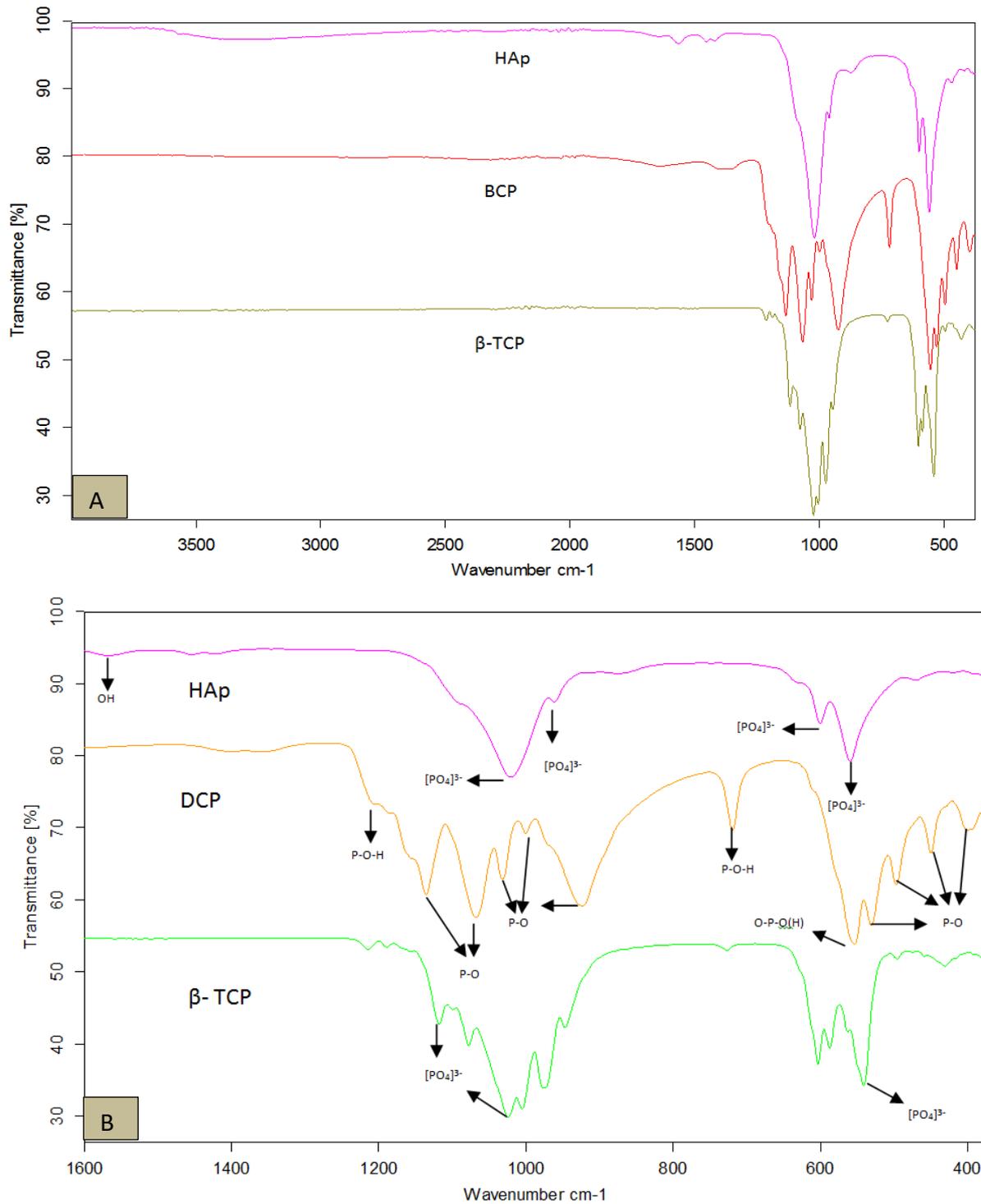
Figure 2.4 FTIR spectra for HA, DCP and β-TCP powders. (A) shows the water absorption band in HA between 3500 to 2700 cm^{-1}. (B) magnified spectra of (A) depicting all the important transmittance peaks from 1600 – 400wavenumber in the three (HA, DCP and β-TCP) powders.

2.3.2 Characterisation of the final composites

SEM observation (Figure 2.5) of the final composites show they were porous structures. The difference in the crystal structure between the three composites is also visible. No PVA clumps were observed in the three composites confirming that the PVA had completely dissolved. Different crystal shapes and sizes were observed in β-TCP composite similar to the TEM images.
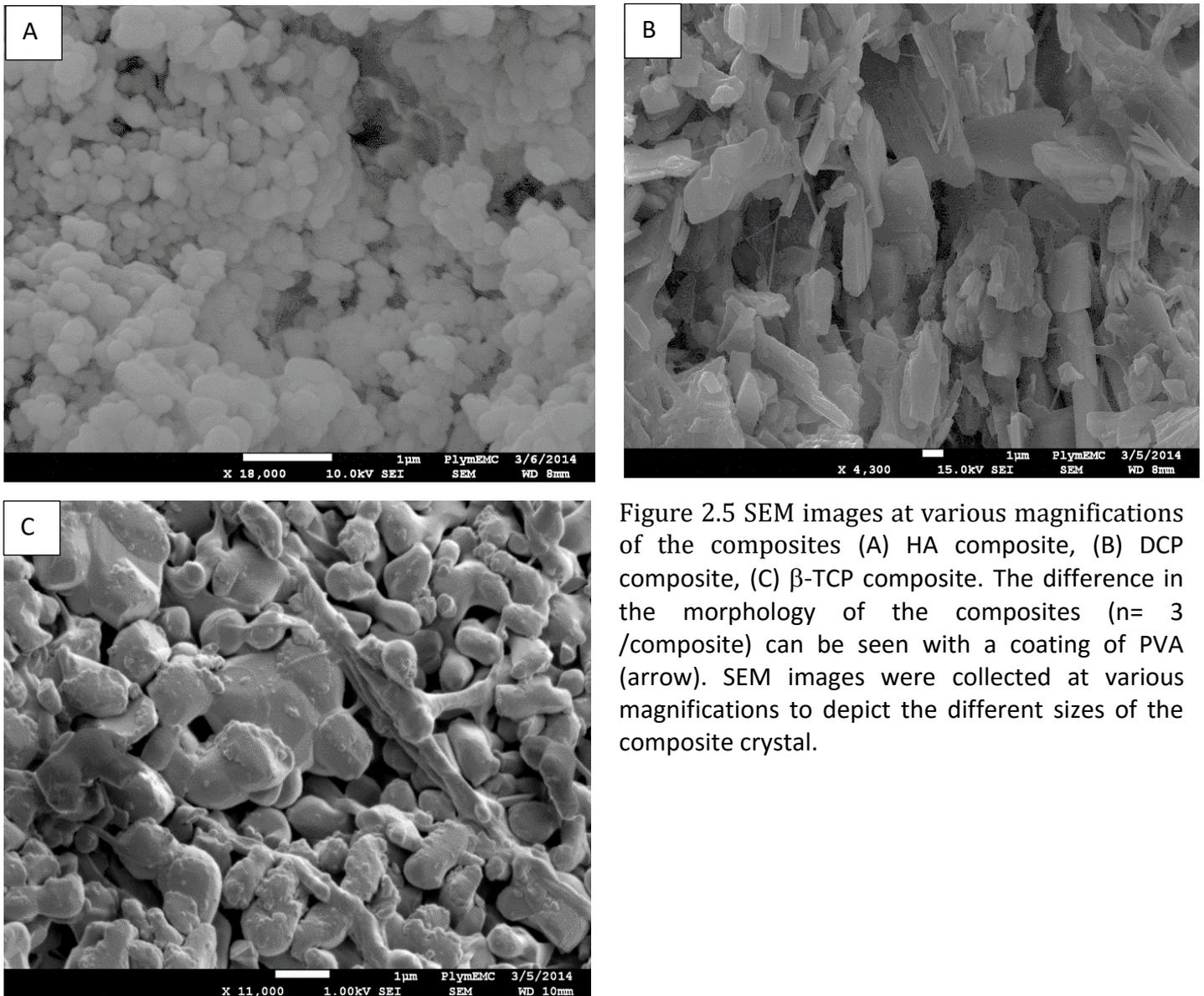
Figure 2.5 SEM images at various magnifications of the composites (A) HA composite, (B) DCP composite, (C) β-TCP composite. The difference in the morphology of the composites (n= 3 /composite) can be seen with a coating of PVA (arrow). SEM images were collected at various magnifications to depict the different sizes of the composite crystal.

FTIR analysis of the final composites (figure 2.6) show that all the peaks present in the powders (Figure 2.4) exist in the composites. Two important peaks were verified at 2907 cm^{-1} which attributes to the stretching of CH_2 and 1141 cm^{-1} that is assigned to the crystallinity of the PVA. The peaks present in PVA can also be observed in all the composites.
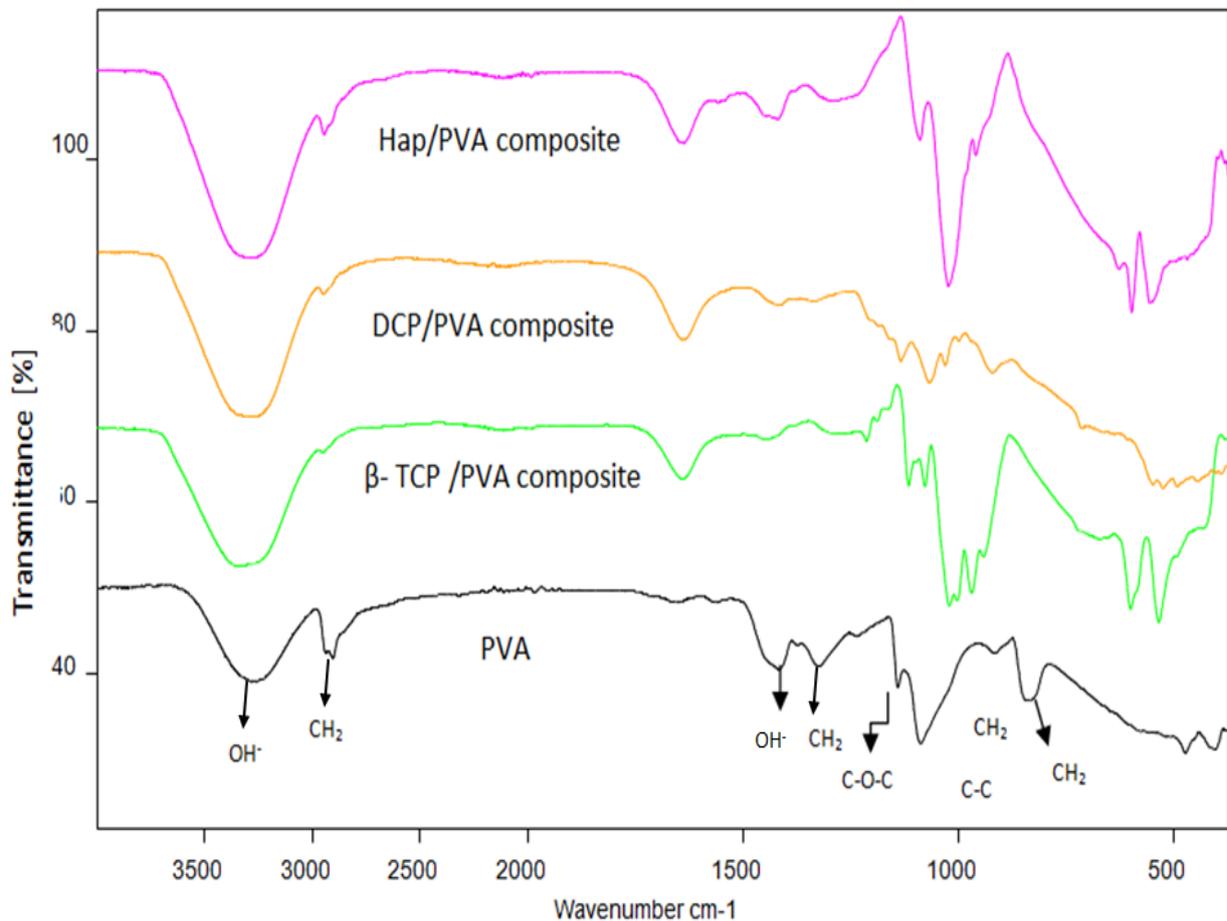
Figure 2.6 FTIR spectrum of the final composites. The spectrums shows the presence of the PVA in composite, as the peak for OH$^-$ at 3200 cm^{-1} is prominent in all the composites.

2.3.3 Growth and Morphology of cultured cells

Quantitative analysis (Figure 2.7) of the samples after 24 h and 7 days revealed that cell growth on all the three types of PVA-composites (HA, DCP and β-TCP) were

significantly different (one way ANOVA, P ≤0.05) to each other. No statistical difference was observed between 24 h and day 7-cell growth within the three different calcium phosphate phases.
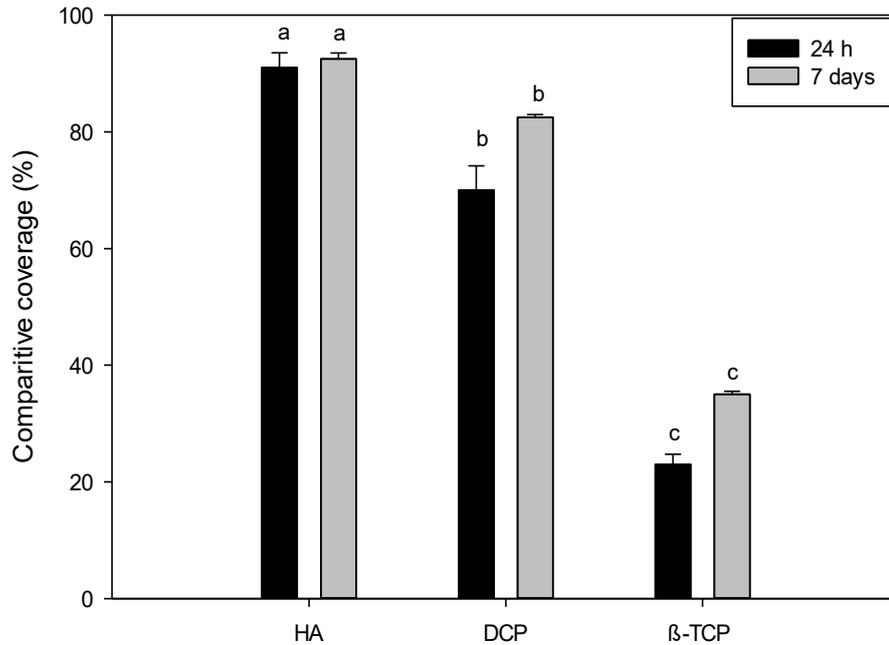
Figure 2.7 Quantitative analysis of the cell growth on the three different types of calcium phosphate-containing PVA composites at the two time points, 24h and day 7.

Initial light microscopy examination of the CHO cells seeded on the 24 well plates after 24h revealed no visible signs of cell death due to toxicity or infection. The Ham's F-12 media appeared normal (no loss of the pH indicator or excessive cell debris). Light microscopy observations showed no signs of deterioration such as necrosis, detachment of cells from the substrate, granularity around the nucleus or obvious disruption of the cell membrane (i.e., no membrane blebs or cell swelling). A closer observation in the SEM (Figure 2.8) after 24 h showed the presence of a monolayer of CHO cells on all of the composites. However, the appearance of the cells was different on each composite. The

cells on the HA-PVA composite samples were healthy in the size range between 12-14 µm with numerous pseudopods and well-defined margins. The cells were flat, had intact homogenous cytoplasm, and were flattened on the substrate surface whereas the cells on DCP-PVA composites appeared to be rounded and did not have healthy pseudopods as seen on HA-PVA composites. The least amount of cells were observed in the β-TCP-PVA composites and they did not appear to have a homogenous cytoplasm. However, at the end of day 7 it can be seen (Figure 2.8 D and E) that the growth of the cells on the DCP-PVP is comparable to those on the HA material, with the presence of a multilayer of cells whereas the cell growth on β-TCP sample is still limited (Figure 2.8 F).
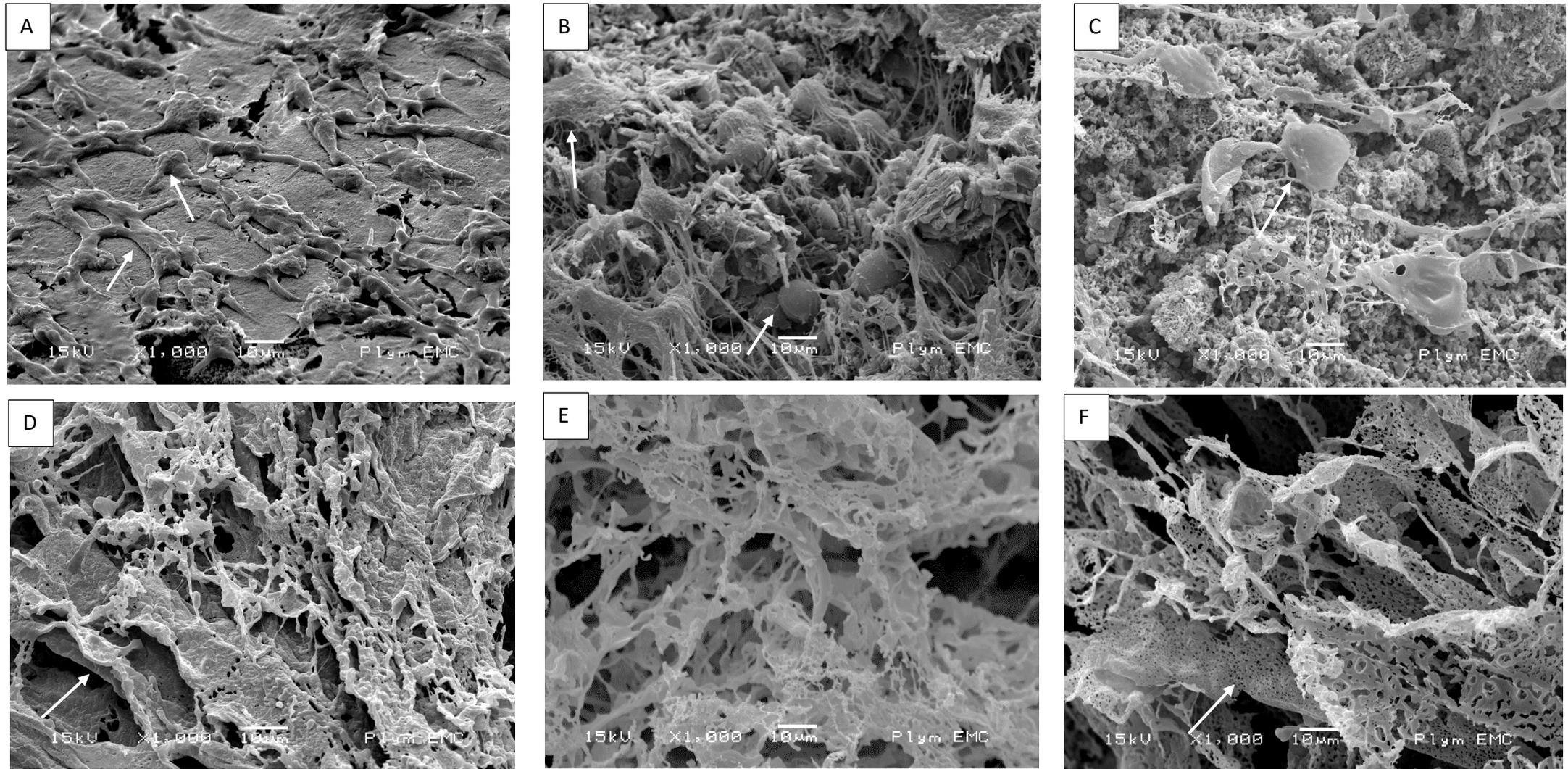
Figure2.8 SEM observation of the CHO cells after 24 h and 7 days. 2.9 A, B and C represents the growth of CHO cells on HA, DCP and β-TCP after 24 h respectively. D, E and F represents the growth of CHO cells on HA, DCP and β-TCP after 7 days respectively. The images are taken in x1000 magnification. The arrows point to the CHO cells on the composites and the difference in the shape of the cells.

2.4   Discussion

The pilot study was undertaken to determine the difference in the biocompatibility of the different phases of calcium phosphate and to elucidate the factors contributing to the biocompatibility of the material. Three phases of calcium phosphate powders (HA, DCP and β-TCP) were synthesized using the wet sol-gel technique and the final composites were produced by mixing the powders with PVA in an equal ratio. The biocompatibility of the composites was tested with CHO cells for 24 h and 7days, at the end of which the composites with the cells were observed under SEM and quantitatively analysed. The main findings of this study was that HA was the most biocompatible phase of calcium phosphate and the sintering temperature plays a crucial role in determining the morphology of the crystals, which in turn affects the biocompatibility properties of the final composite.

2.4.1 Characterisation of the calcium phosphate powders and composites

The need to characterize the calcium phosphate powders and composites prior to any *in vitro* study is crucial, especially due to the potential unintentional synthesis of other phases of calcium phosphates. The powders were analysed using XRD, FTIR and observed by TEM (Figures 2.3 2.4 and 2.2) and the final composites were examined by SEM and FTIR (Figures 2.5 and 2.6).

The XRD patterns of HA and DCP (Figure 2.3) exhibits broad diffraction peaks indicating low crystallinity or more likely nanocrystalline, whereas, high intense peaks were observed in β-TCP powder. This is in accordance with Okazaki et al. (Okazaki et al., 1981), who have stated that the XRD patterns becomes intense with increasing sintering

67

temperature which means that the crystallinity of the synthesized powders increases with temperature. However, no reference material was analysed and the peaks were only compared against published data. XRD is a semi quantitative method as it uses the height of the individual 2Θ peaks in relation to each other to determine the approximate minerals in the powders whereas FTIR spectroscopy is a physical process, which is based on the interaction of the infrared radiation with the material. Functional groups such as CO_3^{2-}, OH^-, PO_4^{3-} groups have a specific absorption ranges in the FTIR Spectroscopy method. By combining XRD and FTIR it is possible to determine the true composition of the materials and also to correlate them with the chemical composition. Comparison of the FTIR analysis of the HA powder and composite (HA-PVA) shows the presence of most characteristic chemical groups that characterize non-stoichiometric HA (Figure 2.4 and 2.6). Additional peaks can be seen at $1086cm^{-1}$ in the HA composite which can be attributed to the interaction with PVA. These spectra also demonstrate low crystallinity degree, which resonates with the TEM observation and XRD analysis. The band shape, width and intensity differ between the powders and composites due to the bonding between the PVA and the respective powders. Similarly, the characteristic peaks of the DCP and β-TCP composites were also observed confirming the desired phases of calcium phosphate were produced.

2.4.2 Biocompatibility effect of the composites

When implanted in the human body, bone implants should provide cell anchorage sites and structural guidance to form a new bone. The viability of the cells were evaluated qualitatively and quantitatively using SEM microscopy (Figure 2.7 and 2.8). Many fibroblasts were easily visible on all the specimens. However, their appearance was different on each material suggesting that some composites were better for cell growth

and that the different phases of calcium phosphate may elicit toxic reaction from the cells. The results (Figure 2.7 and 2.8) show that HA has better biocompatibility compared to DCP and β-TCP. There could be two possible explanations to this, whilst it is known that the shape and size of the particles contribute to the bioactivity of the materials, the chemical composition and presence of functional groups also play a vital role(Galea et al., 2013). Natural HA has a hydroxyl ion channel which runs straight through the centre of the basal plane of its hexagonal lattice and parallel to its c-axis which is responsible for its extraordinary characteristics (Uskoković, 2015). Synthetic HA has an additional OH group which is not present in the other two types of the calcium phosphates. The presence of the additional OH- is thought to enhance the adhesion and proliferation of the CHO cells (Barrère et al., 2006). Another possibility is the similarity with the non-stoichiometric HA which occurs naturally in bone. A healthy cell should be flat with extending pseudopods which is not observed in the morphology of the cells grown on DCP composite suggesting that the cells are under stress which could be due to higher phosphoric content in the composite compared to the HA. Of all the materials studied, β-TCP exhibited the least compatibility (Figures 2.7 and 2.8). It is possible that the size of the crystals may have affected the cell growth. This is in accordance with (Coathup et al., 2013) who suggests that adhesion and proliferation of osteoblast cells increases when the crystal size is decreased.

2.5 Conclusion

The pilot study was undertaken to observe cell response to the various phases of Ca-P. HA-PVA composites showed better biocompatibility with the composites from 24 h whereas DCP was comparable to HA only by day 7. Based on the results, HA composite

was chosen to be improved further by reinforcing it with carbon nanotubes and to make it antibacterial with the addition of silver nanoparticles.

3. Synthesis and characterization of silver nanoparticle decorated carbon nanotube-hydroxyapatite nanocomposites

3.1 Introduction

Since bone is a typical example of a nanocomposite, designing bone graft in the form of nanocomposite is perceived to be beneficial over single phase and microcomposite materials. Nanocomposites are usually made of at least two components; the basic matrix and the reinforcement. In bone implants, the reinforcement serves to improve the strength of the nanocomposite by blocking the growth of cracks in them. This can be achieved by employing a material which has a high aspect ratio: since the higher the aspect ratio, the better the reinforcement(Li et al., 2005). It is because of this reason long thin fibres reinforce better than particulates. In addition to impeding the growth of cracks, the reinforcement should also bear most of the applied load. One such reinforcement is carbon nanotubes (CNTs). Apart from reinforcement, CNTs have the potential to be used in targeted drug delivery (Liu et al., 2010). Therefore, in the case of HA-CNTs nanocomposites, synthetic HA matrix reinforced with CNTs can be anticipated to not only be bioactive and strong, but also be able to deliver drugs and antimicrobial agents.

Silver ions and silver based compounds are highly toxic to microorganisms. Silver nanoparticles (Ag NPs) can be synthesised by chemical reduction using organic or inorganic reducing agents and can be attached to the sidewalls of the MWCNTs. The slow release of silver from the composites over a long period will reduce / prevent infection following surgery. So far, only one study led by Herkendell et al (2014) has been published relating to the development of Ag NPs-MWNCTs-HA composites that are also antimicrobial (See chapter 1, section 1.4). This chapter details the synthesis of the Ag NPs-MWNCTs-HA nanocomposites, their characterisation, mechanical properties and their behaviour in aqueous media.

3.2 Materials and methods

In order to study the effect of Ag NPs decorated MWCNTs in synthetic HA nanocomposites, 4 different types of nanocomposite powders were produced using pristine (as produced) and functionalised (oxidised with nitric acid) MWCNTs with two types of surfactants - Poly Vinyl Alcohol (PVA) and Hexadecyl trimethyl ammonium bromide (HTAB) as follows:

1. Ag NPs-*p*-MWCNTs-PVA – (HA +Ag NPs-Pristine MWCNTs + PVA)

2. Ag NPs-*f*-MWCNTs-PVA – (HA + Ag NPs -Functionalized MWCNTs + PVA)

3. Ag NPs -*p*-MWCNTs-HTAB – (HA + Ag NPs -Pristine MWCNTs + HTAB)

4. Ag NPs-f-MWCNTs-HTAB – (HA +Ag NPs- Functionalized MWCNTs + HTAB)

5. Pure HA composites (control)

The nanocomposite powders were then mixed with PVA to produce the final composites. Analytical grade reagents from Sigma Aldrich were used throughout the production process.

3.2.1 Functionalization of MWCNTs

Pristine MWCNTs are insoluble in water and most solvents owing to their tendency to agglomerate due to their high aspect ratio and high surface energy. CNTs that have been chemically functionalised by oxidation are more soluble than pristine nanotubes, and are more easily incorporated into nanocomposites. Commercially supplied MWCNTs (shenzen Nanotech port, China) with a diameter of 10 -30 nm, length 5 -15 μm and ≥ 95% purity (manufacturer's information) were functionalised in house using concentrated nitric acid (Sigma Aldrich,Dorset, UK) following an established protocol (Datsyuk et al., 2008). Briefly, 0.3 g of the as-received MWCNTs was mixed with 25 ml of 14.5M concentrated nitric acid and refluxed at room temperature for 48 h. The

resulting dispersion was then filtered through a Whatman® glass microfiber filter paper (WHA1827070, Sigma Aldrich, Irvine, UK) with pore size 1.5 μm and washed in deionised water until neutral pH was achieved. The sample was then dried in a vacuum at 40 °C for 24 h.

3.2.2 Decoration of Ag NPs onto pristine/ functionalized MWCNTs

The decoration of Ag NPs onto the surface of MWCNTs was carried out according to the protocol by Xin et al (2011) with some modifications. Silver Nitrate ($AgNO_3$) was reduced to Ag NPs using N,N-Dimethylformamide (DMF) (437573, Sigma Aldrich, Dorset, UK) as a reductant as shown in equation below

$$HCON(CH_3)_2 + 2Ag^+ + H_2O \longrightarrow 2Ag + (CH_3)_2NCOOH + 2H^+$$
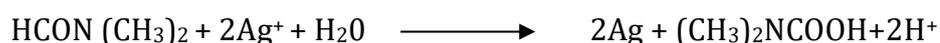
Briefly, 0.5 g of pristine / functionalized MWCNTs and 0.2 g of PVA (MW- 85,000-124,000, 363146, Sigma Aldrich, Dorset, UK) or HTAB (36932, Sigma Aldrich, Dorset, UK) was added to 260 ml of DMF and the mixture was subjected to ultasonication for 1h. The pH value was adjusted to 6.0 using nitric acid (a few drops of 0.1 mol/l HNO_3). To achieve the optimal decoration of the MWCNTs with silver nanoparticles, 60 ml of 10 mmol/l $AgNO_3$ solution was added dropwise to the mixture and was stirred vigorously for 1 h at 60 - 62 °C. Following this, the solution was kept aside without stirring at room temperature for 48 h for the silver to deposit on the MWCNTs. The final product was obtained by filtration using Whatman® filter paper (WHA1001070, Sigma Aldrich, Irvine, UK) with pore size of 11 μm and washed with ethanol, water, acetone and left to dry in a vacuum chamber at 90 °C for 48 h.

3.2.3 Preparation of HA-Ag NPs-MWCNTs powder (precipitation of HA on Ag-MWCNTs)

In order to obtain maximum mechanical strength, nanocomposites containing 0.5 % weight percentages of Ag NPs-MWCNTs were produced using the sol-gel technique (Figure 3.1). The amount of MWCNTs needed for each batch was calculated relative to the expected amount of HA. For example, 0.05 g of MWCNTs was used for a batch expected to produce 10 g of HA with 0.5 wt.% of MWCNTs so the total mass of the powders would be 10.05 g. Figure 3.1 is a schematic representation of the sol-gel process used to produce the powders.
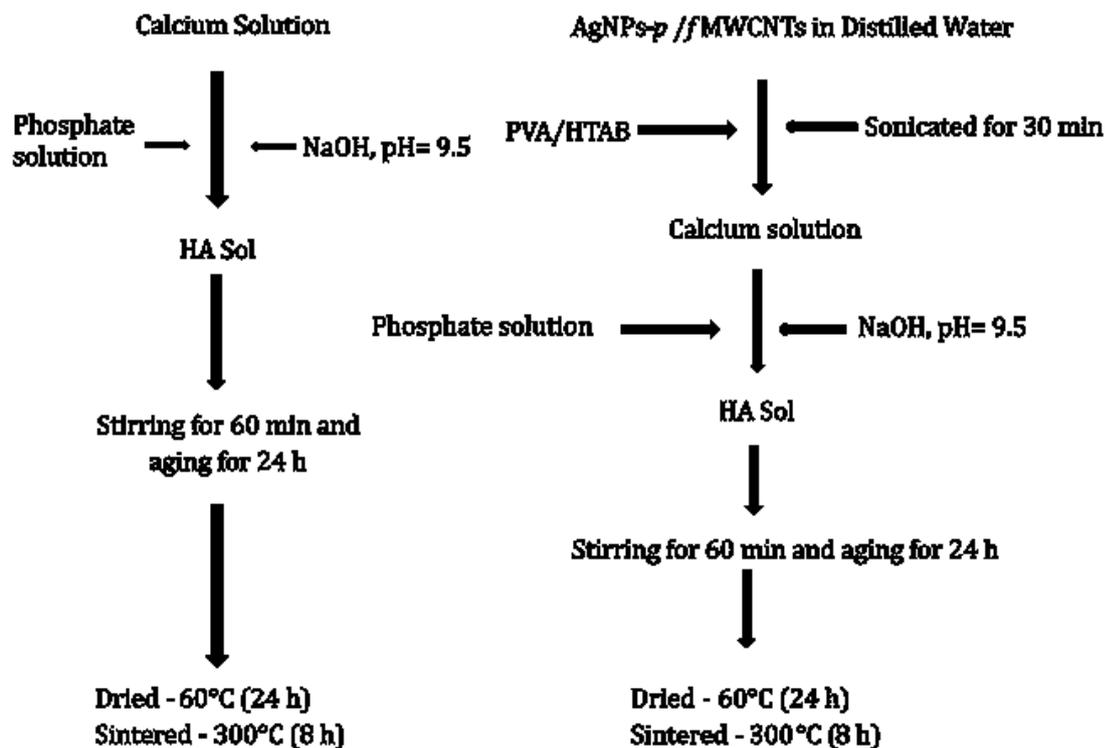
Figure 3.1 Schematic representation of the sol-gel technique used for the synthesis of pure HA (control) and the four different types of composites containing Ag NPs and MWCNTs.

To produce the nanocomposite powders, HA must be nucleated on the walls of the Ag NPs -MWCNTs in the presence of the surfactant. In a typical experiment, to produce

10 g of the nanocomposite powder, 0.005 g of PVA (MW- 70,000-100,000, Sigma Aldrich, UK) or 0.005 g of HTAB (Sigma Aldrich, UK) was added to 100 ml ultrapure water. 0.05 g (0.5 wt. %) of pristine or functionalized Ag NPs - MWCNTs were added to the mixture which was sonicated at 50-60 Hz (Metason 120T, Struers, UK) for 30 min at room temperature until all the Ag NPs - MWCNTs were dispersed. Then, HA was nucleated in to the dispersion by the addition of 200 ml of 0.1 M calcium acetate and 0.06 M of ammonium phosphate to obtain a final calcium: phosphate ratio of 10:6, normally expressed as 1.67. The solution was stirred at the rate of 900-1000 rpm using a magnetic stirrer (dial setting 9, Hotplate/stirrer, RCT basic, IKA Oxford, UK). While stirring, the pH of the solution was checked periodically and maintained at 9.5-10 by the addition of 6M sodium hydroxide solution. The solution was stirred for 1h and left to mature for 24 h at 40 °C. The resulting dispersion containing the HA nucleated on the MWCNTs was then filtered through Whatman® filter paper (WHA1001070, Sigma Aldrich, Irvine, UK) with pore size of 11 μm and the precipitate was washed with ultrapure water which was subsequently dried under a vacuum at 60 °C for 24 h. The dry precipitate was manually crushed with a glass mortar and pestle to make a fine powder and was then sintered at 100 °C for 8h.

In order to obtain pure HA powders, the process above was conducted exactly the same, but without the addition of the MWCNTs. A pilot study was conducted for the synthesis of the pure HA with the addition of PVA and HTAB to determine its effect on the crystal growth. Based on the results obtained, 0.5 wt% of PVA was added during the sol-gel synthesis of pure HA to obtain the crystal structure that is similar to natural bone.

3.2.4 HA-Ag NPs- MWCNTs composite

The nanocomposite powders obtained from the above method was used to prepare the final composites which were produced following established protocols in Plymouth University laboratory (Natesan et al., 2015). Briefly, 1 g of the calcined nanocomposite powder was mixed with 1 ml of 20 % PVA at room temperature. The mixture was inserted and packed in a cylindrical mould whose ends were blocked with short cylinders. Different size of composites were produced for mechanical and biocompatibility tests . This was done to comply with the international testing standards (see below) for mechanical tests and to ensure that the composites fits in a 24 well plate (each well = 15 mm diameter) for biocompatibility and antibacterial tests. Pressure was applied on top of the cylinders using mechanical mini pellet press (GS03940, Specac, Kent, UK) which in turn, compressed the sample inside the mould. The pressure applied on each sample was equivalent to 26 MPa which was held for 1 minute after which, the aluminium cylinders were removed from the moulds. The samples were placed in an oven at 40 °C for 48 h to dry. Afterwards, the samples were carefully removed from the moulds and stored at room temperature, until required for mechanical testing and biocompatibility studies.

3.3 Characterisation of the composite materials

Physico-chemical characterisation was performed at several steps in the synthesis of the composites including the original materials and their functionalised forms in dispersions and the resulting powers that were compressed into pellets to make the final composite. In addition to the manufacturer's information, the MWCNTs were examined by electron microscopy for their appearance and primary size. XRD is the most common technique to determine crystal structures and atomic spacing and was used to identify

the phase purity of the produced nanocomposite powders and FTIR analysis was performed to detect the functional groups and characterise covalent bonding information. The protocols used for the XRD and FTIR measurements is previously described in Chapter 2 (sections 2.2.3.2 and 2.2.3.3)

3.3.1 SEM and TEM analysis

To confirm the primary dimensions (length, tube diameter) and morphology (stiff or flexible tubes that form bundles) the MWCNTs as supplied by the manufacture were examined by transmission electron microscopy. Batches of the functionalized MWCNTs prior to making the nanocomposite powder were also examined followed by examining the nanocomposite powders to analyse the morphology of the HA crystal. Briefly, in a separate run, approximately 0.05 g of the material to be analysed (pristine MWCNTs, functionalised MWCNTs and nanocomposite powders) were dispersed separately in distilled water and sonicated for 5 min which was used as the stock solution. All electron microscope observations were made on 3 sub-samples of each stock. A drop of the relevant dispersion was placed on the copper grid and air dried and subsequently observed at an accelerating voltage of 120 kV using a high resolution TEM (JEOL 1400, JEOL ltd, Japan). On each specimen, 30 random images were collected for quantification of dimensions of the materials. The images were processed using image J software (Windows version) to measure the length and diameter of the tubes. The same process was used to analyse the shape, size and growth of the HA crystals around MWCNTs powder.

Due to their carbonic nature and presence of Van der Waals force, the tubes are hydrophobic and exhibit low dispersibility in water and other organic solvents. To

observe the wettability of the MWCNTs and to determine the effect of the surfactants on the MWCNTs, pristine and functionalised MWCNTs were dispersed in 5ml of deionised water along with PVA and HTAB. In a clean glass bottle, 0.05 g of pristine and functionalised MWCNTs were added to 5 ml deionised water. To this 0.005g of PVA and HTAB was added. A separate glass bottle containing only pristine and functionalised MWCNTs was taken as control. Images were taken immediately and then sonicated for 30 min. Following sonication, the images were taken again and the bottles were left undisturbed for 1 week. Images were taken again and compared to day 1 images.

3.3.2 Dialysis Experiment

Ag NPs may release Ag^+ ions by dissolution and in order to enable interpretation of the Ag NPs response to the bacteria and osteoblast cells in this study, a dialysis experiment was done to measure the dissolution rate of the Ag NPs in simulated body fluid (SBF). The degradation (if any) of the composites in SBF was also studied by measuring the concentration of the electrolytes Na^+, K^+, Ca^{2+}, Mg^{2+}, and P. Table 3.1 details the ion concentration of SBF (Kokubo et al., 1990) compared with human blood plasma.

Table 3.1 Comparison of the ion concentration of the prepared SBF and human blood plasma.

Ion	Simulated body fluid (mmol/l)	Human blood plasma (mmol/l)
Na^+	142.0	142.0
K^+	5.0	5.0
Mg^{2+}	7.5	7.5
Ca^{2+}	2.5	2.5
Cl^-	147.8	147.8
HCO_3^-	4.2	4.2
HPO_4^{2-}	1.0	1.0
SO_4^{2-}	0.5	0.5

The appropriate ion concentration of SBF was obtained by adding appropriate amount of salts listed in Table 3.2 in 1l of deionised (Milli-Q) water. The pH was adjusted to 7.25 using a few drops of sodium hydroxide (2 M)

Table 3.2 Concentration of each salt added to 1l of Milli-Q water.

Salt	g/mol	g/l
Ammonium dihydrogen phosphate	115.03	0.115
Calcium nitrate	236.15	0.59
Magnesium Chloride Hexahydrate	203.3	0.305
Sodium Chloride	58.4	8.39
Ammonium Sulfate	131.14	0.066
Ammonium Hydrogen Carbonate	79.06	0.332
Potassium Chloride	74.55	0.373

The dialysis method was based on Handy et al (1989) with modifications for composites. Briefly, the composites, identical to those used for the biocompatibility and antibacterial studies were prepared as mentioned above. All glassware and dialysis tubing had been acid washed (5% nitric acid) and triple rinsed in deionised (Milli-Q) water. Before the start of the experiment, the dialysis tubing (D9777, cellulose membrane with molecular weight cut off at 12,000 Da, Sigma Aldrich, Dorset, UK) with an approximate exclusion size of 2.5 nm was used to make 70 mm long x 25 mm wide dialysis bags and were soaked in deionised (Milli-Q) water for 10 mins. Following that, the appropriate composites were placed inside the tube and filled with 8 ml of SBF ensuring that the composites were immersed in SBF. The ends of the bags were secured with mediclips to prevent leaking which were also previously acid washed. The filled dialysis bags were then placed immediately in a beaker containing 492 ml of SBF (bringing the total volume to 500 ml). Care was taken to use beakers of identical shape/size for the experiment (n = 3 per treatment and control). Three beakers were also set up for reference control containing only SBF without the presence of any composites. The solutions in the beakers were gently agitated with a multipoint magnetic stirrer (RO 15P power, IKa-Werke GmbH & Co. KG, Staufen, Germany) for 24 h at room temperature. Samples of the external SBF (4.5ml) from each beaker was taken at 0, 30 min, 1, 2, 3, 4, 6, 8, 12, and 24 h. At the end of the experiment, the remaining contents of the dialysis bags were also collected. Total concentrations of Ag, Na^+, K^+, Ca^{2+}, Mg^{2+}, and P were measured by Inductively coupled plasma mass spectrometry (ICP-MS) and Inductively coupled plasma optical emission spectrometry (ICP-OES, Varian 725-ES, Melbourne, Australia fitted with v-groove nebuliser and Sturman-Masters spray chamber). The pH of the samples and the temperature of the media in the beakers was also measured during the experiment.

3.4 Mechanical testing

Mechanical tests were performed to determine the tensile and compressive strength (CS) of the produced composites.

3.4.1 Tensile strength

To determine the tensile strength, the diameteral tensile strength (DTS) method was used (Bresciani et al., 2004). For each material, ten replicates of the final composites were prepared as explained in section 3.2.4 (HA-Ag NPs- MWCNTs composite). The dimensions of the composites were 6.0 mm diameter x 3.0 mm height for the DTS test. The specimens were tested under compressive load in a universal testing machine (3300 single column Instron, Wycombe, UK) at a crosshead speed of 0.5 mm/min. Load was applied vertically on the lateral portion of the cylinder, producing tensile stress perpendicular to the vertical plane passing through the centre of the specimen (Della Bona et al., 2008). The DTS was calculated as follows:

$$DTS = 2F/\pi dh$$

Where, F is the load applied; d is the diameter of the composite; h is the height of the composite; π = 3.14 (constant)

3.4.2 Compressive strength

Similar to the tensile strength five replicates of each final composite were produced and the dimensions of the composites were 6.0 mm diameter x 12.0 mm height. The specimens were placed in a vertical position, with the force incident on the long axis of the specimen. The specimens were tested under compressive load in a universal testing machine (3300 single column Instron, Wycombe, UK) at a crosshead speed of 1.0 mm/min for compressive strength.

3.5 Material Characterisation results

3.5.1 Carbon nanotube characterisation

Morphology and quality of the MWCNTs was studied using TEM. Figure 3.2 shows that both, pristine and functionalized MWCNTs demonstrate a high aspect ratio. On closer observation (Figure 3.2 C and D), the central hollow portion was clearly visible in both the pristine and functionalised MWCNTs which confirms that they are hollow 1D structures. The pristine MWCNTs appeared entangled due to the presence of strong Van der Waals force whereas functionalization with strong acid made the bundles exfoliate and curl. The average length and diameter of the tubes are presented in Table 3.3. While the diameters of the MWCNTs was easily be measured by Image J software from the TEM images, measuring the length of the MWCNTs was not as straightforward. This is because the MWCNTs were long and entwined making it difficult to identify entire individual strands. Care was taken to measure only the length of individual tubes which were separate at the edge of the clusters. It is likely that this is the lower estimate of the length, as within the clusters, no MWCNTs of similar lengths could be found, despite it being possible to follow along the length of many CNTs through the visible part of the image.
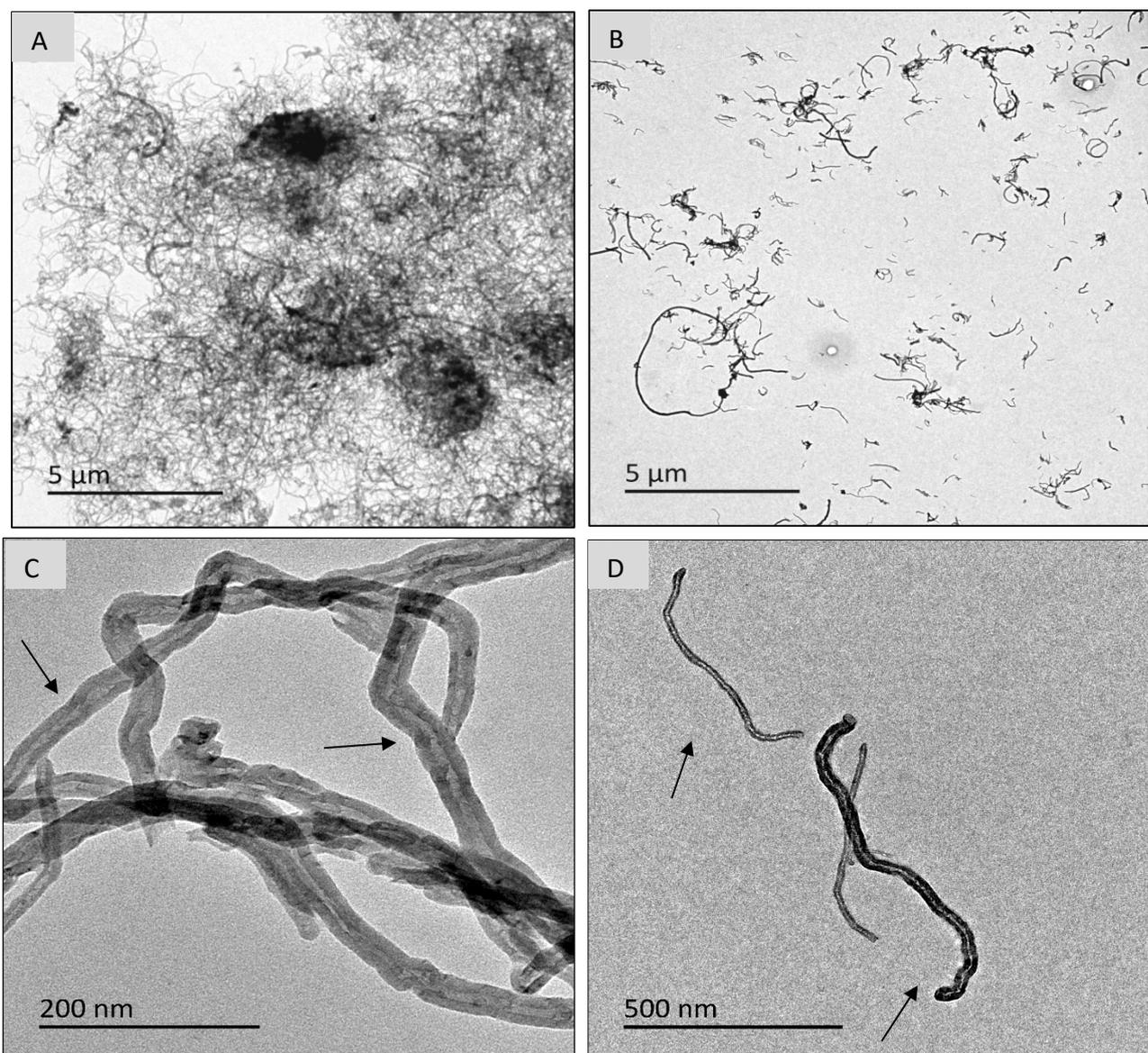
Figure 3.2 TEM micrographs of MWCNTs (A) as received Pristine MWCNTs depicting the clusters, (B) oxidised MWCNTs following functionalization with strong nitric acid, (C) higher magnification of pristine MWCNTs depicting the hollow tubes, (D) higher magnification of functionalised MWCNTs .

Table 3.3 Average diameter and length of Pristine and functionalised MWCNTs

MWCNTs	Average Diameter (nm)	Average Length (µm)
Pristine	27.8 ± 12	2 ± 2.13
Functionalised	23.7 ± 10.7	1.10 ± 1.21

The data represents the average diameter and length of the MWCNTs. Data are mean ± S.D (n = 100 measurements). TEM images were processed through Image J software to obtain the measurements.

The homogeneity of the composites depended on the wettability and dispersability of the MWCNTs in the matrix. This was observed by dispersing MWCNTs in water and observing the difference in the wettability and dispersion of the MWCNTs in the presence of the surfactants. Figure 3.3 and 3.4 shows the dispersion of the pristine and functionalised MWCNTs in Milli-Q water with and without the surfactants. Three elements affected the dispersability of the MWCNTs: 1) whether the MWCNTs were functionalised or pristine; 2) the presence or absence of surfactants and 3) the type of surfactant used (PVA or HTAB). Functionalisation of the MWCNTs with strong nitric acid adds functional bonds to the sidewalls and tips of the MWCNTs, which was intended to improve the wettability and dispersion of the MWCNTs in water. This was demonstrated in Figure 3.4 B. The figures 3.3 and 3.4 shows that pristine and functionalised MWCNTs without the addition of surfactants will result in heterogeneous dispersion. After 1 week, no real difference was observed in the dispersion of the functionalised MWCNTs with and without the presence of PVA or HTAB (Figure 3.4). The dispersion of pristine MWCNTs without the surfactants exhibits hydrophobicity and they are adhered to the walls of the bottle (Figure 3.3).
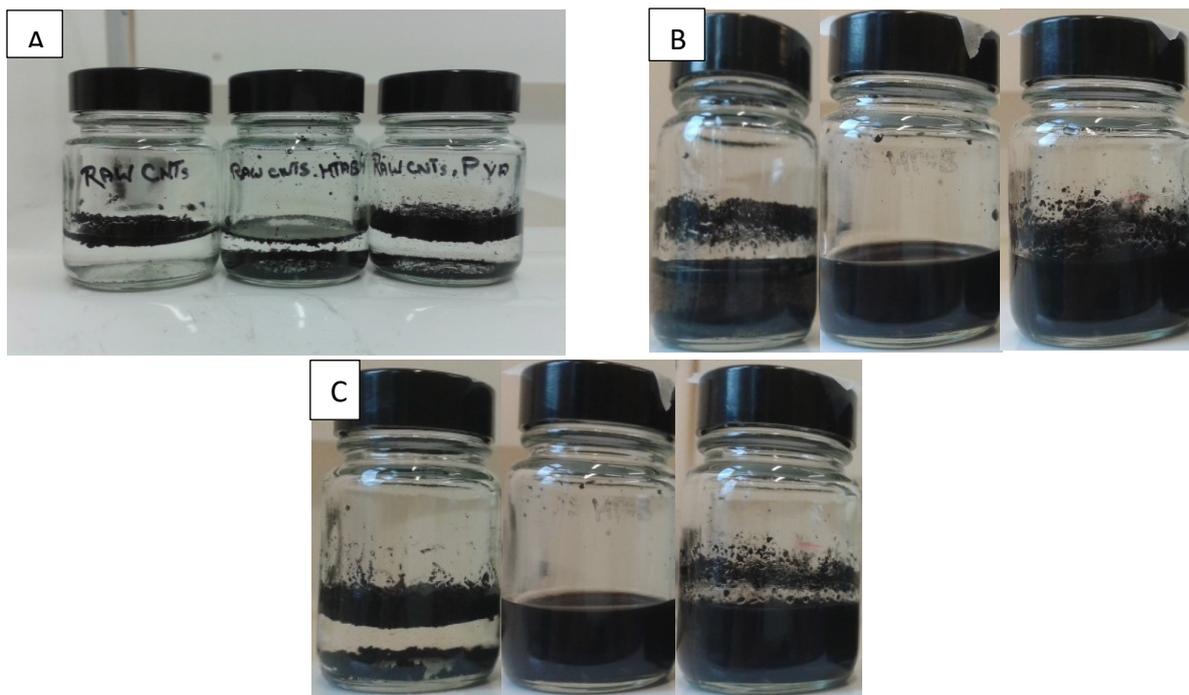
Figure 3.3 Comparison of the wettability and disperability of the pristine MWCNTs. From left to right –p- MWCNTs Control, without the presence of surfactants, p- MWCNTs with HTAB, p- MWCNTs with PVA. (A) Dispersion of MWCNTs immediately after adding it to water, (B) dispersion of MWCNTs after sonicating for 30 min, (C) dispersion of MWCNTs after 1 week.
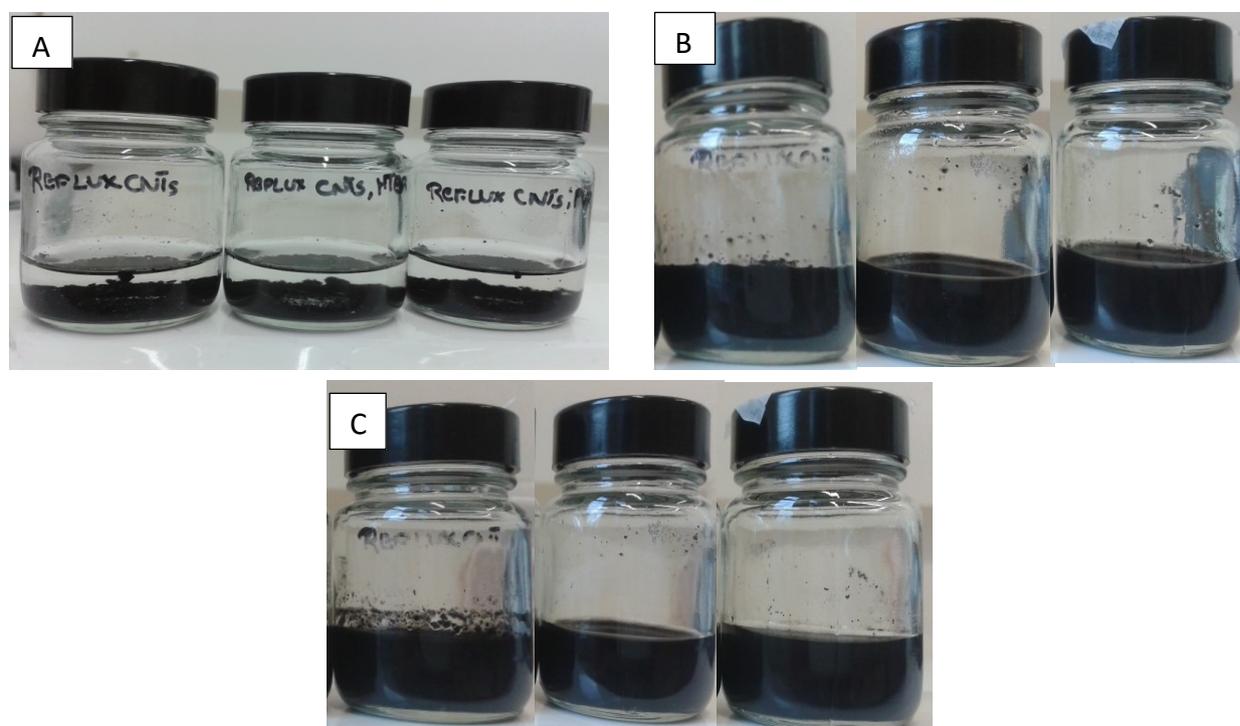
Figure 3.4 Comparison of the wettability and disperability of the functionalised MWCNTs. From left to right –f- MWCNTs Control, without the presence of surfactants, f-MWCNTs with HTAB, f- MWCNTs with PVA. (A) Dispersion of functionalised MWCNTs immediately after adding it to water, (B) dispersion of MWCNTs after sonicating for 30 min, (C) dispersion of MWCNTs after 1 week

3.5.2 Ag NPs-MWCNTs Characterisation

The interaction between the Ag NPs and MWCNTs is crucial to obtain the optimal silver release over a period of time for the composites to prevent bacterial colonisation. Figure 3.5 shows the presence of Ag NPs and their interaction with the pristine and functionalised MWCNTs.
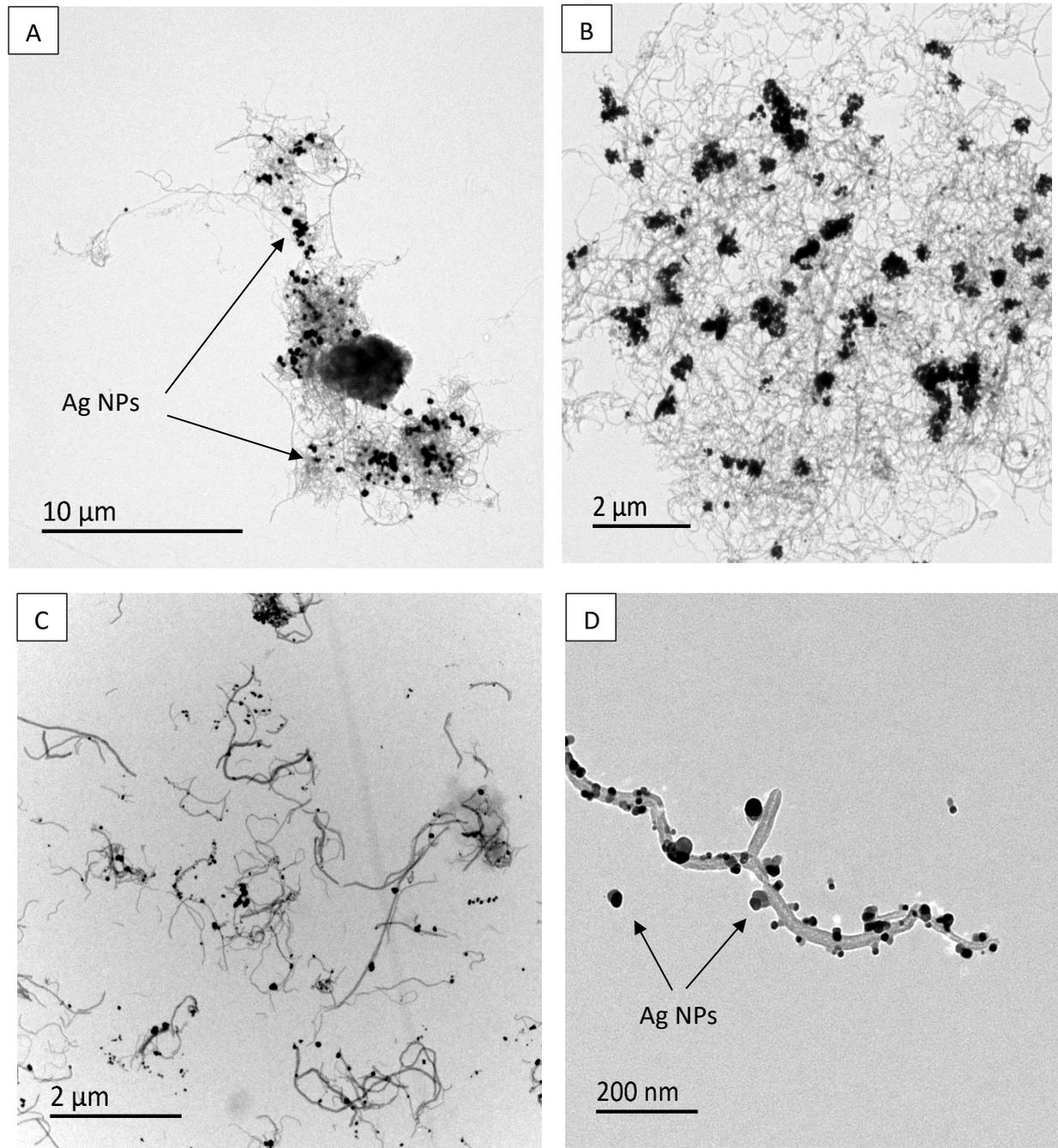
Figure 3.5 TEM images of Ag NPs-MWCNTs (A and B) shows Ag NPs-p-MWCNTs (C and D) shows Ag NPs-f-MWCNTs .Arrows point to the Ag NPs.

Figure 3.5 D shows silver nanaoparticles decorating the sidewalls of *f*-MWCNTs. Compared to the interaction between the Ag NPs and *f*-MWCNTs, the interaction between the Ag NPs and *p*-MWCNTs (Figure 3.5 A and B) was low.

3.5.3 HA-Ag NPs-MWCNTs powders characterisation

The mechanical properties and biocompatibility of the final composites were determined by the morphology and physico-chemical characteristics of the nanocomposite powders. The powders were analysed by TEM, XRD and FTIR. TEM analysis (Figure 3.6) of the nanocomposite powders shows the presence of nano HA in all the samples. The effect of the surfactants on the morphology of the crystals is shown (Figure 3.6). The HA crystals exhibited the typical needle-like-shape morphology similar to natural HA in pure HA, *p*-MWCNTs-PVA and *f*-MWCNTs-PVA (Figure 3.6 A, B, C) nanocomposite powders. The crystals in *p*-MWCNTs-HTAB and *f*-MWCNTs-HTAB nanocomposite powders exhibited short nano-rod morphology. The difference in length is detailed in Table 3.4 with the pure HA powder exhibiting maximum size and the powders containing HTAB surfactant exhibiting the least size. The degree of interaction between the HA and the MWCNTs can also be observed in the images. Figure 3.6 B shows a cluster of MWCNTs which is not completely surrounded by HA. This shows the weak interaction between the HA and *p*-MWCNTs whereas the interaction between HA and *f*-MWCNTs is comparatively higher which is due to the presence of functional groups. Functionalisation tends to break open the ends of the MWCNTs which is also visible in Figure 3.6 C.

Table 3. 4 Average HA crystal size of the nanocomposite powders

Composite powder	Average HA crystal size (nm)
HA (Control)	130.12 ± 127.4
Ag NPs-*p*-MWCNTs-PVA	87.16 ± 36
Ag NPs-*f*-MWCNTs-PVA	80.6 ± 22.4
Ag NPs-*p*-MWCNTs-HTAB	62.6 ± 18.3
Ag NPs-*f*-MWCNTs-HTAB	52.4 ± 13

The data represents mean ± S.D (n = 20 measurements per composite powder). TEM images were processed through Image J software to obtain the measurements.
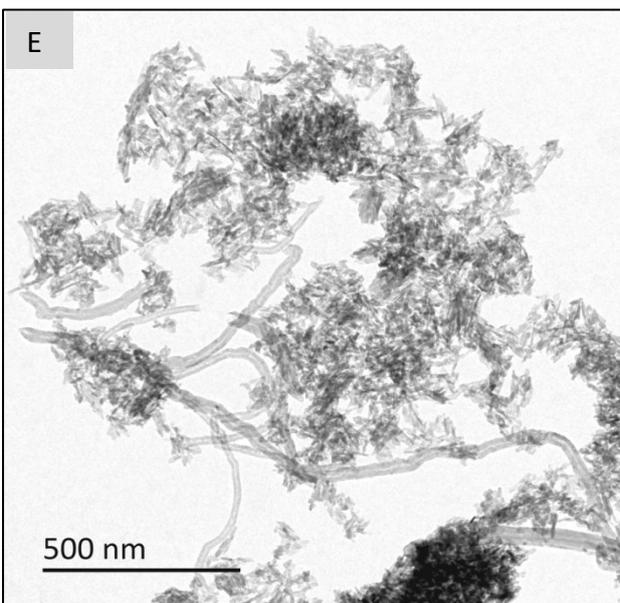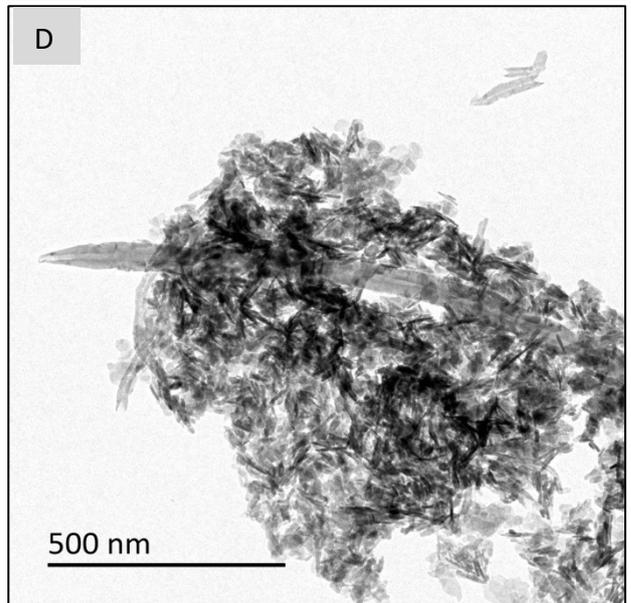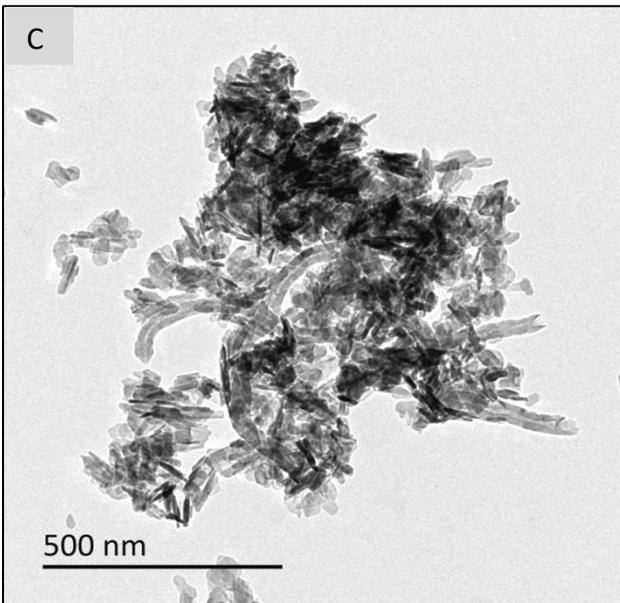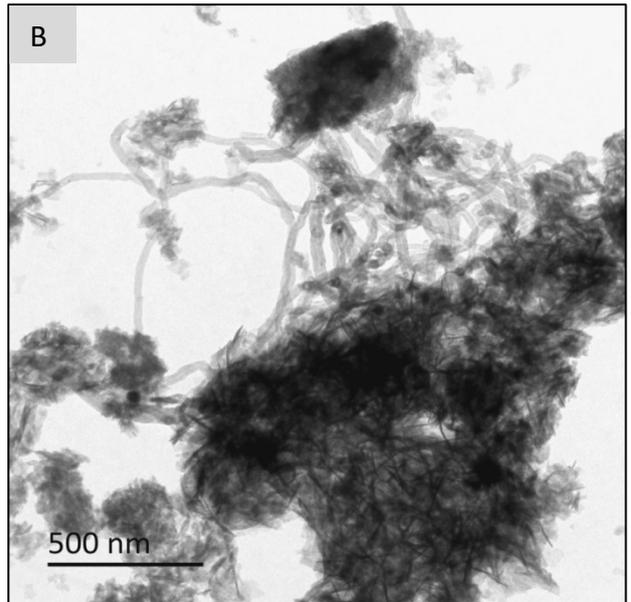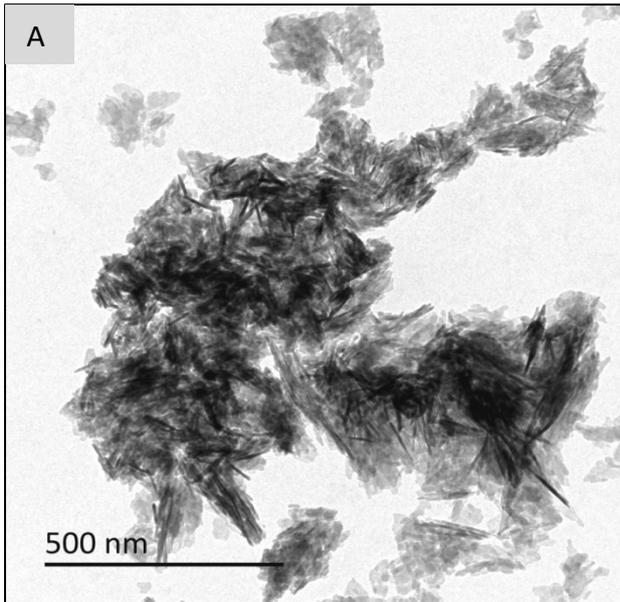
Figure 3.6 TEM images of composite powders (A) Pure HA crystals with the appearance of needle shape; (B) p-MWCNTs-PVA shows clusters of long nanotubes with needle like HA; (c) f-MWCNTs-PVA shows the growth of HA crystal around the CNTs; (D) p-MWCNTs-HTAB shows that the crystals have not obtained the needle structure but have a rod shape (on closer observation); (E) f-MWCNTs-HTAB indicates that CNTS are not clustered and also no presence of needle like HA crystals.

3.5.3.1 XRD analysis

XRD analysis was performed to determine the crystal structure and phase purity of the HA present in the nanocomposite powders. The XRD spectra of the sintered powders are shown in Figure 3.7. The data obtained from XRD compliments the TEM images which indicates that HA phase was produced in all the samples. Broad diffraction peaks are observed in all the nanocomposite powders indicating presence of nanocrystals. However, no peaks corresponding to the presence of Ag NPs and the graphite in MWCNTs were detected suggesting that either the sensitivity limit of the XRD does not allow the detection of the small volume fraction of MWCNTs or MWCNTs have reacted completely with HA. Thus, other methods were employed to confirm the presence of residual Ag NPs-MWCNTs in the composites.
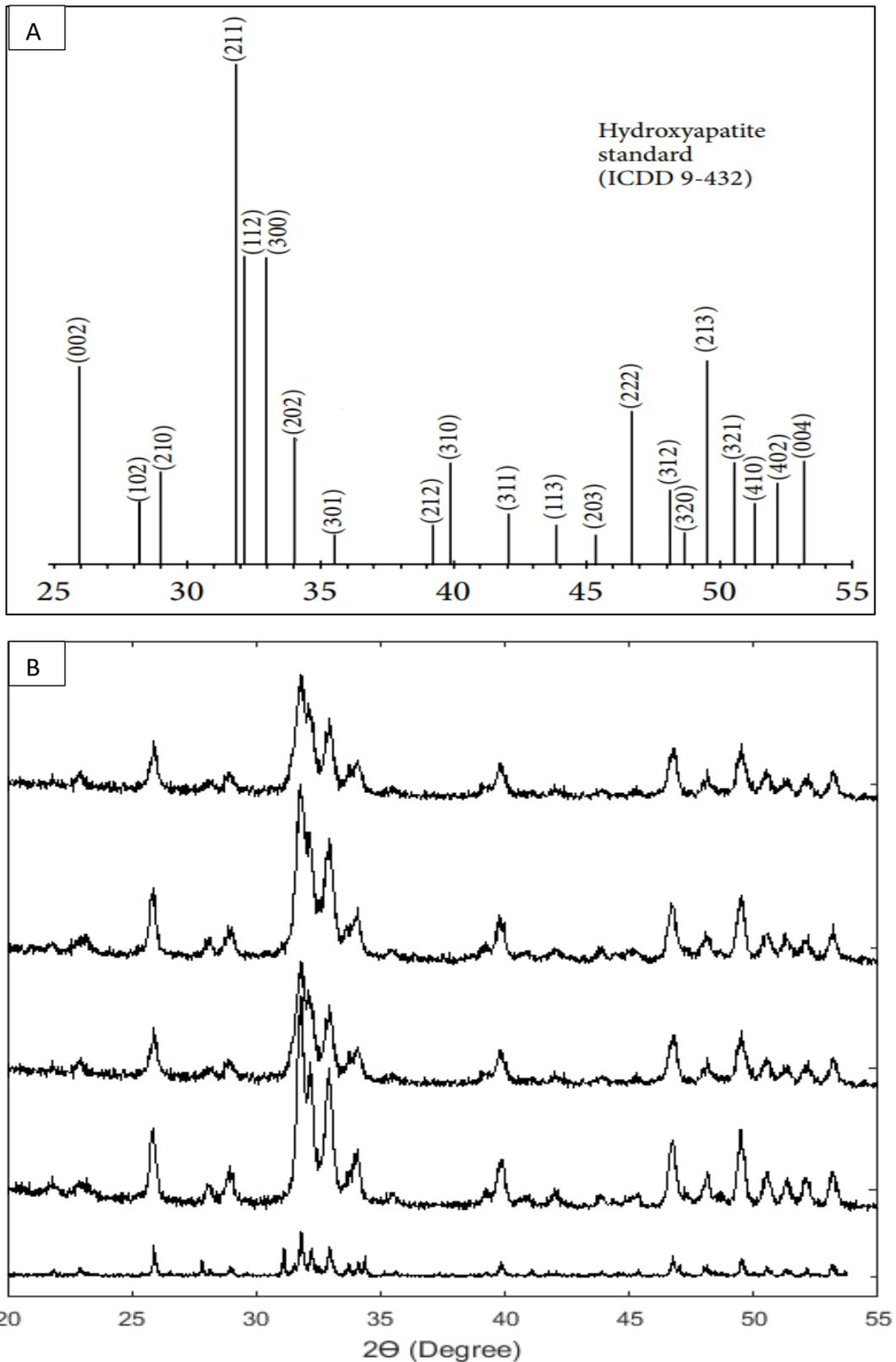
Figure 3.7 XRD analysis of the nanocomposite powders. (A) XRD peaks data for HA from ICDD ref: 9-432(Shahabi et al., 2014)(B) XRD analysis of the powders (i) Pure HA –control ;(ii) p-MWCNTs-PVA ; (iii) f-MWCNTs-PVA; (iv) p-MWCNTs-HTAB ; (v) f-MWCNTs-HTAB. The peaks observed in the powders correspond to reference from ICDD.

3.5.3.2 FTIR analysis

The FT-IR spectroscopy is more sensitive than XRD and is an effective tool for structural investigation and to study the hydroxylation of HA after heat treatment. The FTIR data are represented in the Figure 3.8 and was performed for each batch of material. The expected peaks and observed peaks are presented in Table 3.5. All the peaks were present in the expected location. Additionally, a peak at 2917 cm^{-1} was observed in all the powders except the pure HA . This is due to C-H bond in which is expected from the presence of MWCNTs. The intensity of the peaks suggest chemisorption nature of the bond.

Table 3.5 FTIR peak assignment of HA

Wave number expected (cm-1)	Wave number observed (cm-1)	Assignment
3572	3567	Stretching of OH
3450;1640	3343;1567	Stretching and bending mode of H_2O
1460;875	1454;875	Impurities (CO_3^{2-})
962	962	stretching of HPO_4^{2-}
1046;1087	1021	Symmetric stretching of PO_4^{3-}
565;606	560;600	Symmetric stretching of PO_4^{3-}

Transmittance(%)

V
IV
III
II
I

OH stretch

Absorbed H$_2$O

C-H

Absorbed H$_2$O

CO$_3^{2-}$

CO$_3^{2-}$

HPO$_4^{2-}$

PO$_4^{3-}$

4000   3500   3000   2500   2000   1500   1000   500

Wavenumber (cm-1)
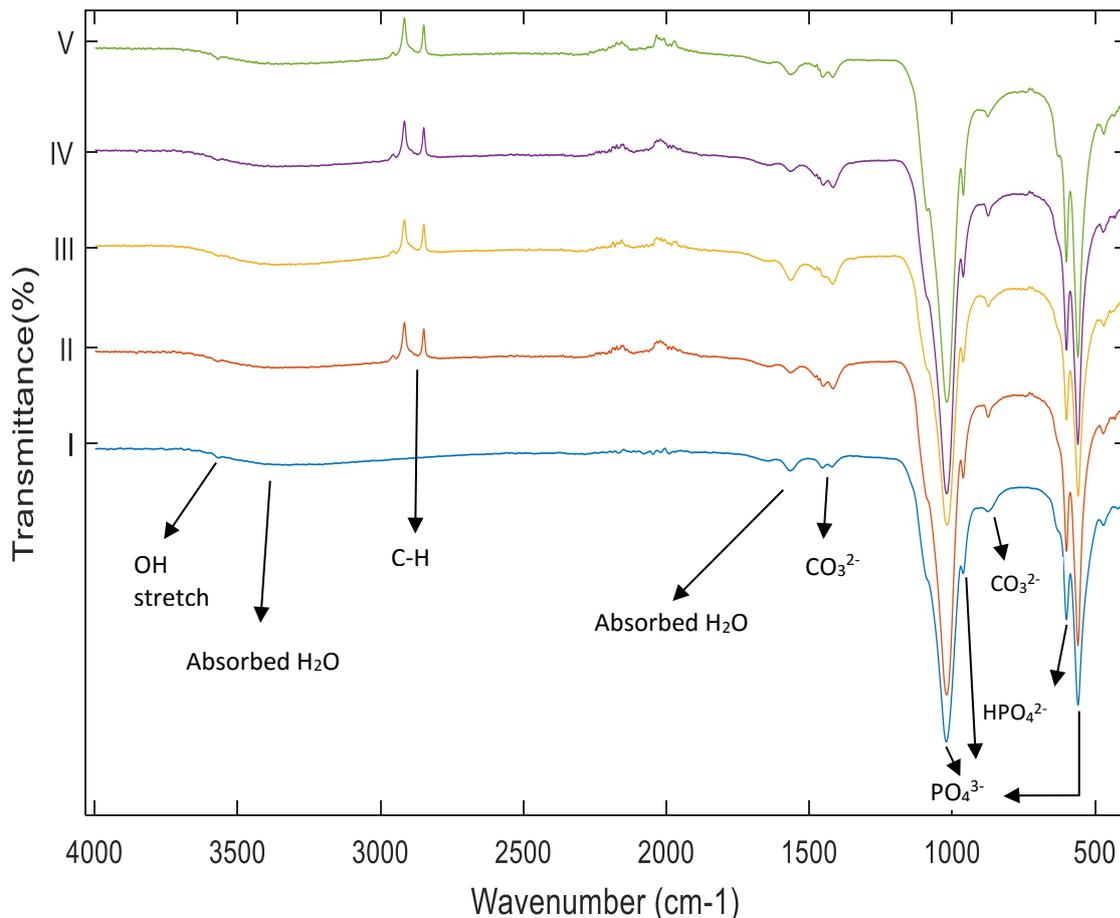
Figure 3.8 FTIR spectra of composite powders .(I) Pure HA, (II) HA-Ag NPs-*p*-MWCNTs-PVA, (III) HA-Ag NPs-*f*-MWCNTs-PVA, (IV) Ag NPs-*p*-MWCNTs-HTAB, (V) Ag NPs-*f* -MWCNTs-HTAB powders. Note the presence of C-H bond in all the powders except Pure HA due to the presence of MWCNTs. The arrows point to the absorbance peaks for the functional groups present in the powders.

3.5.4 HA-Ag NPs-MWCNTs composites characterisation

3.5.4.1 SEM and FTIR analysis of the final composites

The interaction between the HA, MWCNTs and PVA in the final composite is crucial in determining the mechanical strength of the composites. The interaction was investigated using SEM and FTIR analysis, while the degradation or dissolution of the composites in aqueous medium was analysed by performing the dialysis experiment in SBF. Figure 3.9 represents the SEM images of the final composites. The composites were examined following the mechanical test to study the interaction of the HA, MWCNTs and PVA within the composites. Figure 3.9A shows that the pure HA crystals were densely

packed and with no clumps of PVA visible in any of the composites. It can be seen that MWCNTS were forming bridges between the dense HA crystals where a crack has been formed in all the composites but no HA or Ag NPs are observed around the exposed parts of the MWCNTs.
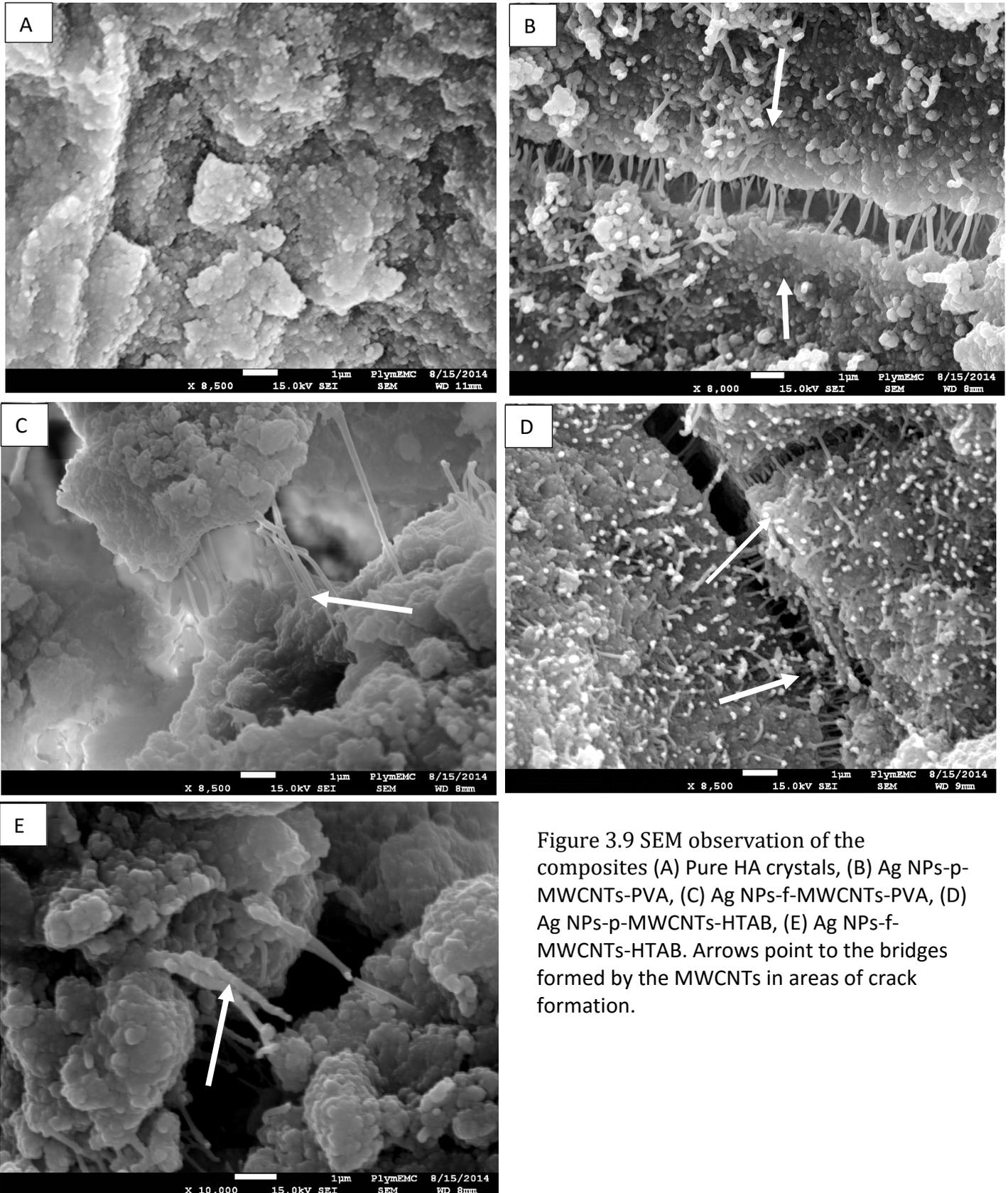
Figure 3.9 SEM observation of the composites (A) Pure HA crystals, (B) Ag NPs-p-MWCNTs-PVA, (C) Ag NPs-f-MWCNTs-PVA, (D) Ag NPs-p-MWCNTs-HTAB, (E) Ag NPs-f-MWCNTs-HTAB. Arrows point to the bridges formed by the MWCNTs in areas of crack formation.

FTIR analysis of the final composites were performed to determine the bonding between the powders and the PVA. Figure 3.10 represents the FTIR spectra for the composites and the reference peak for PVA. Similar to the powders, all the important peaks corresponding to HA were present in the expected positions. The peak corresponding to the MWCNTs was not visible. However, the peaks corresponding to PVA was observed in all the composites.
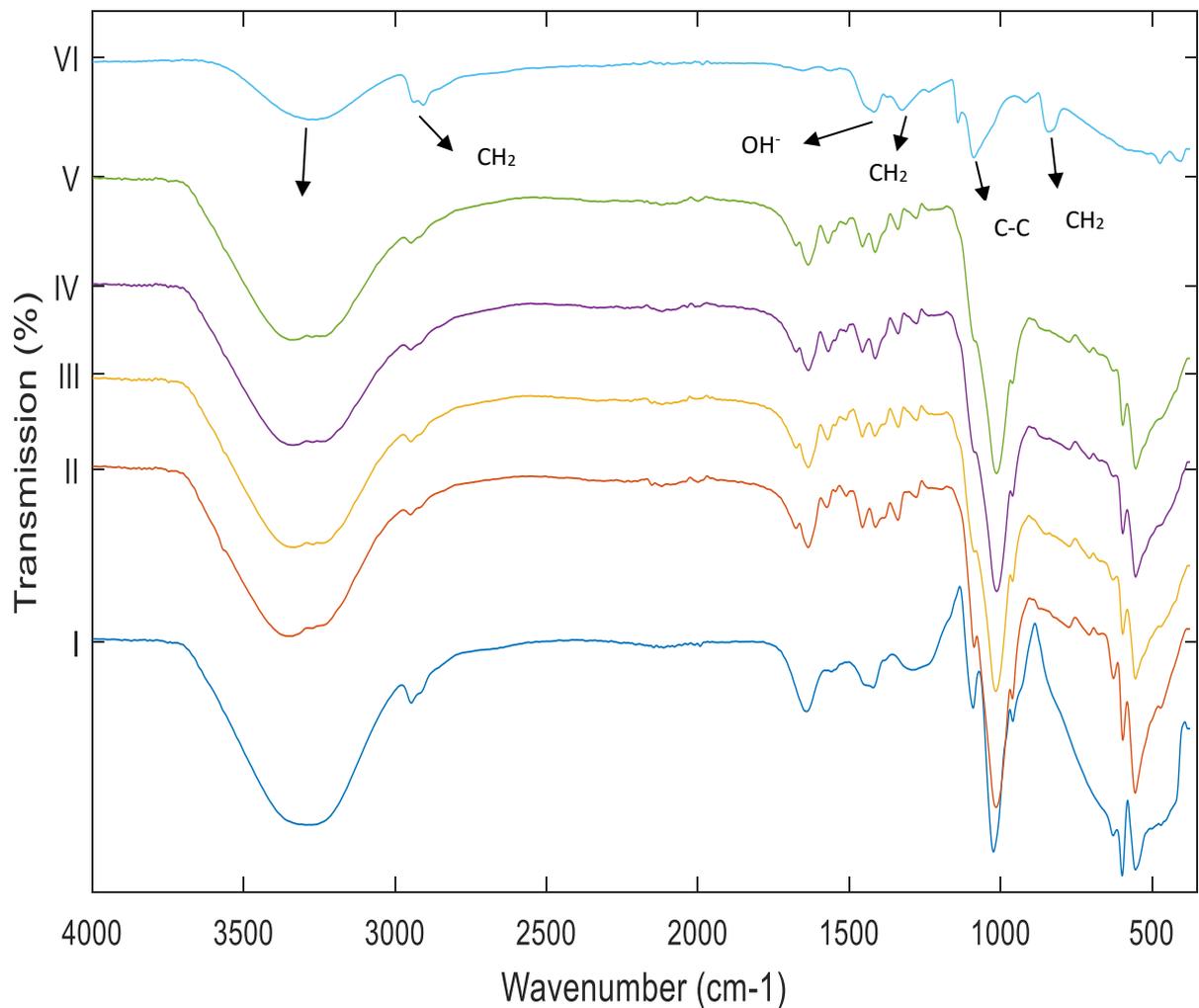
Figure 3.10 FTIR spectra of final composites. (I) pure HA composite, (II) Ag NPs-p-MWCNTs-PVA, (III)Ag NPs-f-MWCNTs-PVA, (IV)Ag NPs-p-MWCNTs-HTAB, (V) Ag NPs-f-MWCNTs-HTAB, (VI)PVA (reference). The arrows point to the absorbance peaks for the functional groups present in PVA .

3.5.4.2 Dissolution of silver from the composite materials

The dialysis experiment was conducted to determine the release of silver from the composites and the possible degradation of the composites in SBF. The results of the dialysis experiment showed that the total Ag release was high from composites containing *p*-MWCNTs. Overall, the maximum total dissolution from the composites was around 6 ug/l or less (Figure 3.11A). The concentration of Ag in the beaker was 3.3, 0.2, 2.2, 0.6 µg/l from p-MWCNTs-PVA, f-MWCNTs-PVA, p-MWCNTs-HTAB, f-MWCNTs-HTAB, respectively at the end of the first hour of the experiment. The saturation point for Ag release from the composites containing *p*-MWCNTs was reached by the sixth hour whereas the concentration of Ag in the beaker had not levelled out even after 24 h in the composites containing *f*-MWCNTs.

To investigate the effect of the composites on electrolytes and to determine the degradation of the composites, the concentration of electrolytes (Calcium, potassium, magnesium and phosphorus) were also measured over 24 h (Figure 3.11). The results show a reduction in the concentration of calcium in the SBF from the beaker for all the composites (Figure 3.11 B) whereas no major changes in the concentration of phosphorus was observed (Figure 3.11 D). Similar to calcium, the concentration of magnesium decreased over time whereas potassium stabilized after 4h (Figure 3.11 C and E).
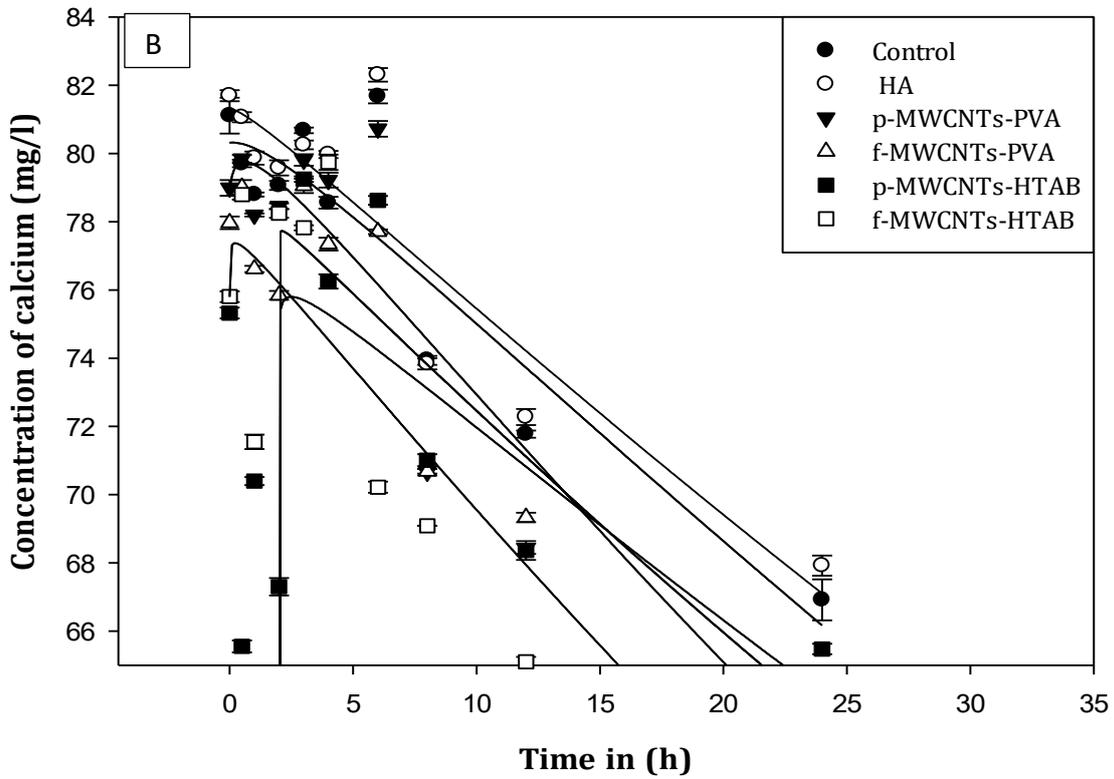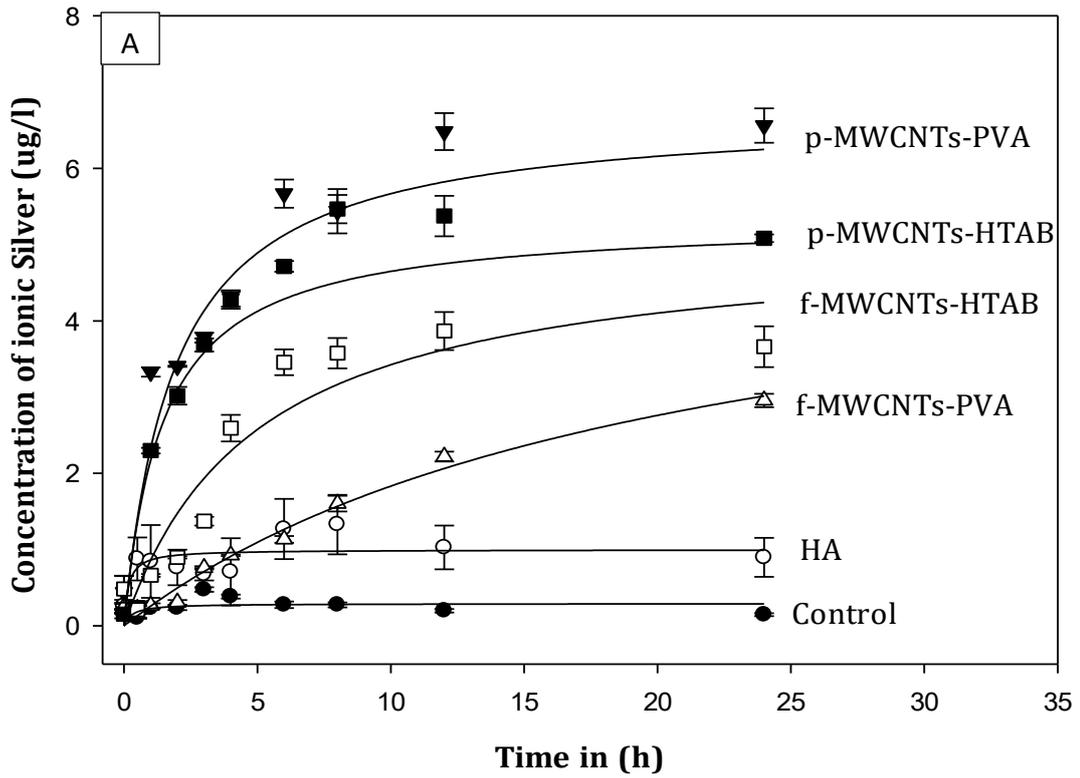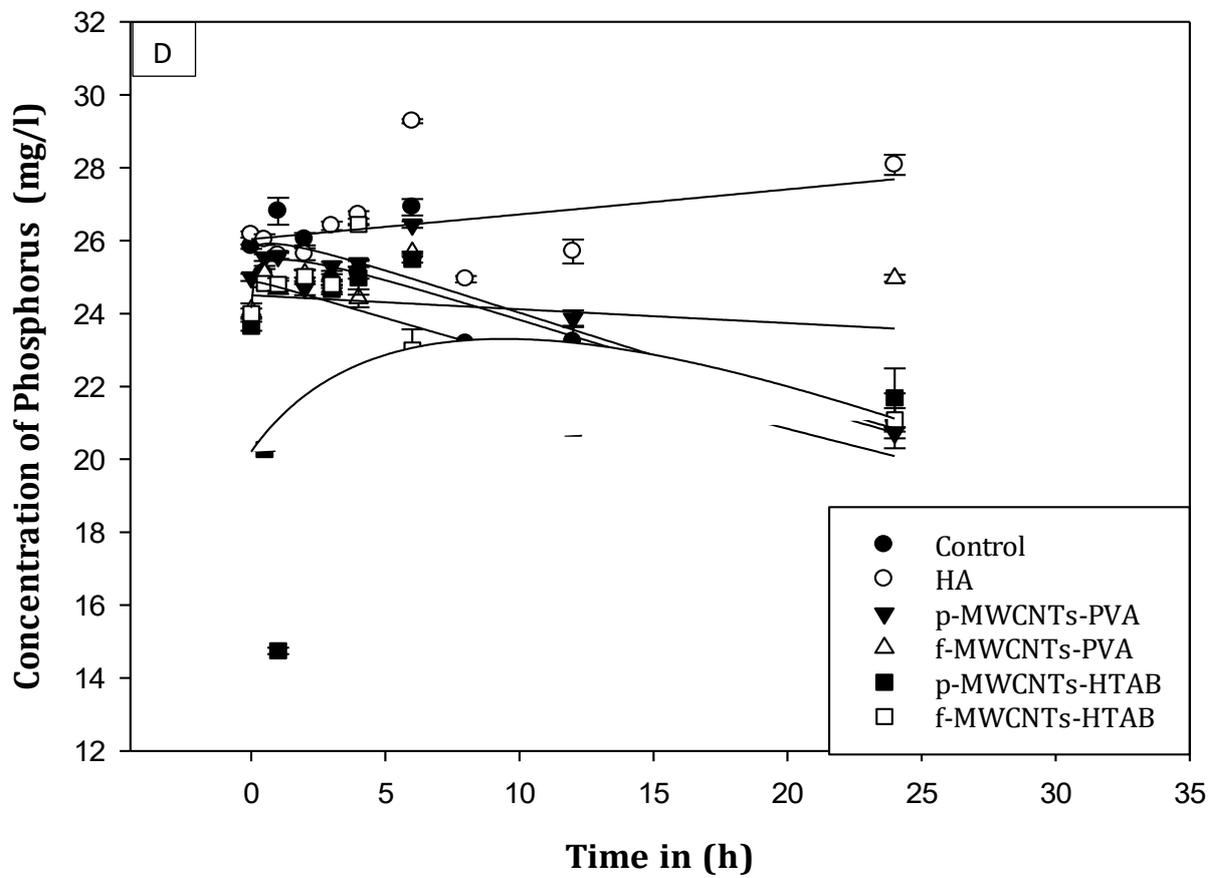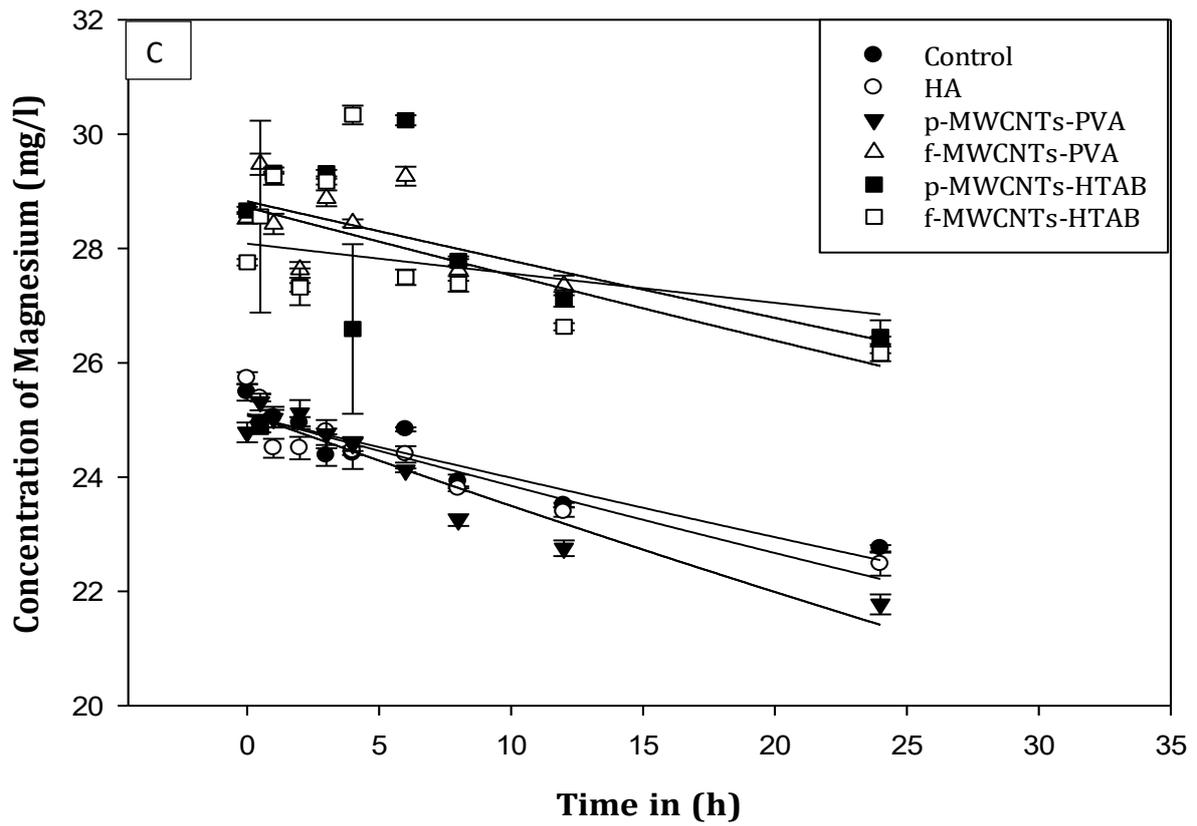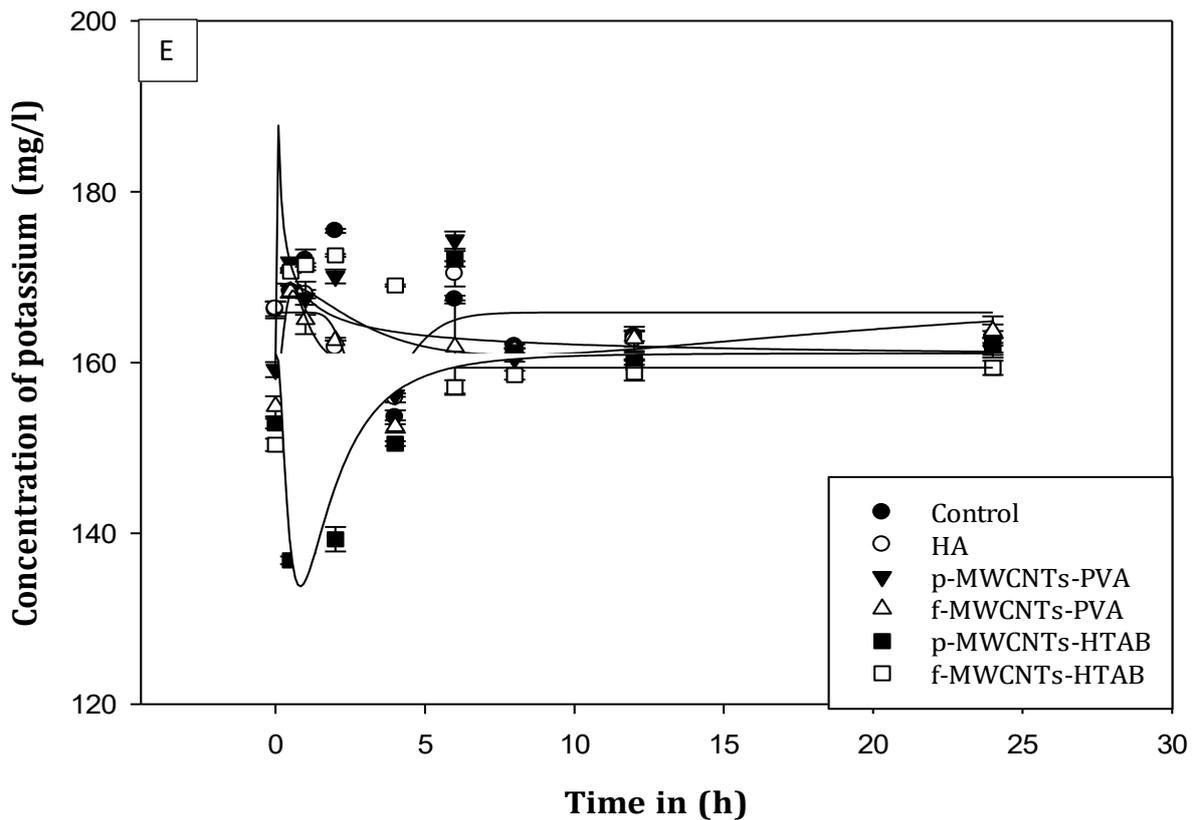
Figure 3.11 Dialysis curve showing the total release of (A) silver (µg/l), (B) Calcium (mg/l), (C) Magnesium (mg/l), (D) Phosphorus (mg/l), (E) Potassium (mg/l) from the different composites through dialysis tubing into the external SBF of the beakers. Data expressed as mean ± S.E.M (n= 3 per treatment). Curves were fitted to the mean data points shown using a single rectangular hyperbola function in SigmaPlot version 13.

3.6 Mechanical strength results

The tensile and compressive strength test results of pure HA nanocomposites (control) and all the treatments (Ag NPs-*p*-MWCNTs-PVA, Ag NPs-*f*-MWCNTs-PVA, Ag NPs-*p*-MWCNTs-HTAB, Ag NPs-*f*-MWCNTs-HTAB) after 48 h curing are presented in Figure 3.12. The tensile strength of all the composites were significantly higher than the pure HA composites. There was a significant difference in the tensile strength between all the composites. The maximum tensile strength was observed in the composite made of *p*-MWCNTS-PVA which was an increase of 215 % compared to the pure HA composite. The least tensile strength among the composites containing MWCNTs was observed in the *p*-MWCNTs-HTAB which was 49 % less than the *p*-MWCNTS-PVA composite.

However, the maximum compressive strength was observed from the composite made of f-MWCNTs-PVA, which was significantly higher than the other composites. This was an increase of 100% compared to the pure HA composite. Unlike tensile strength, no significant difference in compressive strength was observed between the composites containing HTAB surfactant but they were significantly lower compared to the composites containing PVA.
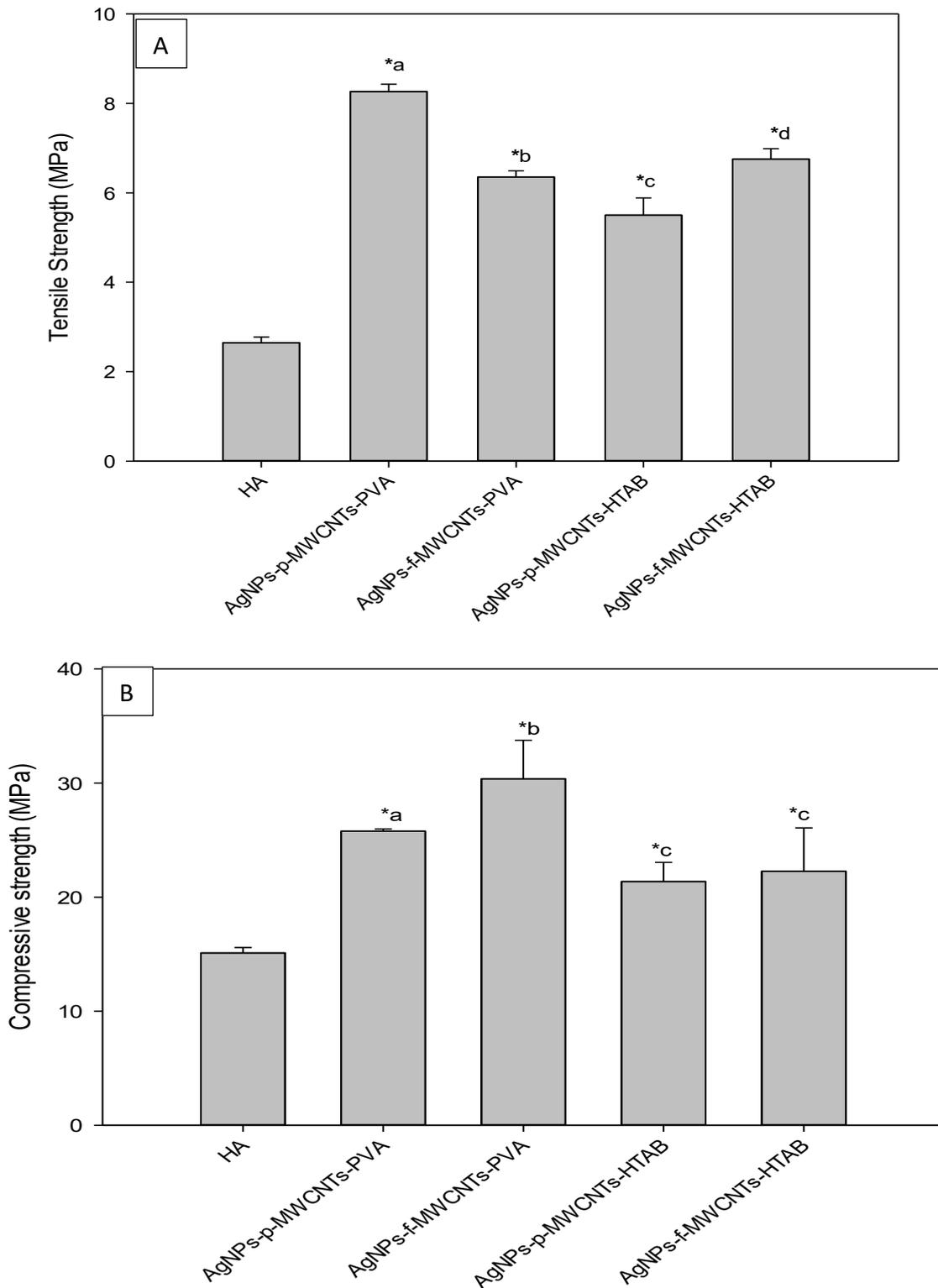
Figure 3.12 Mechanical strength of the composites. (A) tensile strength of the composites after curing for 48 h. (B) Compressive strength of the composites after curing for 48 h (n= 5 per composite for each test). * statistically different from the control (pure HA composite). Within each test, different letters represent statistical difference between the composites.

3.7 Discussion

This chapter focuses on the synthesis of the Ag NPs-MWCNTs-HA composites, their characterisation and their mechanical properties. The Ag NPs were doped onto the MWCNTs which was then dispersed in the presence of PVA or HTAB as a surfactant during the synthesis of the HA. The powders were produced by the wet sol-gel technique and the final composites were made by mixing 20% PVA with the powders in a 1:1 ratio and cured at 40 ° C for 48 h. Overall, the results show that HA was the primary constituent of the powders. The reinforcement of the MWCNTs in the HA matrix improved the mechanical properties of the composites.

3.7.1 Interaction between Ag NPs and MWCNTs

The difference in the interaction between the *p*-MWCNTs and *f*-MWCNTs can be observed in the TEM images (Figure 3.5). On the surface of the *f*-MWNTs the Ag NPs were uniformly distributed without agglomeration and their sizes were also uniform. The oxidation process adds the oxygen containing functional groups such as OH, COOH on the surface of the MWCNTs. The functional groups along with the surfactant enables the dispersion of the MWCNTs in aqueous media with high stability due to charge repulsion and colloidal dispersion. The functional groups introduce more anchoring sites for the silver ions. During the reduction process of $AgNO_3$, the Ag NPs anchor to these site resulting in their uniform distribution on the outer walls of the MWCNTs. In the case of *p*-MWCNTs, many clumps of Ag NPs were randomly distributed hence it is possible that no uniform bonding between the Ag NPs and MWCNTs existed. Although DMF has an oxidation property, the effect was not sufficient to anchor the Ag NPs on the sidewalls of the MWCNTs and achieve a uniform distribution. Some Ag NPs were also found inside the

MWCNTs which must have formed by the diffusion of the Ag ions into the tubes forming silver particles.

3.7.2 Effect of the surfactants in the dispersion of the MWCNTs and its effect on the growth of HA crystals

Observation by eye were made of the MWCNTs dispersion in water (Figure 3.3 and 3.4). The f-MWCNTs-HTAB had the most homogeneous dispersion whereas *p*-MWCNTs without the addition of surfactants showed the least dispersion. This is because, even if the MWCNTs solution was subjected to sonication, the dispersion is unstable and the nanotubes rebundled quickly. With the presence of surfactants, when individual nanotubes are cleaved from the bundle through the force induced by sonication, the surfactant acts on the entire length of the tube in an unzipping mechanism until full separation of the tube occurs (Fernandes et al., 2015). The solution then becomes a kinetically stabilized colloidal dispersion which is stable due to the presence of steric repulsion (Fernandes et al., 2015). The presence of the functional groups on the sidewalls of the oxidised MWCNTs aids this process by increasing the wettability of the nanotubes. However, the exact mechanism by which the surfactant absorbs on the entire length of the MWCNTs is still not clearly understood.

The presence of PVA or HTAB in the Ag NPs-MWCNTs powders cannot be verified using XRD and FTIR due to the miniscule amount being used during the synthesis process. Furthermore, during the filtration process the surfactants would have been filtered out. However, the TEM images (Figure 3.6) show that the surfactants also play a role in determining the morphology of the nucleating HA. Surfactants can stabilize the nucleating HA and reduce the agglomeration (Zhang and Dong, 2015). The adsorption property of the surfactants forms a layer of molecular resistance on the solid liquid

interface to stop the collision between the growing grains. Another way to look at this is that surfactants lower the surface tension at the interface between the particles. PVA is a non-ionic, polar, water-soluble polymer with -CH, -CH$_2$, and -OH as side groups and HTAB is a cationic surfactant with -CH$_3$, -CH$_2$, and -Br. When the calcium source (calcium acetate) is added to the solution in the presence of dissolved PVA, the Ca^{2+} ions attach to the OH$^-$ group in the PVA and when phosphate source (ammonium phosphate) is added, PO$_4^{3-}$ ions bind to the –OH-Ca^{2+} group. The PVA then regulates the growth of the HA crystals along the c-axis giving the crystals the needle structure (Mollazadeh et al., 2007, Rajkumar et al., 2010). In our study, 0.05 wt% of PVA was added to disperse the MWCNTs in the solution. This low concentration of PVA has created a positive effect on the nucleating HA. However, Rajkumar et al. (Rajkumar et al., 2010) has reported that if the concentration of PVA in the solution is increased by 2.5 wt % it results in the formation of crystals with irregular structures combined with a reduction of the crystal size, so high concentrations of PVA should be avoided.

Conversely, HTAB is an organic cationic surfactant, which has the same charge sign as the nucleating HA which causes a coulombic repulsion (Shiba et al., 2016). Coulombic repulsion is the force between like charges as described by Coulomb's law. Hence, the interaction of the surfactant and HA is weaker compared to that of PVA. The HTAB molecules are mainly absorbed with their positively charged head group directed towards the HA surface. According to Chen et al. (Chen et al., 2004) the absorption density of HTAB is higher compared to anionic surfactants. Owing to the higher absorption density and the presence of coulombic repulsion, the small HA particles are much more stable in the presence of HTAB.

3.7.3 Factors contributing to the mechanical properties of the composites

The main intention of reinforcing HA with MWCNTs was to improve the mechanical strength of synthetic HA and to serve as anchorage points for the Ag NPs. Significant increase in both the tensile and compressive strength was observed in all the composites containing MWCNTs and the maximum tensile strength was observed in the composite containing *p*-MWCNTs. The SEM images (Figure 3.9) of the composites shows that the MWCNTs were forming bridges between the cracks. One main factor that contributes to improve the strength of the composite is the interfacial bonding between the matrix and MWCNTs (Shin et al., 2011, Khalid et al., 2015).

In biomedical applications, functionalised MWCNTs are preferred since pristine MWCNTs tend to agglomerate due to the presence of Van der Waals force (Rosca et al., 2005, Datsyuk et al., 2008). This reduces the uniform dispersion of CNTs in a composite, which in turn might affect the mechanical strength of the composite as the interfacial bonding will be affected ultimately affecting the load transfer between the HA and CNTs. Furthermore, based on the synthesis technique, pristine CNTs are sometimes covered in toxic catalytic metals which were used during the synthesis process. These impurities induce the formation of reactive oxygen species in-vitro and causes oxidative damage (Chłopek et al., 2006). To purify, breakdown the bundles of CNTs to individual tubes and to introduce functional groups on the sidewalls that increase the surface area, CNTs are chemically functionalized using strong acids. However, the acidic oxidative treatment causes major alteration to the structural properties of the carbon rings. Acid treatment introduces structural carbon defects and atomic vacancies that degrade the mechanical strength of CNTs by an average value of 15% (Garg and Sinnott, 1998). This effect can be observed in the tensile strength of the composite (Figure 3.12). (Rosca et al., 2005)

suggest that concentrated acids not only generates functional groups, but also amorphous carbon by shortening and thinning of the MWCNTs. These processes cause a continuous increase of the defective sites. Thus, most of the short thin MWCNTs in pristine MWCTs will be lost during the functionalization process and the long thin MWCNTs will be reduced to short thin MWCNTs which affects the mechanical properties of the composites.

Nevertheless, the mechanical behaviour of MWCNTs in composites is much more intricate. Various other factors play a crucial role in determining the overall mechanical properties of the composite such as the crystal structure of the nucleating HA, the effect of surfactants on the nucleating HA , the aging time which includes dissolution of smaller crystals to favour recrystallization of the larger ones and the interfacial bonding between the HA and the MWCNTs. The results obtained in this study establishes that pristine MWCNTs with PVA as surfactant have superior mechanical properties compared to the composites with functionalised MWCNTs. It is hypothesised that the presence of PVA as a surfactant combined with the longer MWCNTs are contributing factors to the improved mechanical strength (since all the other parameters were the same during the composite preparation).

3.7.4 Behaviour of the composites in aqueous media

Since the intended application of the composites is in the human body, it is essential to know the behaviour of the composites in aqueous media. Hence, the dialysis experiment was conducted by immersing the composites in SBF over a period of 24 h. The results shows that maximum release of Ag NPs was observed in the composites containing p-MWCNTs (Figure 3.11). This could be because the Ag NPs were not anchored

to the sidewalls of the nanotubes resulting in the release within the dialysis tubing. The higher presence of Ag NPs in the tube containing p-MWCNTs composites results in high concentration of dissolved Ag ions leaking to the SBF in the beaker. The Ag NPs could easily escape through the pores in the composite which is specifically beneficial as it wold immediately prevent the attachment of bacteria following surgery and reduce the possibility of infection. There is a constant decrease in the concentration of calcium over the 24 h. This could be either due to the precipitation of HA, since SBF contains calcium and phosphorus, it is expected that precipitation of HA would have commenced. Lu and Leng (2005) has shown that HA can precipitate in SBF and is stable compared to the other phases of calcium phosphate. The other possible explanation is the adsorption of calcium into the composites. Since the same effect is seen in magnesium and phosphorus, the latter might be true as the composites are porous. There is an initial fluctuation in the concentration of the electrolytes but they seem to stabilize after a few hours. This could be due to the porous nature of the material where the SBF inside the dialysis tubing could enter the composites and be trapped enabling the movement of the electrolytes from outside the bag to maintain equilibrium.

3.8 Conclusion

The aim of the study was to develop a composite which is mechanically strong, biocompatible to allow the proliferation of cells and provide bacterial resistance following surgery. The sol-gel technique was used to synthesise the Ag NPs- MWCNTs-HA composites. The overall characterisation of the synthesised powders and final composites show that HA was the primary phase of calcium phosphate. The Ag NPs had better interaction with the *f*-MWCNTs due to the presence of functional groups, which served as anchoring points compared to Ag NPs anchorage to *p*-MWCNTs. The surfactant played a role in determining the morphology of the HA crystals. The overall strength of the composites containing MWCNTs was significantly higher than the pure HA composites.

4. Investigation of the biocompatibility of the HA-MWCNTs composites with human osteoblast cells

4.1 Introduction

Biocompatibility is one of the prerequisites for the safety and efficacy of biomaterials that are used as bone implants since the material will be in intimate contact with the bone and connective tissues for a long period. Most of the composites that are used as implants will eventually undergo some form of degradation. Initially, degradation would be due to the sheer force during implant insertion whereas the long term factors which affect the degradation of the composites could be due to dissolution, pore size, porosity, and degree of crystallinity of the HA. This will lead to release of the reinforcement which in this case will be CNTs. Hence, attention should be paid to the biocompatibility of the composites and particularly the reinforcement (CNTs) on specific human cells because the toxicity of the material differs from one cell type to another. Hence, most of the studies that investigate the biocompatibility of the implant use bone or bone like cells such as primary human osteoblasts, osteoclasts and sarcoma cells (Saos-2) (Chlopek et al., 2006, Dawei et al., 2007, Coathup et al., 2013)

The aim of this study was to investigate the biocompatibility of the HA-CNTs composites on human cells. For this purpose, primary human osteoblast cells were used, since the composites will be in direct contact with the osteoblast cells in a real patient receiving a bone implant. The cell viability and metabolic activity of the osteoblasts were determined by performing biochemical assays such as lactate dehydrogenase activity, protein assays and alkaline phosphatase (ALP) assay to evaluate the biocompatibility of the composites. ALP is commonly used as a biomarker to evaluate the metabolic activity of the osteoblast cells as it plays an important role in the mineral formation by increasing the local concentration of inorganic phosphate (mineralization promoter) and by

decreasing the extracellular pyro phosphate (mineralization inhibitor) (Golub and Boesze-Battaglia, 2007). Moreover, the dissolution of the HA composite was also measured by measuring the concentration of the Ca^{2+} and PO_4^{3-} in the external media and cell homogenate. The concentration of the K^+, Na^+ and Mg^{2+} was also measured to investigate changes in the presence of the electrolytes in the presence of the composites.

4.2   Methodology

To determine the biocompatibility of the HA-MWCNTs composites they were produced without the addition of silver nanoparticles. The same synthesis process as described in section 3.2.3 and 3.2.4 was used to produce the following composites:

i.   *p*-MWCNTs-PVA – (HA + Pristine MWCNTs + PVA)

ii.   *f*-MWCNTs-PVA – (HA + Functionalized MWCNTs + PVA)

iii. *p*-MWCNTs-HTAB – (HA + Pristine MWCNTs + HTAB)

iv.   *f*-MWCNTs-HTAB – (HA + Functionalized MWCNTs + HTAB)

v.   HA - Pure HA composites (control)

4.2.1 Cell culture

Human osteoblast (HOB) cells (2nd passage) were obtained from Sigma Aldrich, Dorset, UK (Product code: 406-05A). The cells were thawed and grown in Dulbecco's modified eagle medium (DMEM, Product code: 11530596, Fisher Scientific, Loughborough, UK) supplemented with 10% fetal bovine serum (FBS, Product Code: 11563397, Fisher Scientific, Loughborough, UK) and 1% Antibiotic-antimycotic (contains penicillin, streptomycin and Gibco Amphotericin B; Product code: 11580486, Fisher Scientific, Loughborough, UK) referred to hereafter as "DMEM". Cells were cultured at the

density $1 \times 10^4/cm^2$ in 75 cm^2 flasks (Product code : CLS3290, Corning® CellBIND® Surface cell culture flasks, Sigma Aldrich, Dorset, UK) containing 15 ml of DMEM. The media was routinely changed every 3 days and the cells were sub-cultured when confluence reached 80-85%. To subculture, the cells were washed twice with phosphate buffer saline, D-PBS, (without added calcium and magnesium, Fisher scientific, 10708144) then tryptinized (2 ml of 0.1% trypsin and 1 mM EDTA, Fisher Scientific, 11560626) and suspended in fresh media, and then counted using a haemocytometer. The cells were grown in a humidified incubator at 37°C with 5% CO_2 and 95% air. The cells of passage 9 and 10 were used for the experiment below.

4.2.2 Experimental design

The experimental design involved exposing the osteoblast cells to the composites (Figure 4.1). Before exposing the cells, the composites were sterilized using Gamma radiation (dosage: 36.42-40.72 kGy, BD Biosciences, Plymouth, UK). Then, using sterile forceps, the composites (diameter of15 mm) were each carefully placed at the bottom of a 24 well plate (flat bottom sterile, tissue culture treated polystyrene microplate; 662160, Greiner bio-one, Stonehouse, UK). The cell culture plate containing all the controls and treatments was a unit of replication in the experimental design. Composites made of pure HA served as a positive control, while HOB cells grown in wells without the presence of any composites served as reference controls on each cell culture plate. The treatments were p-MWCNTs-PVA, f-MWCNTs-PVA, p-MWCNTs-HTAB, f-MWCNTs-HTAB. Each plate also had a well containing only DMEM without the presence of any cells to measure changes in pH. A total of 9 replicates (plates) were conducted on at least three separate days (i.e., triplicate runs of plates). Each well was cultivated with 600 µl of cell culture (2 $\times 10^4$ cells/ml) from the 9th and 10th passage of the stock cell culture and additional 400

µl of DMEM was added. The microplates were then incubated for seven days at 37°C under 5% CO_2 in atmospheric air to allow the cells to grow. The DMEM media was changed at 24 and 96 h to ensure the culture conditions were not limiting. Changes in pH, electrolytes (Na^+, K^+, Ca^{2+}, P and Mg^{2+}) and the presence of lactate dehydrogenase activity (LDH) were measured from the collected media at the two time points (24 and 96 h). Six of the replicates were used for biochemistry and 3 for microscope observation (see below).

For biochemistry, cell homogenates were prepared in hypo-osmotic buffer at the end of the experiment according to Gitrowski et al. (2014). Briefly, cells were carefully washed twice with 2 ml of isosmotic sucrose buffer ($300 mmol\ l^{-1}$ sucrose, 0.1 mmol l^{-1} ethylenediaminetetraacetic acid (EDTA), 20mmol l^{-1} 4-(2-hydroxyethyle)-1-piperazineethanesulfonic acid (HEPES), buffered to pH 7.4 with a few drop of 2 molar Trizma base). The cells attached to each composite were then treated with 1 ml of a lysis buffer (hypo-osmotic version of the buffer above consisting of $30 mmol\ l^{-1}$ of sucrose) for 5 min and then pipetted vigorously several times to remove the cells. The lysis buffer containing the cell homogenate was sonicated in a bath for 30 s to ensure the homogenate was well mixed and that any remaining cells were lysed prior to storage at -80 ˚C.

Materials tested

Blank (cells, reference control)

HA (Positive Control)

T1 - *p*-MWCNTs-PVA

T2 - *f*-MWCNTs-PVA

T3 - *p*-MWCNTs-HTAB

T4- *f*-MWCNTs-HTAB

X9 repeats; incubated at 37 ° C with 5% CO_2 for 24 h

X6 repeats for Assays

X3 repeats for SEM analysis

Cell culture

Composite at the bottom of the well

X6 repeats for Assays

From the external media (Days 1,4 and 7)
1. pH
2. Lactate dehydrogenase activity x3 /repeat/treatment
3. Ion concentration measurement (Na^+, K^+, Ca^{2+} and PO_4^{3-})

External media was removed on day 7, the composites were washed twice, and the cell homogenate was prepared in hypo-osmotic buffer

From the cell homogenate
1. Protein assay x3 /repeat/treatment
2. Lactate production x3 /repeat/treatment
3. Alkaline phosphatase x 3 /repeat/treatment
3. Ion concentration measurement (Na^+, K^+, Ca^{2+} and PO_4^3)

Figure 4.1 Schematic representation of the experimental design. The different treatments and control were placed in the 24 well plates (n=9 plates). The media was changed on day 1, 4 and 7 of which six repeats were used to measure pH, electrolytes, LDH. The cell homogenate was obtained at the end of the experiment on day 7 which was used to measure the electrolytes, LDH, ALP and protein content. Three repeats were used for SEM analysis.

115

Fresh aliquots of the cell homogenate were used for the assessment of LDH activity, ALP activity, protein content and the electrolyte composition (total Na^+, K^+, Ca^{2+}, P and Mg^{2+}) of the cells.

4.2.3 Lactate Dehydrogenase activity

The presence of lactate dehydrogenase activity in the external media (DMEM) was used to assess the general health of the cells (i.e., membrane leak of this normally cytosolic enzyme). In addition, the LDH activity in the cell homogenates was also measured. Briefly, LDH activity was measured according to (Campbell et al., 1999) with minor modification. The collected DMEM and cell homogenates were gently centrifuged for 1 min at approx. 13,000x g (Heraeus pico 17 centrifuge, Product code: 75002401, Thermo electron crop, Paisley, UK) to remove debris. Then, 100 µl of the supernatant from each sample was added to 2.9 ml of a reaction mixture consisting of 2800 µl of 6mM pyruvate in 50mM of phosphate buffer (pH 7.4) and 100 µl of 6mM nicotinamide adenine dinucleotide (Product code: B3012, Melford Laboratories Ltd, Suffolk, UK), directly in a 3 ml cuvette. The change in absorbance was measured immediately over 2 min at 340 nm (Helios β Spectrophotometer, Product code: 14-2982046, Fisher Scientific, Loughborough, UK). LDH activity was calculated using the extinction coefficient of NADH at 340 nm of 6.3 mM and a 1 cm path length. The cell homogenate LDH was normalized with the homogenate protein content.

4.2.4 Alkaline phosphatase activity

Alkaline phosphatase is involved in the calcification of bone and is therefore of functional significance to osteoblasts as developing bone cells. The activity of alkaline phosphatase enzyme was measured using a colorimetric assay based on the hydrolysis

of para-nitrophenylphosphate (pNPP) to p-nitrophenol (PNP), a yellow-coloured substrate. Briefly, 65 µl of the cell homogenate was added to 595 µl of the reagent assay (265 µl of 0.1 M glycine buffer + 330 µl of 0.5 mmol l^{-1} pNPP in glycine buffer). The appearance of p-nitrophenol was measured spectrophotometrically at 405 nm (Helios β Spectrophotometer, Thermo scientific, England). ALP activity was calculated using an extinction coefficient of 18.3 mM for a path length of 1 cm. The cell homogenate ALP activity was normalized with cell protein content as above.

4.2.5 Acid digestion for electrolyte concentration analysis

The ion concentration in the external media and the cell homogenate was measured by following the protocol by (Gitrowski et al., 2014). Briefly, 500 µl of the external media and cell homogenate was transferred to 15 ml test tubes (Product code: 10262861, Fisher scientific, Loughborough, UK) to which 1 ml of concentrated nitric acid (70%) was added at 70 °C in a water bath for 4 h. The test tubes were allowed to cool overnight before opening them. The resulting acid digested samples were used to measure the electrolytes in the external media and the cell homogenate by inductively coupled plasma optical emission spectrophotometry (ICP-MS).

4.2.6 Protein Assay

The total protein content in cell homogenates was measured using the Pierce BCA protein assay kit (Product number: 23227, Thermo Fisher scientific, Loughborough UK). The assay was performed according to the manufacturer's instructions. Briefly, a working reagent was prepared by mixing reagents A and B in a 50:1 ratio. Twenty µl of the cell homogenate (in triplicate) was transferred to a 96-well microplate, to which 200 µl of the working reagent was added and carefully mixed. Plates were covered and incubated at

37°C for 30 min and absorbances were read at 562 nm on microplate reader (OptiMax Tunable microplate reader, Molecular devices, UK). A series of bovine serum albumin standards (2000, 1500, 1000,750, 500, 250, 125, 25, 0=blank mg/l) was used for calibration. Protein assay was used to normalise the biochemical assays (LDH and ALP) data and electrolytes from the cell homogenate.

4.2.7 Cell morphology

Morphology (shape and appearance) of the cells was regularly observed by light microscope to determine the health of the cells. The DMEM media appeared normal (no loss of the pH indicator or excessive cell debris). Light microscopy observations showed no signs of deterioration such as necrosis, detachment of cells from the substrate, granularity around the nucleus or obvious disruption of the cell membrane (i.e., no membrane blebs or cell swelling). At the end of the experiment, the presence and health of the cells were determined using a scanning electron microscope (SEM) (JEOL JSM - 5600LV, JEOL ltd, Japan). A separate run (n = 3) replicates were done for SEM work. After the media was removed, samples were washed twice with phosphate buffered saline (PBS) and fixed using 2.5% glutaraldehyde in 0.05 M cacodylate buffer at pH 7.4 for 2h. Fixed samples were dehydrated through a series of ethanols and then critical point dried. Samples were mounted on conducting carbon stubs and coated with gold in a sputter coater (EMITECH K550, Quorum Technologies, UK). SEM images were collected using a 15 kV accelerating voltage. The observations were conducted systematically, starting at a lower magnification (X30) to examine the distribution of the cells on the composites, and then at a higher magnification (X1000) to observe the morphology of the cell membrane, organelles and nucleus as well as to determine the attachment of cells on the composites.

4.2.8 Statistics

All data are presented as mean $\pm$ standard error and were analysed using statgraphics software for windows (version XVI.I). After descriptive statistics to determine normality, skewness or kurotosis, parametric data were analysed by ANOVA following a variance check (Levene's test) and non- parametric data analysed by Kruskal-Wallis. The differences between the treatments and controls at each time point, and time effects within treatment were evaluated using one-way analysis of variance (ANOVA). For treatment x time effects, a two-way ANOVA was also applied to the data. All statistical analysis used a 95% confidence limit, so the *p* values <0.05 were considered statistically significant.

4.3 Results

4.3.1 Growth and morphology of cultured cells

Initial light microscopy examination of the cells seeded on the 24 well plate after the seeding stage (24h) revealed no signs of cell death due to toxicity or infection. To determine the structural integrity and presence of any infection, cells were observed with naked eye and under light microscope throughout the experiment and the cell membranes were intact. A closer observation in SEM after seven days (Figure 4.2), displayed a typical osteoblast morphology with regular cell structure in the controls and the treatments. No major morphological differences were observed between the cells maintained under the various treatments. The cells had intact homogenous cytoplasm and were attached and flattened on the substrate surface. In all the treatments, the cells spread to cover essentially all available regions of the disk. Since the treatments had areas of uneven surfaces, the cells were often seen to form bridges between the gaps.
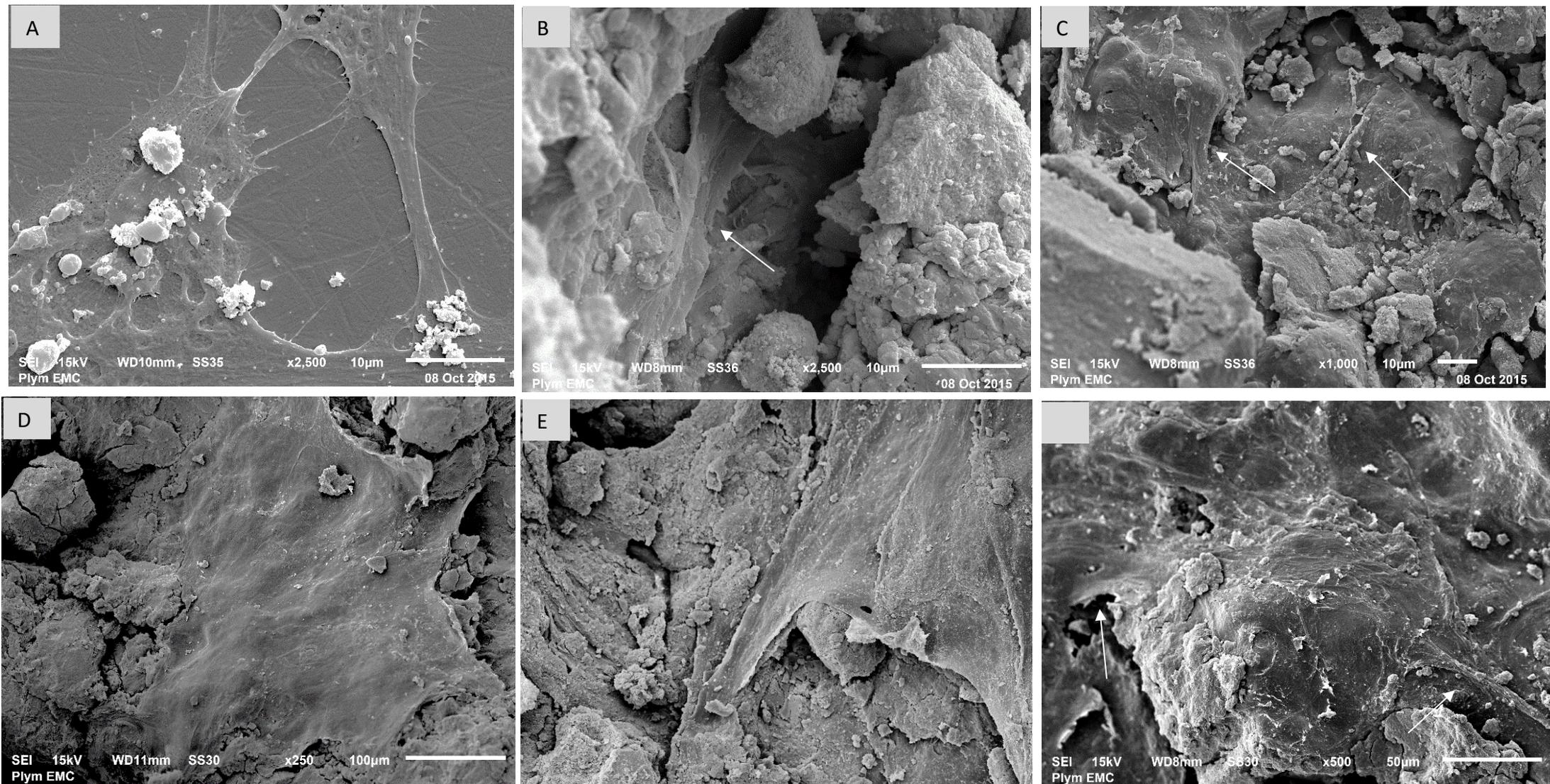
Figure 4.2 SEM images of the osteoblasts at various magnifications. (A) Control cells grown on the plastic plate; (B) cells grown on pure HA control, it can be seen that the cells have infiltrated into the pores (arrow); (C) shows cells grown on *p*-MWCNTs-PVA (arrow); (D) shows cells on *f*-MWCNTs-PVA, note that the cells are flat and extending to cover large surfaces of the substratum; (E) shows cells on *p*-MWCNTs-HTAB; (F)shows cells on *f*-MWCNTs-HTAB.

4.3.2 pH and ion concentrations in media and cell homogenates

The pH measurements of both the controls (reference and HA composites) and treatments were assessed and the values were compared against the reference DMEM. A drop in pH was observed in the media of the +ve control (pure HA composites), and all the treatments (Table 4.1) on all the days. This was significantly different ($p < 0.05$) to the values of reference control (HOB cells) and reference media (DMEM). No statistically significant difference in pH was observed between the reference control (HOB cells) with reference DMEM value. At the end of day 1, the pH value of the media for the pure HA and p-MWCNTs-PVA was found to be statistically more acidic (6.84±0.08; 6.76 ± 0.17) than the other treatments (all above pH 7). However, by the end of the experiment, recovery had commenced and the pH value of all the treatments was above 7.2. The value of negative control was at 7.9 which is slightly more alkaline than normal pH.

Table 4.1 pH measurements of the DMEM media exposed to the composites.

Material	Day 1	Day 4	Day 7
Media (no cells)	7.77 ± 0.02a	7.73 ± 0.01a	7.75 ± 0.04a
Blank (cells in DMEM)	7.75 ± 0.03a	7.74 ± 0.03a	7.91 ± 0.02a
HA	6.84 ± 0.08b	7.24 ± 0.04b	7.51 ± 0.02b
p-MWCNTs-PVA	6.76 ± 0.17b	7.20 ± 0.12bc	7.40± 0.09bc
f-MWCNTs-PVA	7.16 ± 0.06c	7.33 ± 0.04bcd	7.54 ± 0.08b
p-MWCNTs-HTAB	7.24 ± 0.03c	7.37 ± 0.03bd	7.62 ± 0.02b
f-MWCNTs-HTAB	7.18 ± 0.04c	7.26 ± 0.02bcd	7.59 ± 0.03b

Data expressed as means ±S.E.M (n=6 for each treatment). Different letters are statistically different from each other within the column (one-way ANOVA, p<0.05)

The electrolytes Na^+, K^+, Ca^{2+}, Mg^{2+} and P were measured in the external media on days 1,4 and 7 and from the cell homogenate (Table 4.2). The electrolyte composition of the media is as expected. The concentration of calcium and phosphorus in the treatments is significantly lower on days 4 and 7 compared to the reference control whereas in the cell homogenate it is significantly higher. Similarly, the concentration of the electrolytes

are higher in the treatments than the reference control (HOB cells) in cell homogenate

(Table 4.2)

Table 4.2 The total concentration of the electrolytes, Na$^+$, K$^+$, Ca^{2+}, Mg$^{2+,}$ and P (mg/l) in the media after exposing the osteoblasts to the composites for 7 days and from the cell homogenates (mmol/mg cell protein).

	Treatment	Day 1 (mg/l)	Day 4(mg/l)	Day 7(mg/l)	Cell homogenate (mmol/mg cell protein)
Sodium	Blank	259.6 ± 224.6	439.5 ± 476.5	395.5 ± 704.6	0.6 ± 0.1
	HA	413.4 ± 454.7*a	407.3 ± 600.2a	284.8 ± 270.3	16.1 ± 12.0*
	p-MWCNTs-PVA	238.8 ± 109.5b	318.6 ± 706.5ab	237.2 ± 283.1*	16.3 ± 13.8 *
	f-MWCNTs-PVA	281.1 ± 131.6b	241.5 ± 361.0*b	303.3 ± 350.5	20.3 ± 45.5*
	p-MWCNTs-HTAB	254.6 ± 83.3b	391.6 ± 551.7ab	278.6 ± 271.6	16.8 ± 7.2*
	f-MWCNTs-HTAB	238.6 ± 140.0b	327.8 ± 336.3ab	310.5 ± 413.2	17.3 ± 15.3*
Potassium	Blank	29.7 ± 25.6	49.7 ± 53.5	32.2 ± 58.2	0.2 ± 0.1
	HA	27.6 ± 39.4	38 ± 48.9ab	21.8 ± 20.5*	2.4 ± 0.7*a
	p-MWCNTs-PVA	25.3 ± 11.5	35.3 ± 77.6 ab	20 ± 29.3*	3.7 ± 1.2*ab
	f-MWCNTs-PVA	29.9 ± 11.2	26.3 ± 38.0*a	25 ± 30.5	6.2 ± 2.2*b
	p-MWCNTs-HTAB	25.1 ± 12.8	43.2 ± 63.6b	23 ± 24.1	4.3 ± 0.6*ab
	f-MWCNTs-HTAB	26.1 ± 17.6	38.8 ± 33.1ab	26.8 ± 33.8	5.4 ± 1.6*ab
Calcium	Blank	39.3 ± 3.3	67.7 ± 7.3	53.4 ± 9.4	0.6 ± 0.1
	HA	32.2 ± 6.7ab	34 ± 4.8*a	5.2 ± 1.9*a	1.3 ± 0.2 ac
	p-MWCNTs-PVA	19.8 ± 3.7*a	6.3 ± 2.3*b	12.8 ± 6.5*ab	1.5 ± 0.4*ac
	f-MWCNTs-PVA	38.2 ± 7.3b	9.3 ± 2.9*b	13.1 ± 2.8 *ab	1.8 ± 0.2*ac
	p-MWCNTs-HTAB	22.7 ± 5.5*ab	9.8 ± 1.5*b	24.5 ± 6.5*b	2.1 ± 0.3*b
	f-MWCNTs-HTAB	29.4 ± 4.5ab	3.1 ± 1.1*b	2.3 ± 0.3*a	1.2 ± 0.1ac

	Treatment	Day 1 (mg/l)	Day 4(mg/l)	Day 7(mg/l)	Cell homogenate (mmol/mg cell protein)
Phosphorus	Blank	122.1 ± 10.2	179.5 ± 20.9	142.3 ± 26.3	0.7 ± 0.2
	HA	202.7 ± 19.9 * a	180.5 ± 32.0a	90.6 ± 10.7ab	9 ± 19.1*a
	p-MWCNTs-PVA	125.6 ± 23.1b	120.5 ± 28.4*b	171.3 ± 43.0a	4 ± 14.1*b
	f-MWCNTs-PVA	90.7 ± 16.4b	46.5 ± 4.8*c	97.7 ± 36.8ab	6 ± 1.3*c
	p-MWCNTs-HTAB	107 ± 34.4b	50 ± 9.2*c	80.6 ± 19.3b	7.2 ± 1.5c*
	f-MWCNTs-HTAB	119.2 ± 20.3b	73.3 ± 9.7*bc	101.3 ± 28.8ab	2.6 ± 2.0b
Magnesium	Blank	22.2 ± 1.9	37.9 ± 4.1	30.6 ± 5.4	0.03 ± 0.0
	HA	1.2 ± 0.2*	1.3 ± 0.2*	0.4 ± 0.1*	0.06 ± 0.0a
	p-MWCNTs-PVA	1.1 ± 0.1*	1 ± 0.2*	0.8 ± 0.3*	0.1 ± 0.0*ad
	f-MWCNTs-PVA	1.5 ± 0.2*	0.8 ± 0.1*	0.7 ± 0.2*	0.1 ± 0.0*b
	p-MWCNTs-HTAB	1.1 ± 0.2*	1.3 ± 0.3*	0.6 ± 0.1*	0.1 ± 0.0*cb
	f-MWCNTs-HTAB	2 ± 0.3*	0.1 ± 0.0*	0.4 ± 0.1*	0.08 ± 0.0 *ad

Data expressed as means ±S.E.M (n=6 for each treatment). Different letters are statistically different form each other within the column. * indicate significant difference from the control within each column (one-way ANOVA or Kruskal –Wallis test, $p < 0.05$).

4.3.3 Total protein concentration in cell homogenate

At the end of the experiment, the protein concentration in the cells was stable and higher in the positive control (pure HA composites) and the treatments compared to the reference control (HOB cells) grown directly on the culture plates (Figure 4.3).
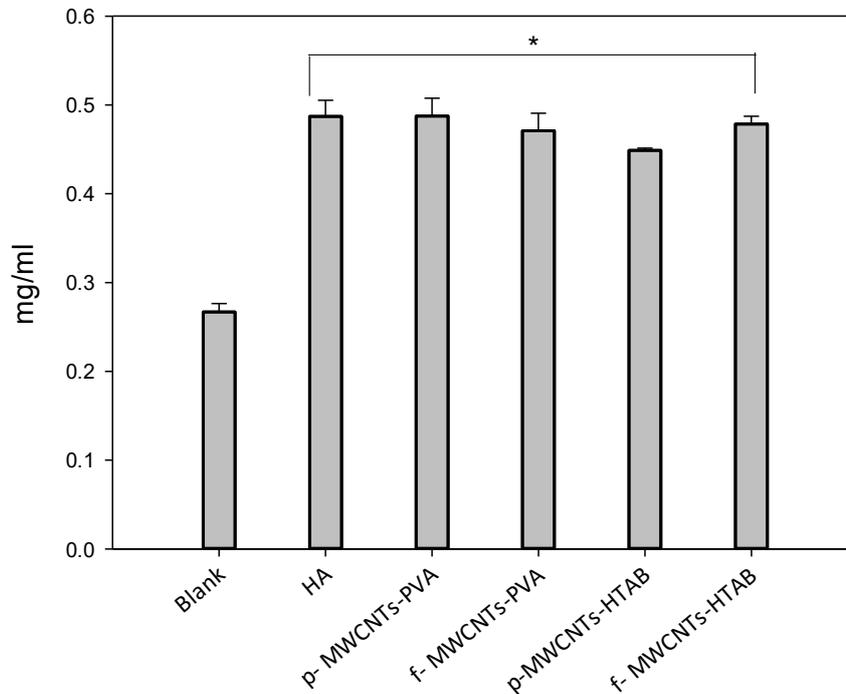
Figure 4.3 Total protein concentration from the cell homogenate after 7 days of proliferation on culture plate (blank, reference control), positive control (Pure HA composites), treatments (p-MWCNTs-PVA, f-MWCNTs-PVA, p-MWNTs-HTAB, f-MWCNTs-HTAB). Data are mean ± S.E.M (n=6), * indicates statistical difference (p=0.00) between the blank (reference control) and the composites. There were no differences between the composites.

4.3.4 Lactate Dehydrogenase

The LDH release to the media is one of the parameters that indicate cell injury. Table 4.3 shows the specific activity of LDH in the external media after 1, 4 and 7 days. Overall, the result shows that the treatments had higher LDH activity on day 1and the least on day 7, in contrast to the reference control (HOB cells). At day one, there was significant differences between *f*- MWCNT treatment compared to reference control

(HOB cells), whereas by day 4 and 7 there was no significant difference in the LDH activity between the treatments and the reference control (HOB cells) .

The activity of LDH was also measured in the cell homogenate to investigate the viability of the cells after 7 days incubation. The pure HA composite (positive control) did not show a statistical difference with the reference control (HOB cells). There was a significant difference in LDH activity of all the composite treatments compared to the blank with cells alone. No statistical difference was observed between the HA (Control) and p-MWCNTs–PVA treatments. Within the CNT treatments, statistical difference was observed between pristine and functionalised MWCNTs.

Table 4.3 Lactate Dehydrogenase activity in the external media (IU/ml of media) during exposure of the osteoblast cells to the HA composites reinforced with MWCNTs over 7 days.

Material	Day 1	Day 4	Day 7	Cumulative release
Control (HOB cells)	0.0063 ± 0.002	0.0119 ± 0.002	0.0127 ± 0.006	0.0310 ± 0.01
HA	0.0111 ± 0.003	0.0095 ± 0.003	0.0024 ± 0.001	0.0230 ± 0.008
p-MWCNTs-PVA	0.0135 ± 0.003	0.0063 ± 0.004	0.0024 ± 0.001	0.0222 ± 0.009
f-MWCNTs-PVA	0.0254 ± 0.008*	0.0119 ± 0.003	0.0048 ± 0.002	0.0421 ± 0.01
p-MWCNTs-HTAB	0.0190 ± 0.004	0.0056 ± 0.003	0.0127 ± 0.006	0.0373 ± 0.01
f-MWCNTs-HTAB	0.0262 ± 0.008*	0.0048 ± 0.001#	0.0048 ± 0.001	0.0357 ± 0.01

The data are presented as mean ± S.E.M (n=6); different letters within columns indicate significant difference, and absence of the letters means there is no significant difference. * Statistical significant difference from reference control within column. # statistically different from previous time point within row (one way ANOVA, $p < 0.05$)
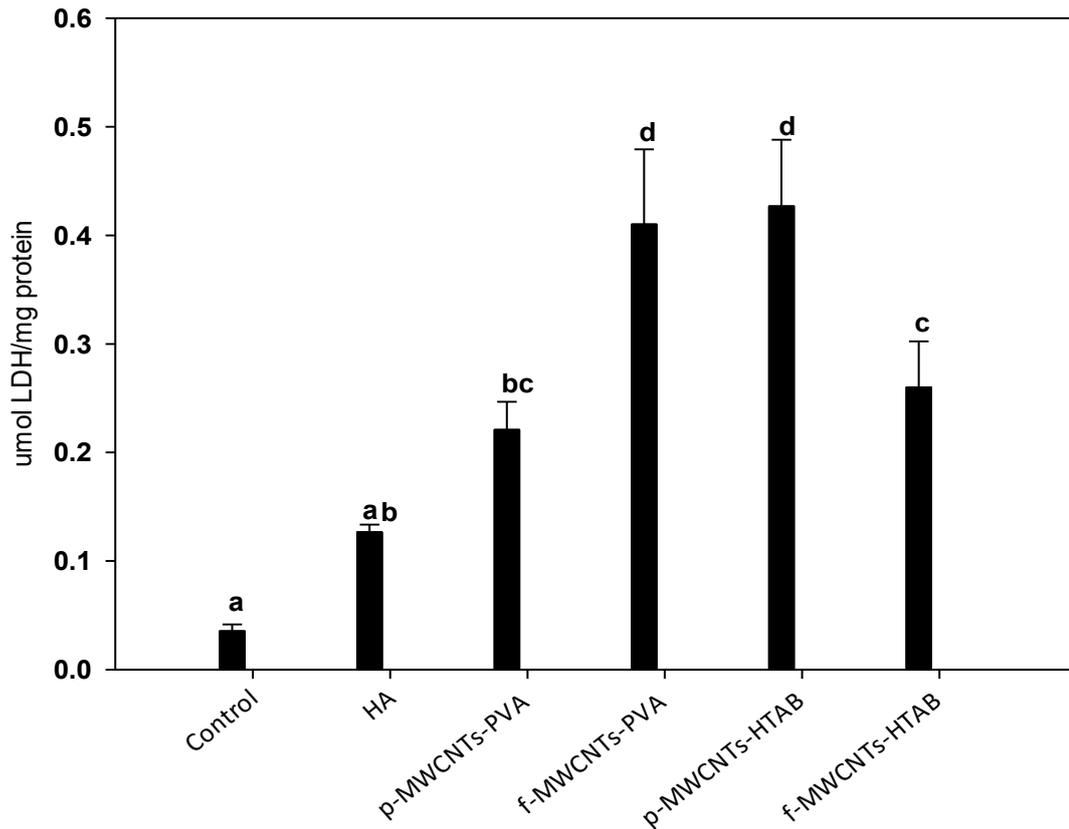
Figure 4.4. Comparison of the LDH activity from cell homogenate after 7 days of growth in DMEM on culture plate (Control, HOB cells), pure HA composite (positive control), *p*-MWCNTS-PVA, *f*-MWCNTS-PVA, *p*-MWCNTS-HTAB, *f*-MWCNTs-HTAB. Data are mean ±S.E.M (n=6), bars with different letter indicate statistical difference from each other (one way ANOVA, P<0.05)

4.3.5 Alkaline phosphatase activity

The presence of alkaline phosphatase activity in the cell homogenate was used as a measure of metabolically active osteoblast cells. Figure 4.5 shows the ALP activity (μmol/min/mg protein) in the cell homogenate after 7 days incubationtt. No significant difference was observed between the controls (Blank and HA composite). Significant differences were observed between *p*-MWCNTs-PVA, *f*-MWCNTs–PVA and *f*-MWCNTs-HTAB and the blank. However, no significant difference was observed between the MWCNT treatments.
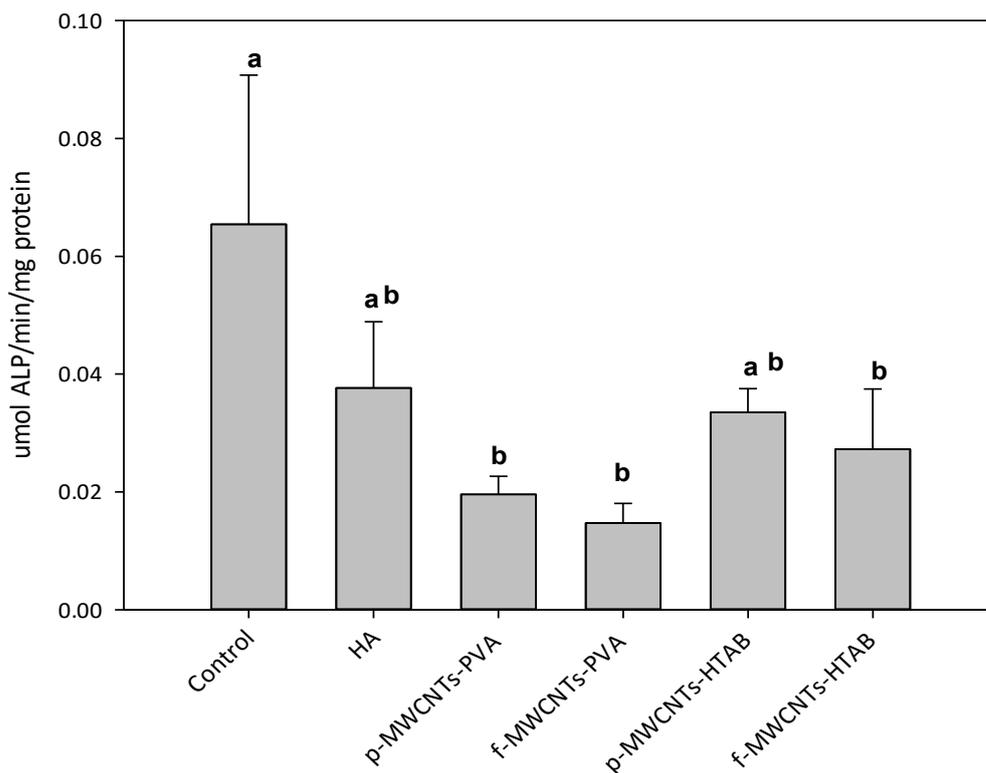
Figure 4.5 Alkaline phosphatase activity (ALP) from cell homogenates of osteoblasts after 7 days growth in DMEM on culture plate (reference, HOB cells), pure HA composite (positive control), p-MWCNTS-PVA, f-MWCNTS-PVA, p-MWCNTS-HTAB, f-MWCNTs-HTAB. Data are mean ± S.E.M (n=6), bars with different letters are statistically different from each other (one-way ANOVA, $P < 0.05$).

4.4 Discussion

The aim of the study was to evaluate the biocompatibility of the MWCNTs reinforced HA composites with human osteoblast cells. The main findings of this study was that the presence of MWCNTs did not adversely affect the growth of the osteoblast cells; and healthy-looking cells were observed on all the composites. Another finding was that no major difference in cell growth on the composites containing pristine and functionalised MWCNTs was observed, but the biochemical activity of the cells were different.

4.4.1 Effects of composites on DMEM media and evidence of dissolution

pH and electrolytes were measured in the external media since calcium phosphate based biomaterials can interact with their ionic environment in many ways including crystal growth, degradation and ion exchange (substitution). The overall pH and electrolyte measurements (Table 4.1 and 4.2) of the external media showed that the composites did not produce major changes in composition of the DMEM except for transient pH changes. Although, the physiological pH of the human body is approximately 7.4, it has been shown that local pH at wound site does not remain at physiological range and fluctuates between 5.45 to 8.65 at the various wound healing stages (Percival et al., 2014). Hence, from the clinical perspective, it is advantageous that the cells can survive in the transient acidity, as the implant will be introduced through surgery which would be similar to the wound environment.

The concentration of sodium and potassium in the external media is in the normal range (Table 4.2). Since sodium makes most of the osmotic content of the media, huge variation of this salt will result in cell death. However, that effect is not observed suggesting that the cells were healthy. Similar effect is also observed in the concentration of potassium which does not show significant difference between the control. However, the concentration of calcium in the media is significantly lower than the control confirming there was no dissolution of the composite. Calcium and phosphate from the DMEM was absorbed by the composite for apatite nucleation and crystal growth. Kokubo et al have shown apatite nucleation and growth of HA in SBF at physiologic temperature and pH (Kokubo et al., 1990). There are only trace amounts of calcium present inside the cells. If there is a membrane damage, the calcium could be released to the external media but no such effect is observed in cell homogenate of the osteoblasts grown on the

composites (Table 4.2). Similar to calcium, significantly higher quantities of phosphorus are observed in the cell homogenate of the composites suggesting that the osteoblasts were reserving calcium and phosphorus for the mineralization process. This result correlates with the reduction of phosphorus in the external media.

4.4.2 Effect of the composites on human osteoblast cells

Total protein content measurements from the cell homogenate (Figure 4.3) indicates cell growth. The higher protein content in the composites could be due to the adsorption of the proteins from the media to the composites. This could have been released into the lysis buffer during the vigorous pipetting used to lyse the cells while collecting the cell homogenate. Another possibility is that it could be an indication of the biocompatibility of the composites, as it is known that the surface topography of the composites plays a role in determining the adhesion and proliferation of the osteoblast cells. Studies led by (Yamashita et al., 2009, Zareidoost et al., 2012) have shown that cell attachment and proliferation on rougher titanium surfaces were significantly greater than smooth surfaces. Since the culture plate on which the reference control (HOB cells) were grown was smooth while the composites were rough uneven porous surfaces, it is possible that the adhesion and proliferation of cells were better. However, the other biochemical assays results (LDH and ALP) suggests that the former is more likely.

The LDH assay was used to measure the cytotoxicity of the composites on osteoblast cells due to cell membrane damage (Fotakis and Timbrell, 2006). The result of the LDH in the external media shows that the composites had no toxic effect on the cells because the concentration of the LDH in the external media from the treatments is not significantly different to the reference control (Table 4.3). One possible explanation

for the non-toxicity of the MWCNTs could be that when HA is nucleated in the presence of MWCNTs, the side walls of the tubes are covered with calcium phosphate and the cells do not come into direct contact with the MWCNTs. This can be seen in the TEM images from chapter 3, Figure 3.5 which shows that the MWCNTs are surrounded by HA particles.

Compared to the LDH activity in the external media, high amount of LDH activity was detected in the cell homogenate, which indicates that the cells were viable until the end of the experiment on day 7. However, compared to the blank (control), significantly high amounts of LDH activity was detected in the cell homogenate of the composites (Figure 4.4). There are two possible explanations for this. Since the composites are porous, it allows the cells to infiltrate into the composites providing higher surface area for the cells to proliferate. Osteoblasts adhere and proliferate well on rough and porous material, especially materials with pores size of 100μm magnitude (Boyan et al., 2002, Gough et al., 2004). The high LDH release could mean that the cell growth was higher in the composites compared to the control resulting in higher LDH activity. The other possible explanation is that the cells grown on the composites were damaged as a result of oxidative stress leading to the immediate release of the cell contents during the pipetting process.

The specific activity of ALP was measured as it increases the local concentration of the inorganic phosphate (Golub and Boesze-Battaglia, 2007). Hence, it is considered as an important biomarker to evaluate the activity of the bone cells; however, the exact mechanism by which ALP functions in hard tissues is still not clearly understood. The activity of this enzyme means the osteoblast cells are active and have the ability to differentiate and mineralize. The results showed that the activity of alkaline phosphatase

was decreased by the presence of the composites (Figure 4.5) which means that there is some impairment on the metabolic activity of the cells.

SEM analysis (Figure 4.2) of the cells grown on the composites shows that the cells are proliferating and covering the surface of the composites. Cells can also be seen infiltrating the pores and proliferating within the composites suggesting that favourable conditions for cell proliferation exists within the composites. However, a correlation exists between the LDH and the ALP results suggesting that although the human osteoblast cells grew and proliferated on the composites, they might be under stress resulting in reduced metabolic functions.

4.5 Conclusion

The intention of the current study was to determine the biocompatibility of the MWCNTs composites with human osteoblast cells. Overall results suggest that although cells proliferated on the treatment composites suggesting that they were biocompatible there was a decrease in the ALP activity suggesting that the mineralization ability of the cells could be compromised. Since the results are contradicting, further *in vitro* analysis needs to be performed for a longer period to analyse further changes in the LDH and ALP activity as ALP is a marker to determine the differentiation and mineralization ability of the osteoblast cells. Nevertheless, it can be concluded that MWCNTs when entrapped in a composite do not reduce cell viability.

5. Investigation of the antibacterial activity of the silver nanoparticle-multiwall carbon nanotube-hydroxyapatite composites against *Staphylococcus aureus*

5.1 Introduction

Among the most promising nanomaterials with antimicrobial properties are silver nanoparticles (Ag NPs). Ag NPs have been incorporated mainly into metal based implants as coatings to improve their antimicrobial properties (Juan et al., 2010, Zhao et al., 2011). However, the use of Ag NPs in the development of composites with other nanomaterials or micron scale biomaterials has not been adequately explored. Assuming that the antibacterial properties of any Ag-coated implant are derived from Ag ion toxicity, it is the stable controlled release of Ag ions from the composite that is one of the essential criteria that is difficult to obtain as most of the composites contain varying pore sizes and composition and will act differently when they come into contact with body fluids. In addition, the hazards of toxic metal particles in the systemic circulation are not fully understood, and so from a medical safety perspective it is desirable to ensure the Ag NPs remained fixed on the structure of the implant.

The aim of this study was to determine the antibacterial activity of the Ag NPs decorated MWCNTs–HA composites. This was done by exposing the composites to *S. aureus* for 24 h and determining the viability of the microbial cells both quantitatively and qualitatively.

5.2 Methodology

The methodology and experimental design was based on the work published by (Besinis et al., 2014) with some modifications. *S. aureus* as the major cause of implant related infection was chosen as the organism of study. The NCTC 6571 strain of *S. aureus*

was obtained from National Collection of Type Cultures, Public Health England and grown in Brain Heart Infusion broth (BHI, Product code: LAB049, LAB A Neogen company, Lancashire, UK) and incubated at 37°C in a shaker incubator overnight. A bacterial suspension having an optical density (OD, Helios Epsilon, UNICAM, Cambridge, UK) of 0.19 turbidity units containing approximately 10^7 CFU/ml was used for the experiments. An optimisation study was undertake prior to the main experiment to determine the appropriate optical density and to determine the incubation period for *S. aureus.*

5.2.1 Optimisation Study

The optimisation study involved using OD as a means to determine turbidity measurements which were used to calculate the number of CFU. Briefly, 100 μl of broth containing microbes were transferred to a sterile tube containing 10 ml of fresh sterile broth and mixed. 1 ml of this was transferred to a cuvette (Product code: 11954395, Fisher scientific, Loughborough, UK) and the OD was measured immediately. Additional broth containing microbes were transferred to the 10 ml broth and OD was measured until the value of 0.1 was achieved which is approximately 1×10^7 CFU/ml. To optimise the correct OD, the same procedure was repeated with varying OD values (0.25, 0.2, 0.15, 0.1 and 0.05). The varying concentrations were used to make serial dilution to reduce the dense culture of cells to a more manageable CFU which is in the range of 10-200 individual CFU. Serial dilutions were made up to 10^{-7} and 100 μl from 10^{-4}, 10^{-5}, and 10^{-6} dilutions were used to make spread plates. The plates were incubated overnight at 37 °C and the plates with countable colonies were counted. A graph was obtained (Figure 5.1) based on which the OD required for the study was determined.
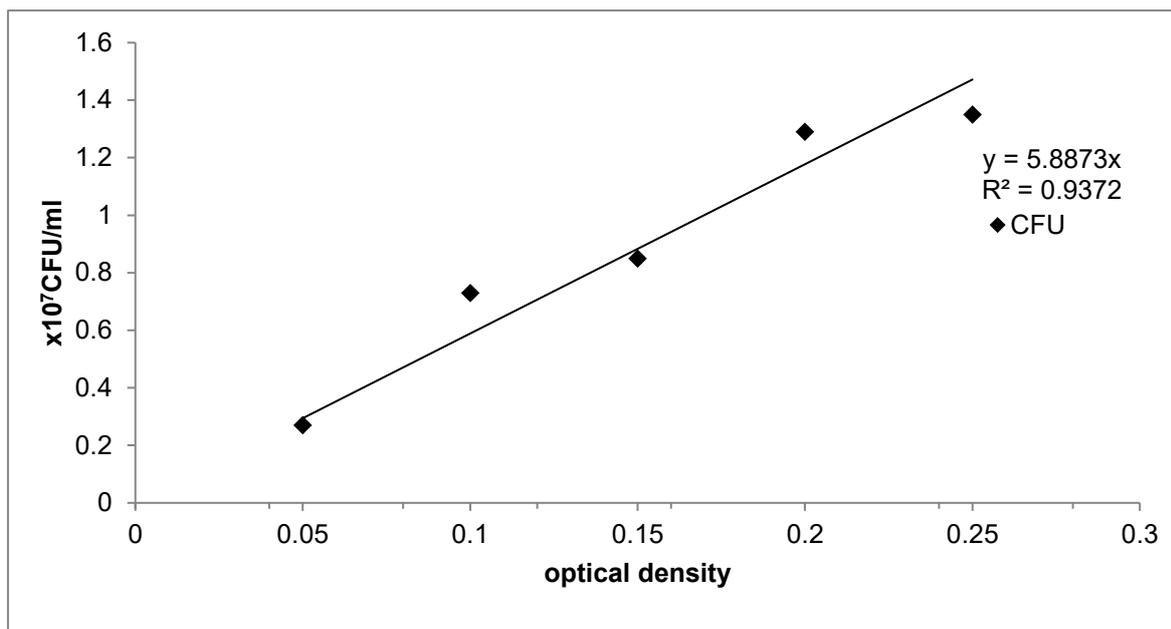
Figure 5.1 Representation of the CFU at the various OD values following incubation at 37 °C overnight. The optimal OD value for the study was chosen based on this optimisation study.

To determine the bacterial attachment to the composites following the initial 24 h incubation, the bacteria adhered to the composites were removed and incubated (see below). A growth curve study was undertaken to determine the optimum incubation period, which was based on the time (hours) it took for the bacteria to be in the log phase of growth. To determine the growth curve, 100 μl of broth containing mocrobes with an initial OD value of 0.01 was introduced into a flask containing 100 ml of fresh sterile broth which was then incubated at 37 °C on a shake table (MaxQTM 4450, Benchtop Orbital Shaker, ThermoFisher Scientific, Paisley, UK) for 24 h. The turbidity was measured every hour and the OD values were recorded. The growth curve was plotted based on the value obtained (Figure 5.2).
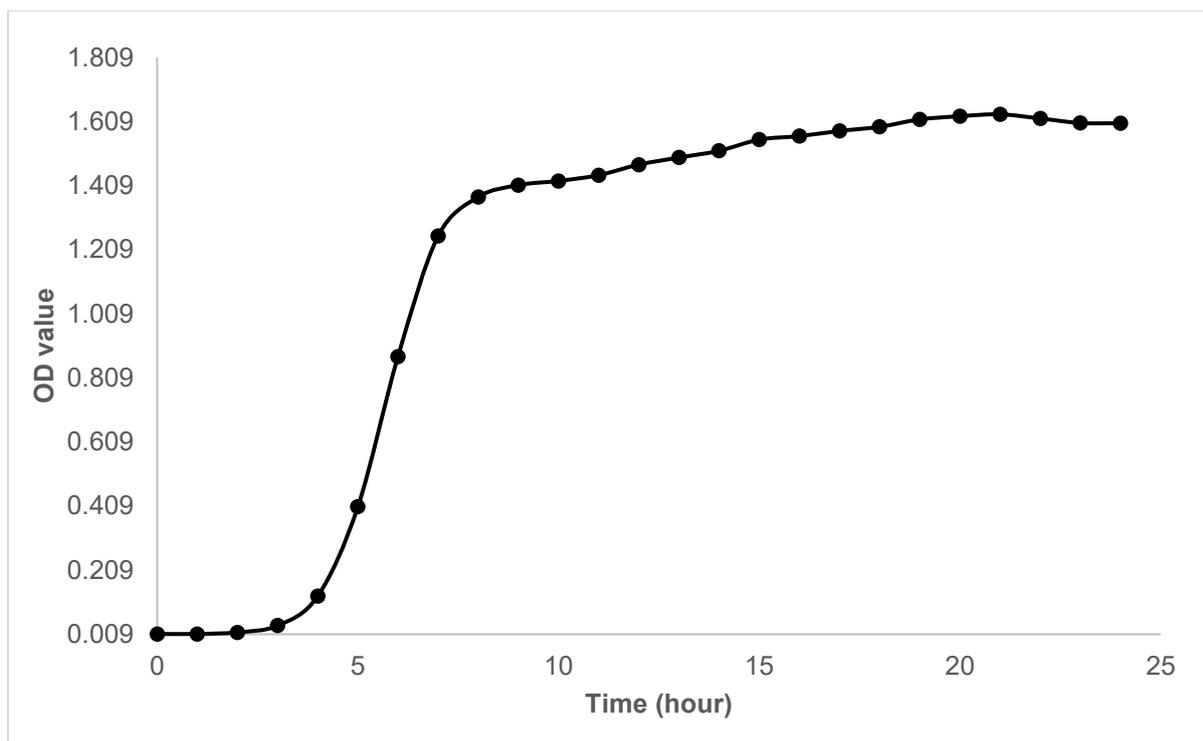
Figure 5.2 Growth curve of *S. aureus* over 24 h. The initial OD value was 0.009 and the values were read every hour for 24 h. Lag phase was observed for the first 3 hours following which log phase was observed for 4 hours. The microbes entered the stationary phase at the 8th hour.

5.2.2 Experimental design

The experimental design involved exposing *S. aureus* to the composites containing Ag NPs for 24 h in 24 well microplates (flat bottom sterile, tissue culture treated polystyrene microplate, Product code: 662160, Greiner bio-one, Stonehouse, UK) and compare it to its equivalent metal salt, AgNO$_3$ as a positive control. A pure HA composite was used as a negative control and the treatment composites were :

1. Ag NPs-*p*-MWCNTs-PVA – (HA +Ag NPs-Pristine MWCNTs + PVA)
2. Ag NPs-*f*-MWCNTs-PVA – (HA + Ag NPs -Functionalized MWCNTs + PVA)
3. Ag NPs -*p*-MWCNTs-HTAB – (HA + Ag NPs -Pristine MWCNTs + HTAB)
4. Ag NPs-*f*-MWCNTs-HTAB – (HA +Ag NPs- Functionalized MWCNTs + HTAB)

AgNO$_3$ solution (0.4 mg/l) was prepared to have the same dissolved amount of Ag available, as it would be from the composites sterilized by autoclaving (121 °C for 15 min

at 15 psi pressure). This was based on the results from the dialysis experiment (Chapter 3, section 3.5.4.2). The highest amount of Ag detected in the dialysis bags was used to determine the quantity of the $AgNO_3$ to be used for this study. All the composites were sterilised by Gamma irradiation (36.42-40.72 KGy for 10 h) due to concern that high autoclave temperature might affect the crystal structure and pore size of the composites. Figure 5.3 shows a schematic representation of the experimental design. The composites were placed at the bottom of 24 well plate using sterile technique. Due to the porous nature of the composites, 1ml of sterile broth was added to the wells and removed after 1 h. Following this, as shown in Figure 5.3, 1 ml of bacterial suspension was added to the wells. For the $AgNO_3$, 0.5 ml of the solution and 1ml of the bacterial suspension was introduced into a well simultaneously. The plates were then incubated at 37 °C on a shake table (MaxQ™ 4450, Benchtop Orbital Shaker, ThermoFisher Scientific, Paisley, UK) for 24 h. The 24 well microplate was a unit of replication (n= 9 plates/ treatment); one of each type of composite was added to each plate (Figure 5.3). Additional treatments included the pure HA composite (negative control), the $AgNO_3$ solution (positive control), and a blank well with just the bacterial suspension (reference) (Figure 5.3). After 24 h of exposure, the external media from 6 replicates was assessed for bacterial growth by measuring the lactate production and cell viability using the live/dead kit. The integrity of the composites was also assessed by measuring concentrations of calcium, phosphorus and silver in the external media and media from the attached cells using ICP-MS as detailed in chapter 4 ,section 4.2.5. Briefly, 0.5 ml of the media transferred to acid washed Eppendorf tubes and a few drops of 70% nitric acid was added to the tubes to digest the metal and other electrolyte which was then analysed using ICP-MS. Biofilm formation on the composites was also investigated. Three replicates were used for SEM observation which is explained in detail below
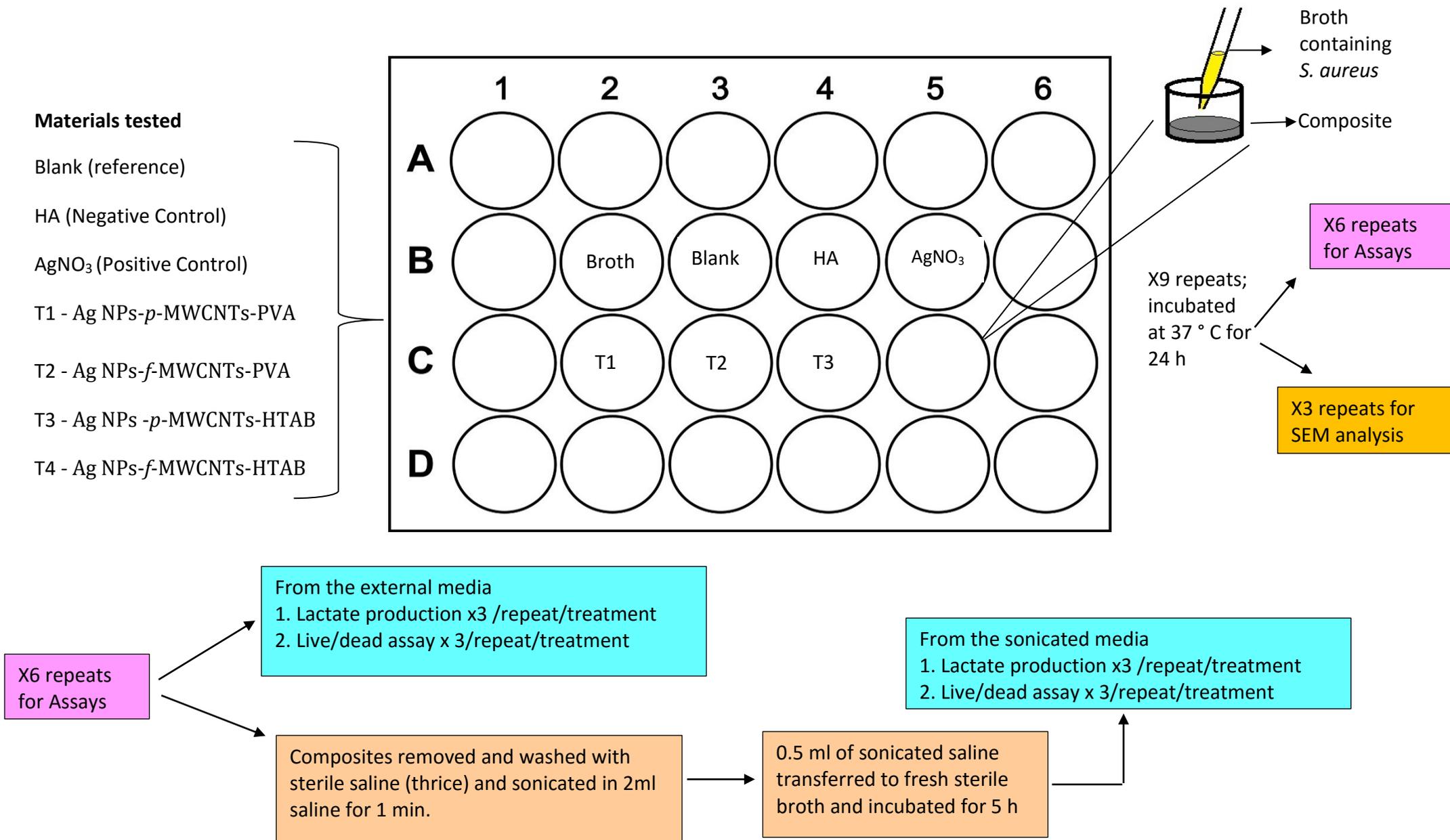
Figure 5.3 Schematic representation of the experimental setup for the bacterial study. The figure shows the control for the experiment and the treatments tested. The placement of the controls and treatment composites in the 24 well plate (n=9 plates) followed by the different types of assays performed on the external media and the assays performed bacteria grown on the composites and controls.

5.2.3 Assessment of bacterial attachment

The viability of the bacteria attached to the composites was tested by following the method of (Besinis et al., 2014), with some modifications. In brief, the composites were carefully removed from the 24 well microplates using sterile tweezers and then washed thrice with sterile saline (0.85% NaCl) to remove any unattached bacteria. Each composite was placed separately into sterile glass bottles containing 2 ml of sterile 0.85% NaCl and sonicated in an ultrasonic bath (35 KHz frequency, Fisherbrand FB 11010, Germany) for 1 min to remove the attached cells from the surface of the composite. The composites were removed and the remaining solutions were vortexed for a few seconds to homogenize them. Then, 0.5 ml of the saline from the sonicated composites was aliquoted into new sterile BHI broth and incubated in the shaker incubator at 37 °C for 5 h. The incubation time was decided based on the growth curve of *S. aureus* which was assessed before the start of the experiment (Refer optimisation study, growth curve). The media from the blank well with no composites and well containing AgNO$_3$ solution were mixed well with a pipette and centrifuged for 10 min at 2000 rpm (2040 rotors microplate centrifuge, Centurion Scientific Ltd, Ford, UK). The supernatant was discarded and the pellet was washed twice with saline and re-suspended in 2 ml of 0.85% saline. Then, 0.5 ml of this solution was aliquoted into new sterile BHI broth and incubated in the shaker incubator at 37 °C for 5 h.

5.2.4 Determination of lactate production

S. aureus is a facultative anaerobe that is capable of fermenting the supplements in the broth to lactic acid. The appearance of lactate in the external medium is therefore an indication of metabolically active viable cells. After 24 h exposure of the bacteria to the composites, 100 μl of the supernatant from each well was transferred to V-bottom 96 well

microplates (Produce code: 3896, Corning, Flintshire, UK) which was centrifuged at 2000 rpm for 10 min to pellet the bacteria. According to (Besinis et al., 2014), 10µl of the supernatant was then transferred to a new V-bottom 96 well microplate to perform the lactate assay. Briefly, 10 µl of the supernatant from each well was mixed with 211 µl of a lactate assay reagent. The assay reagent was made of 200 µl of 0.4 M hydrazine and 0.5 M glycine solution (buffered to pH 9 with few drops of 6 M KOH), 10 µl of 40 mM nicotinamide adenine dinucleotide (NAD+, Melford Laboratories Ltd, Suffolk, UK) and 1 µl of 1000 units/ml lactate dehydrogenase (LDH, Sigma-Aldrich Ltd, Dorset, UK). Samples were then incubated for 2 h at 37°C, and absorbance read with VersaMax plate reader (VersaMax microplate reader with SoftMax Pro4.0 software, Molecular Devices, Sunnyvale, USA) at 340 nm wavelength. Absorbance values were converted to molar concentration using a calibration curve of lactic acid standards in triplicates (0, 0.125, 0.25, 0.5, 1.0, 2.0, 4.0 and 8 mM). The standards were prepared by adding 480 µl of 30% lactic acid to 100 ml Milli-Q- ultrapure water to get 16 mM, and then a 50% serial dilution was made to get 8, 6, 4, 2, 1, 0.5, 0.25, 0.125 mM. Similar to the suspended bacteria in the external media, lactate production was measured in the media of the attached bacteria after 5 h.

5.2.5 Live/ dead assay

The viability of *S. aureus* after 24 h exposure to the composites and 5 h growth in the broth was assessed using the L7012 Live/Dead ® Backlit Kit (Invitrogen ltd, Paisley, UK) according to the manufacturer's protocol. The kit contains SYTO 9, a green fluorescent DNA stain for all kinds of cells, and a red fluorescent DNA stain (propidium iodide) for cells with a compromised membrane. To perform the assay the staining solution was prepared by mixing the two stains provided in the kit at a 1:1 ratio and then

adding Milli-Q- ultrapure water to obtain a final stain concentration of 0.6%. Then 100 µl of the samples (external media after 24 test and supernatant after 5 h incubation) were transferred into a 96-well plate (flat-bottom sterile polystyrene Microplates, Product code: 11319163, Fisher Scientific, Loughborough, UK). Equal quantity of the dye (100 µl) was also transferred into the wells and this was mixed well. The microplates were then incubated for 15 min in dark at room temperature. The samples were examined immediately using a Cytofluor II, fluorescence plate reader (perspectives Biosystems, Framingham, MA, USA). The excitation wavelength was set at 480 nm for both the dyes, whereas the emission wavelength for SYTO 9 was set at 530 nm and 645nm for propidium iodide and gain was 70.

Prior to performing the assay with the bacteria from the samples, the assay was calibrated to convert the fluorescence data of live/dead assay to an equivalent live cells percentage values. This was done according to Besinis et al., (2014) and the manufacturer's instructions with some modifications. To calibrate the assay for *S. aureus* 5 ml of cells from the stock culture was added to 15 ml of sterile broth and this was centrifuged at 4000 rpm for 10 min. The supernatant was discarded and the pellet was suspended in 10 ml saline which was again centrifuged at 4000 rpm for 10 min. This was repeated twice and the pellet was suspended in 2ml saline. Then 1ml of this suspension was added to 15 ml of 70% isopropyl alcohol and incubated for 1 h to kill the cells. The remaining 1 ml was suspended in 15 ml saline to obtain an OD of 0.19 (10^7 CFU/ml) which was read at the wavelength of 595 nm. After 1 h the tube containing isopropyl alcohol was centrifuged at 4000 rpm for 10 min and the supernatant was discarded. The pellet was washed twice in saline. Finally, the pellet obtained was resuspended in 15 ml saline to achieve an OD of 0.19 absorbance units. Care was taken to ensure the OD of both the

live and dead cells were the same. To obtain the calibration curve (Figure 5.4), the ratio of integrated green/ red fluorescence against the known percentage of live cells of the standard cell suspension was plotted as follows:

Live cells %	100	90	80	70	60	50	40	30	20	10	0
Dead cells %	0	10	20	30	40	50	60	70	80	90	100
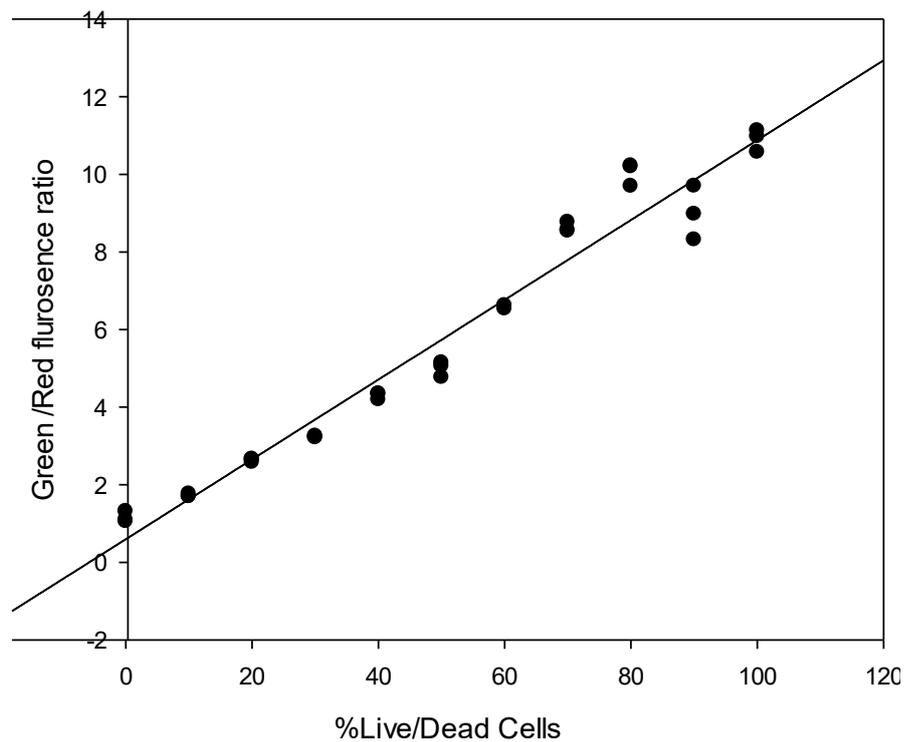
Figure 5.4 Calibration curve for % live dead cells. A typical calibration gave a linear response (e.g., R^2 =0.9805, y= 0.1029x+0.5956)

5.2.6 Electron microscopy observation

To qualitatively asses the bacterial growth on the composites, SEM observation was performed. Briefly, the composites, positive control ($AgNO_3$) negative control (Pure HA) and reference (blank well with only bacteria) were exposed to *S. aureus* for 24 h as described previously (n=3). Since $AgNO_3$ and blank wells only had fluids, circular disks

from the bottom of another similar 24 well microplate was cut and sterilised by soaking in absolute ethanol for 1h. After drying, the disks were placed at the bottom of the 24 well microplates which were used for the experiment and the fluids were introduced. At the end of the exposure, the disks and the composites were washed twice with 0.85% NaCl to remove the detached bacteria and were subsequently fixed with 2.5% glutaraldehyde in 0.05 M cacodylate buffer at pH 7.4 for 2h. The specimens were subjected to a graded series of ethanol which involved immersing the specimens in 30, 50, 70, 95 and 100% ethanol for 30 min at each concentration. The specimens were then immersed in 50/50 ethanol/ hexamethyldisilazane (HMDS) for 30 min and finally 100% HDMS for 20 min. The specimens were left undisturbed in the fume cupboard to air dry. The resultant specimens were mounted on conducting carbon stubs and coated first with carbon to perform EDS analysis, followed by gold in a sputter coater (EMITECH K550, Quorum Technologies, and UK). SEM images were collected using a 15 kV accelerating voltage.

5.2.7 Statistical analysis

All data are presented as mean $\pm$ standard error and were analysed using statgraphics software for windows (version XVI.I). After descriptive statistics to determine normality, skewness or kurotosis, data were analysed by one way ANOVA following a variance check (Levene's test). All statistical analysis used a 95% confidence limit, so the p values < 0.05 were considered statistically significant.

5.3 Results

5.3.1 Investigation of the bacterial growth in external media (suspension)

The growth inhibition of *S. aureus* on the composites containing the Ag NPs was investigated by measuring the amount of lactate (Figure 5.5A) produced by the bacteria, as it is an indicator of metabolically active living cells. Lactate production was observed in all the composite treatments. However, they were significantly lower than the control groups (blank and pure HA composites, one-way ANOVA, < 0.05). Significant difference (one-way ANOVA, < 0.05) was observed in the lactate production among the composites, wherein lactate production was significantly higher in composites containing functionalised MWCNTs. No significant difference was observed between the composites made of pristine MWCNTs and positive control ($AgNO_3$ solution).

The proportion of viable cells in the external media was also measured using the live/dead assay (Figure 5.5C). The data was normalised against the blank (bacteria grown without any treatment); assuming that the bacterial growth was 100% in the blank. Similar to the lactate assay, significantly lower growth was observed in the treatment composites compared to the control (pure HA composites) by approximately 80%. No significant difference was observed between the treatment composites but the composites containing functionalised MWCNTs showed significantly higher amount of live cells compared to the positive control ($AgNO_3$ solution).

5.3.2. Assessment of bacterial attachment to the composites

Determination of the bacterial attachment on the composites was done by incubating the media obtained from the composites for 5 h. Similar to the lactate production in the external media; lower lactate production was observed in the treatment composites. The lactate production (Figure 5.5B) was significantly less compared to the controls (blank and pure HA composites). However, no significant difference was observed between the treatments and the positive control ($AgNO_3$ solution). Figure 5.5D depicts the results of live/dead assay for the attached bacteria. The data was normalised against the blank (bacteria grown without any treatment) similar to the external media. The viability of the bacterial cells was significantly reduced in the composites compared to the control by approximately 25%. No significant difference was observed between the composites. Although, no significant difference in the presence of viable cells was observed between the positive control and the composites.
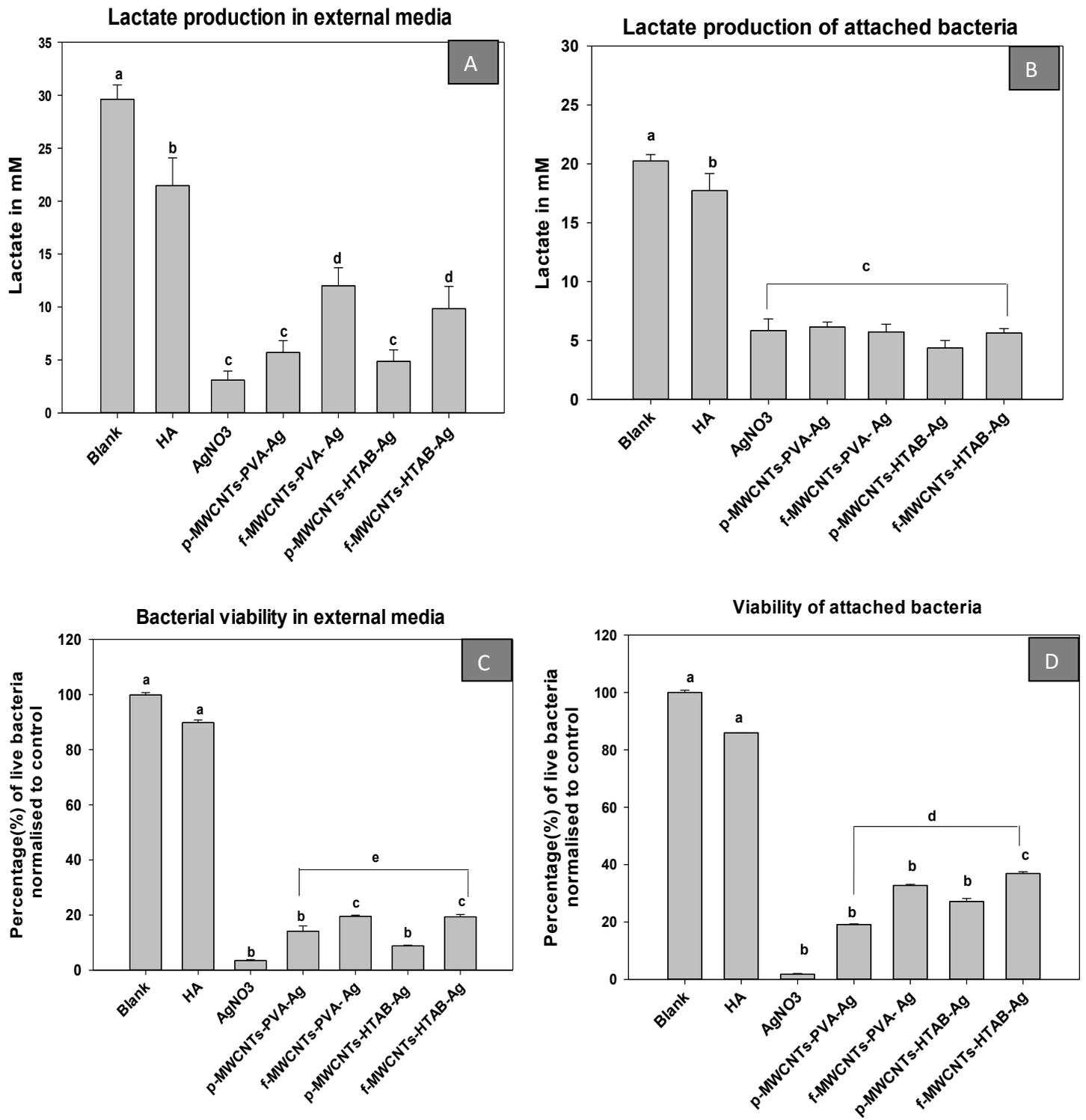
Figure 5.5 Growth inhibition of *S. aureus* **A)** Lactate production in external media, **B)** Lactate production of bacteria attached to the composites after 5 h incubation, **C)** Proportion of live bacterial cells in external media after normalization with control, **D)** Proportion of live bacterial cells attached to the composites after 5 h incubation (normalized with control). Different letter indicates significant different between the groups (ANOVA, P < 0.05).

5.3.3 Investigation of the stability of the composites

To determine the stability of the composites and leaching of Ag NPs from the composites, the concentration of silver was measured in both the external media and the sonicated media. In the external media (Table 5.1), silver release from all the composites was significantly lower compared to the positive control. The maximum concentration released from the positive control was 3.48±0.74 ug/l (mean ± S.E.M., n=6). Within the treatment groups, the composites with PVA surfactant had a higher release of silver compared to composites with the HTAB surfactant. Silver release from the sonicated media showed that f-MWCNTs-PVA-Ag showed significantly higher release (0.65 ± 0.07 ug/l) compared to the other composites. Overall, silver release in the external media was higher compared to the silver release from sonicated media (Table 5.1), indicating that most of the silver was released from the composites into the external media during the incubation period.

Table 5.1 Total concentration of Ag (ug/l), Ca (mg/l) and P (mg/l) from the external and sonicated media.

	Treatment			
External media		Ag	Ca	P
	Blank	0.005 ± 0.0a	8.72 ± 0.7a	1285.33 ± 117.8a
	HA	0.005 ± 0.0a	49.05 ± 11.7b	1238.09 ± 178.4a
	AgNO$_3$	3.48 ± 0.7b	7.90 ± 0.1a,e	777.11 ± 12.6b
	p-MWCNTs-PVA-Ag	1.58 ± 0.1a	11.23 ± 3.7a,e,f	184.29 ± 11.8c
	f-MWCNTs-PVA- Ag	0.91 ± 0.04a	36.19 ± 4.3b,c	104.28 ± 13.3c
	p-MWCNTs-HTAB-Ag	0.87 ± 0.02a	23.4 ± 0.7c,d	129.58 ± 8.4c
	f-MWCNTs-HTAB-Ag	0.80 ± 0.1a	19.31 ± 1.5a,d,e,f	470.16 ± 10.3d
Sonicated Media	HA	0.005 ± 0.0a	38.34 ± 13.07a	151.08 ± 13.5a
	p-MWCNTs-PVA-Ag	0.49 ± 0.01b	30.59 ± 3.8a	44.61 ± 3.3b
	f-MWCNTs-PVA- Ag	0.65 ± 0.07c	38.51 ± 4.7a	64.7 ± 5.1b
	p-MWCNTs-HTAB-Ag	0.49 ± 0.01b	13.89 ± 0.9b	30.71 ± 7b
	f-MWCNTs-HTAB-Ag	0.59 ± 0.08b,c	22.35 ± 2.1a	92.53 ± 8.7c

Data are expressed as mean± S.E.M (n=6 for each treatment). Different letters are statistically different from each other within the column (one-way ANOVA, $p < 0.5$).

The concentration of calcium and phosphorus (Table 5.1) was also measured in the media as an indication of composite degradation. Highest release of calcium in both the external and sonicated media was from the pure HA composites. In the external media, there was a significant difference between the treatments in calcium concentration (one-way ANOVA, $p < 0.05$). The concentration of calcium release was highest in pure HA composites (negative control) 49.05±11.74 mg/l followed by f-MWCNTs-PVA- Ag (36.19±4.38 mg/l). The least amount of calcium was detected in $AgNO_3$ solution which was the positive control. In the sonicated media, *p*-MWCNTs-HTAB-Ag had significantly less quantities of calcium compared to the other composites. Phosphorus concentration in the external media showed significant difference between treatments. Both blank and pure HA composites showed significantly higher amount of phosphorus release compared to the treatment composites. The least amount of phosphorus release was observed in all the treatment composites, except *f*-MWCNTs-HTAB-Ag, which was significantly higher than the other composites. Phosphorus release (Table 5.1) in sonicated media followed the same pattern as the external media with the highest amount of release from pure HA composite (negative control) followed by *f*-MWCNTs-HTAB-Ag (one-way ANOVA, $p < 0.05$).

5.3.4 Qualitative assessment of bacterial attachment (SEM observation)

The bacterial growth on the composites was qualitatively analysed using SEM. Biofilm formation was observed in the blank well (bacteria grown without any treatment). Multilayer of bacterial cells was also observed on pure HA composite (negative control) surface and within the pores of the composites. *S. aureus* did not show any signs of stress and grew in multiple layers (Figure 5.6A and B). On the other hand, minimum to no bacterial cells were observed in $AgNO_3$ as expected (Figure 5.6c). Among

the treatment composites, relatively higher amount of bacterial cells was observed on the surface of composites containing functionalised MWCNTs (Figures 5.6E and G). The bacterial cells had also filtered into the pores of the composites. Less bacterial cell adhesion and growth was observed in the composites containing pristine MWCNTs (Figures 5.6D and F) with the least on *f*-MWCNTs-HTAB-Ag composite.
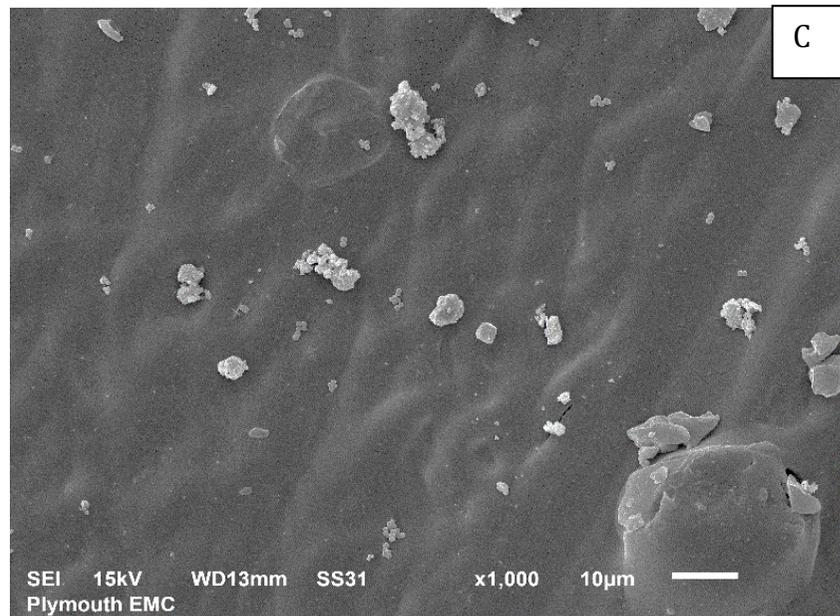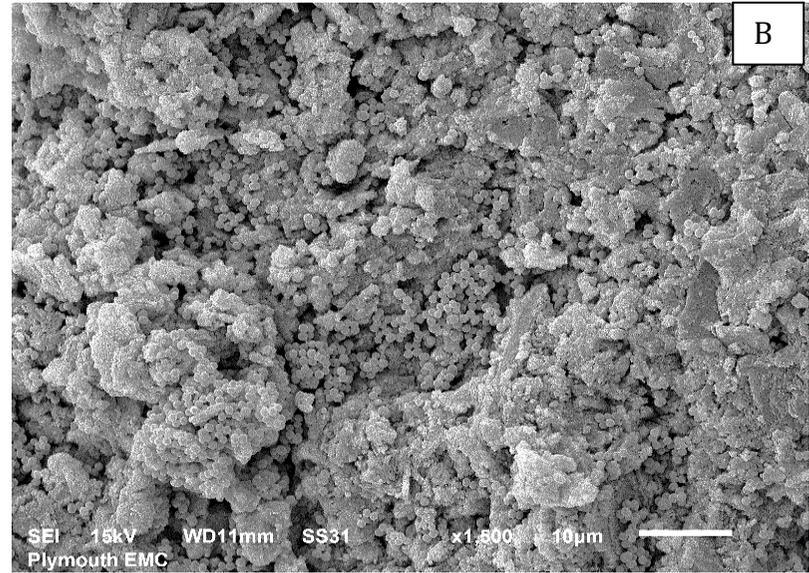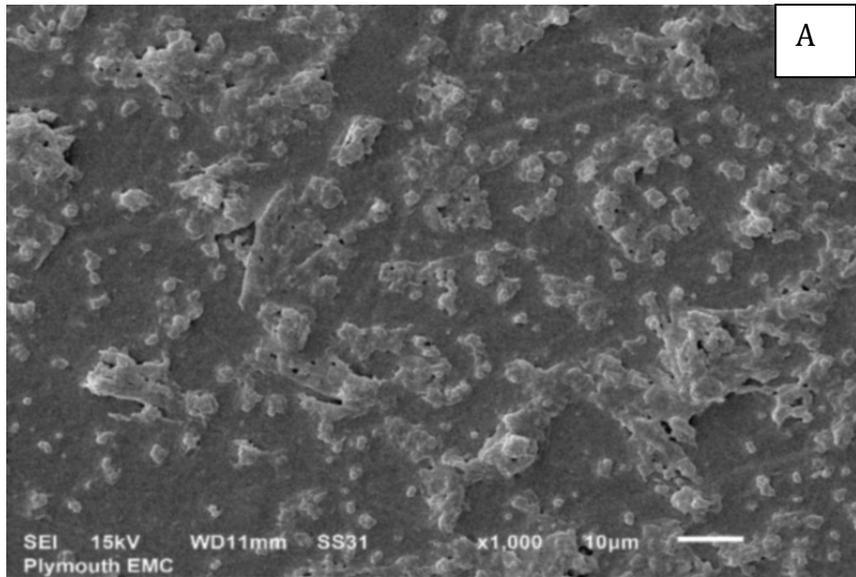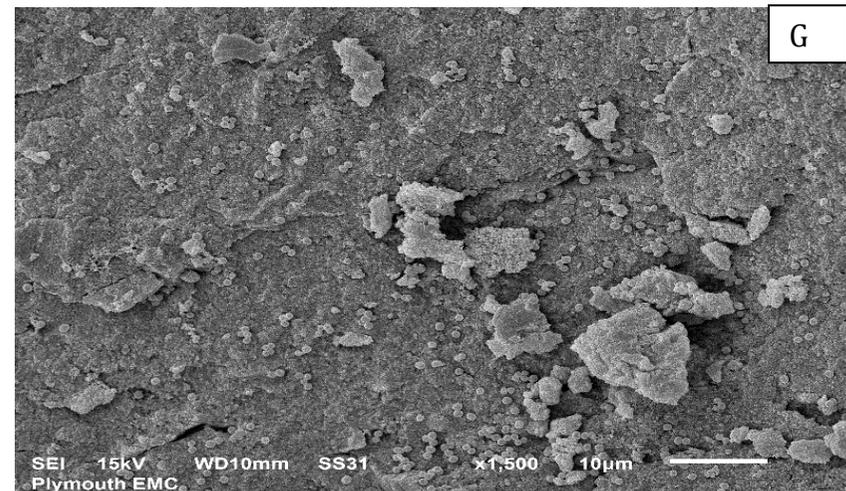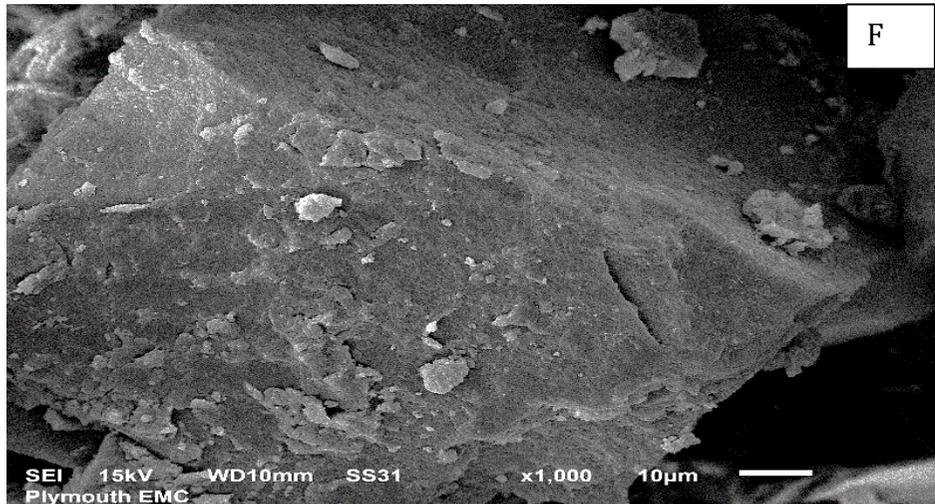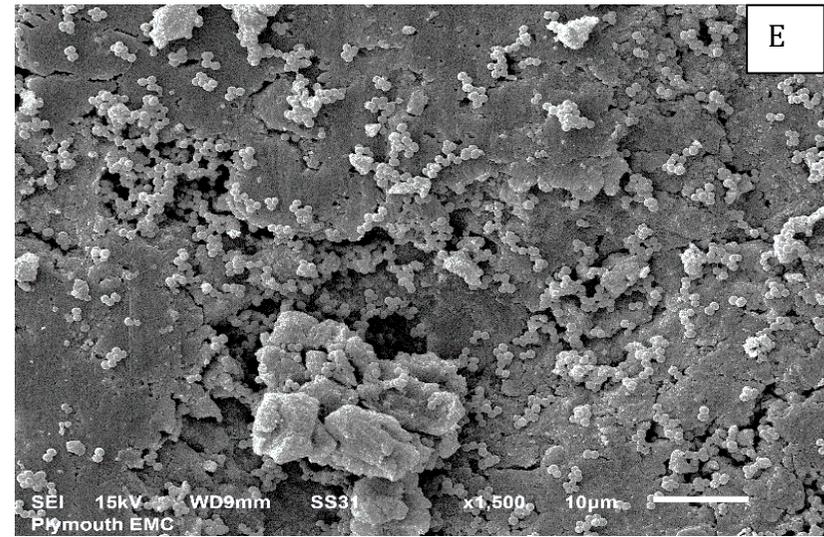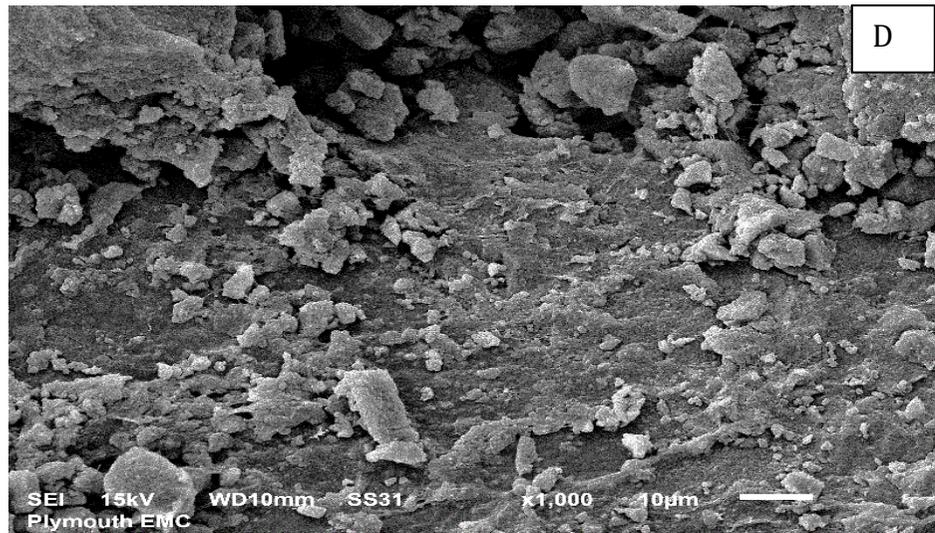
Figure 5.6 Scanning electron micrographs of the composites exposed to *S. aureus* for 24 h, A) Blank (bacteria grown without any treatment) shows presence of bacterial biofilm, B) Pure HA composite (negative control) which shows full bacterial growth, C) Silver nitrate solution (positive control) which shows no bacterial growth, D) p-MWCNTs-PVA-Ag composite, E) f-MWCNTs-PVA-Ag composite, F) p-MWCNTs-HTAB-Ag composite, G) f-MWCNTs-HTAB- Ag composite. More bacterial cells are present on the composites containing functionalised MWCNTs (E and G).

5.4 Discussion

This study reports the antibacterial activity of silver nanoparticles against clinically relevant bacteria *S. aureus* and their potential use in the development of composites for bone implants. The main finding was that the incorporation of Ag NPs in the composites enhanced the antibacterial effect compared to the pure HA composite, which provided a favourable condition for the bacteria to attach and proliferate.

5.4.1 Integrity of the composites

The concentration of calcium and phosphate was measured to investigate the degradation of all the composites. Significantly high amount of calcium and phosphorus was detected in the external media for the HA composite (control) suggesting a possible degradation (Table 5.1). The same effect was not observed with the treatments suggesting that since HA was nucleated in the presence of the MWCNTs they were held together strongly preventing the degradation of the treatment composites. The amount of calcium and phosphorus in the external media was higher than the sonicated media. Taking into consideration that no composites were present in the sonicated media after sonication, this could be because of calcium and phosphorus precipitation in the media.

5.4.2 Antibacterial effect

The bioassay results confirmed that the composites containing Ag NPs had antibacterial activity against *S. aureus.* It is well known that the antibacterial effect of $AgNO_3$ is due to the release of silver ions which are toxic to microbes (Zarubina et al., 2015). However, for Ag NPs, there are two possible explanations for this, either it is due

to the silver ion release from the composites or the direct contact of the microbe with the silver nanoparticles (Jose Ruben et al., 2005). The former is more likely, because the ICP-MS results showed silver ion release from the composites to the external media (Table 5.1). It is assumed that the potency of silver is related to its active form (soluble silver ions). (Schreurs and Rosenberg, 1982) found that silver ions can bind to the electron donor groups in biological molecules containing sulphur, oxygen or nitrogen, which causes defects in cell membrane and bacterial death.

It was shown that the composites containing Ag NPs and pristine MWCNTs showed the highest antibacterial activity among all the tested groups (Figure 5.5 A and C) which could be attributed to the poor adhesion of Ag NPs to the sidewall of the pristine CNTs (as explained in chapter 3). This means that, once broth was introduced into the well containing the composites, the broth filled up the pores in the composite washing out the trapped Ag NPs which were loosely adhered to the MWCNTs. It is hypothesised that this quick release of the Ag NPs in the first few hours of introducing the bacterial broth would have killed a partial amount of microbes resulting in the higher antibacterial effect as seen in the results (Figure 5.5 A and C).

SEM analysis shows the presence of bio film formation in the blank and pure HA composites (Figure 5.6A and B). The same was not observed in the treatment composites suggesting that the composites containing Ag NPs had potential anti-biofilm activity by decreasing the colonisation and attachment of the bacteria to the composite surface (Figure 5.2 B and D). There are two possible mechanisms by which the colonisation of the composites leading to the formation of biofilm could have been prevented. The large surface area of the Ag NPs provide better contact with the microbes. This results in high

percentage of interaction with the microbes compared to silver micro particles or other bulk forms of silver. Lok et al., (2007) had suggested that direct contact of the Ag NPs with the bacteria may result in membrane rupture. Another explanation is that the bacteria would be killed in the suspension before settling down on the composites due to the effect of the silver released from the composites into the media (Table 5.1) preventing the biofilm formation. Furthermore, (Sondi and Salopek-Sondi, 2004a) revealed that Ag NPs could accumulate in the bacterial membrane and increase the permeability of the cell wall that leads to loss of cell content and eventually result in bacterial death.

According to the assay results and SEM observation (Figure 5.5A and B; 5.6 B) complete growth of bacteria was observed in the pure HA composites (external media and sonicated media) confirming that HA had no antibacterial activity against *S. aureus,* but enhances their growth instead. This finding further supports the idea of (Rameshbabu et al., 2007) who suggested that HA could absorb many proteins, amino acids and other organic materials, which favour the attachment and colonisation of bacteria.

Although live/dead results (Figure 5.2C and D) was in agreement with the lactate production assays, the data values must be interpreted with caution as the calibration curve was not performed on the same day as the measurements of the fluorescence. Differences in the performance of the dyes was observed each day and it became clear that the calibrations are best conducted with each use of the dyes in the kit. The source of error may be small differences in dye concentration or quenching effects each day, which when converted from a calibration curve led to difference in the apparent live and dead ratios in sample resulting in negative values. For that reason, the data were

normalised to control, assuming that the growth of bacteria in the control (blank) was 100%.

Examination of the composites at the end of the 24 h incubation period by SEM (Figure 5.6) showed varying levels of bacterial adhesion on the composites under investigation. Bank (plastic disks) and HA composites (Figure 5.3 A and B) were fully covered with a multilayer of *S. aureus* biofilm. In contrast, wells that contained $AgNO_3$ solution (plastic disk, see above) showed minimal or no bacterial presence on the disk, as expected. Within the composite treatments, the composites containing pristine MWCNTs were the least susceptible to bacterial adhesion followed by the composites containing functionalised MWCNTs. A possible explanation for this could be the presence of MWCNTs as proposed by (Kang et al., 2008). According to Kang et al, (Kang et al., 2008) the direct contact between the MWCNTs and the microbes inactivate the cells. Hence, the size of the MWCNTs plays a crucial role. For the functionalised CNTs, during the oxidation process the CNTs are exfoliated reducing the size of the CNTs (see chapter 3) suggesting that more pristine MWCNTs would have been available to be exposed to the microbes. Further studies of the composites without the presence of Ag NPs needs to be performed to validate this.

5.5 Conclusion

In the present study, the suitability of HA composites containing MWCNTs decorated with Ag NPs to provide good antibacterial and anti-biofilm activity to the implants was determined. The evidence from this study supports the idea that the antibacterial activity of Ag NPs is mainly due to silver ion release. Further, the study also supports the idea that MWCNTs could be antibacterial in nature. However, there is concern about the biological safety of MWCNTs-silver releasing implant material. Therefore, further *in vitro* and *in vivo* studies are needed to investigate the biosafety of the Ag NPs and to determine the antibacterial properties of MWCNTs.

6. Investigation of osteoblast cell differentiation and mineralization in the presence of silver nanoparticle-multiwall carbon nanotube-hydroxyapatite composites

6.1 Introduction

Osteoblasts are specialized fibroblasts with the ability to secrete and mineralize the bone matrix. Mineralization refers to cell mediated deposition of extracellular calcium and phosphorus salts where anionic matrix molecules take up the calcium and phosphate ions and serve as nucleation and growth sites leading to calcification. The ideal scaffolds should promote early mineralization of osteoblasts and support new bone formation.Since the introduction in Chapter 4 details the benefits and concerns about the application of MWNCNTs in implants, emphasis is placed on the same for Ag NPs biocompatibility in this chapter introduction. Ag NPs are known to exhibit cytotoxic effect on osteoblast cells in a time and dose dependent manner, along with affecting the functional expression of the differentiation genes in the cells. So far there is only one study led by (Herkendell et al., 2014) which focused on the biocompatibility of the combined application of Ag NPs–MWCNTs in HA matrix composites. They have compared varying quantities of MWCNTs and Ag NPs in HA matrix and have shown that the cytotoxicity of the composites are increased with the increase in Ag NPs.

Short-term *in vitro* studies that cultivate osteoblasts on composites can provide vital information about the biocompatibility of the cells with the implants. In the present study, synthetic HA composites containing Ag NPs were produced which were intended to have the ability to release Ag ions. Therefore, it is necessary to carefully consider the effects silver might exert at the nano scale to the cells and to understand the mechanism enabling the biocidal properties of the composite. The influence of the Ag NPs-MWCNTs-HA composites on the bioactivity of human osteoblasts was studied by allowing the cells to proliferate, differentiate and mineralize on the composites. The effect of the composites was analysed at the molecular level by examining the expression of various

targeted differentiation and inflammation genes. Additionally, total glutathione concentration assay and lactate dehydrogenase activity assay were used to evaluate the oxidative stress and viability of the cell, respectively. ALP plays an important role in mineral formation by increasing the local concentration of inorganic phosphate (mineralization promoter) and by decreasing the extracellular pyro phosphate (mineralization inhibitor) (Golub and Boesze-Battaglia, 2007) and was used as a biomarker to evaluate the metabolic activity of the osteoblast cells. Moreover, the dissolution of the Ag NPs-MWCNTS-HA composites and cellular uptake of silver was also investigated by measuring the total concentration of Ca^{2+} , P and Ag^{2+} in the external media and cell homogenate along with the concentration of the electrolytes (K^+, Na^+ and Mg^{2+}).

6.2 Methodology

The biocompatibility of silver nanoparticles in the HA-MWCNTs composites, and the overall bioactivity was determined by growing human osteoblast cells on the composites and allowing them to differentiate. The composites were prepared and the following composites were exposed to osteoblast cells: pure HA (control), Ag NPs-*p*-MWCNTs-PVA, Ag NPs-*f*-MWCNTs-PVA, Ag NPs-*p*-MWCNTs-HTAB, Ag NPs-*f*-MWCNTs-HTAB. Human osteoblast cells were grown as mentioned in chapter four (section 4.2.1 – cell culture). The cells of passage 3, 4 and 6 were used for the experiment below.

6.2.1 Experimental Design

The experimental design is similar to the experimental setup explained in chapter four (section 4.2.2 – experimental design). In brief, the composites were sterilized using

gamma radiation and placed aseptically at the bottom of 24 well plates. The cell culture plate containing all the controls and treatments was a unit of replication. The composites were soaked in DMEM for 24 h before seeding with cells. The media were then removed and 1 ml of fresh DMEM containing 4×10^4 cells/ml from the stock was introduced into the wells. After 24 h the media was replaced with fresh DMEM, from there on media was changed every two days. Two time points, day 7 and 21 were used in this study (culture time was calculated from the day of cell seeding). A schematic representation of the test performed at the two time points is presented in Figure 6.1. Two separate runs were performed for the two time points (day 7 and 21). Each run had eight replicates of which 4 were used for RT-qPCR studies and 4 for biochemical studies. A separate run consisting of 3 replicates were used for SEM analysis for which day 7 time point was not performed. To enable the osteoblasts to mineralize, the differentiation supplements, ascorbic acid – 50 µg/ml (A4403, sigma Aldrich, Irvine, UK), Dexamethasone – 10nM (D4902, Sigma Aldrich, Irvine, UK), and β-Glycerolphosphate – 7mM (G9422, Sigma Aldrich, Irvine, UK) were added to the DMEM media from day 7, referred to hereafter as "Supplemented DMEM". The treated media were also collected to measure LDH and ALP activity along with ion concentrations.
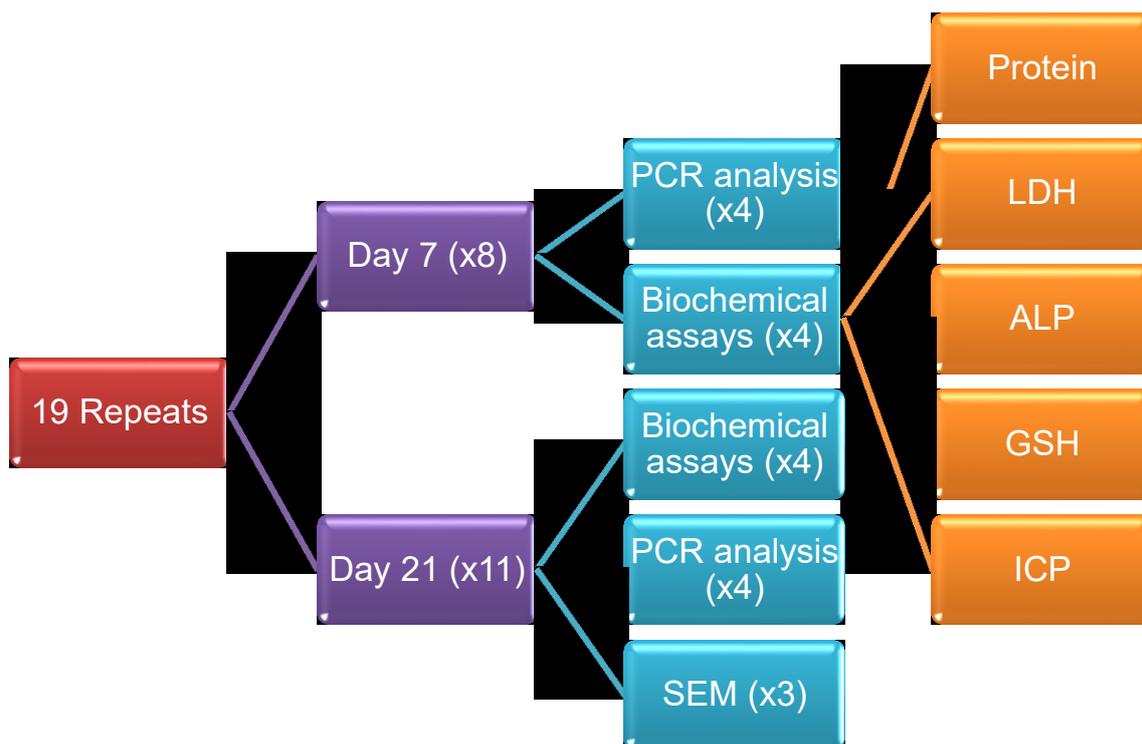
Figure 6.1 Schematic representation of the tests performed at the two time points of the study. Two runs with eight replicates were performed of which four repeats were used for PCR and biochemical assays on day 7 and four repeats for PCR, biochemical assays on day 21. A separate run with three replicates was performed for day 21 SEM analysis.

6.2.2 RNA extraction and RT-qPCR (Reverse transcription - quantitative polymerase chain reaction) analysis

At the end of day 7 and 21, total RNA was extracted using RNeasy mini Kit (Product code: 74104, Qiagen, Manchester, UK) according to the manufacturer's specifications. The control and treatment composites containing the cells were washed twice with 2 ml of phosphate buffered saline (PBS 1x without calcium and magnesium, Product code: 10708144, Fisher scientific, Loughborough, UK). Following this, 600 µl of prepared buffer RLT was added for 10 min to lyse the cells (buffer RLT was previously prepared by adding 10 µl of β-Mercaptonethanol per 1 ml of RLT buffer) according to manufacturer's

instructions. The lysate was collected and centrifuged for 2 min at approximately 13,000 x g (Heraeus pico 17 centrifuge, Thermo electron crop, Paisley, UK). Then, one volume of 70% ethanol was added to the lysate and mixed well by pipetting. This lysate was then transferred to an RNeasy spin column and centrifuged for 30 s at 10,000 x g. The flow through was discarded and the spin column membrane was washed by adding 350 µl of buffer RW1 and centrifuged for 30 s at 10,000 x g. To ensure that all the DNA was removed efficiently, on-column digestion of DNA was performed during the RNA purification procedure. This was done by adding 80 µl of DNase I incubation mix directly to the spin column membrane for 15 min followed by the addition of 350µl of RW1 buffer. The spin column along with the contents was centrifuged again for 30 s at 10,000 xg. Following this, the spin column membrane was washed twice with 500 µl of buffer RPE and centrifuged for 4 min at 10,000 xg. Finally, 30 µl of RNase-free water was added to the spin column and centrifuged for 2 min at 10,000 x g. The flow through containing the RNA was collected in a centrifuge tube to perform RT-qPCR.

PCR was done for one housekeeping gene: β-actin, and eight target genes: ALP, Osteocalcin, runx2, tumour necrosis factor (TNF-α), interleukin-6(IL-6), Osterix (OSX), DLX-5 and osteopontin (OPN). The target genes were selected to represent the health (response for any toxic reaction) and differentiation capability of the osteoblast cells. A description of the target genes and their function in the osteoblast cells is presented in Figure 6.2. The forward and reverse primer for the housekeeping and the target genes are detailed in Table 6.1.
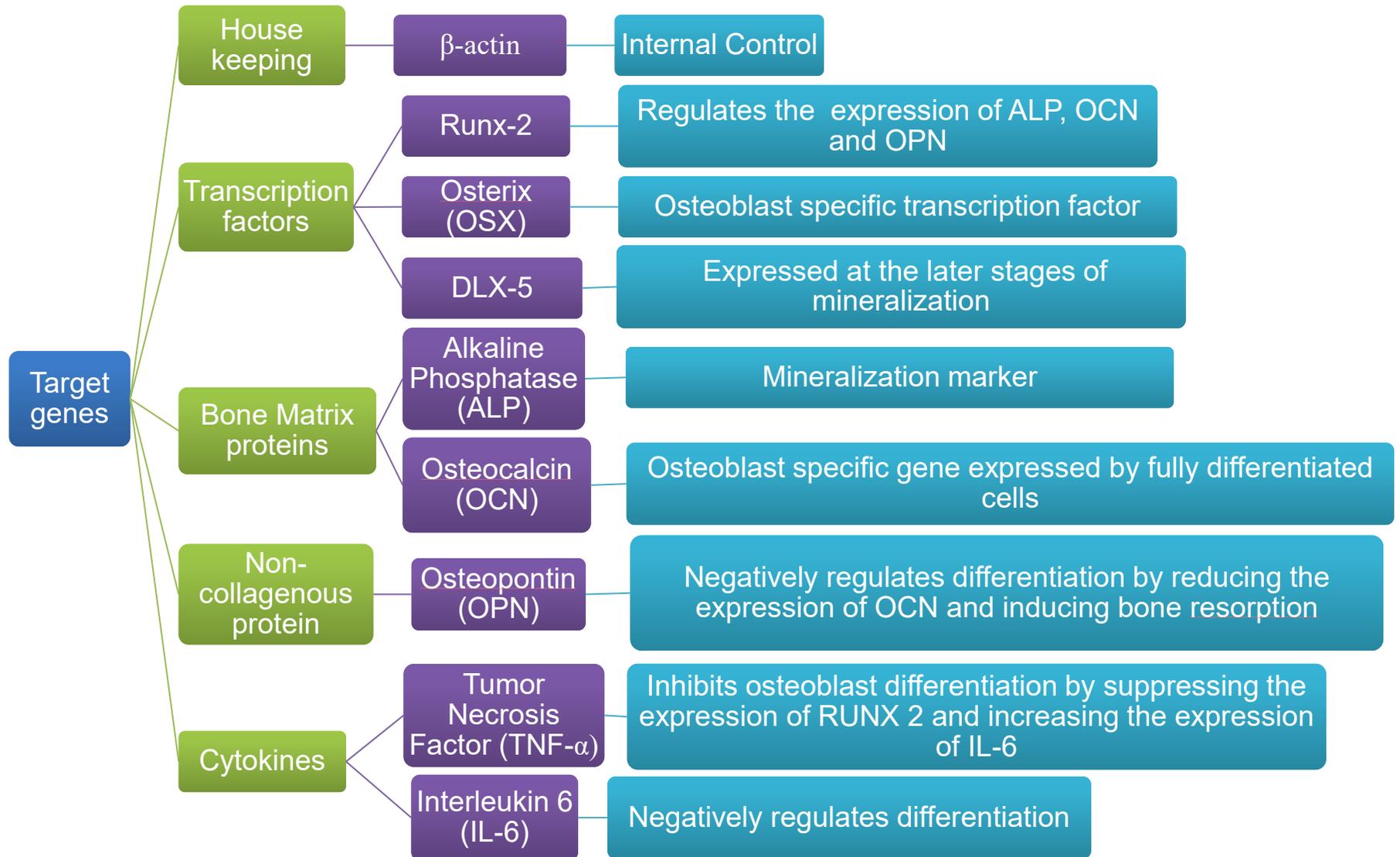
Figure 6.2 Description of the various target genes selected for the RT-qPCR study. The expression of these genes sever as an indicator of the effect of the composites on the osteoblast cells at the molecular level. The genes were selected to represent health and differentiation capability of the cells in the presence of the composites.

Table 6.1 Description of the forward and reverse primers for the housekeeping and target genes

Name	Forward Primer	Reverse Primer	Reference
β-Actin	CCCAAGGCCAACCG CGAGAAGATG	GTCCCGGCCAGCCAGGT CCAGA	(Cheng et al., 2015)
ALP	GACAATCGGAATGA GCCCACAC	GTACTTATCCCGCGCCT TCACCAC	(Cheng et al., 2015)
Osteocalcin	AGCCCAGCGGTGCA GAGTCCA	GCCGTAGAAGCGCCGAT AGG	(Cheng et al., 2015)
RUNX 2	TGCGGCCGCCCCAC GACAA	ACCCGCCATGACAGTAA CCACAGT	(Cheng et al., 2015)
TNF-α	AGCCCCCAGTCTGT ATCCTT	CTCCCTTTGCAGAACTC AGG	(Neacsu et al., 2014)
IL 6	AGTTGCCTTCTTGG GACTGA	TCCACGATTTCCCAGAG AAC	(Neacsu et al., 2014)
Osterix	GCAGCTAGAAGGGA GTGGTG	GCAGGCAGGTGAACTT CTTC	(Sunk et al., 2006)
DLX-5	CCAACCAGCCAGAG AAAGAA	GCAAGGCGAGGTACTG AGTC	(Morsczeck, 2006)
Osteopontin	TTGCAGCCTTCTCA GCCAA	GGAGGCAAAAGCAAAT CACTG	(Bahrambeigi et al., 2012)

RT-qPCR was performed in duplicates (per treatment on each plate, per gene) using QuantiNova SYBR Green RT-PCR Kit (Product code: 208154, Qiagen, Manchester, UK) in Quantstudio 12K Flex real time PCR system (Product code: 4471134, Applied Bioscience, Thermo Fisher scientific, Loughborough, UK). A total volume of 10 μl of PCR mixture was loaded in each well of the 368 well PCR plate (Product code: AB1384, ThermoFisher Scientific, Loughborough, UK). The PCR mixture was made up of 5 μl of 2x SYBR Green RT-PCR Master Mix, 0.1μl of QN SYBR Green RT-Mix and 0.5μl of 20x primer mix (0.5 μM forward primer and 0.5 μM reverse primer), 1 μl of template RNA and 3.4 μl of Nuclease free ultrapure water. PCR amplification was conducted with an initial 10 min RT-step at 50° C followed by 2 min PCR initial heat activation step at 95° C , then 40 cycles of 5 s denaturation step at 95° C and 10 s combined annealing/extension step at 60° C was performed. The fluorescent signal from SYBR Green was detected immediately after

the extension step of each cycle and the cycle at which the product was first detectable was recorded as the cycle threshold. The housekeeping gene (β-actin) was used as the internal control gene to normalize the mRNA of the target genes.

A cycle threshold (Ct) value was obtained for each amplified sample using the Quantstudio 12K Flex Real-Time PCR System thermocycler analysis software. The mean value of the two replicas analysed for each gene/ each repeat of the treatment (4 repeats /treatment) was calculated and a final average Ct value was obtained (Schmittgen and Livak, 2008). The correspondent housekeeping gene β-actin was subtracted to normalize those values, obtaining a dCt (ΔCt) value. The level of gene expression showed by cells grown on their own (blank) were taken as a reference for both the time points. To estimate gene expression relative to this reference, the mean dCt value corresponding to each gene calculated from the positive control (pure HA) and treatments was subtracted from the mean dCt values of the reference, obtaining a ddCt (ΔΔCt) value. Finally, mean fold change value, the times a gene is expressed in a treatment compared to the expression level in a control (Pure HA composite), taken as reference, was calculated from the ddCt value of the treatments on the two time points (Day 7 and 21) .

6.2.3 Biochemical assays and cell morphology

At the two time points (day 7 and 21), cell homogenates were prepared in hypo-osmotic buffer as mentioned in chapter 4 (section 4.2.2–experimental design). Aliquots of the cell homogenates was stored at -80 ° C and were later used to measure lactate dehydrogenase and alkaline phosphatase activity, total protein and total glutathione (GSH) concentration. The electrolyte composition (Na^+, K^+, Ca^{2+}, P^+ and Mg^{2+}) of the cells and the concentration of total Ag in the cell homogenate was measured from fresh

aliquots by acid digestion followed by ICP-MS and/or ICP-OES analysis. The protocols used for the measurement of, LDH, ALP and electrolyte and metal analysis and protein content is previously described in Chapter 4 (Sections 4.2.3, 4.2.4 and 4.2.5, 4.2.6). The LDH, ALP assays and ion concentration measurements were also performed with the external media from days 1, 4, 7, 10, 13, 16, 19 and 21.

Glutathione (GSH) is a tripeptide synthesised in the cytoplasm of all cells and acts as a chemical antioxidant. Hence, the presence of GSH in the cell homogenate is an indication of oxidative stress in the cell caused by reactive oxygen species such as silver accumulation. GSH was measured according to (Owens and Belcher, 1965) with minor modifications. Briefly, 20 µl of the cell homogenate was added to 300 µl of the reaction mixture consisting of 260 µl assay buffer (100 mmol/l potassium phosphate + 5mmol/l potassium EDTA, pH 7.4), 10mmol/l of buffered DTNB (Ellman's reagent – 5, 5' – dithiobis – 2- nitrobenzoicacid) and 20 µl of 2 U/ml glutathione reductase. After equilibration for 1 min, the reaction was started by adding 20 µl of 3.63 mmol/l NADPH. Since this is a kinetic assay which is time critical, the NADPH was added simultaneously in all the wells by pipetting with a multichannel pipette. Absorbance was read at 412 nm for 15 min using microplate reader (SpectraMax 190 Microplate reader, Molecular Devices, Wokingham, UK). A series of glutathione reductase standards (0, 4, 8, 12, 16, and 20) µmol/l was used for calibration. The assay was performed in triplicates for each sample.

Morphology (shape and appearance) of the cells was regularly observed by light microscope to determine the health of the cells. The DMEM media appeared normal (no loss of the pH indicator or excessive cell debris). Light microscopy observations showed no signs of deterioration such as necrosis, detachment of cells from the substrate,

granularity around the nucleus or obvious disruption of the cell membrane (i.e., no membrane blebs or cell swelling). The mineralization of the cells was observed after adding supplemented DMEM. At the end of the experiment, the presence and health of the cells were determined using a scanning electron microscope (SEM) (JEOL JSM -5600LV, JEOL ltd, Japan). A separate run (n = 3) replicates were done for SEM work as mentioned previously. Only one time point (day 21) was done for SEM analysis. The composites containing the cells were processed and fixed as mentioned in chapter 4 (section 4.2.6 – cell morphology). SEM images were collected using a 15 kV accelerating voltage. The observations were conducted systematically, starting at a lower magnification (X30) to examine the distribution of the cells on the composites, and then at a higher magnification (X1000) to observe the morphology of the cell membrane as well as to determine the attachment of cells on the composites.

6.2.4 Statistics

All data are presented as mean ± standard error and were analysed using statgraphics software for windows (version XVI.I). After descriptive statistics to determine normality, skewness or kurotosis, parametric data were analysed by one way ANOVA following a variance check (Levene's test) and non- parametric data analysed by Kruskal-Wallis. The differences between the treatments and controls at each time point, and time effects within treatment were evaluated using one-way analysis of variance (ANOVA). For treatment x time effects, a two-way ANOVA was also applied to the data. All statistical analysis used a 95% confidence limit, so the p values < 0.05 were considered statistically significant.

6.3 Results

6.3.1 Growth and morphology of cultured cells

The morphology of the osteoblast cells was investigated after the inoculation stage (24h) using light microscopy (Figure 6.3 A). No signs of cell death due to toxicity or infection was observed. To determine the structural integrity and presence of any infection, cells were observed with naked eye and under light microscope throughout the experiment. The osteoblasts appeared flat with extending pseudopods before the addition of supplemented DMEM. After the addition of supplemented DMEM to the wells, the cells appear to cluster to form a single layer with calcium deposition on the surface (Figure 6.3 B).
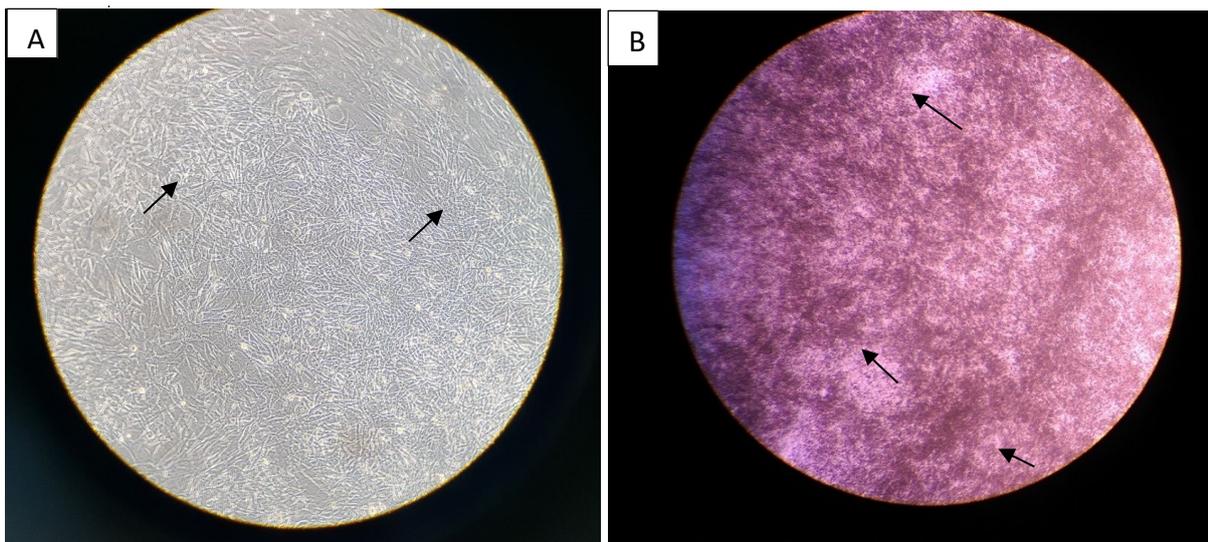
Figure 6.3 Light microscope observation of the osteoblast cells (Control) (A) Osteoblast cells after 24 h, arrows point to the individual cells which can be clearly observed. (B) Osteoblast cells after 21 days incubations. Mineralization of the cells is evidenced by the presence of the mineral deposit.
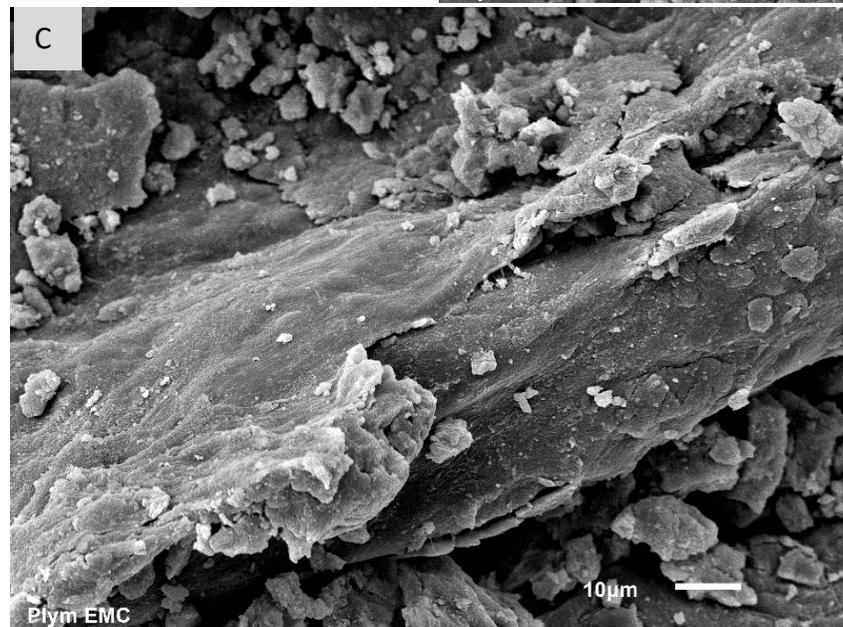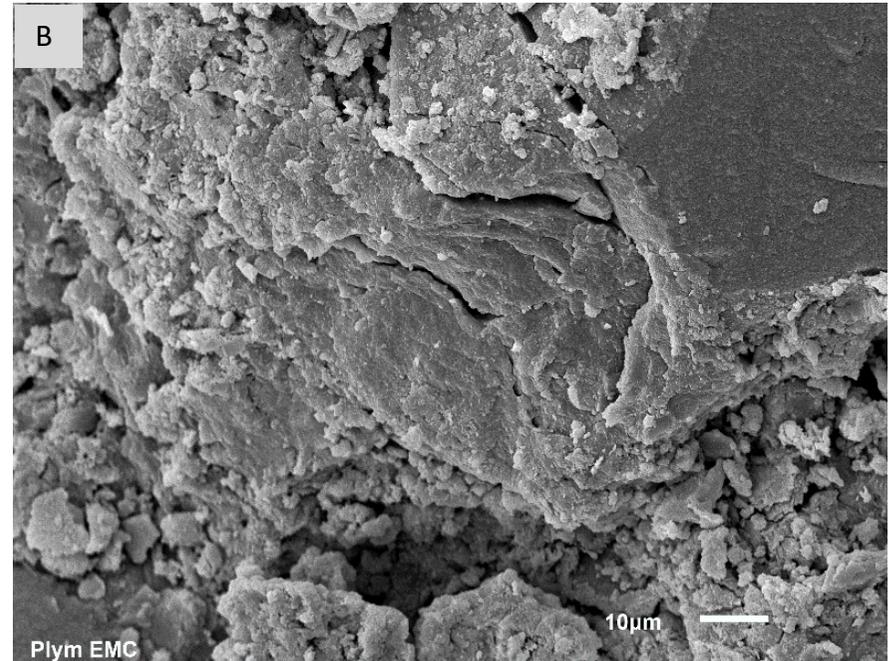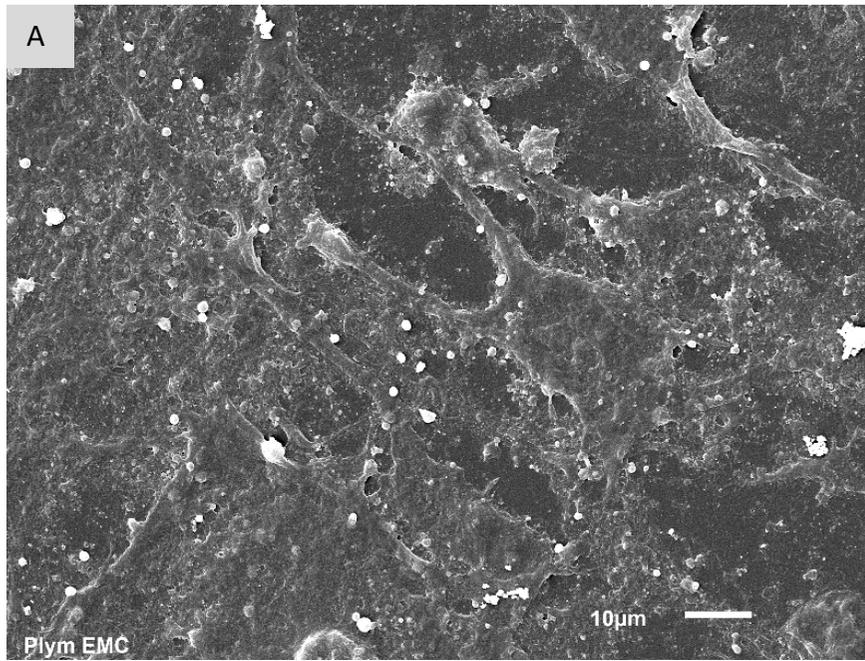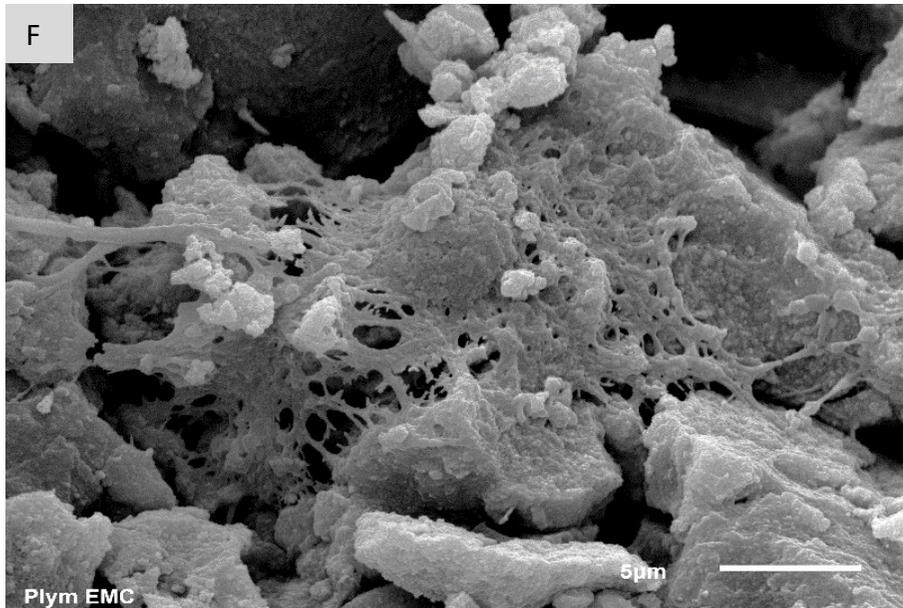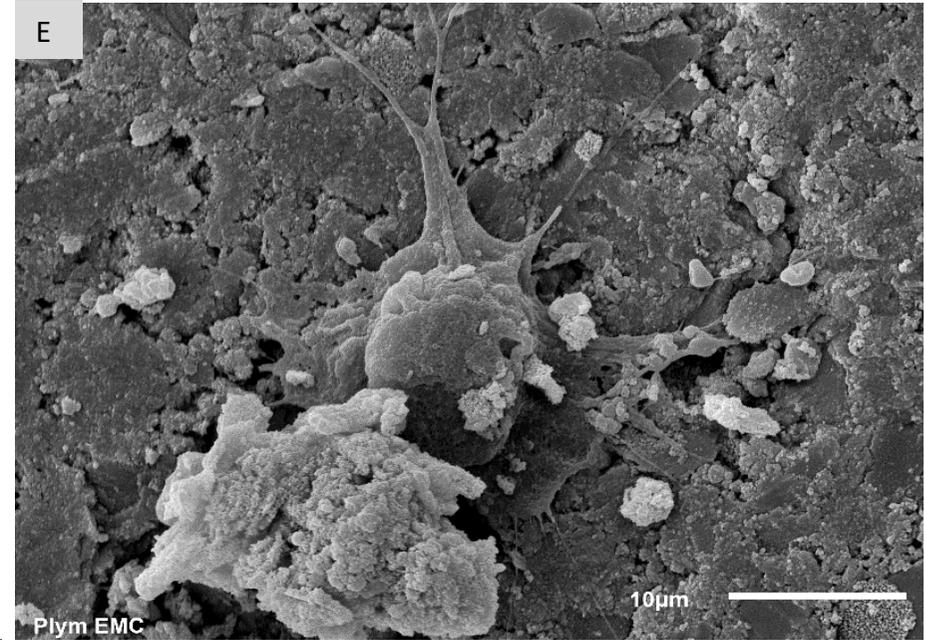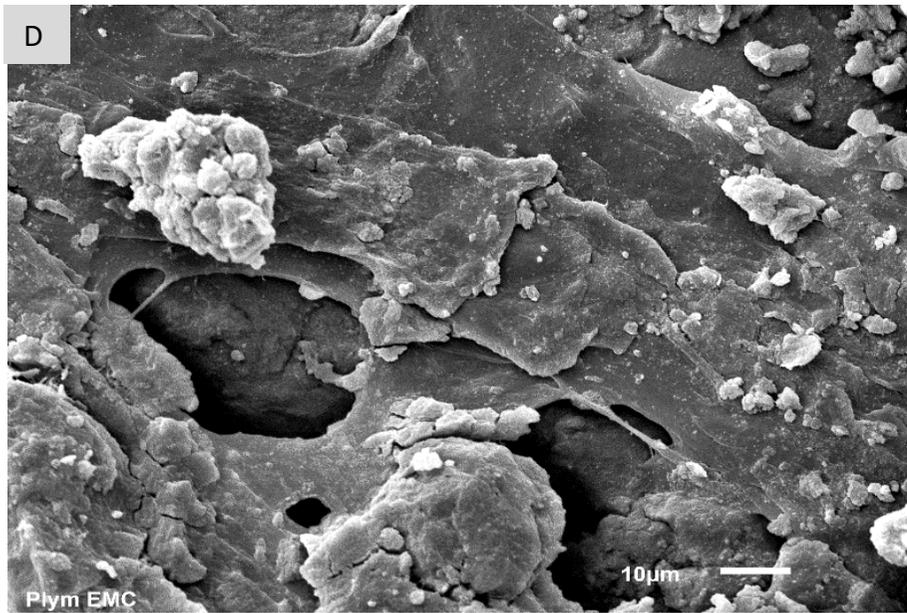
Figure 6.4 SEM images of the osteoblasts after 21 days of growth and mineralization on the composites. Various magnification has been used for the treatments to show the presence of nodules (A) Control cells grown on the plastic plate; (B) cells grown on pure HA , it can be seen that the cells have infiltrated into the pores; (C) shows cells grown on p-MWCNTs-PVA (D) shows cells on f-MWCNTs-PVA; (E) shows a single cell with the presence of a nodule on p-MWCNTs-HTAB; (F)shows cells on f-MWCNTs-HTAB forming bridges. Arrows in (A, B ,C, D and F) indicate the nodules formed by the cells Arrow in (E) shows the podia extending from a cells.

171

After 21 days of culture, the controls and the treatment samples were visualized using SEM (Figure 6.4). The white solid crystalline structures on the blanks and the treatments were mineralized crystals deposited by the cells (Figure 6.4, arrows in the images). Crystal nodules were also observed in the areas were the cells had in filtered through the pores. Since the treatments had areas of uneven surfaces, the cells were often seen to form bridges between the gaps (Figure 6.4 F).

6.3.2 Quantification of specific mRNA

Quantification of relative expression of the different genes related to differentiation and inflammation was performed to understand the potential regulatory effect of the composites on human osteoblast cells. This was done by calculating the value of ΔΔCt, using the endogenous expression of the gene β-actin as a control, to normalise the expression levels. The Figure 6.5 show the mean value of fold change of selected gene expression after 7 and 21 days of osteoblast cell cultures on the treatments relative to the cells on pure HA composites. The genes were classified into groups according to the known or proposed function of the encoded protein .The categories are: transcription factors (Dlx-5, Runx2, Osterix), bone matrix proteins (ALP, osteocalcin), non-collagenous protein (osteopontin) and cytokines (IL-6, TNF –α). As shown in (Figure 6.5 A, B and C) the transcription factor Dlx5 is downregulated on both the days whereas Runx2 and osterix are upregulated on day 7, but downregulated on day 21 except for genes from *p*-MWCNTs-PVA, where they are downregulated on day 7 as well. The bone matrix proteins (Figure 6.5 D and E) ALP and osteocalcin are as expected (ALP is upregulated on day 7 and downregulated on day 21 and vice versa for osteocalcin). The only exception is the *p*-MWCNTs-PVA which are downregulated for both the genes on both the days. The cytokines IL-6 and TNF–α (Figure 6.5 G and H) are both upregulated on both the days

reaching a maximum of 16.15 and 7.1 fold change for Il-6 and TNF -α respectively on day 7 and 6.5 and 2.4 fold change on day 21.

C OSX

(chart: Delta Delta ct (fold change respective to HA) vs p-MWCNTs-PVA, f-MWCNTs-PVA, p-MWCNTs-HTAB, f-MWCNTs-HTAB; Day 7, Day 21)

D ALP

(chart: Delta Delta ct (FOld change respective to HA) vs p-MWCNTs-PVA, f-MWCNTs-PVA, p-MWCNTs-HTAB, f-MWCNTs-HTAB; Day 7, Day21)

E OCN

(chart: Delta Delta ct (Fold change respective to HA) vs p-MWCNTs-PVA, f-MWCNTs-PVA, p-MWCNTs-HTAB, f-MWCNTs-HTAB; Day 7, Day 21)

174
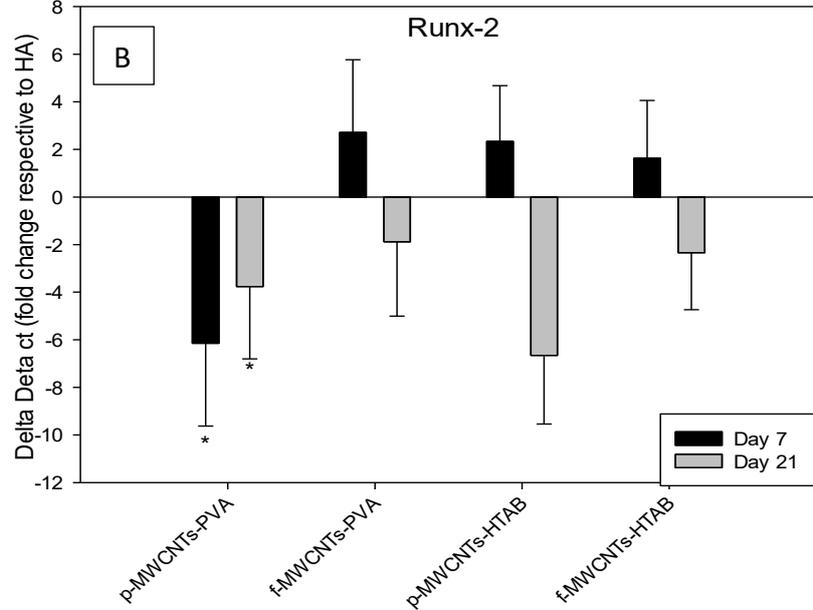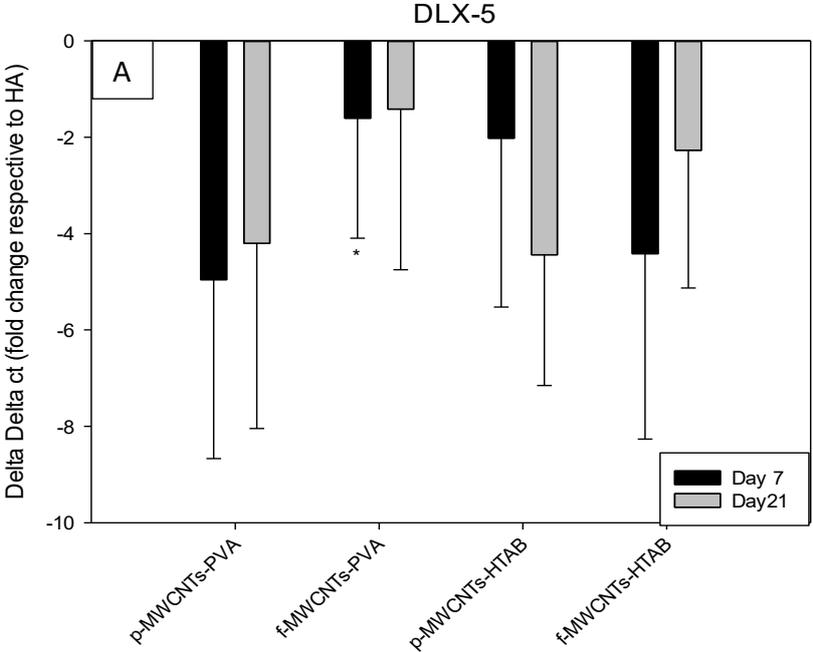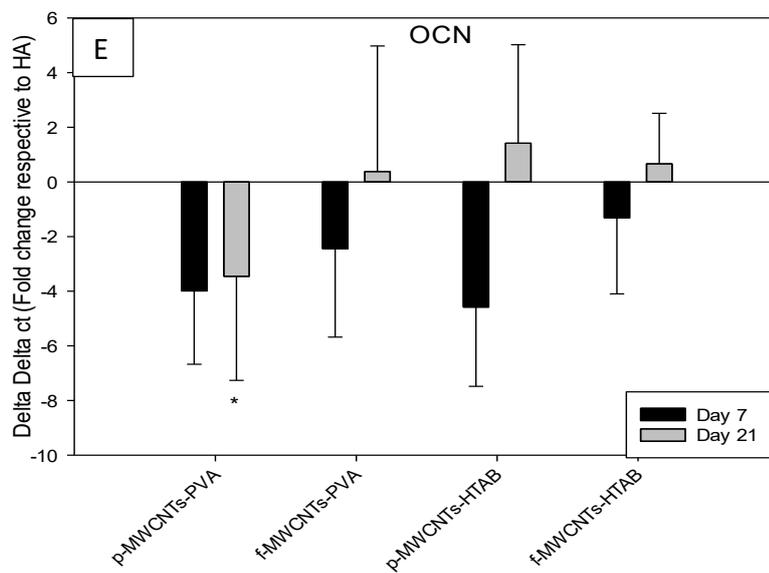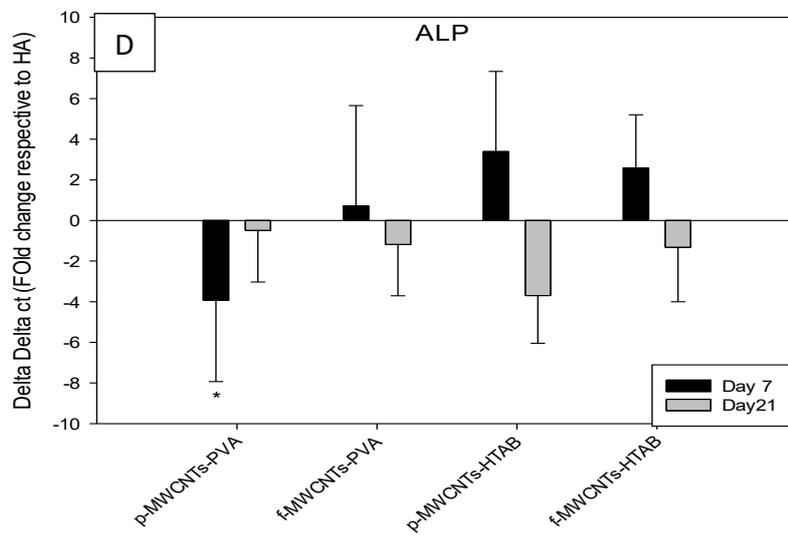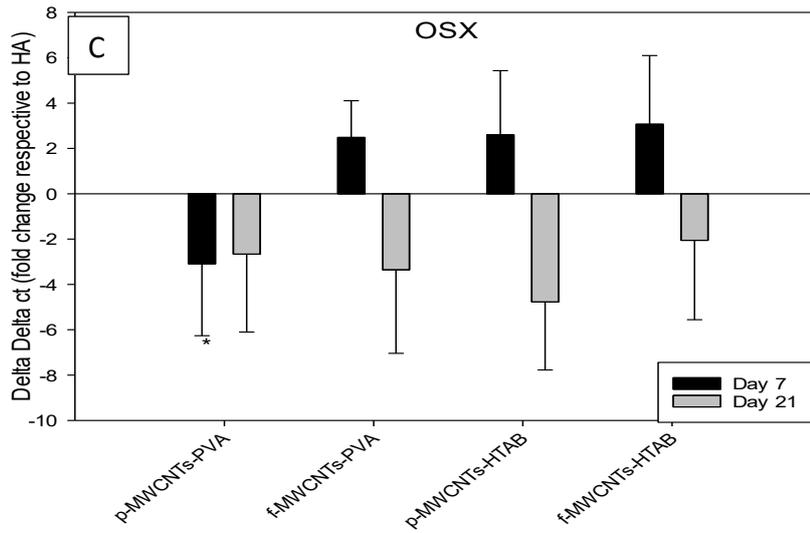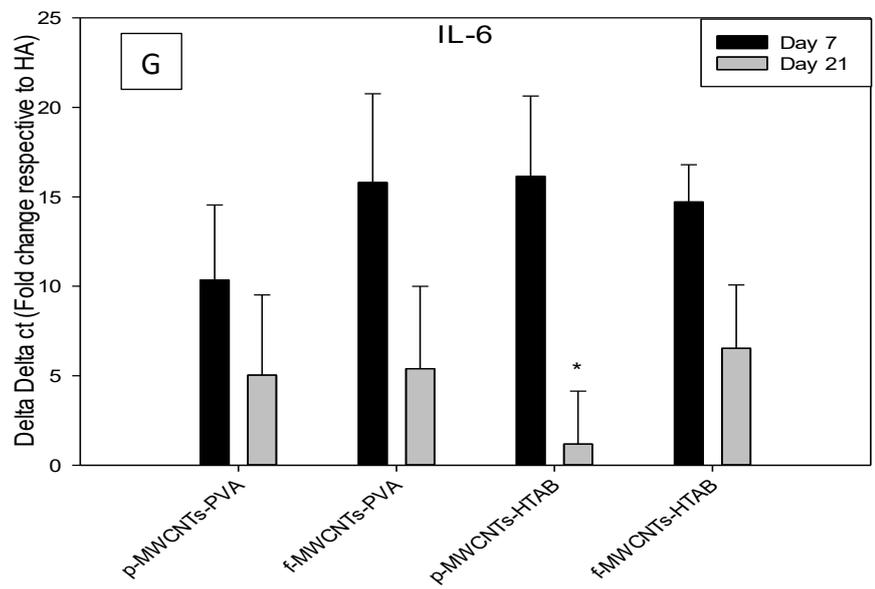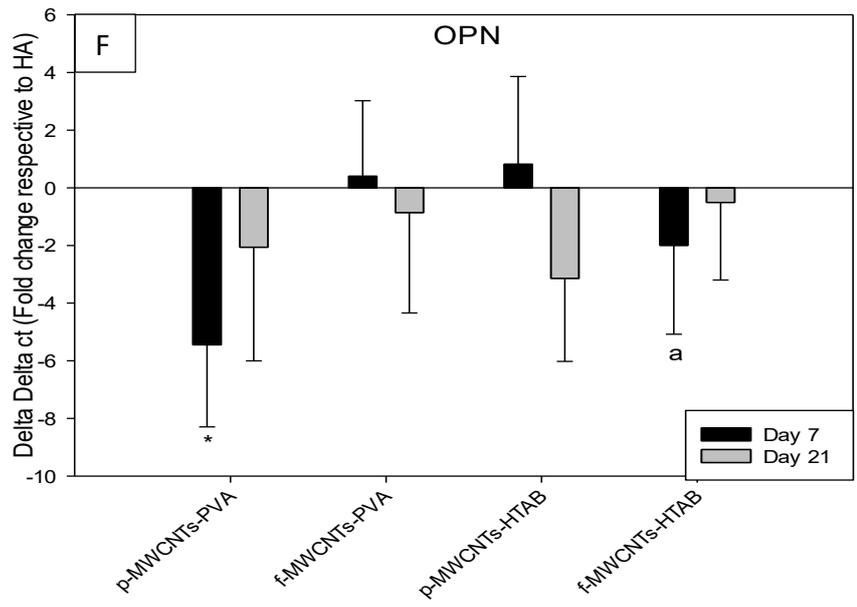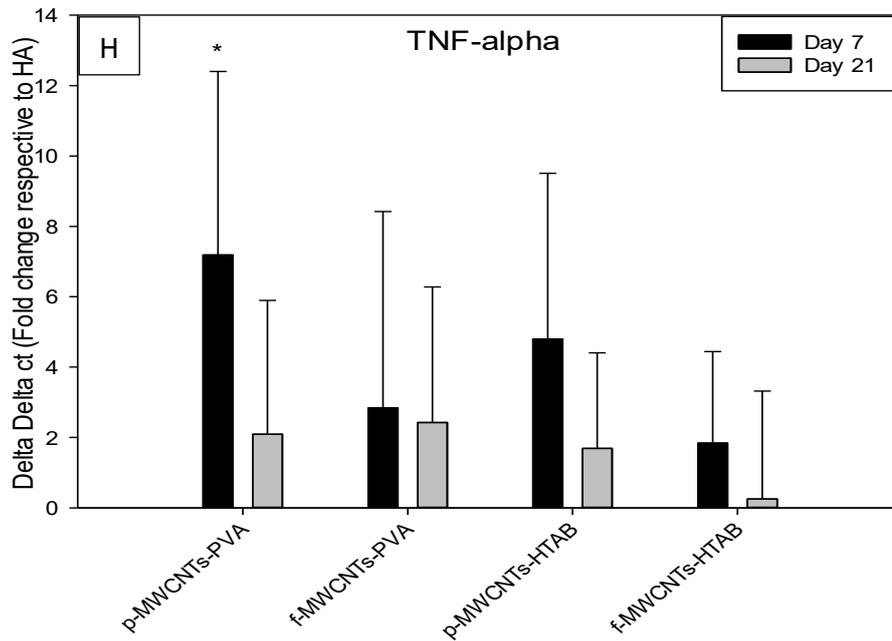
Figure 6.5 RT-qPCR measurement of targeted mRNA levels of the osteoblast cells adhered to the composites. Total RNA was isolated from cells on day 7 and 21 from AgNP-p-MWCNTs-PVA, AgNP- f-MWCNTs-PVA, AgNP- p-MWCNTs-HTAB, AgNP- f-MWCNTs-HTAB. Data are mean ± S.D (n=4 per treatment per end point). Expression levels (fold change) for (A) Dlx-5, (B) RunX2, (c) Osterix, (D) Alkaline Phosphatase, (E) Osteocalcin, (F) Osteopontin, (G) Interleukin -6, (H) Tumour Necrosis Factor-Alpha are compared for all the treatments. The results are shown as fold change (ddCt method, relative to cells on pure HA composites).* significantly different from the other treatments (one way ANOVA or Kruskal – Wallis test, $p < 0.05$)

6.3.3 Investigation of the silver exposure and ion concentration in the media and cell homogenates

The total silver concentration was measured in the external media on days 1, 4, 7, 10, 13, 16, 19 and 21 (Table 6.2). The concentration of the silver in the media of composites containing *p*-MWCNTs was high over 21 days. There was a significant difference in silver concentration between the groups (Ag NP-*p*-MWCNTs and Ag NP-*f*-MWCNTs). The highest concentration of silver (µg/l) was observed after one day in the

external media of the p-MWCNTs–HTAB and p-MWCNTs-PVA treatments; the concentration was 22.1 ± 2.5 and 20.7 ± 2.3 respectively. There is an initial release of Ag from all the treatment composites which decreases over time. The concentration of silver in the media from control (blank) and Pure HA composite was below the detection limit (detection limit $<0.03\mu g/l$).

In the cell homogenate, silver accumulation was observed in all the treatment composites. The concentration of silver was significantly higher on day 21 in all the p-MWCNTs treatments compared to day 7. Low concentration of silver (day 7 - 0.03 (blank and HA), day 21 – 0.1 (control), 0.0 (pure HA) $\mu g/l$) was detected on both the days in the control (blank) and pure HA composite.

The electrolytes Na^+, K^+, Ca^{2+}, Mg^{2+}, and P were also measured in the external media and cell homogenate (Tables 6.2 and 6.3). No significant difference in the concentration of Na^+, K^+ and P between the treatments and control was observed whereas significant difference was observed in the concentration of Ca^{2+} and Mg^{2+} in the external media. The concentration of Ca^{2+} in the media was significantly lower in the pure HA composite and significantly higher in the p-MWCNTs treatments compared to the control. The concentration of Mg^{2+} in the media was significantly lower in pure HA composite and all the treatments compared to the control (Blank). In the cell homogenates, the concentration of the electrolytes was significantly higher in the treatments and pure HA composite compared to the control (Blank).

Table 6.2 The total concentration of Ag (µg/l) and electrolytes, Na$^+$, K$^+$, Ca^{2+}, Mg^{2+}, and P (mg/l) in the media after exposing the osteoblasts to the composites for 21 days.

			Silver			
Days	**Control**	**HA**	**p-MWCNTs-PVA**	**f-MWCNTs-PVA**	**p-MWCNTs-HTAB**	**f-MWCNTs-HTAB**
1	0.12±0.03	0.13±0.05a	20.7 ± 2.3*b	2.2 ± 0.7a	22.1 ± 2.5*b	5.7 ± 4.2a
4	0.15±0.06	0.21±0.02a	13.2 ± 0.3*b	1.5 ± 0.1a	21.2 ± 3.5*b	3.7 ± 2.1a
7	0.24±0.03	0.05±0.03a	8.4 ± 3.1*b	1 ± 0.3a	16.4 ± 2.4*b	1.5 ± 1a
10	0.12±0.08	0.15±0.07a	7 ± 2.1*b	0.3 ± 0.1a	8.6 ± 1.3*b	0.5 ± 0.1a
13	0.17±0.08	0.08±0.08a	13.2 ± 1.2*b	0.8 ± 0.05a	7 ± 1.5*b	7.6 ± 0.2a
16	0.44±0.01	0.30±0.02a	6.6 ± 0.7*b	0.2 ± 0.1a	9.3 ± 3.5*b	0.2 ± 0.1a
19	0.4±0.05	0.10±0.04a	9.3 ± 3.3*b	0.3 ± 0.4a	4 ± 1*b	0.04 ± 0.1a
21	0.31±0.1	0.42±0.005a	8.3 ± 1.8*b	1.6 ± 0.2a	8.4 ± 1.8*b	0.07 ± 0.1a

			Sodium			
Days	**Control**	**HA**	**p-MWCNTs-PVA**	**f-MWCNTs-PVA**	**p-MWCNTs-HTAB**	**f-MWCNTs-HTAB**
1	251.4 ± 6.8	257.2 ± 11.5a	333.5 ± 14*b	384.2 ± 18*	324.2 ± 15.5*b	276.8 ± 18.8a
4	217.4 ± 8.2#	203 ± 12.4a#	253.3 ± 17.8b#	261.6 ± 13*b#	243.2 ± 11b#	233.8 ± 14ab#
7	240.8 ± 13.4	207.8 ± 9.2a	283.7 ± 29b	258 ± 4.6bc	220.4 ± 8.6acd	210.2 ± 8.07ad
10	262.5 ± 15.8	261 ± 13.2a#	221.4 ± 12.1*#	243.2 ± 10a	233.5 ± 4.7a	231.7 ± 17.7a
13	252 ± 5	224.5 ± 13.4*a	248 ± 10b	273 ± 6.2c	252.1 ± 7.1bc	239.5 ± 4.3ab
16	235.5 ± 7.4	220 ± 7.5a	256 ± 3.4b	269.8 ± 9*bc	264.6 ± 3.7*bc	204.4 ± 16.5*a
19	312.5 ± 10.6#	354.8 ± 14.1*#	475.7 ± 11.6*a#	457.8 ± 10.8*a#	456 ± 4.6*a#	444 ± 16.5*a#

| 21 | 527.4 ± 17.8# | 544.2 ± 16.7# | 539.3 ± 18.3# | 555.1 ± 19.4# | 539.1 ± 15.2# | 527.4 ± 9.8# |

Potassium

Days	Control	HA	p-MWCNTs-PVA	f-MWCNTs-PVA	p-MWCNTs-HTAB	f-MWCNTs-HTAB
1	19.8 ± 0.4	21.7 ± 2.3	20.8 ± 2.3	19.6 ± 1	19.4 ± 0.6	19.6 ± 0.6
4	17.7 ± 0.7	16.7 ± 1#	16.3 ± 1.4#	17 ± 1.3	16.1 ± 0.5	18 ± 1.3
7	19.6 ± 1.1	18.6 ± 1.6	19 ± 1.7	18.8 ± 1.4	18 ± 2	17 ± 2
10	18.8 ± 1.3	18.4 ± 1.7a	14.5 ± 0.6*b#	18.2 ± 1.3abc	18.5 ± 1.7ac	15.1 ± 0.8abc
13	18.8 ± 0.4	17.2 ± 1	18.4 ± 1.3	19.2 ± 0.8	18.2 ± 0.4	17.7 ± 0.6
16	17.6 ± 0.4	16.6 ± 0.4a	18.3 ± 0.3ab	19 ± 0.6bc	19.1 ± 0.1bc	15.3 ± 1.4*a
19	24.2 ± 1.1#	30.1 ± 1.1*#	34.5 ± 1.7*a#	36.6 ± 1.2*a#	35.3 ± 1.2*a#	35.5 ± 0.7*a#
21	34.4 ± 1.7#	37.3 ± 2.1#	40.1 ± 1.2*#	38.3 ± 1.1	38.8 ± 1.5	36.3 ± 1.3

Calcium

Days	Control	HA	p-MWCNTs-PVA	f-MWCNTs-PVA	p-MWCNTs-HTAB	f-MWCNTs-HTAB
1	7 ± 0.7	1.1 ± 0.1*a	29.2 ± 2.4*b	6.6 ± 2.8c	40.1 ± 0.8*d	14.2 ± 1.5*e
4	5.8 ± 0.2	1.6 ± 0.1*a	25.3 ± 1.3*b	5 ± 1a	23.3 ± 1.9*b#	9.4 ± 1.2*#
7	6.6 ± 0.4	1.0 ± 0.2*	13.5 ± 1.9*#	8 ± 0.8a	21.2 ± 10*	5.3± 1.0a#
10	6 ± 0.5	0.4 ± 0.1*	21.2 ± 0.5*#	3.4 ± 0.7*a#	16.6 ± 1.4*	4.4 ± 0.4a
13	5.3 ± 0.1	0.4 ± 0.07*	26.1 ± 0.3*#	5 ± 1a	12 ± 0.8*	4.5 ± 0.3a
16	3.6 ± 0.5#	0.4 ± 0.1*	12.5 ± 0.7*a#	5.2 ± 1ab	14.8 ± 1.2*a	3.5 ± 1ab
19	2 ± 0.3#	0.3 ± 0.06a	15 ± 15.4*b	2.1 ± 0.5a	10.5 ± 3.3*b	6 ± 1
21	2 ± 0.1	1.6 ± 0.8#	24.2 ± 2*#	17.4 ± 1.2*a#	19.1 ± 2.4*a#	14.1 ± 0.4*a#

Phosphorus

Days	Control	HA	*p*-MWCNTs-PVA	*f*-MWCNTs-PVA	*p*-MWCNTs-HTAB	*f*-MWCNTs-HTAB
1	3.4 ± 0.4*	21.5 ± 1.4*a	32.1 ± 3.3*	28 ± 2.3*a	30.6 ± 2.6*	28.7 ± 1.7*
4	2.7 ± 0.1	16 ± 0.2*a#	23.7 ± 1.2*b#	26.3± 2.4*b	21 ± 1.8*#	19.3 ± 2.5*a#
7	3 ± 0.1	16.3 ± 1*a	15 ± 1.2*ab#	21.8 ± 1*a	23.1 ± 4.1*	15.7 ± 1.7*ab
10	20 ± 0.5#	22 ± 1.5#	20 ± 2.2	23.4 ± 1.1	21.1 ± 0.8	21.5 ± 1.5
13	14 ± 1ab#	21 ± 0.4ab	31 ± 0.8a#	25.06 ± 1b	20.8 ± 1.4ab	23.3 ± 1.1ab
16	11.8 ± 0.5	20.5 ± 0.7*ab	21.7 ± 0.7*ab#	24 ± 1.6*b	21.6 ± 1.3*ab	19 ± 1.6*a
19	16.8 ± 2	29.2 ± 2*#	35 ± 1.1*#	30.6 ± 2*#	29 ± 2.4*#	32.6 ± 3.1*#
21	21.5 ± 4.4	31.7 ± 2.8*a	43.7 ± 1.3*	36.5 ± 3.6*ab	25.5 ± 2ac	31.1 ± 2.3*abc

Magnesium

Days	Control	HA	*p*-MWCNTs-PVA	*f*-MWCNTs-PVA	*p*-MWCNTs-HTAB	*f*-MWCNTs-HTAB
1	2 ± 0.2	0.2 ± 0.04*	0.1 ± 0.03*	0.1 ± 0.01*	0.1 ± 0.04*	0.1 ±0.00*
4	1.5 ± 0.05	0.07 ± 0.0*#	0.08 ± 0.01*	0.05 ± 0.01*	0.1 ± 0.04*	0.06 ± 0.01*#
7	1.7 ± 0.1	0.06 ± 0.0*	0.04 ± 0.02*	0.06 ± 0.00*	0.1 ± 0.03*	0.04 ± 0.00*
10	1.6 ± 0.1	0.07 ± 0.0*	0.08 ± 0.03*	0.06 ± 0.01*	0.06 ± 0.01*	0.05 ± 0.00*
13	1.6 ± 0	0.07 ± 0.0*a	0.1 ± 0.04*b	0.06 ± 0.00*a	0.06 ± 0.01*a	0.2 ± 0.01*b
16	1.4 ± 0.1	0.08 ± 0.0*	0.1 ± 0.01*	0.07 ± 0.00*	0.1 ± 0.04*	0.04 ± 0.00*
19	1.8 ± 0.1	0.1 ± 0.01*	0.2 ± 0.07*	0.1 ± 0.03*	0.1 ± 0.02*	0.1 ± 0.01*#
21	2.3 ± 0.2#	0.2 ± 0.01*#	0.2 ± 0.04*	0.2 ± 0.05*#	0.3 ± 0.07*#	0.2 ± 0.02*#

Data expressed as mean ± S.E.M (n=4 for each treatment).Different letters are statistically different from each other within the column and absence of letters means there is no significant difference.*significantly different from the control in each row. # Significantly different from previous time point within the column (one way ANOVA or Kruskal-wallis test, P<0.05)

Table 6.3 The total concentration of Ag in (µg/l) and electrolytes, Na$^+$, K$^+$, Ca^{2+}, Mg^{2+} and P (mg/l) in the cell homogenate after 7 and 21 days

	Treatment	Day 7 Cell Homogenate	Day 21 cell homogenate
Silver	Control	0.03 ± 0.01	0.03 ± 0.01
	HA	0.03 ± 0.0	0.03 ± 0.0
	p-MWCNTs-PVA	20.1 ± 2.6*b	57.7 ± 9.7*c
	f-MWCNTs-PVA	15.4 ± 1.2*b	16.6 ± 1.8*b
	p-MWCNTs-HTAB	18 ± 2.4*b	68.7 ± 7.5*c
	f-MWCNTs-HTAB	1.7 ± 0.3a	3.4 ± 1a
Sodium	Control	3.1 ± 0.9	5.3 ± 0.7
	HA	39 ± 1.6*	44 ± 6.7*
	p-MWCNTs-PVA	71.4 ± 3.5*a	132.4 ± 8.8*ab
	f-MWCNTs-PVA	70 ± 5.3*a	109 ± 7.1*ab
	p-MWCNTs-HTAB	74 ± 3.8*a	136 ± 12*ab
	f-MWCNTs-HTAB	69.8 ± 6.1*a	73.4 ± 7.9*a

	Treatment	Day 7 Cell Homogenate	Day 21 cell homogenate
Potassium	Control	1.3 ± 0.06	1.1 ± 0.3
	HA	3.7 ± 0.3*a	4 ± 0.5*a
	p-MWCNTs-PVA	4.7 ± 0.7*a	8.1 ± 0.5*
	f-MWCNTs-PVA	4.2 ± 0.4*a	6.2 ± 1*b
	p-MWCNTs-HTAB	5.3 ± 0.3*	6.2 ± 1.1*b
	f-MWCNTs-HTAB	5.3 ± 0.5*	5.5 ± 0.6*a
Calcium	Control	0.03 ± 0.008	9.2 ± 0.6
	HA	34.6 ± 3.2*a	122.5 ± 7.7*a
	p-MWCNTs-PVA	135.5 ± 11*b	456 ± 16.3*b
	f-MWCNTs-PVA	223.1 ± 14*c	278.7 ± 18.4*c
	p-MWCNTs-HTAB	287.5 ± 17.3*d	662 ± 32.2*d
	f-MWCNTs-HTAB	133.7 ± 6.5*b	277.1 ± 25.6*c

	Treatment	Day 7 Cell Homogenate	Day 21 cell homogenate
Phosphorus	Control	0.1 ± 0.08	5.8 ± 0.8
	HA	17.8 ± 2.7*a	58.5 ± 3.2*a
	p-MWCNTs-PVA	89 ± 1.7*b	212 ± 17*b
	f-MWCNTs-PVA	142 ± 10*c	141.8 ± 10.6*c
	p-MWCNTs-HTAB	52.3 ± 6*d	312.3 ± 24.4*d
	f-MWCNTs-HTAB	68.8 ± 2.7*e	152.4 ± 15.1*c
Magnesium	Control	0.1 ± 0.002	6.3 ± 0.1
	HA	1 ± 0.02a	3 ± 0.1a
	p-MWCNTs-PVA	6.3 ± 1.6*b	12.8 ± 1.7*b
	f-MWCNTs-PVA	3.5 ± 0.1a	12.3 ± 0.3*b
	p-MWCNTs-HTAB	10.7 ± 1.8*b	11.6 ± 0.1*b
	f-MWCNTs-HTAB	5.3 ± 1*b	7.8 ± 2.2a

Data expressed as mean ± S.E.M (n=4 per treatment per end point). Different letter are statistically different from each other.*significantly different from the control within the column (one way ANOVA or Kruskal – Wallis test, $P<0.05$)

6.3.4 Lactate dehydrogenase

The presence of LDH activity in the external media is one of the parameters that indicate cell injury. Table 6.4 represents the concentration of LDH (IU/ml media) in the external media after 1, 4, 7, 10, 13, 16, 19 and 21 days which was negligible. No statistical difference was observed between the treatments on all the days. Significant difference between the control (blank) and pure HA composite was observed on day 13. No significant difference was observed between the control (blank) and the treatments on all the other days. Within the controls and treatments, no significant difference was observed between the different days except for f-MWCNTs-PVA on day 10 and 13 and p-MWCNTs – HTAB on day 7 and 16. In the cell homogenate, the LDH was low and < 1um/mg protein on day 7 in both the controls and treatment composites but as the cells matured there was an increase (Figure 6.6). Statistical difference was observed between the control (blank), pure HA composite and all the treatments on day 7 whereas no statistical difference was observed between the control and the treatments on day 21 except f-MWCNTs-PVA which was significantly lower than control.
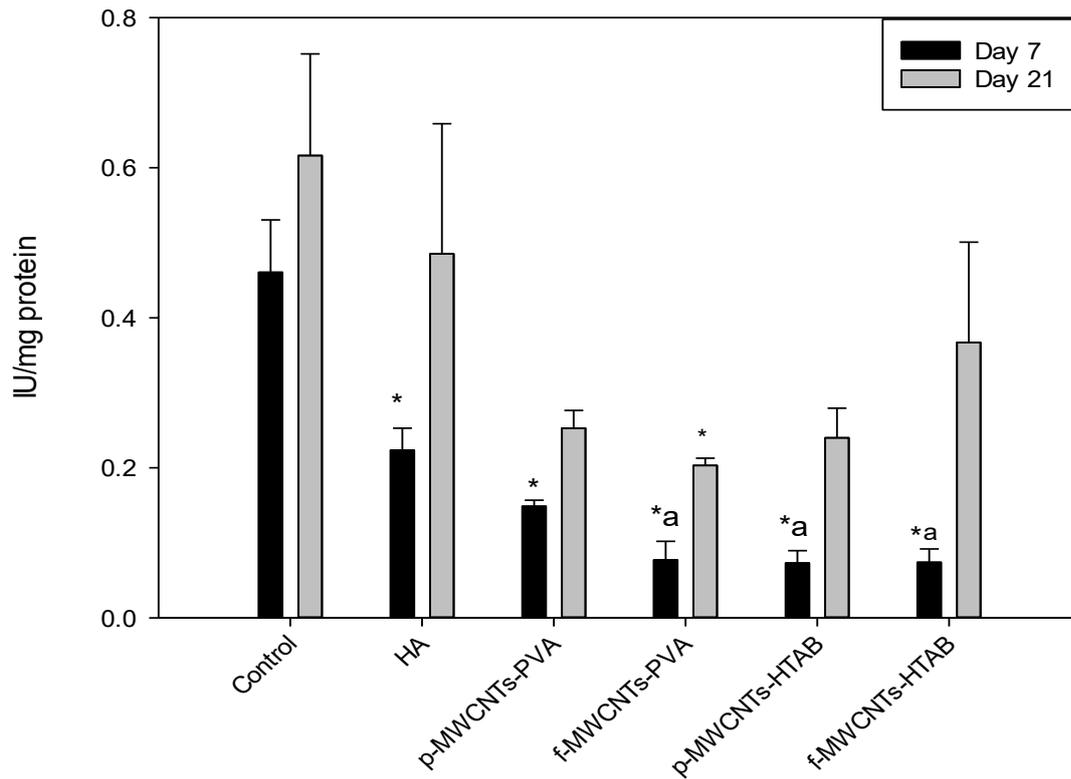
Figure 6.6 LDH activity from cell homogenate after 7 and 21 days. Data are mean ± S.E.M (n = 4 per treatment per end point);* statistically different from control. Bars with letter 'a' are statistically differ from the others (p < 0.05).

Table 6.4 Lactate dehydrogenase activity in the external media (IU/ml media) during exposure of the osteoblast cells to the pure HA composite and the treatments containing MWCNTs and Ag NPs.

	Control	HA	*p*-MWCNTs-PVA	*f*-MWCNTs-PVA	*p*-MWCNTs-HTAB	*f*-MWCNTs-HTAB
Day 1	0.011 ± 0.05	0.042 ± 0.03	0.002 ± 0.002	0.014 ± 0.01	0.013 ± 0.005	0.018 ± 0.01
Day 4	0.036 ± 0.02	0.029 ± 0.01	0.011 ± 0.007	0.002 ± 0.001	0.048 ± 0.01	0.008 ± 0.004
Day 7	0.025 ± 0.01	0.007 ± 0.003	0.026 ± 0.02	0.000 ± 0.000a	0.014 ± 0.01#	0.064 ± 0.04b
Day 10	0.024 ± 0.02	0.110 ± 0.1	0.011 ± 0.01	0.061 ± 0.04#	0.000 ± 0.000	0.007 ± 0.007
Day 13	0.000 ± 0.00	0.035 ± 0.020*a	0.002 ± 0.002	0.000 ± 0.000#	0.000 ± 0.000	0.000 ± 0.000
Day 16	0.012 ± 0.006	0.001 ± 0.001	0.014 ± 0.01	0.033 ± 0.02	0.012 ± 0.009#	0.044 ± 0.04
Day 19	0.038 ± 0.02	0.007 ± 0.007	0.021 ± 0.02	0.012 ± 0.01	0.005 ± 0.005	0.000 ± 0.000
Day 21	0.033 ± 0.01	0.001 ± 0.001	0.036 ± 0.02	0.017 ± 0.01	0.013 ± 0.005	0.010 ± 0.01

The data is presented as mean ± S.E.M (n= 4 per treatment); different letters within rows are statistically different from each other and absence of the letters means there is no significate difference. * statistically different from the control within each row. # Significantly different from previous time point within the column (one way ANOVA or Kruskal-wallis test, $P < 0.05$

6.3.5 Alkaline Phosphatase

The presence of alkaline phosphatase in the media indicates the metabolic activity of the osteoblast cells. Table 6.5 shows the ALP activity (IU/ml) in the external media on days 1, 4, 7, 10, 13, 16, 19 and 21. The data did not show any significant differences between the control (blank) and the treatments on all the days. Significant difference between the control (blank) and pure HA composite was observed on day 4 and 13. Within the control and treatments no significant difference as observed within the days except pure HA composite which had a significant difference between day 13 and 16. An increase in ALP activity was observed in the media of all the composites from day 1 to day 21. After 7 and 21 day incubation, ALP activity of the cell homogenates were also measured (Figure 6.7). No significant difference was observed between the controls and treatments on both the days (one way ANOVA, P =0.102 (day 7) 0.209(day 21)).
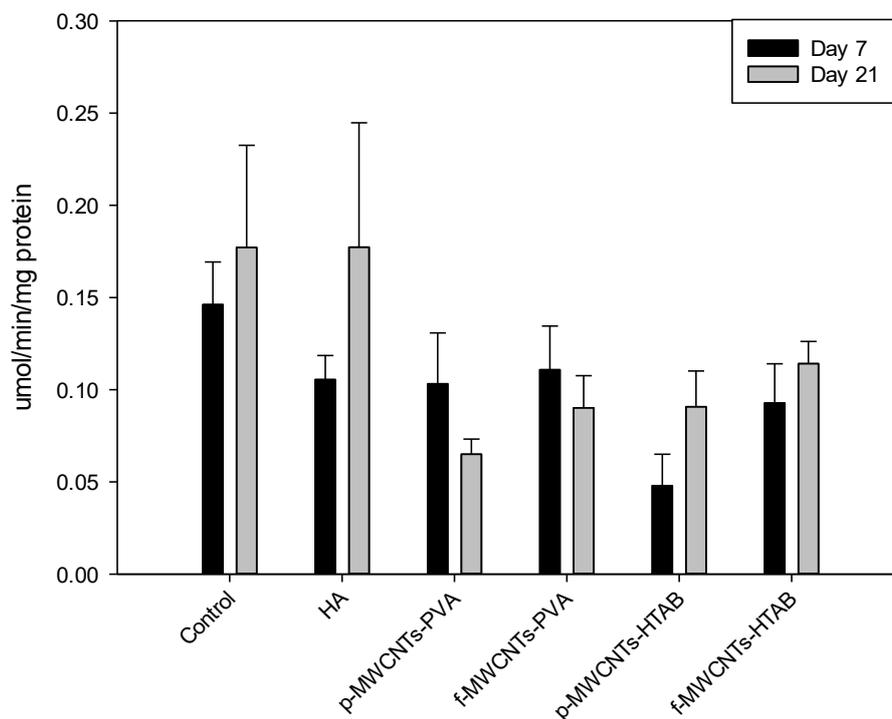
Figure 6.7 Alkaline Phosphatase activity (ALP) from the cell homogenates after 7 and 21 days. Data are mean ± S.E.M (n=4 per treatment per end point). No statistical difference was observed between the treatments and control on both the days, one way ANOVA, P = 0.102 (day 7) 0.209(day 21)

Table 6.5 Alkaline phosphatase activity of the osteoblast cells in external media (µmol/min/ml) after exposing the osteoblasts cells to the composites over 21 days.

Day	Control	HA	*p*-MWCNTs-PVA	*f*-MWCNTs-PVA	*p*-MWCNTs-HTAB	*f*-MWCNTs-HTAB
1	0.023 ± 0.006	0.016 ± 0.003	0.017 ± 0.003	0.016 ± 0.005	0.022 ± 0.01	0.019 ± 0.007
4	0.032 ± 0.003	0.012 ± 0.002*	0.026 ± 0.004	0.024 ± 0.01	0.028 ± 0.01	0.024 ± 0.01
7	0.021 ± 0.01	0.014 ± 0.003	0.028 ± 0.008	0.017 ± 0.004	0.016 ± 0.004	0.020 ± 0.007
10	0.022 ± 0.01	0.024 ± 0.006	0.015 ± 0.006	0.015 ± 0.005	0.026 ± 0.01	0.021 ± 0.008
13	0.029 ± 0.007	0.011 ± 0.002*a#	0.029 ± 0.007	0.026 ± 0.006b	0.032 ± 0.01	0.038 ± 0.01
16	0.028 ± 0.01	0.029 ± 0.007#	0.020 ± 0.003	0.022 ± 0.01	0.022 ± 0.01	0.028 ± 0.008
19	0.029 ± 0.004	0.025 ± 0.006	0.014 ± 0.007	0.025 ± 0.007	0.033 ± 0.01	0.031 ± 0.01
21	0.038 ± 0.007	0.028 ± 0.005	0.040 ± 0.01#	0.024 ± 0.007	0.024 ± 0.01	0.028 ± 0.01

The data are presented as mean ± S.E.M (n=4 per treatment); different letters within rows are statistically different from each other and absence of the letters means there is no significate difference. * statistically different from the control within each row. # Significantly different from previous time point within the column (one way ANOVA, $P<0.05$)

6.3.6 Total Glutathione assay

Glutathione is involved in protecting cells against cytotoxicity by counteracting the effects of oxidative stress in cells and maintaining the intracellular redox balance. The total concentration of GSH was measured in cell homogenate after day 7 and 21 (Figure 6.8). No statistical difference was observed between the controls and treatments on both the days (one-way ANOVA, p = 0.743(day 7), 0.27 (day 21)).
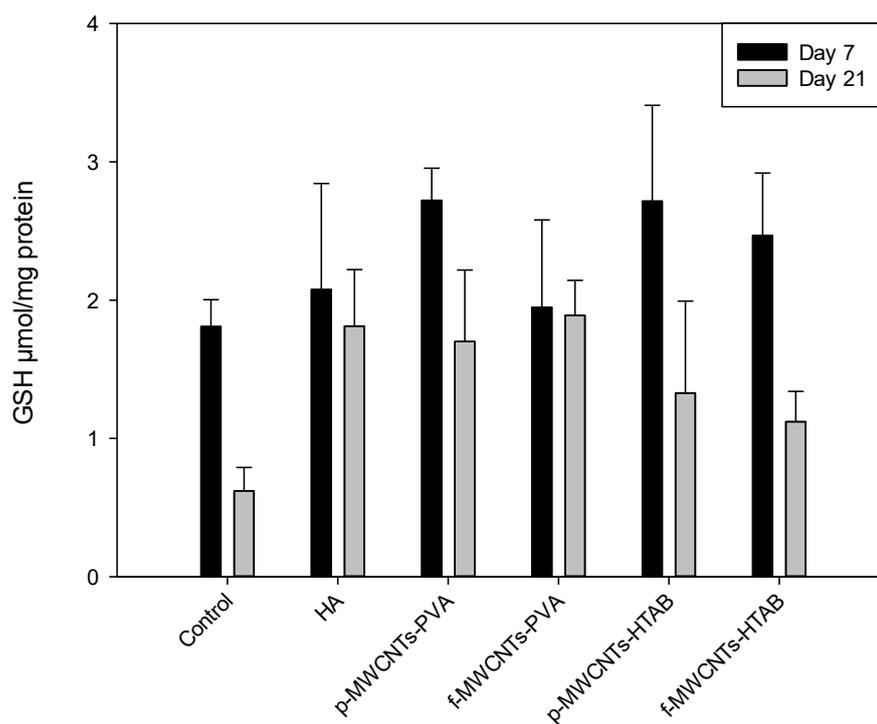

Figure 6.8 Total Glutathione activity (GSH) from the cell homogenates after 7 and 21 days. Data are mean ± S.E.M (n=4 per treatment per end point). No statistical difference was observed between the treatments and control on both the days, one way ANOVA, P = 0.743 (day 7) 0.27(day 21)

6.4 Discussion

The aim of this study was to test the biosafety of the Ag NPs-MWCNTS-HA composites for clinical application by allowing human osteoblast cells to differentiate and mineralize on the composites. Osteogenesis was induced by specific culture media conditions and was monitored by measuring the bone specific proteins and protein encoding mRNA expression. Osteoblastic differentiation and mineralization was observed for all the treatment substrates, pure HA control and for the cultures grown on tissue culture plastic (reference, control).

6.4.1 The exposure of the DMEM media and cells to the composites and silver accumulation

The total silver concentration was measured in the external media and cell homogenates (Table 6.2 and 6.3) in order to determine the exposure of the osteoblast to silver. High concentrations of silver was observed in the external media of the composites with p-MWCNTs, specifically after 24 h incubation which then starts to decrease with the media being changed every 48 h. This high dissolution of silver from the p-MWCNTs compared to the f-MWCNTs could be due to the difference in the decoration of Ag NPs on the outer walls of the MWCNTs. Compared to the p-MWCNTs, higher amount of silver nanoparticles decorated the outerwalls of the f- MWCNTs which was evident from the TEM images (Chapter 3, Section 3.3.2). This result correlates with the dialysis experiment results (Section 3.3.2) which also showed higher silver release in SBF from the p-MWCNTs composites. Also, the Ag NPs surface will be modified in DMEM media and once an insoluble coat of AgCl or protein corona is formed, then the particles will be less likely to leach. Another possible explanation lies in the medium, which bathes the composites.

Hansen et al. (Hansen and Thünemann, 2015) have shown that silver dissolution was higher in DMEM media supplemented with 10 % FBS compared to pure water due to the presence of proteins. The presence of amino acids such as L-cysteine (63mg/l) from FBS could have enhanced silver release from the composites. The cysteine –SH group has a very high affinity for Ag which is an irreversible binding. This would stimulate an outward diffusion gradient from the particle surface. Furthermore, accumulation of silver in the cell homogenate of the treatments and controls was analysed for both the days. Silver accumulation was observed in all the cell homogenate from all the treatments, except the controls. Day 7 cell homogenates had an approximate concentration between 20 -15 μg/l except f-MWCNTs-HTAB which was significantly lower. However, by day 21 the concentration of silver in p-MWCNTs composites and f-MWCNTs-HTAB increased by ~ 170%. This result seems to be consistent with Zhang et al (Zhang et al., 2016) who showed that silver could accumulate in human cells such as fibroblasts and osteoblasts. The electrolytes Mg $^{2+}$, Ca^{2+},P, Na$^+$, K$^+$ were measured in the media and significantly higher concentration of Ca^{2+} and P was observed in the p-MWCNTs composites suggesting possible dissolution or degradation of the material. Further studies needs to be undertaken to confirm this effect.

6.4 2 Effect of the composites on biochemistry

The cytotoxicity of the composites against the osteoblast cells was measured by the LDH and glutathione assay. LDH activity in the external media was very low and supports the idea that the composites did not exhibit a toxic effect on the cells. Although silver was detected in the media (Table 6.2), the proteins (cysteine) in the media might bind with any free silver reducing the bioavailability of the silver to cause toxicity to the cells. Another possible explanation is the formation of insoluble AgCl at high chloride

concentrations [120Mm] present in DMEM (Huynh and Chen, 2011). Also, the total concentration of the LDH in the cell homogenate (Figure 6.6) was generally low suggesting that there was not sufficient LDH to leak out into the external media.

However, day 7 cell homogenates showed a low level of LDH activity in the treatments compared to the reference control (blank, Figure 6.6), which infers to less number of viable cells in the composites but by the end of 21 days no significant difference was observed in the LDH activity between the reference and the treatments (Figure 6.6). Contrary to the LDH result, no significate difference was observed in the concentration of GSH on both the days. The LDH results correlates with the concentration of silver released in the media (Table 6.2) as the concentration of silver being released into the media has decreased gradually over time. It seems possible that the concentration of silver in the media was at sub-lethal dose as the silver did not kill the cells but slowed the proliferation of the cells temporarily.

GSH is an antioxidant and is the first defence in the cell against oxidative stress as it scavenges of reactive oxygen species. No significant change in the GSH measurement was observed in both the days (Figure 6.8) suggesting that the cells were not under stress. Many studies involving Ag NPs have suggested oxidative stress as the main route by which Ag NPs decrease proliferation of cells and cause toxicity (Carlson et al., 2008, Piao et al., 2011, Lee et al., 2014). Oxidative stress is caused by an imbalance between the production of reactive oxygen species and antioxidant capacity of the cells. The results from this study show that oxidative stress might not be the primary toxic mechanism for Ag NPs. This result is in accordance with Nguyen et al (Nguyen et al., 2013) who showed that the toxicity route of the Ag NPs differ based on the physiochemical properties such

as shape, size and coating of the Ag NPs. They have shown that Ag NPs have stimulatory and suppressive effects on the production of cytokines. Similarly, the cytokines, Il-6 and TNF-α are upregulated in this study (Figure 6.5 G and H) which are discussed in detail below.

A small fraction of dissolved silver from the Ag NPs will instantaneously form silver chloride and be lost. The GSH present in the cells will bind to the silver at it enters the cells. When the GSH pool is depleted, the genes encoding cytokines will be upregulated (Tew and Townsend, 2011). The cells are also capable of transporting total glutathione across the cell membrane and GSH along with other solutes may leak from damaged cells (Perrone et al., 2005). However, the possibility of cell damage and leak of enzymes in the media is not supported by the other assays such as LDH, ALP and qualitative analysis by SEM. To exemplify, as the release of silver was reduced over time, the cells were able to proliferate and no significant difference was observed between the reference control and treatments by day 21in LDH assay. This is in accordance with the fact that cytotoxicity of silver is time and dose dependent and the cells are able to revive as the concentration of the silver reduces.

Similarly, no significant difference in the ALP activity was detected in the cell homogenate on both the days (Figure 6.7). ALP is an enzyme bound to the inositol-phosphate membrane on the outer surface of osteoblasts. The mechanism with which this enzyme carries out its function is not completely understood but it appears to act both to increase the local concentration of inorganic phosphate, a mineralization promoter, and to decrease the concentration of extracellular pyrophosphate, an inhibitor of mineral phosphate (Golub and Boesze-Battaglia, 2007). The presence of ALP in the

media (Table 6.5) suggests that the cells were healthy and had the ability to mineralise as ALP is released from the osteoblast cells into the media during active bone formation. The results show that the presence of silver did not decrease the ALP activity which confirms that silver has no adverse effect on the activity of the osteoblasts. This finding is consistent with the study done by Pauksch et al (2014) who suggested that silver at sublethal dose (10 mg/l) does not inhibit the alkaline phosphate activity in human osteoblast cells. The biochemical assay results are reflected in the SEM observation as no major differences in the presence of nodule formation on the cells was observed.

6.4.3 Effect of the composites on the cells at molecular level

As cells undergo differentiation, various markers are induced in an ordered and sequential manner; although the details of the steps can be overlapping and difficult to elucidate. The most frequently used bone matrix protein markers of the osteoblast differentiation process (ALP, OPN and OCN, Figure 6.5) are all expressed in the treatments confirming the differentiation and mineralization of the cells. Many studies have suggested that the osteoblast gene expression and subsequent mineralization are affected by the surface topographies of the implants (Boyan et al., 1996, Schneider et al., 2003, Masaki et al., 2005). Since the topography of the composites are not comparable to that of the cell culture plate the expression of the genes are relative to the pure HA composite. Further, the cells grown on the composites were not expected to outperform the control (reference cells) grown on the plastic culture plate which is evidenced by the biochemical assay results.

The transcription factors Runx2, Dlx5 and OSX (Figure 6.5 A, B and C) are all expressed on both the days and their expression has been either upregulated or

downregulated depending on their role in osteoblast differentiation. Runx2 is considered as the osteoblast master regulator as it is the first transcription factor required for the determination of the osteoblast lineage from the mesenchymal cells, while the Sp7 and Wnt-signalling block their differentiation into other cell types such as osteoclasts and chondrocytes (Komori, 2010). Runx2 is upregulated by day 7 as they are still immature cells and differentiation was induced by the addition of supplemented DMEM which reduced the expression of Runx2 by day 21. This is because Runx2 is first detected in preostoblasts and the expression increases in immature osteoblasts but during maturation the expression of Runx2 is reduced and do not express a significant amount in mature osteoblasts (Komori, 2010) whereas the expression of DLX-5 which is usually expressed during mineralization stage is also downregulated. The downregulation of DLX-5 could be due to the upregulation of cytokines, which suggests possible inflammation reaction of the osteoblasts to the composites. Following Runx2, OSX is the next transcription factor crucial for osteoblast differentiation which is expressed during the maturation of pre-osteoblasts to immature osteoblasts (Cao et al., 2005, Komori, 2006). The expression of OSX also follows the same pattern as Runx2 which is upregulated on day 7 and downregulated on day 21 which suggests that the molecular function mainly coding differentiation of the cells is not affected by the presence of the composites.

Factors secreted by the osteoblasts also control the differentiation and activity of the bone –resorbing osteoclast (Zhou et al., 2010). Cytokines reduce osteoblastic bone formation and stimulate osteoclastic bone resorption. The cytokines TNF-α and IL- 6 are both upregulated in all the treatments on both the days (Figure 6.5 G and H) with a maximum of 15 fold change on day 7. TNF-α is one of the most important

proinflammatory cytokines that is induced in response to the early phase of injury which inturn activates IL-6 expression (Kurokouchi et al., 1998). The results from this study correspond to the study by Kaneshiro et al. (Kaneshiro et al., 2014) who suggested that IL-6 negatively regulates the osteoblast differentiation by reducing the expression of Runx2, osterix and osteocalcin and differentiation in a dose dependent manner. Similarly, all the genes encoding differentiation are downregulated on both the days in cells from the composite AgNP-*p*-MWCNTs –PVA which could be due to the relatively higher upregulation of IL-6 associated with the relatively high Ag NPs release from these composites compared to the other composites. The upregulation of the cytokines in the other treatments is also higher on day 7 compared to day 21 which again corresponds with the relatively higher silver release on day 7 compared to day 21. However, the expression of the bone matrix proteins (ALP and OCN) and non-collagenous protein (OPN) are as expected.

In all the treatments, ALP is upregulated on day 7 and downregulated on day 21, except for AgNP-*p*-MWCNTs –PVA (Figure 6.5). In general, ALP as early marker of osteoblast differentiation, is among the first functional genes expressed in the process of calcification, and appear in relatively immature osteoblasts. On the other hand, OCN appears later with the onset of mineralization which occurs at the same time as the expression of DLX-5 transcription factor (Ryoo et al., 1997, Golub and Boesze-Battaglia, 2007, Komori, 2010). An upregulation in the expression of OPN is observed on day 7 and downregulated on day 21. OPN mediates the binding of osteoclasts to the mineral matrix protein resulting in bone resorption. The high expression of TNF-α and IL-6 due to inflammation promotes the upregulation of OPN leading to the promotion of bone resorption. This result has been observed by Kutokouchi et al (Kurokouchi et al., 1998)

196

who observed that TNF-α upregulates the IL-6 which leads to the cascading events leading to high bone resorption in cases of osteoporosis and inflammatory diseases such as rheumatoid arthritis.

6.5 Conclusion

The goal of the study was to determine the biocompatibility of the Ag NPs-MWCNTs –HA by allowing human osteoblast cells to differentiate and mineralize on the composites. The main outcome of this study is that the nature of the MWCNTs (pristine or functionalised) affect the release of the Ag NPs which was significantly higher in the presence of *p*-MWCNTs. At sub lethal dose, Ag NPs release temporarily affect the proliferation of osteoblasts but with the reduction in the release of silver, the cells are able to resume proliferation but the activity (mineralization) is not affected. The study of the genes suggested that the cells were subjected to inflammation reaction but it does not manifest as an effect on cell health. Literature suggests that high expression of cytokines may trigger bone resorption by activating osteoclast cells. Hence, for clinical purposes, these composites are not yet ready and further studies are needed to investigate the expression of the cytokines after extended periods and the exact mechanism by which silver affects the expression of the genes.

7. General Discussion

There is a rise in the demand for long term artificial bone implants which do not have to be replaced as a result of implant failure. Currently, implants fail as a result of either infection following surgery, inflammation / adverse reaction from the body due to non-biocompatibility of the implant or poor mechanical properties in load bearing areas. So far, there is no single ideal treatment and all the alternatives have their own advantages and disadvantages. The main hypothesis of the current study was to develop a composite which is biocompatible and mechanically strong with the ability to prevent infection following surgery. To achieve this, the initial pilot study was undertaken which confirmed that HA was the most biocompatible type of calcium phosphate with human osteoblast cells. Following that, Ag NPs were incorporated to provide antibacterial properties while MWCNTs were used to reinforce the HA to improve the mechanical strength and to serve as anchor points for the silver nanoparticles. The suitability of the composites for the intended purpose was tested by subjecting the composites to mechanical, biocompatible and antibacterial testing and the main conclusions of the study are as follows.

Ag NPs-MWCNTs-HA composite powders with a MWCNTs loading of 0.5 wt. % were successfully synthesized using the sol-gel technique. The powders mainly contained phase pure HA as shown by XRD, FTIR and TEM analysis (Figures 3.5, 3.6 and 3.7). The morphology of the HA crystals was influenced by the presence of surfactants (section 3.7.2). Composites containing pristine MWCNTs and needle shaped HA crystals (Ag NPs-*p*MWCNTs-PVA) presented the highest mechanical properties compared to the pure HA composites. The functionalisation of the MWCNTs using nitric acid resulted in defects on the walls of the MWCNTs, which affected the tensile strength of the composite, but not the compressive strength (Figure 3.11). Human osteoblast cells were grown and allowed

to differentiate on the pure HA control and the four treatment composites. Cells proliferated and differentiated on all the composites. mRNA studies showed that the molecular activity of the cells encoding differentiation were upregulated although the genes encoding the cytokines were also upregulated meaning that the cells were subjected to stress. However, the biochemical analysis showed that the stress did not affect the health of the cells and they were able to proliferate and mineralize. The viability of *S. aureus* was reduced in all the composites containing Ag NPs compared to pure HA composites after 24 h. The silver ion release was low and controlled.

7.1 Mechanical strength of the composites

All bones are bearing loads to different extents. The mechanical strength results showed a promising outcome for the Ag NPs-MWCNTs-HA composites. This is because the tensile and compressive strength of the composites were improved significantly compared to pure HA composites. Both the nature of the MWCNTs (Pristine or functionalised) and the HA crystal morphology played a crucial role in determining the overall mechanical properties of the composite. The tensile strength values of the Ag NPs-MWCNTs-PVA composites are approaching that of cancellous bones which is approximately 10-20 MPa, whereas the compressive strength values have exceeded the values of cancellous bone which are between 7- 10 MPa by approximately 200% (Murugan and Ramakrishna, 2005). Based on the results obtained, the composites can be mainly used in less load bearing areas such as the upper extremity bones or clavicle bone. The results also confirm that the addition of the MWCNTs and Ag NPs do not negatively affect the mechanical properties of the final composite.

7.2 Biocompatibility and toxicity of the composites to human cells and bacteria

In this study, both the antibacterial activity and the biocompatibility of the composites were investigated. The investigation against *S. aureus* showed the ability of the composites to reduce/ prevent infection compared to pure HA composites (Section 5.3; Figure 5.5 and 5.6). This is especially promising as the Ag NPs were able to significantly reduce bacterial growth in the composites with very low silver ion release of 1.6 µg/l (Table 5.1). The result suggest that the Ag NPs- *p*-MWCNTs-PVA composite will meet the antimicrobial criteria for an implant to be translated to clinical use. Nevertheless to use these composites clinically, their toxicity and biocompatibility to human cells should also be studied. Hence, the human osteoblast cells were used to evaluate the biocompatibility of these composites *in vitro* first without the presence of Ag NPs for 7 days. The results showed that the MWCNTs-HA composites were biocompatible and allowed the proliferation of the cells (Figure 4.2 and 4.4). However, the ALP results suggested that the mineralization ability of the cells grown on the MWCNTs-HA composites might be reduced (Figure 4.5). Hence, an extended biocompatibility study of the final Ag NPs–MWCNTs-HA composites involving the differentiation and mineralization of the osteoblast cells in the presence of the composites for 21 days was performed. The overall results showed that the cells were able to proliferate with healthy morphology and mineralize in the presence of the composites (Figure 6.4). The ALP analysis showed that the metabolic activity of the cells were also not affected in the presence of the composites (Figure 6.7). Although the genes encoding mineralization had been upregulated, the mRNA analysis also suggested that the cells were under stress as the cytokines (TNF - α and IL – 6, Figure 6.5) were also upregulated. The overall biocompatibility studies have shown that the composites are biocompatible and the osteoblast cells were able to proliferate, differentiate and mineralize. The

biocompatibility of the composites are in accordance with the study led by Herkendell et al., (2014) which is the only other study which has examined the impact of HA, MWCNTs and Ag NPs composites. However, from the clinical perspective, the biocompatibility study should also be performed with other cell types, which are involved in wound healing such as fibroblasts , endothelial cells and angiogenesis.

Humans are exposed to low quantities of heavy metals such as silver and gold every day from food, cosmetics and clothing. For example, silver is approved as a foil for consumption by the European Union as food additive E174 (Aguilar et al.,2016) . This is because silver is generally considered to exhibit low toxicity in the human body. Minimal risk is also expected due to the clinical exposure by the use of silver in implants. Free silver (Ag^+) which are released from the composites will bind avidly to the –SH groups almost irreversibly. So, any free silver will be neutralised by the plasma proteins like albumins. Also, Ag^+ will react with the copious amount of chloride (Cl-) to form AgCl which is an insoluble particulate precipitate and can enter into circulation. Similarly, Ag NPs which could be released from the composites would normally be digested by the immune cells and any undigested particle will be processed by the liver into the bile and excreted by the gut lumen. If the Ag NPs are reabsorbed into circulation by resorption rather than excreted, it will only cause imbalance in the microbial flora resulting in gastrointestinal tract disturbances in patients. Hence, the silver used in the development of the composites which is at sub lethal levels should not pose a risk to the human health in the long term but they are able to reduce microbial infection. Another main concern would be the use of MWCNTs as CNTs have a toxic effect on human cells similar to the toxicity effect of asbestos (Donaldson et al., 2013, Poland et al., 2008, Pacurari et al., 2010). However, the results suggest that MWCNTs are biocompatible, promote the proliferation

of the osteoblast cells and do not elicit a toxic response. Furthermore, most of the toxicology studies are based on the bioaccumulation of CNTs in internal organs following respiratory exposure whereas, the effect of CNTs leaching from implants has not been explored (Muller et al., 2005, Poland et al., 2008, Teeguarden et al., 2010). Furthermore, the toxicity of CNTs should not be compared to asbestos as the mechanism by which asbestos cause toxicity is different to that of CNTs. Asbestos toxicity is due to the rigid needle like nature which causes cell injury and are not phagocytosed by macrophages whereas CNTs are flexible and non-rigid and they can undergo phagocytosis (Smart et al., 2006, Muller et al., 2009, Nagai and Toyokuni, 2012).

7.3 Clinical perspective

The process of translating a new medical product into a clinically approved product involves acquiring the approval of European Medicines Agency (EMA). There are specific requirements stipulated by both the EMA and Food and Drug Administration (FDA) in the United States of America for medical implants. For the European Union, the Clinical Trials Directive (Directive 2001/20 /EC) which details the implementation of good clinical practice for the clinical trials overview the process of conducting a clinical trial for human medicines. Additionally, Basins et al (2015) suggests that there are regulations set by the EMA that lays down the procedures for the authorization and supervision of medicinal products which gives the EMA some oversight of national authority within Europe. Outside the European Union, regulations are often established at national level. There are three main principles behind the regulations of both the EMA and FDA which are: (i) the efficiency of the medical product for its intended clinical use; (ii) if the medial product is replacing an existing product, its effectives compared to the existing product and (iii) the safety of the new product – is it safe or safer than the existing

product (Juillerat-Jeanneret et al., 2015). In the case of Dental and bone implants, Annex I of the Medical Device Directive 93/42/EC details the legal requirements for the use of bone/dental implants but there are no specific directives for the use of nanoparticles in bone/dental implants. The use of the various nanoparticles in the composite poses some complexity for the regulations. For example, the Ag NPs might be regarded as medicine since their main intended purpose is to provide antibacterial properties to the composite whereas the MWCNTs and HA falls under then medical device regulation. In essence, the main purpose of the composites is to be used as a medical device and that would be the starting point to get health agency approval.

Nevertheless, the important aspect of getting approval for the composite is to ensure that the above mentioned criteria are met and the benefits outweigh the risks of the composite. Risk assessment of the composites will include the hazard (toxicity) potential of the composites for the intended use. Although, some investigation has been undertaken to determine this, further investigations on the erosion of the composite and bioavailability of the Ag NPs and MWCNTs may be needed. Consequently, animal models will be relevant to determine the toxicity and *in vivo* reaction of the composites.

In conclusion, the study set out to develop a composite that is mechanically strong, biocompatible with antibacterial properties and the specific objectives were either achieved or partially achieved:

1. Investigate the biocompatibility of HA and compare it with different types calcium phosphate such as dicalcium phosphate and β-tricalcium phosphate –

achieved, HA showed better biocompatibility than the other two types of calcium phosphates;

2. Synthesise Ag NPs-MWCNTs-HA composites (with pristine and functionalised MWCNTs and surfactants) and characterize them using various techniques- **achieved**;

3. Demonstrate the mechanical properties of the composites by performing the diametral tensile strength test and compressive strength test- **partially achieved, the results showed that the composites exceed the compressive strength but not the tensile**;

4. Determine the biocompatibility of the MWCNTS- HA composites without the presence of Ag NPs *in vitro* by testing the viability and cytotoxic response to the cells to the composites- **achieved, the biocompatibility of the composites was better than pure HA composites**;

5. Demonstrate the antibacterial activity of the Ag NPs- MWCNTs-HA composites against *Streptococcus aureus* and select the composites with good antibacterial property for further study – **achieved, the composites containing pristine MWCNTs had higher antibacterial effect compared to the other composites**;

6. Investigate the biocompatibility of the Ag NPs- MWCNTs-HA composites with the human osteoblast cells by allowing the cells to differentiate and mineralize in the presence of the composites and study the viability of the cells by analysing gene expression and cytotoxic response to the composites- **achieved, the cells were able to proliferate and mineralize in the presence of all the composites.**

7.4 Future work suggestions

Based on the results obtained the following future work needs to be undertaken before the composites can be approved for human use. Adding functional groups to the MWCNTs surface to improve the dispersability in the HA matrix is most commonly achieved through treatments with strong acids. This affects the morphology and structural integrity of the MWCNTs, which damages the strength of the composite as shown in the mechanical results. A focus of the future work should be to find alternate less disruptive methods to add functional groups which would improve the homogeneity of the MWCNTs.

As a result of this study, it is evident that the mechanical properties of the final composite are dependent on the starting material and the HA crystals morphology which can be manipulated by the presence of surfactants. It would be interesting to compare the mechanical strength of different HA crystal to achieve the maximum necessary strength using various surfactants which might also improve the dispensability of the MWCNTs. Based on the literature survey only one type of MWCNTs loading (0.5% wt. %) was tried in this study. It would be beneficial to try different weight loadings above 5% as no results are available for composites with higher CNTs Wt.%. The mechanical study undertaken in the current research work was only preliminary investigation. It would be useful to try a wide range of mechanical tests such as 3-point bending test. It would also be beneficial to study the alignment of CNTs, the current method does not allow the alignment of CNTs in any one given direction. This will have a major effect on the mechanical properties of the final composite.

It would also be useful to test the antibacterial nature of the MWCNTs which might enhance the current antibacterial properties Ag NPs. Further investigation of the composites with varying quantities of Ag NPs will be useful to determine the exact quantity / release of Ag NPs required to fully prevent bacterial growth without compromising the biocompatibility of the materials. Furthermore, testing with one type of microbe is not sufficient to confirm their efficiency and the composites need to be exposed to other strains of microbes. The *in vitro* study is still a preliminary work and further investigation needs to be undertaken to study the effect of the composites on the various molecular and metabolic activities of the cells. Animal testing needs to be undertaken to determine the effect of the composites on other organs if there is MWCNTs dissolution from the composite.

7.5 Conclusion

There is a great potential to translate the Ag NPs-MWCNTs-PVA composites into clinically approved product. Ag NPs is a suitable alternative to the antibiotics and with the current surge in antibiotic resistance microbes, Ag NPs have the potential to prevent bacterial infection following surgery. This study has shown that the CNTs are biocompatible. However, even if the biological community eventually rules out CNTs due to their toxicity and prohibits their use in human body, this study and further investigations will be useful in understanding the mechanism by which CNTs reinforce ceramics which could be translated to a wide range of applications.

References

Abarrategi, A., Gutierrez, M. C., Moreno-Vicente, C., Hortiguela, M. J., Ramos, V., Lopez-Lacomba, J. L., Ferrer, M. L. & Del Monte, F. (2008). Multiwall carbon nanotube scaffolds for tissue engineering purposes. Biomaterials, 29, 94-102.

Aguilar,F., Cvrebelli,R., Domenico,A.,EFSA ANS Panel (EFSA Panel on Food Additives and Nutrient Sources Added to Food), 2016. Scientific opinion on the re-evaluation of silver (E 174) as food additive. EFSA Journal2016;14(1):4364, 64.

Afzal, M. a. F., Kalmodia, S., Kesarwani, P., Basu, B. & Balani, K. (2013). Bactericidal effect of silver-reinforced carbon nanotube and hydroxyapatite composites. Journal of Biomaterials Applications, 27, 967-978.

Ahrland, S., Chatt, J. & Davies, N. (1958). The relative affinities of ligand atoms for acceptor molecules and ions. Quarterly Reviews, Chemical Society, 12, 265-276.

Ajayan, P. M. (1999). Nanotubes from Carbon. Chemical Reviews, 99, 1787-1800.

Albee, F. H. (1920). Studies in bone growth: triple calcium phosphate as a stimulus to osteogenesis. Ann Surg, 71, 32-9.

Albers, C. E., Hofstetter, W., Siebenrock, K. A., Landmann, R. & Klenke, F. M. (2013). In vitro cytotoxicity of silver nanoparticles on osteoblasts and osteoclasts at antibacterial concentrations. Nanotoxicology, 7, 30-36.

Allegri, M., Perivoliotis, D. K., Bianchi, M. G., Chiu, M., Pagliaro, A., Koklioti, M. A., Trompeta, A.-F. A., Bergamaschi, E., Bussolati, O. & Charitidis, C. A. (2016). Toxicity determinants of Multi-Walled Carbon Nanotubes: the relationship between functionalization and agglomeration. Toxicology Reports.

Ambard, A. J. & Mueninghoff, L. (2006). Calcium phosphate cement: review of mechanical and biological properties. J Prosthodont, 15, 321-8.

Anderson, H. C. (2003). Matrix vesicles and calcification. Current rheumatology reports, 5, 222-226.

Anderson, H. C., Garimella, R. & Tague, S. E. (2005). The role of matrix vesicles in growth plate development and biomineralization. Front Biosci, 10, 822-837.

Andrade, F. a. C., Vercik, L. C. D. O., Monteiro, F. J. & Rigo, E. C. D. S. (2016). Preparation, characterization and antibacterial properties of silver nanoparticles–hydroxyapatite composites by a simple and eco-friendly method. Ceramics International, 42, 2271-2280.

Arrington, E. D., Smith, W. J., Chambers, H. G., Bucknell, A. L. & Davino, N. A. (1996). Complications of iliac crest bone graft harvesting. Clinical orthopaedics and related research, 329, 300-309.

Asran, A. S., Henning, S. & Michler, G. H. (2010). Polyvinyl alcohol–collagen–hydroxyapatite biocomposite nanofibrous scaffold: Mimicking the key features of natural bone at the nanoscale level. Polymer, 51, 868-876.

Bahrambeigi, V., Salehi, R., Hashemibeni, B. & Esfandiari, E. (2012). Transcriptomic comparison of osteopontin, osteocalcin and core binding factor 1 genes between human adipose derived differentiated osteoblasts and native osteoblasts. Advanced Biomedical Research, 1, 8.

Baker, M. I., Walsh, S. P., Schwartz, Z. & Boyan, B. D. (2012). A review of polyvinyl alcohol and its uses in cartilage and orthopedic applications. Journal of Biomedical Materials Research Part B: Applied Biomaterials, 100B, 1451-1457.

Barrère, F., Van Blitterswijk, C. A. & De Groot, K. (2006). Bone regeneration: molecular and cellular interactions with calcium phosphate ceramics. International Journal of Nanomedicine, 1, 317-332.

Barrientos-Durán, A., Carpenter, E. M., Zur Nieden, N. I., Malinin, T. I., Rodríguez-Manzaneque, J. C. & Zanello, L. P. (2014). Carboxyl-modified single-wall carbon nanotubes improve bone tissue formation in vitro and repair in an in vivo rat model. International Journal of Nanomedicine, 9, 4277-4291.

Bauer, T. W. & Muschler, G. F. (2000). Bone Graft Materials: An Overview of the Basic Science. Clinical Orthopaedics and Related Research, 371, 10-27.

Berendt, T. & Byren, I. (2004). Bone and joint infection. Clinical Medicine, 4, 510-518.

Berthomieu, C. & Hienerwadel, R. (2009). Fourier transform infrared (FTIR) spectroscopy. Photosynthesis Research, 101, 157-170.

Besinis, A., De Peralta, T. & Handy, R. D. (2014). The antibacterial effects of silver, titanium dioxide and silica dioxide nanoparticles compared to the dental disinfectant chlorhexidine on *Streptococcus mutans* using a suite of bioassays. Nanotoxicology, 8, 1-16.

Best, S. M., Porter, A. E., Thian, E. S. & Huang, J. (2008). Bioceramics: Past, present and for the future. Journal of the European Ceramic Society, 28, 1319-1327.

Bigi, A., Boanini, E. & Rubini, K. (2004). Hydroxyapatite gels and nanocrystals prepared through a sol–gel process. Journal of Solid State Chemistry, 177, 3092-3098.

Bloor, D., Donnelly, K., Hands, P. J., Laughlin, P. & Lussey, D. (2005). A metal–polymer composite with unusual properties. Journal of Physics D: Applied Physics, 38, 2851.

Bohner, M., Galea, L. & Doebelin, N. (2012). Calcium phosphate bone graft substitutes: Failures and hopes. Journal of the European Ceramic Society, 32, 2663-2671.

Bonilla, J., Fortunati, E., Atarés, L., Chiralt, A. & Kenny, J. M. (2014). Physical, structural and antimicrobial properties of poly vinyl alcohol–chitosan biodegradable films. Food Hydrocolloids, 35, 463-470.

Boulanger, G., Andujar, P., Pairon, J.-C., Billon-Galland, M.-A., Dion, C., Dumortier, P., Brochard, P., Sobaszek, A., Bartsch, P., Paris, C. & Jaurand, M.-C. (2014). Quantification of short and long asbestos fibers to assess asbestos exposure: a review of fiber size toxicity. Environmental Health, 13, 59.

Boyan, B., Bonewald, L., Paschalis, E., Lohmann, C., Rosser, J., Cochran, D., Dean, D., Schwartz, Z. & Boskey, A. (2002). Osteoblast-mediated mineral deposition in culture is dependent on surface microtopography. Calcified tissue international, 71, 519-529.

Boyan, B. D., Hummert, T. W., Dean, D. D. & Schwartz, Z. (1996). Role of material surfaces in regulating bone and cartilage cell response. Biomaterials, 17, 137-146.

Bresciani, E., Barata, T. D. J. E., Fagundes, T. C., Adachi, A., Terrin, M. M. & Navarro, M. F. D. L. (2004). Compressive and diametral tensile strength of glass ionomer cements. Journal of Applied Oral Science, 12, 344-348.

Bunyaratavej, P. & Wang, H.-L. (2001). Collagen Membranes: A Review. Journal of Periodontology, 72, 215-229.

Campbell, H. A., Handy, R. D. & Nimmo, M. (1999). Copper uptake kinetics across the gills of rainbow trout (Oncorhynchus mykiss) measured using an improved isolated perfused head technique. Aquatic Toxicology, 46, 177-190.

Cao, Y., Zhou, Z., De Crombrugghe, B., Nakashima, K., Guan, H., Duan, X., Jia, S.-F. & Kleinerman, E. S. (2005). Osterix, a Transcription Factor for Osteoblast Differentiation, Mediates Antitumor Activity in Murine Osteosarcoma. Cancer Research, 65, 1124-1128.

Carlson, C., Hussain, S. M., Schrand, A. M., K. Braydich-Stolle, L., Hess, K. L., Jones, R. L. & Schlager, J. J. (2008). Unique Cellular Interaction of Silver Nanoparticles: Size-Dependent Generation of Reactive Oxygen Species. The Journal of Physical Chemistry B, 112, 13608-13619.

Chao Le Meng, B., Erin, Y. T., Mark, S. K. C., Yuchun, L., Mahesh, C. & Jerry, K. Y. C. (2013). Advances in Bone Tissue Engineering.

Charlena, Nuzulia, N. A. & Handika (2017). Synthesis and Characterization of Composite Hydroxyapatite-Silver Nanoparticles. IOP Conference Series: Earth and Environmental Science, 58, 012064.

Chen, C.-W., Oakes, C. S., Byrappa, K., Riman, R. E., Brown, K., Tenhuisen, K. S. & Janas, V. F. (2004). Synthesis, characterization, and dispersion properties of hydroxyapatite prepared by mechanochemical-hydrothermal methods. Journal of Materials Chemistry, 14, 2425-2432.

Cheng, M., Qiao, Y., Wang, Q., Jin, G., Qin, H., Zhao, Y., Peng, X., Zhang, X. & Liu, X. (2015). Calcium Plasma Implanted Titanium Surface with Hierarchical Microstructure for Improving the Bone Formation. ACS Appl Mater Interfaces, 7, 13053-61.

Chłopek, J., Czajkowska, B., Szaraniec, B., Frackowiak, E., Szostak, K. & Beguin, F. (2006). In vitro studies of carbon nanotubes biocompatibility. Carbon, 44, 1106-1111.

Coathup, M. J., Cai, Q., Campion, C., Buckland, T. & Blunn, G. W. (2013). The effect of particle size on the osteointegration of injectable silicate-substituted calcium phosphate bone substitute materials. Journal of Biomedical Materials Research. Part B, Applied Biomaterials, 101B, 902-910.

Coleman, J. N., Khan, U., Blau, W. J. & Gun'ko, Y. K. (2006). Small but strong: a review of the mechanical properties of carbon nanotube–polymer composites. Carbon, 44, 1624-1652.

Constanda, S., Stan, M. S., Ciobanu, C. S., Motelica-Heino, M., Gu, Gan, R., Gis, Lafdi, K., Dinischiotu, A. & Predoi, D. (2016). Carbon Nanotubes-Hydroxyapatite Nanocomposites for an Improved Osteoblast Cell Response. Journal of Nanomaterials, 2016, 10.

Correa-Duarte,M.A., Wagner,N., Rojas-Chapana,R., Morsczeck, C., Thie, M.,& Giersig,M. (2004). Fabrication and Biocompatibility of Carbon Nanotube-Based 3D Networks as Scaffolds for Cell Seeding and Growth.Nano letters 11, 2233-2236.

Costa, H. S., Mansur, A. a. P., Pereira, M. M. & Mansur, H. S. (2012). Engineered hybrid scaffolds of poly(vinyl alcohol)/bioactive glass for potential bone engineering applications: synthesis, characterization, cytocompatibility, and degradation. J. Nanomaterials, 2012, 4-4.

Daculsi, G. (1998). Biphasic calcium phosphate concept applied to artificial bone, implant coating and injectable bone substitute. Biomaterials, 19, 1473-1478.

Dai, H. (2002). Carbon Nanotubes: Synthesis, Integration, and Properties. Accounts of Chemical Research, 35, 1035-1044.

Daniels, A. U., Chang, M. K. O. & Andriano, K. P. (1990). Mechanical Properties of Biodegradable Polymers and Composites Proposed for Internal Fixation of Bone. Journal od applied biomaterials, 1, 57-78.

Datsyuk, V., Kalyva, M., Papagelis, K., Parthenios, J., Tasis, D., Siokou, A., Kallitsis, I. & Galiotis, C. (2008). Chemical oxidation of multiwalled carbon nanotubes. Carbon, 46, 833-840.

Della Bona, Á., Benetti, P., Borba, M. & Cecchetti, D. (2008). Flexural and diametral tensile strength of composite resins. Brazilian oral research, 22, 84-89.

Demczyk, B. G., Wang, Y. M., Cumings, J., Hetman, M., Han, W., Zettl, A. & Ritchie, R. O. (2002). Direct mechanical measurement of the tensile strength and elastic modulus of multiwalled carbon nanotubes. Materials Science and Engineering: A, 334, 173-178.

Dereszewski, G. & Howell, D. S. (1978). The role of matrix vesicles in calcification. Trends in Biochemical Sciences, 3, 151-153.

Eatemadi, A., Daraee, H., Karimkhanloo, H., Kouhi, M., Zarghami, N., Akbarzadeh, A., Abasi, M., Hanifehpour, Y. & Joo, S. W. (2014). Carbon nanotubes: properties, synthesis, purification, and medical applications. Nanoscale Research Letters, 9, 1-13.

Etheridge, M. L., Campbell, S. A., Erdman, A. G., Haynes, C. L., Wolf, S. M. & Mccullough, J. (2013). The big picture on nanomedicine: the state of investigational and approved nanomedicine products. Nanomedicine: Nanotechnology, Biology and Medicine, 9, 1-14.

Felix, R. & Fleisch, H. 1976. The Role of Matrix Vesicles in Calcification. In: NIELSEN, S. P. & HJØRTING-HANSEN, E. (eds.) Calcified Tissues 1975: Proceedings of the XIth European Symposium on Calcified Tissues. Berlin, Heidelberg: Springer Berlin Heidelberg.

Fernandes, R. M. F., Abreu, B., Claro, B., Buzaglo, M., Regev, O., Furó, I. & Marques, E. F. (2015). Dispersing Carbon Nanotubes with Ionic Surfactants under Controlled Conditions: Comparisons and Insight. Langmuir, 31, 10955-10965.

Ferraro, J. W. (1979). Experimental evaluation of ceramic calcium phosphate as a substitute for bone grafts. Plastic and reconstructive surgery, 63, 634-640.

Firme Iii, C. P. & Bandaru, P. R. (2010). Toxicity issues in the application of carbon nanotubes to biological systems. Nanomedicine: Nanotechnology, Biology and Medicine, 6, 245-256.

Fotakis, G. & Timbrell, J. A. (2006). In vitro cytotoxicity assays: Comparison of LDH, neutral red, MTT and protein assay in hepatoma cell lines following exposure to cadmium chloride. Toxicology Letters, 160, 171-177.

Franci,G., Falanga, A., Galdiero,S., Palomba, L., Rai, M., Morelli,G., Galdiero,M.(2015). Silver Nanoparticles as Potential Antibacterial Agents.Molecules, 20, 8856-8874.

Galea, L., Bohner, M., Thuering, J., Doebelin, N., Aneziris, C. G. & Graule, T. (2013). Control of the size, shape and composition of highly uniform, non-agglomerated, sub-micrometer β-tricalcium phosphate and dicalcium phosphate platelets. Biomaterials, 34, 6388-6401.

Garg, A. & Sinnott, S. B. (1998). Effect of chemical functionalization on the mechanical properties of carbon nanotubes. Chemical Physics Letters, 295, 273-278.

Gasser, B. (2000). About composite materials and their use in bone surgery. Injury, 31 Suppl 4, 48-53.

Geiger, M., Li, R. H. & Friess, W. (2003). Collagen sponges for bone regeneration with rhBMP-2. Advanced Drug Delivery Reviews, 55, 1613-1629.

Ghazanfari, S. M. H. & Zamanian, A. (2013). Phase transformation, microstructural and mechanical properties of hydroxyapatite/alumina nanocomposite scaffolds produced by freeze casting. Ceramics International, 39, 9835-9844.

Gitrowski, C., Al-Jubory, A. R. & Handy, R. D. (2014). Uptake of different crystal structures of TiO2 nanoparticles by Caco-2 intestinal cells. Toxicology Letters, 226, 264-276.

Goldenberg, D. L. (1998). Septic arthritis. The Lancet, 351, 197-202.

Golub, E. E. & Boesze-Battaglia, K. (2007). The role of alkaline phosphatase in mineralization. Current Opinion in Orthopaedics, 18, 444-448.

Gonçalves, E. M., Oliveira, F. J., Silva, R. F., Neto, M. A., Fernandes, M. H., Amaral, M., Vallet-Regí, M. & Vila, M. (2015). Three-dimensional printed PCL-hydroxyapatite scaffolds filled with CNTs for bone cell growth stimulation. Journal of Biomedical Materials Research Part B: Applied Biomaterials.

Gorgieva, S. & Kokol, V.(2011). Collagen-vs. gelatine-based biomaterials and their biocompatibility: review and perspectives, INTECH open access publisher Croatia.

Gough, J., Notingher, I. & Hench, L. (2004). Osteoblast attachment and mineralized nodule formation on rough and smooth 45S5 bioactive glass monoliths. Journal of Biomedical Materials Research Part A, 68, 640-650.

Greeves, N. Hydroxyapatite Ca5(OH)(PO4)3. *In:* CA5(OH)(PO4)3, H. (ed.) Materials Studio, PyMOL, CrystalMaker. ChemTube3D: The University of Liverpool.

Haaparanta, A.-M., Haimi, S., Ellä, V., Hopper, N., Miettinen, S., Suuronen, R. & Kellomäki, M. (2010). Porous polylactide/β-tricalcium phosphate composite scaffolds for tissue engineering applications. Journal of Tissue Engineering and Regenerative Medicine, 4, 366-373.

Hansen, U. & Thünemann, A. F. (2015). Characterization of Silver Nanoparticles in Cell Culture Medium Containing Fetal Bovine Serum. Langmuir, 31, 6842-6852.

Harrison, B. S. & Atala, A. (2007). Carbon nanotube applications for tissue engineering. Biomaterials, 28, 344-353.

Herkendell, K., Shukla, V. R., Patel, A. K. & Balani, K. (2014). Domination of volumetric toughening by silver nanoparticles over interfacial strengthening of carbon nanotubes in bactericidal hydroxyapatite biocomposite. Materials Science and Engineering: C, 34, 455-467.

Hernigou, P. & Homma, Y. (2012). Tissue bioengineering in orthopedics. Clin Cases Miner Bone Metab, 9, 21-3.

Hooshmand, T., Abrishamchian, A., Najafi, F., Mohammadi, M., Najafi, H. & Tahriri, M. (2014). Development of sol-gel-derived multi-wall carbon nanotube/hydroxyapatite nanocomposite powders for bone substitution. Journal of Composite Materials, 48, 483-489.

Huang, C. & Cao, P. (2016). Tuning Ca:P ratio by NaOH from monocalcium phosphate monohydrate (MCPM). Materials Chemistry and Physics, 181, 159-166.

Huynh, K. A. & Chen, K. L. (2011). Aggregation Kinetics of Citrate and Polyvinylpyrrolidone Coated Silver Nanoparticles in Monovalent and Divalent Electrolyte Solutions. Environmental Science & Technology, 45, 5564-5571.

Jacobs, J. J. (1998). Current Concepts Review - Corrosion of Metal Orthopaedic Implants. The Journal of Bone and Joint Surgery, 268-282.

Janaćkovića, D., Petrović-Prelevićb, I. & Kostić-Gvozdenovića, L. (2007). Influence of synthesis parameters on the particle sizes of nanostructured calcium-hydroxyapatite. Calcium phosphate Ceramics-Bioresorbable Polymer Composite Biomaterials: from synthesis to applications:(1999-2007), 192, 103.

Jose Ruben, M., Jose Luis, E., Alejandra, C., Katherine, H., Juan, B. K., Jose Tapia, R. & Miguel Jose, Y. (2005). The bactericidal effect of silver nanoparticles. Nanotechnology, 16, 2346.

Juan, L., Zhimin, Z., Anchun, M., Lei, L. & Jingchao, Z. (2010). Deposition of silver nanoparticles on titanium surface for antibacterial effect. Int J Nanomedicine, 5, 261-267.

Juillerat-Jeanneret, L., Dusinska, M., Fjellsbø, L. M., Collins, A. R., Handy, R. D. & Riediker, M. (2015). Biological impact assessment of nanomaterial used in nanomedicine. Introduction to the NanoTEST project. Nanotoxicology, 9, 5-12.

Kalmodia, S., Goenka, S., Laha, T., Lahiri, D., Basu, B. & Balani, K. (2010). Microstructure, mechanical properties, and in vitro biocompatibility of spark plasma sintered hydroxyapatite–aluminum oxide–carbon nanotube composite. Materials Science and Engineering: C, 30, 1162-1169.

Kaneshiro, S., Ebina, K., Shi, K., Higuchi, C., Hirao, M., Okamoto, M., Koizumi, K., Morimoto, T., Yoshikawa, H. & Hashimoto, J. (2014). IL-6 negatively regulates osteoblast differentiation through the SHP2/MEK2 and SHP2/Akt2 pathways in vitro. J Bone Miner Metab, 32, 378-92.

Kang, S., Herzberg, M., Rodrigues, D. F. & Elimelech, M. (2008). Antibacterial Effects of Carbon Nanotubes: Size Does Matter! Langmuir, 24, 6409-6413.

Kasemo, B. (1983). Biocompatibility of titanium implants: surface science aspects. The Journal of prosthetic dentistry, 49, 832-837.

Kay, M. I., Young, R. A. & Posner, A. S. (1964). Crystal Structure of Hydroxyapatite. Nature, 204, 1050-1052.

Kealley, C., Elcombe, M., Van Riessen, A. & Ben-Nissan, B. (2006). Development of carbon nanotube-reinforced hydroxyapatite bioceramics. Physica B: Condensed Matter, 385–386, Part 1, 496-498.

Kealley, C. S., Latella, B. A., Van Riessen, A., Elcombe, M. M. & Ben-Nissan, B. (2008). Micro- and Nano-Indentation of a Hydroxyapatite-Carbon Nanotube Composite. Journal of Nanoscience and Nanotechnology, 8, 3936-3941.

Khalid, P., Hussain, M., Rekha, P. & Arun, A. (2015). Carbon nanotube-reinforced hydroxyapatite composite and their interaction with human osteoblast in vitro. Human & Experimental Toxicology, 34, 548-556.

Khanal, S. P., Mahfuz, H., Rondinone, A. J. & Leventouri, T. (2016). Improvement of the fracture toughness of hydroxyapatite (HAp) by incorporation of carboxyl functionalized single walled carbon nanotubes (CfSWCNTs) and nylon. Materials Science and Engineering: C, 60, 204-210.

Kini, U. & Nandeesh, B. N. (2012). Physiology of Bone Formation, Remodeling, and Metabolism, 29-57.

Kivrak, N. & Tas, A.C. (1998). Synthesis of calcium hydroxyapatite-tricaclium phosphate (HA-TCP) composite bioceramic powders and their sintering behaviour.Americal ceramic society, 81, 2245–2252

Klug, H. P. & Alexander, L. E. 1954. *X-ray diffraction procedures*, Wiley New York.
Kokubo, T., Ito, S., Huang, Z. T., Hayashi, T., Sakka, S., Kitsugi, T. & Yamamuro, T. (1990). Ca,P-rich layer formed on high-strength bioactive glass-ceramic A-W. J Biomed Mater Res, 24, 331-43.

Komori, T. (2006). Regulation of osteoblast differentiation by transcription factors. Journal of Cellular Biochemistry, 99, 1233-1239.

Komori, T. (2010). Regulation of Osteoblast Differentiation by Runx2. *In:* CHOI, Y. (ed.) Osteoimmunology: Interactions of the Immune and skeletal systems II. Boston, MA: Springer US.

Koutsopoulos, S. (2002). Synthesis and characterization of hydroxyapatite crystals: A review study on the analytical methods. Journal of Biomedical Materials Research, 62, 600-612.

Kurokouchi, K., Kambe, F., Yasukawa, K., Izumi, R., Ishiguro, N., Iwata, H. & Seo, H. (1998). TNF-α Increases Expression of IL-6 and ICAM-1 Genes Through Activation of NF-κB in Osteoblast-like ROS17/2.8 Cells. Journal of Bone and Mineral Research, 13, 1290-1299.

Lee, K. Y. & Mooney, D. J. (2001). Hydrogels for tissue engineering. Chemical reviews, 101, 1869-1880.

Lee, Y.-H., Cheng, F.-Y., Chiu, H.-W., Tsai, J.-C., Fang, C.-Y., Chen, C.-W. & Wang, Y.-J. (2014). Cytotoxicity, oxidative stress, apoptosis and the autophagic effects of silver nanoparticles in mouse embryonic fibroblasts. Biomaterials, 35, 4706-4715.

Lew, D. P. & Waldvogel, F. A. (2004). Osteomyelitis. The Lancet, 364, 369-379.

Li, G. Y., Wang, P. M. & Zhao, X. (2005). Mechanical behavior and microstructure of cement composites incorporating surface-treated multi-walled carbon nanotubes. Carbon, 43, 1239-1245.

Liao, C. Z., Wong, H. M., Yeung, K. W. & Tjong, S. C. (2014). The development, fabrication, and material characterization of polypropylene composites reinforced with carbon nanofiber and hydroxyapatite nanorod hybrid fillers. Int J Nanomedicine, 9, 1299-310.

Liao, S., Xu, G., Wang, W., Watari, F., Cui, F., Ramakrishna, S. & Chan, C. K. (2007). Self-assembly of nano-hydroxyapatite on multi-walled carbon nanotubes. Acta Biomaterialia, 3, 669-675.

Lin, X., Li, X., Fan, H., Wen, X., Lu, J. & Zhang, X. (2004). In situ synthesis of bone-like apatite/collagen nano-composite at low temperature. Materials Letters, 58, 3569-3572.

Liu, H. & Webster, T. J. (2007). Nanomedicine for implants: A review of studies and necessary experimental tools. Biomaterials, 28, 354-369.

Liu, Z., Tabakman, S., Welsher, K. & Dai, H. (2010). Carbon nanotubes in biology and medicine: In vitro and in vivo detection, imaging and drug delivery. Nano Research, 2, 85-120.

Lok, C.-N., Ho, C.-M., Chen, R., He, Q.-Y., Yu, W.-Y., Sun, H., Tam, P. K.-H., Chiu, J.-F. & Che, C.-M. (2007). Silver nanoparticles: partial oxidation and antibacterial activities. JBIC Journal of Biological Inorganic Chemistry, 12, 527-534.

Low, K. L., Tan, S. H., Zein, S. H. S., Mcphail, D. S. & Boccaccini, A. R. (2011). Optimization of the mechanical properties of calcium phosphate/multi-walled carbon nanotubes/bovine serum albumin composites using response surface methodology. Materials & Design, 32, 3312-3319.

Lu, X. & Leng, Y. (2005). Theoretical analysis of calcium phosphate precipitation in simulated body fluid. Biomaterials, 26, 1097-108.

Mackie, E. J., Ahmed, Y. A., Tatarczuch, L., Chen, K. S. & Mirams, M. (2008). Endochondral ossification: How cartilage is converted into bone in the developing skeleton. The International Journal of Biochemistry & Cell Biology, 40, 46-62.

Maho, A., Linden, S., Arnould, C., Detriche, S., Delhalle, J. & Mekhalif, Z. (2012). Tantalum oxide/carbon nanotubes composite coatings on titanium, and their functionalization with organophosphonic molecular films: A high quality scaffold for hydroxyapatite growth. Journal of colloid and interface science, 371, 150-158.

Martinez-Gutierrez, F., Boegli, L., Agostinho, A., Sánchez, E. M., Bach, H., Ruiz, F. & James, G. (2013). Anti-biofilm activity of silver nanoparticles against different microorganisms. Biofouling, 29, 651-660.

Masaki, C., Schneider, G. B., Zaharias, R., Seabold, D. & Stanford, C. (2005). Effects of implant surface microtopography on osteoblast gene expression. Clin Oral Implants Res, 16, 650-6.

Michel, R., Nolte, M., Reich, M. & Löer3, F. (1991). Systemic effects of implanted prostheses made of cobalt-chromium alloys. Archives of Orthopaedic and Trauma Surgery, 110, 61-74.

Mollazadeh, S., Javadpour, J. & Khavandi, A. (2007). In situ synthesis and characterization of nano-size hydroxyapatite in poly(vinyl alcohol) matrix. Ceramics International, 33, 1579-1583.

Monroe, E., Votava, W., Bass, D. & Mullen, J. M. (1971). New calcium phosphate ceramic material for bone and tooth implants. Journal of dental research, 50, 860-861.

Morones, J. R., Elechiguerra, J. L., Camacho, A., Holt, K., Kouri, J. B., Ramírez, J. T. & Yacaman, M. J. (2005). The bactericidal effect of silver nanoparticles. Nanotechnology, 16, 2346.

Morsczeck, C. (2006). Gene Expression of runx2, Osterix, c-fos, DLX-3, DLX-5, and MSX-2 in Dental Follicle Cells during Osteogenic Differentiation In Vitro. Calcified Tissue International, 78, 98-102.

Mukherjee, S., Kundu, B., Sen, S. & Chanda, A. (2014). Improved properties of hydroxyapatite–carbon nanotube biocomposite: Mechanical, in vitro bioactivity and biological studies. Ceramics International, 40, 5635-5643.

Mukherjee, S., Nandi, S. K., Kundu, B., Chanda, A., Sen, S. & Das, P. K. (2016). Enhanced bone regeneration with carbon nanotube reinforced hydroxyapatite in animal model. Journal of the Mechanical Behavior of Biomedical Materials, 60, 243-255.

Müller-Mai, C. M., Voigt, C. & Gross, U. (1990). Incorporation and degradation of hydroxyapatite implants of different surface roughness and surface structure in bone. Scanning microscopy, 4, 613-22; discussion 622-4.

Muller, J., Delos, M., Panin, N., Rabolli, V., Huaux, F. & Lison, D. (2009). Absence of Carcinogenic Response to Multiwall Carbon Nanotubes in a 2-Year Bioassay in the Peritoneal Cavity of the Rat. Toxicological Sciences, 110, 442-448.

Murugan, R. & Ramakrishna, S. (2005). Development of nanocomposites for bone grafting. Composites Science and Technology, 65, 2385-2406.

Nagai, H. & Toyokuni, S. (2012). Differences and similarities between carbon nanotubes and asbestos fibers during mesothelial carcinogenesis: Shedding light on fiber entry mechanism. Cancer Science, 103, 1378-1390.

Natesan, K., Shah, W., Le, H. & Tredwin, C. (2015). A Critical Comparison on Biocompatibility of Different Phases of Sol–Gel Derived Calcium Phosphates as Bone Graft Materials. Journal of Biomaterials and Tissue Engineering, 5, 655-664.

Nayak, A. K. (2010). Hydroxyapatite synthesis methodologies: an overview. International Journal of ChemTech Research, 2, 903-907.

Neacsu, P., Mazare, A., Cimpean, A., Park, J., Costache, M., Schmuki, P. & Demetrescu, I. (2014). Reduced inflammatory activity of RAW 264.7 macrophages on titania nanotube modified Ti surface. Int J Biochem Cell Biol, 55, 187-95.

Nguyen, K. C., Seligy, V. L., Massarsky, A., Moon, T. W., Rippstein, P., Tan, J. & Tayabali, A. F. (2013). Comparison of toxicity of uncoated and coated silver nanoparticles. Journal of Physics: Conference Series, 429, 012025.

Nie, L., Chen, D., Suo, J., Zou, P., Feng, S., Yang, Q., Yang, S. & Ye, S. (2012). Physicochemical characterization and biocompatibility in vitro of biphasic calcium phosphate/polyvinyl alcohol scaffolds prepared by freeze-drying method for bone tissue engineering applications. Colloids and Surfaces B: Biointerfaces, 100, 169-176.

Nuttelman, C. R., Henry, S. M. & Anseth, K. S. (2002). Synthesis and characterization of photocrosslinkable, degradable poly(vinyl alcohol)-based tissue engineering scaffolds. Biomaterials, 23, 3617-3626.

Okazaki, M., Aoba, T., Doi, Y., Takahashi, J. & Moriwaki, Y. (1981). Solubility and Crystallinity in Relation to Fluoride Content of Fluoridated Hydroxyapatites. Journal of Dental Research, 60, 845-849.

Olmedo, D. G., Duffó, G., Cabrini, R. L. & Guglielmotti, M. B. (2008). Local effect of titanium implant corrosion: an experimental study in rats. International Journal of Oral and Maxillofacial Surgery, 37, 1032-1038.

Owens, C. W. I. & Belcher, R. V. (1965). A colorimetric micro-method for the determination of glutathione. Biochemical Journal, 94, 705-711.

Paiyz, E. M., Ami, R. A., Joysurya, B., Arellano-Jimenez, M. J., Cato, T. L., Mary, M. S., Carter, C. B. & Syam, P. N. (2014). Functionalized carbon nanotube reinforced scaffolds

for bone regenerative engineering: fabrication, in vitro and in vivo evaluation. Biomedical Materials, 9, 035001.

Percival, S. L., Mccarty, S., Hunt, J. A. & Woods, E. J. (2014). The effects of pH on wound healing, biofilms, and antimicrobial efficacy. Wound Repair and Regeneration, 22, 174-186.

Perrone, G. G., Grant, C. M., & Dawes, I. W. (2005). Genetic and Environmental Factors Influencing Glutathione Homeostasis in Saccharomyces cerevisiae. Molecular Biology of the Cell, 16(1), 218–230.

Piao, M. J., Kang, K. A., Lee, I. K., Kim, H. S., Kim, S., Choi, J. Y., Choi, J. & Hyun, J. W. (2011). Silver nanoparticles induce oxidative cell damage in human liver cells through inhibition of reduced glutathione and induction of mitochondria-involved apoptosis. Toxicology Letters, 201, 92-100.

Potocni, J. 2011. *COMMISSION RECOMMENDATION of 18 October 2011on the definition of nanomaterial* [Online]. Available: http://ec.europa.eu/research/industrial_technologies/policy_en.html [Accessed 10 2016].

Rai, M., Yadav, A. & Gade, A. (2009). Silver nanoparticles as a new generation of antimicrobials. Biotechnology Advances, 27, 76-83.

Rajendran, A., Barik, R. C., Natarajan, D., Kiran, M. S. & Pattanayak, D. K. (2014). Synthesis, phase stability of hydroxyapatite–silver composite with antimicrobial activity and cytocompatability. Ceramics International, 40, 10831-10838.

Rajkumar, M., Sundaram, N. M. & Rajendran, V. (2010). In-situ preparation of hydroxyapatite nanorod embedded poly (vinyl alcohol) composite and its characterization. International Journal of engineering science and Technology, 2, 2437-2444.

Ramakrishna, S., Mayer, J., Wintermantel, E. & Leong, K. W. (2001). Biomedical applications of polymer-composite materials: a review. Composites Science and Technology, 61, 1189-1224.

Rameshbabu, N., Sampath Kumar, T. S., Prabhakar, T. G., Sastry, V. S., Murty, K. V. G. K. & Prasad Rao, K. (2007). Antibacterial nanosized silver substituted hydroxyapatite: Synthesis and characterization. Journal of Biomedical Materials Research Part A, 80A, 581-591.

Razak, S. A., Sharif, N. & Rahman, W. (2012). Biodegradable polymers and their bone applications: a review. Int J Basic Appl Sci, 12, 31-49.

Rejda, B., Peelen, J. & De Groot, K. (1977). Tri-calcium phosphate as a bone substitute. Journal of bioengineering, 1, 93-97.

Rho, J.-Y., Kuhn-Spearing, L. & Zioupos, P. (1998). Mechanical properties and the hierarchical structure of bone. Medical Engineering & Physics, 20, 92-102.

Rosca, I. D., Watari, F., Uo, M. & Akasaka, T. (2005). Oxidation of multiwalled carbon nanotubes by nitric acid. Carbon, 43, 3124-3131.

Ryoo, H. M., Hoffmann, H. M., Beumer, T., Frenkel, B., Towler, D. A., Stein, G. S., Stein, J. L., Van Wijnen, A. J. & Lian, J. B. (1997). Stage-specific expression of Dlx-5 during osteoblast differentiation: involvement in regulation of osteocalcin gene expression. Mol Endocrinol, 11, 1681-94.

Sadat-Shojai, M., Khorasani, M.-T., Dinpanah-Khoshdargi, E. & Jamshidi, A. (2013). Synthesis methods for nanosized hydroxyapatite with diverse structures. Acta Biomaterialia, 9, 7591-7621.

Salahil, E. R. A. (2016). Fabrication and Characterization of Hydroxyapatite-Carbon Nano Tubes Composites. American Journal of Nanosciences, 2, 41-45.

Salehi, S. & Fathi, M. H. (2010). Fabrication and characterization of sol–gel derived hydroxyapatite/zirconia composite nanopowders with various yttria contents. Ceramics International, 36, 1659-1667.

Schmittgen, T. D. & Livak, K. J. (2008). Analyzing real-time PCR data by the comparative CT method. Nature protocols, 3, 1101.

Schneider, C. A., Rasband, W. S. & Eliceiri, K. W. (2012). NIH Image to ImageJ: 25 years of image analysis. Nat Methods, 9, 671-5.

Schneider, G. B., Perinpanayagam, H., Clegg, M., Zaharias, R., Seabold, D., Keller, J. & Stanford, C. (2003). Implant Surface Roughness Affects Osteoblast Gene Expression. Journal of Dental Research, 82, 372-376.

Schreurs, W. J. & Rosenberg, H. (1982). Effect of silver ions on transport and retention of phosphate by Escherichia coli. Journal of Bacteriology, 152, 7-13.

Seal, B. L., Otero, T. C. & Panitch, A. (2001). Polymeric biomaterials for tissue and organ regeneration. Materials Science and Engineering: R: Reports, 34, 147-230.

Seeman, E. (2007). Bone's material and structural strength. Current Opinion in Orthopaedics, 18, 494-498.

Seeman, E. (2008). Structural basis of growth-related gain and age-related loss of bone strength. Rheumatology (Oxford), 47 Suppl 4, iv2-8.

Seeman, E. & Delmas, P. D. (2006). Bone Quality-The Material and Structural basis of Bone Strength and Fragility. The New England Journal of Medicine, 354, 2250-2261.

Shahabi, S., Najafi, F., Majdabadi, A., Hooshmand, T., Haghbin Nazarpak, M., Karimi, B. & Fatemi, S. M. (2014). Effect of Gamma Irradiation on Structural and Biological Properties of a PLGA-PEG-Hydroxyapatite Composite. The Scientific World Journal, 2014, 9.

Shiba, K., Motozuka, S., Yamaguchi, T., Ogawa, N., Otsuka, Y., Ohnuma, K., Kataoka, T. & Tagaya, M. (2016). Effect of Cationic Surfactant Micelles on Hydroxyapatite Nanocrystal Formation: An Investigation into the Inorganic–Organic Interfacial Interactions. Crystal Growth & Design, 16, 1463-1471.

Shibuya, N. & Jupiter, D. C. (2015). Bone graft substitute: allograft and xenograft. Clin Podiatr Med Surg, 32, 21-34.

Shin, U. S., Yoon, I. K., Lee, G. S., Jang, W. C., Knowles, J. C. & Kim, H. W. (2011). Carbon nanotubes in nanocomposites and hybrids with hydroxyapatite for bone replacements. J Tissue Eng, 2011, 674287.

Singh, M. K., Gracio, J., Leduc, P., Goncalves, P. P., Marques, P. a. a. P., Goncalves, G., Marques, F., Silva, V. S., Capela E Silva, F., Reis, J., Potes, J. & Sousa, A. (2010). Integrated biomimetic carbon nanotube composites for in vivo systems. Nanoscale, 2, 2855-2863.

Sionkowska, A. (2011). Current research on the blends of natural and synthetic polymers as new biomaterials: Review. Progress in Polymer Science, 36, 1254-1276.

Smart, S. K., Cassady, A. I., Lu, G. Q. & Martin, D. J. (2006). The biocompatibility of carbon nanotubes. Carbon, 44, 1034-1047.

Socrates, R., Sakthivel, N., Rajaram, A., Ramamoorthy, U. & Kalkura, S. N. (2015). Novel fibrillar collagen–hydroxyapatite matrices loaded with silver nanoparticles for orthopedic application. Materials Letters, 161, 759-762.

Sondi, I. & Salopek-Sondi, B. (2004a). Silver nanoparticles as antimicrobial agent: a case study on E. coli as a model for Gram-negative bacteria. Journal of colloid and interface science, 275, 177-182.

Sondi, I. & Salopek-Sondi, B. (2004b). Silver nanoparticles as antimicrobial agent: a case study on E. coli as a model for Gram-negative bacteria. Journal of Colloid and Interface Science, 275, 177-182.

Suchanek, W. & Yoshimura, M. (1998). Processing and properties of hydroxyapatite-based biomaterials for use as hard tissue replacement implants. Journal of Materials Research, 13, 94-117.

Sunk, I.-G., Trattnig, S., Graninger, W. B., Amoyo, L., Tuerk, B., Steiner, C.-W., Smolen, J. S. & Bobacz, K. (2006). Impairment of chondrocyte biosynthetic activity by exposure to 3-tesla high-field magnetic resonance imaging is temporary. Arthritis Research & Therapy, 8, R106-R106.

Suzuki, O. (2013). Octacalcium phosphate (OCP)-based bone substitute materials. Japanese Dental Science Review, 49, 58-71.

Tew, K. D., & Townsend, D. M. (2011). Regulatory functions of glutathione S-transferase P1-1 unrelated to detoxification. Drug Metabolism Reviews, 43(2), 179–193.

Toh, R. J., Ambrosi, A. & Pumera, M. (2012). Bioavailability of Metallic Impurities in Carbon Nanotubes Is Greatly Enhanced by Ultrasonication. Chemistry – A European Journal, 18, 11593-11596.

Tong, Q., Qingzhi, W., Honglian, D., Xinyu, W., Youfa, W., Shipu, L. & Junli, L. (2014). A comparative study on the effects of pristine and functionalized single-walled carbon nanotubes on osteoblasts: ultrastructural and biochemical properties. Journal of Materials Science: Materials in Medicine, 25, 1915-1923.

Tranquilli Leali, P., Doria, C., Zachos, A., Ruggiu, A., Milia, F. & Barca, F. (2009). Bone fragility: current reviews and clinical features. Clinical Cases in Mineral and Bone Metabolism, 6, 109-113.

Uskoković, V. (2015). The Role of Hydroxyl Channel in Defining Selected Physicochemical Peculiarities Exhibited by Hydroxyapatite. RSC advances, 5, 36614-36633.

Usui, Y., Aoki, K., Narita, N., Murakami, N., Nakamura, I., Nakamura, K., Ishigaki, N., Yamazaki, H., Horiuchi, H., Kato, H., Taruta, S., Kim, Y. A., Endo, M. & Saito, N. (2008). Carbon Nanotubes with High Bone-Tissue Compatibility and Bone-Formation Acceleration Effects. Small, 4, 240-246.

Vallet-Regí, M. & González-Calbet, J. M. (2004). Calcium phosphates as substitution of bone tissues. Progress in Solid State Chemistry, 32, 1-31.

Vandrovcova, M. & Bacakova, L. (2011). Adhesion, growth and differentiation of osteoblasts on surface-modified materials developed for bone implants. Physiol Res, 60, 403-17.

Venkatesan, J., Qian, Z.-J., Ryu, B., Ashok Kumar, N. & Kim, S.-K. (2011). Preparation and characterization of carbon nanotube-grafted-chitosan – Natural hydroxyapatite composite for bone tissue engineering. Carbohydrate Polymers, 83, 569-577.

Wagner, H., Lourie, O., Feldman, Y. & Tenne, R. (1998). Stress-induced fragmentation of multiwall carbon nanotubes in a polymer matrix. Applied physics letters, 72, 188-190.

Wang, M., Li, Y., Wu, J., Xu, F., Zuo, Y. & Jansen, J. A. (2008). In vitro and in vivo study to the biocompatibility and biodegradation of hydroxyapatite/poly(vinyl alcohol)/gelatin composite. Journal of Biomedical Materials Research Part A, 85A, 418-426.

Wang, Y., Zhang, S., Wei, K., Zhao, N., Chen, J. & Wang, X. (2006). Hydrothermal synthesis of hydroxyapatite nanopowders using cationic surfactant as a template. Materials Letters, 60, 1484-1487.

White, A. A., Best, S. M. & Kinloch, I. A. (2007). Hydroxyapatite–Carbon Nanotube Composites for Biomedical Applications: A Review. International Journal of Applied Ceramic Technology, 4, 1-13.

Xu, H. H. & Simon, C. G., Jr. (2005). Fast setting calcium phosphate-chitosan scaffold: mechanical properties and biocompatibility. Biomaterials, 26, 1337-48.

Xu, J. L., Khor, K. A., Sui, J. J. & Chen, W. N. (2009). Preparation and characterization of a novel hydroxyapatite/carbon nanotubes composite and its interaction with osteoblast-like cells. Materials Science and Engineering: C, 29, 44-49.

Yadav, S. K., Bera, T., Saxena, P. S., Maurya, A. K., Garbyal, R. S., Vajtai, R., Ramachandrarao, P. & Srivastava, A. (2010). MWCNTs as reinforcing agent to the Hap–Gel nanocomposite for artificial bone grafting. Journal of Biomedical Materials Research Part A, 93A, 886-896.

Yamada, S., Heymann, D., Bouler, J. M. & Daculsi, G. (1997). Osteoclastic resorption of calcium phosphate ceramics with different hydroxyapatite/β-tricalcium phosphate ratios. Biomaterials, 18, 1037-1041.

Yamashita, D., Machigashira, M., Miyamoto, M., Takeuchi, H., Noguchi, K., Izumi, Y. & Ban, S. (2009). Effect of surface roughness on initial responses of osteoblast-like cells on two types of zirconia. Dental Materials Journal, 28, 461-470.

Yang, W., Thordarson, P., Gooding, J. J., Ringer, S. P. & Braet, F. (2007). Carbon nanotubes for biological and biomedical applications. Nanotechnology, 18, 412001.

Yang, Y., Kim, K.-H., Agrawal, C. M. & Ong, J. L. (2004). Interaction of hydroxyapatite–titanium at elevated temperature in vacuum environment. Biomaterials, 25, 2927-2932.

Yu, M.-F., Lourie, O., Dyer, M. J., Moloni, K., Kelly, T. F. & Ruoff, R. S. (2000). Strength and Breaking Mechanism of Multiwalled Carbon Nanotubes Under Tensile Load. Science, 287, 637-640.

Yunoki, S., Ikoma, T., Monkawa, A., Ohta, K. & Tanaka, J. (2007). Preparation and Characterization of Hydroxyapatite/Collagen Nanocomposite Gel. Journal of Nanoscience and Nanotechnology, 7, 818-821.

Zareidoost, A., Yousefpour, M., Ghaseme, B. & Amanzadeh, A. (2012). The relationship of surface roughness and cell response of chemical surface modification of titanium. Journal of Materials Science. Materials in Medicine, 23, 1479-1488.

Zarubina, A. P., Deev, L. I., Parkhomenko, I. M., Parshina, E. Y., Sarycheva, A. S., Novoselova, L. A., Lukashev, E. P., Netrusov, A. I. & Rubin, A. B. (2015). Evaluation

of toxicity of silver ions and nanoparticles using model bacteria with luminescent phenotype. Nanotechnologies in Russia*, 10*, 475-483.

Zeng, S., Fu, S., Guo, G., Liang, H., Qian, Z., Tang, X. & Luo, F. (2011). Preparation and Characterization of Nano-Hydroxyapatite/Poly(vinyl alcohol) Composite Membranes for Guided Bone Regeneration. Journal of Biomedical Nanotechnology*, 7*, 549-557.

Zhang, X.-F., Shen, W. & Gurunathan, S. (2016). Silver Nanoparticle-Mediated Cellular Responses in Various Cell Lines: An in Vitro Model. International Journal of Molecular Sciences*, 17*, 1603.

Zhang, Y. & Dong, Y. (2015). Effect of Surfactant on Morphology of Hydroxyapatite. Synthesis and Reactivity in Inorganic, Metal-Organic, and Nano-Metal Chemistry*, 45*, 411-414.

Zhang, Y., Petibone, D., Xu, Y., Mahmood, M., Karmakar, A., Casciano, D., Ali, S. & Biris, A. S. (2014). Toxicity and efficacy of carbon nanotubes and graphene: the utility of carbon-based nanoparticles in nanomedicine. Drug Metabolism Reviews*, 46*, 232-246.

Zhao, L. & Gao, L. (2004). Novel in situ synthesis of MWNTs-hydroxyapatite composites. Carbon*, 42*, 423-426.

Zhao, L., Wang, H., Huo, K., Cui, L., Zhang, W., Ni, H., Zhang, Y., Wu, Z. & Chu, P. K. (2011). Antibacterial nano-structured titania coating incorporated with silver nanoparticles. Biomaterials*, 32*, 5706-5716.

Zhou, X., Zhang, Z., Feng, J. Q., Dusevich, V. M., Sinha, K., Zhang, H., Darnay, B. G. & De Crombrugghe, B. (2010). Multiple functions of Osterix are required for bone growth and homeostasis in postnatal mice. Proc Natl Acad Sci U S A*, 107*, 12919-24.